UNIVERSITY OF WOLLONGONG AUSTRALIA

Fabrication and Preclinical Assessment of Drug Eluting Wet Spun Fibres for Pancreatic Cancer Treatment

Samantha Jane Wade

Supervisor:
Dr. Kara Vine-Perrow

This thesis is presented as part of the requirement for the conferral of the degree:
DOCTOR OF PHILOSOPHY

This research has been conducted with the support of a matching scholarship from the Faculty of Science, Medicine and Health and the Intelligent Polymer Research Institute

The Illawarra Health and Medical Research Institute
School of Chemistry and Molecular Bioscience
University of Wollongong
Dec 2019

Abstract

Pancreatic ductal adenocarcinoma (PDAC) is an insidious disease with an abysmal 5-year survival rate of 9 % in Australia. This rate has only marginally improved over the last 20 years, highlighting the need for improved therapeutic approaches. Chemotherapy is the current standard of care of PDAC, with a combination of *nab*-paclitaxel and gemcitabine one of the major first line treatments for locally advanced, non resectable and metastatic PDAC. Depending on the patients overall health (performance status), chemotherapy can be combined with radiotherapy but only moderately improves survival by approximately 13 months. The notoriously poor survival of PDAC is attributed to a number of factors including the typically advanced stage of the disease at the time of diagnosis and the rapid development of resistance to therapy. The tumour biology plays a major role in hindering chemotherapy uptake by the tumour. Desmoplasia is a characteristic of PDAC which consists of a stromal environment composed of extracellular matrix (ECM) components, activated fibroblast- and myofibroblast-like cells called pancreatic stellate cells (PSC) and inflammatory cells which contribute to the lack of response to chemotherapy by creating a tumour environment with high intratumoural tumour pressure and low vascularity. These factors combined mean therapeutic concentrations of drug often cannot be reached without intolerable toxicity to the patient.

This thesis describes a novel way of delivering currently used, but largely ineffective drugs to treat pancreatic tumours – through the development of dual drug loaded chemotherapy implants. The single-use drug delivery device is designed to be implanted intratumourally to overcome the physical barriers described above and deliver high concentrations of drugs locally, without systemic toxicity. Chapter 2 describes the optimisation of gemcitabine loading into single alginate or chitosan fibres for localised drug delivery. This involved optimisation of the wet spinning fabrication process to form the fibres with a range of gemcitabine concentrations. The fibres were characterised by scanning electron microscopy (SEM) imaging to observe surface and internal morphology, and the drug release profile assessed. The release profile of all fibre formulations displayed a large burst release, in which ~80 % of the drug was released within the first 10 h. This was then followed by efficacy assessment using two

human PDAC cell lines (Mia-PaCa-2 and PANC-1) grown as 2D monolayers. Here, alginate fibres without drug showed biocompatibility, as there was no reduction in cell viability after 72 h, while gemcitabine loaded alginate fibres showed a 23-56 % reduction in viability. Conversely, wet-spun chitosan fibres without drug showed significant toxicity in all *in vitro* studies so was not tested in subsequent chapters. A 3D spheroid model using MCF-7 cells was utilised as a more clinically relevant model, and over a 5 day period showed up to 52 % reduction in cell viability after treatment with gemcitabine loaded fibres.

In order to better recapitulate the standard of care chemotherapy regimen used in the clinic and potentially improve upon the therapeutic efficacy of the fibre formulation developed in Chapter 2, a coaxial fibre formulation containing gemcitabine and paclitaxel was developed and characterised in Chapter 3. Poly lactic-co-glycolic acid (PLGA) and poly-ε-caprolactone (PCL) were assessed in a number of solvents to determine the most appropriate formulation for wet spinning. PCL was determined to be superior and was therefore selected for formation of the outer layer which was loaded with paclitaxel, while alginate was used to form the inner core and was loaded with gemcitabine. Coaxial fibres were formed using a novel coaxial spinneret. Similarly to the *in vitro* testing of single gemcitabine fibres, 2D monolayer and 3D spheroids models were utilised for assessing the efficacy of the dual-drug loaded fibres and found that the dual-drug loaded fibres reduced cell viability by up to 82.5 %. Further in Chapter 3, a clonogenic survival assay was utilised to assess the effect of combining treatment of our dual-drug loaded fibres with radiotherapy. This study showed that the dual-drug loaded fibre in combination with 1 Gy radiation reduced the colony forming ability of the surviving Mia-PaCa-2 cells by 87.1 %, and was the superior treatment when compared to the equivalent amount of free drug with 1 Gy radiation. Interestingly, the Alg/PCL fibre itself showed significant radiosensitising ability, which may have increased the effect of the chemotherapy/radiotherapy combination.

In Chapter 4 the dual-drug loaded fibres were formed into implants for subcutaneous injection into mice, and an *in vivo* efficacy study performed in a subcutaneous Mia-PaCa-2 xenograft mouse model. A rigid PCL capsule was fabricated to house the dual-drug loaded coaxial fibre to form the implant, in order to increase the mechanical strength required for implantation into an animal. The implants were inserted adjacent to human PDAC tumours growing on the flanks of mice for a period of 42 days, and tumour volume measured by vernier callipers. The implantation procedure was well tolerated, and there were no adverse effects at the implantation site. There was no implant migration, and no weight loss was observed throughout the study, indicating the implants were well tolerated. There was no significant difference in tumour volume of the mice treated with the dual-drug loaded implant and empty implants, likely due to lack of hydration and swelling of the alginate polymer leading to insufficient drug release from the implant over the study period. A cytokine panel was performed to assess whether there was an immune response occurring, and it was determined there was no immune response to the implants.

Finally, in Chapter 5, the wet spinning method was further explored as a means to fabricate single alginate fibres loaded with the monoclonal antibody nivolumab, an anti PD-1 checkpoint inhibitor used for cancer immunotherapy. The method of loading and release conditions showed that there was no significant effect on the activity of the nivolumab, which opens the door for further evaluation of a localised immunotherapy treatment option using our Alg/PCL drug delivery technology.

In summary, the work presented in this thesis demonstrates the feasibility of using the wet spinning method to create drug eluting implants that show preclinical efficacy. It has provided the groundwork into further developing this technology to form an implantable drug delivery system that with further testing could be suitable for implantation into humans for the treatment of locally advanced, non-resectable PDAC.

Acknowledgements

Firstly, to my supervisor Dr Kara Vine-Perrow. I initially chose your lab because I admired your confidence, success and passion for this project. This hasn't waned over the last 5 years, which is something that I greatly admire. Thankyou for pushing me to be better, and providing numerous opportunities to further myself personally and professionally. Thankyou for caring about me as a person, and not just a data generating research student. Thankyou for always having time for me, even when stretched to your own limits. I didn't think I would even make it through undergrad, so thankyou for taking a chance on me 5 years ago in my honours year. I'm really excited to see where this project goes and am ecstatic to continue working in your lab.

Thankyou to the researchers I've had the pleasure working with over the last 4 years. My co-supervisors Prof Simon Moulton, Prof Mori Aghmesheh, Prof Gordon Wallace and Dr Javad Foroughi, as well as the wider cancer research group – notably Dr Ann-Katrin Piper, Bryce Keenan, Dr Lisa Belfiore, Prof Marie Ranson, Dr Benjamin Buckley and Elahe Minaei – for all your help with experiments (and life advice). I wish to acknowledge the technical support staff that facilitate all of the research at both IHMRI and the animal house. Special mention to Maria Catacouzinos, who provided constant reassurance and kindness during my first animal experiment when I was breaking down and stressed. You saved my mental health during those few months and I am incredibly grateful.

To Jay Perry and Claudia Kielkopf, for the constant distractions, toast and jokes, tuna and crackers – I probably would have finished this much earlier without you both, but definitely without my sanity. Thankyou for making a tough journey incredibly enjoyable. Thankyou for making this office space more like a second home (considering the time we've spent here!). I'm better for knowing you both. Now get back to work.

To Mum, Dad, Steph, Alex and Zaz – Thank you for always listening as I *constantly* talked, ranted, practiced speeches (over and over and over), and for proudly telling people about my amazing research on "flesh eating bacteria". Thankyou for your unwavering and unconditional support for the 10 long years I've been at uni. You are all my safe space and remind me what's most important.

I recently read the quote "*I so rarely meet a scientist who is single. I refuse to believe this is because people find socks and sandals attractive. It's because it's nearly impossible to do what they do, on their own*" Thankyou Joel, for being my #1 cheerleader, for believing in me more than I ever did, and always finding ways to pick me up at my lowest. We (finally!) did it and I'm really excited to see where our next adventure goes.

Certification

I, Samantha Jane Wade, declare that this thesis submitted in fulfilment of the requirements for the conferral of the degree Doctor of Philosophy, from the University of Wollongong, is wholly my own work unless otherwise referenced or acknowledged. This document has not been submitted for qualifications at any other academic institution.

Samantha Jane Wade
19th Dec 2019

Table of Contents

List of Figures

List of Tables

Cytokine	Saline	Empty Implant + i.v. saline		Empty Implant + i.v. Drugs		Dua
	Mean (pg/mL)	Mean (pg/mL)	Fold change	Mean (pg/mL)	Fold change	Mean
CXCL1	51.75±7.13	138.21±3.23	2.67	252.76 ±56.23	4.88	66.68
TGF-β1	49.81±8.72	13.46±2.92	0.27	40.24±11.18	0.81	62.18
IL-1β	4.00±0.91	4.58±1.04	1.14	5.64±1.22	1.41	3.84
IL-23	2.89±1.26	12.91±2.50	4.46	4.65±1.56	1.60	45.40
CCL22	287.66±33.54	250.82±17.62	0.87	276.53±23.69	0.96	329.0
IL-10	1.15±1.16	2.09±1.40	1.81	0	0	20.6
IL-12p70	0.72±0.31	0.25±0.17	0.35	0.45±0.26	0.63	0.59
IL-6	68.90±19.54	14.45±1.60	0.21	31.62±5.86	0.46	40.04
TNF-α	39.45±5.45	21.00±1.13	0.53	24.85±2.71	0.63	35.1
G-CSF	113.53±59.39	19.40±7.36	0.17	4.55±2.54	0.04	43.23
CCL17	241.43±33.76	204.22±10.51	0.85	261.71±32.07	1.08	285.9
IL-12p40	367.37±22.57	445.05±34.98	1.21	448.86±41.38	1.22	378.4
IL-1β	0	1.51±1.06	-	0	0	12.1

Presentations & Manuscripts

Oral Presentations

Invited speaker: Controlled Delivery Workshop – Australian Institute for Innovative Materials, University of Wollongong. Talk title: Drug Eluting Implants for Non-Resectable Pancreatic Cancer Wollongong, 2017

Invited speaker: Translational Cancer Research Workshop – Centre for Oncology Education and Research Translation. Talk title: Drug Eluting Implants for Non-Resectable Pancreatic Cancer, Wollongong Sept 2017, Sydney Sept 2019)

Poster Presentations

Wade, SJ. Talebian, S. Foroughi, J. Moulton, SE. Aghmesheh, M. Vine, KL. Fabrication and *in vitro* Assessment of Dual Drug Eluting Polymeric Fibres for the Treatment of Pancreatic Cancer. Poster presented at Controlled Release Asia meeting, Singapore, Sept 2018

Wade, SJ. Talebian, S. Foroughi, J. Moulton, SE. Aghmesheh, M. Vine, KL. Fabrication and *in vitro* Assessment of Dual Drug Eluting Polymeric Fibres for the Treatment of Pancreatic Cancer. Poster presented at Drug Delivery Australia Conference, Wollongong, Sept 2017

Wade, SJ. Zuzic A. Foroughi, J. Talebian, S. Moulton, SE. Aghmesheh, M. Vine, KL. Changing the Treatment Paradigm: Gemcitabine Eluting Degradable Polymeric Fibres for the Treatment of Pancreatic Cancer. Poster presented at the Sydney Cancer Conference, Sydney, Sept 2016

Wade, SJ. Zuzic A. Foroughi, J. Talebian, S. Moulton, SE. Aghmesheh, M. Vine, KL. Changing the Treatment Paradigm: Gemcitabine Eluting Degradable Polymeric Fibres for the Treatment of Pancreatic Cancer. Poster presented at the Australian Society for Medical Research, Sydney, June 2016.

Manuscripts

Talebian, S. Foroughi, J. **Wade, SJ.** Vine, KL. Dolatshahi-Pirouz, A. Mehrali, M. Conde, J. Wallace, GG. Biopolymers for Antitumor Implantable Drug Delivery Systems: Recent Advances and Future Outlook. Advanced materials, 2018

Wade, SJ. Zuzic, A. Foroughi, J. Talebian, S. Aghmesheh, M. Moulton, SE. Vine, KL. Preparation and In Vitro Assessment of Wet-Spun Gemcitabine-Loaded Polymeric Fibres: Toward Localised Treatment for the Treatment of Pancreatic Cancer. Pancreatology, 2017, 17(5) p795-804

List of Abbreviations

5FU	5-fluoruracil
APH	Acid phosphatase assay
CA	Coeliac axis
CHA	Common hepatic artery
CTLA-4	Cytotoxic T lymphocyte associated protein 4
DDS	Drug delivery system
DMF	Dimethylformamide
EUS	Endoscope ultrasound guided
FNA	Fine needle aspiration
FNI	Fine needle injection
GEMM	Genetically engineered mouse model
Ig	Immunoglobulin
IL-	Interleukin-
IP	Intraperitoneal
i.v.	Intravenous
Mw	Molecular weight
Nab-	Nanoparticle albumin bound
NK	Natural killer
NMP	N-methyl-2-pyrrolidine
OS	Overall survival
PBS	Phosphate buffered saline
PDAC	Pancreatic ductal adenocarcinoma
PCL	poly-ε-caprolactone
PD-1	Programmed cell death protein 1
PD-L1	Programmed cell death protein ligand 1
PDX	Patient derived xenograft
PLGA	Poly(lactic-co-glycolic acid)
PV	Portal vein
SEM	Standard error of the mean / scanning electron microscopy
SMA	Superior mesenteric artery
SMV	Superior mesenteric vein
TCR	T cell receptor
ULA	Ultra-low adhering

Chapter 1: Introduction to Implantable, Polymeric Drug Delivery Systems for Cancer Therapy

Portions of this chapter have been published in the following work:

Talebian, S. Foroughi, J. **Wade, SJ.** Vine, KL. Dolatshahi-Pirouz, A. Mehrali, M. Conde, J. Wallace, GG. Biopolymers for Antitumor Implantable Drug Delivery Systems: Recent Advances and Future Outlook. Advanced materials, 2018

Author contributions: S Talebian wrote the manuscript. All other authors edited the manuscript for submission

1.1 Introduction to Cancer

Cancer is one of the leading causes of death in Australia with an estimated 145,000 newly diagnosed cases and 50,000 deaths predicted for 2019.* Cancer is comprised of a broad range of diseases that involve abnormal cell proliferation, invasion and metastasis. There are 10 hallmarks that describe the capabilities that enable cancer growth and metastasis which are summarised in Fig 1.1 (Hanahan and Weinberg 2011).

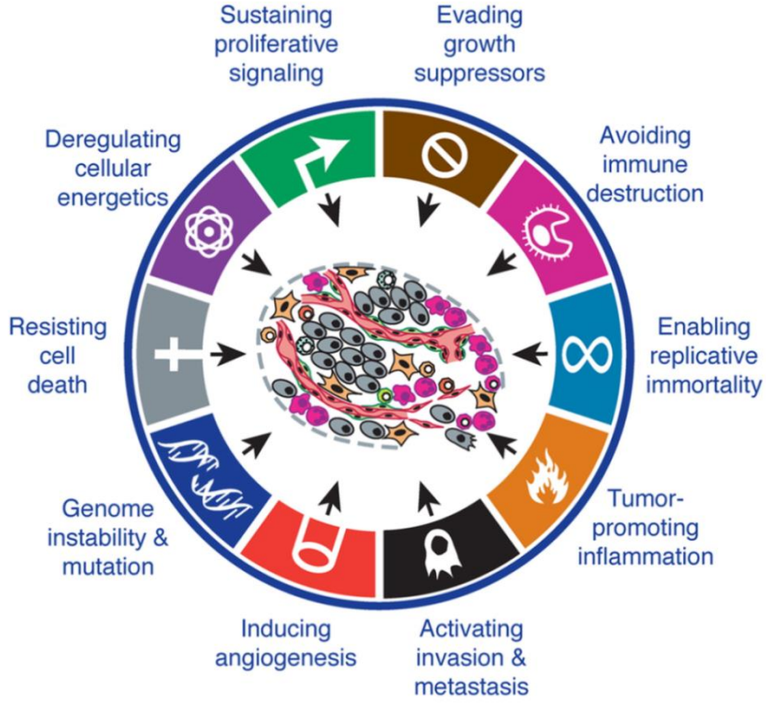

Figure 1.1: The hallmarks of cancer. Taken from Hanahan and Weinberg (2011)

The majority of cancers are treated with cytotoxic agents (e.g. chemotherapy), and while some cancer types respond very well, primarily haematological cancers, others such as pancreatic ductal adenocarcinoma (PDAC) respond poorly. As chemotherapy targets all rapidly proliferating cells, it not only targets and kills cancer cells, but also hair follicles, mucous membranes (mouth and gastrointestinal tract), reproductive organs, blood cells in the bone marrow

* Cancer Council
www.cancer.org.au

and skin (Moran 2000). This non-specific toxicity caused by chemotherapy treatment can affect the treatment regimen. Dose reductions and delays are often implemented when the toxicity is intolerable, along with supportive measures (such as medications to prevent nausea and vomiting). If the toxicity is still too high and a decision to stop the treatment is made, this therefore will lead to tumour progression. These treatments have the ability to be effective, but the severe side effects highlight the need to deliver the treatments specifically to the site of disease. Given our understanding of the hallmarks of cancer and the identification of some of the key genetic drivers, there has been a shift in the field towards targeted therapy. Targeted therapies are substances that stop cancer growth by interfering with specific pathways or molecular mechanisms of cancer cells. There are a number of approved targeted therapies on the market, many of which have shown considerable improvements in overall survival. Trastuzumab is a humanised monoclonal antibody developed to target the HER2 receptor, which is overexpressed in 25% of breast cancer (Dean-Colomb and Esteva 2008). Addition of trastuzumab to chemotherapy in early stage breast cancer was associated with a 37 % reduction in mortality risk over long-term follow-up (Perez *et al.,* 2014). While this is a shining example of the potential of targeted therapy, resistance to trastuzumab is still a significant problem, primarily for metastatic breast cancer. There are a number of other HER2 targeted therapies that can help overcome these issues such as pertuzumab which showed that when administered in combination with trastuzamab and docetaxel improved overall survival in HER2 positive metastatic breast cancer cases by 15.7 months (Swain *et al.,* 2015). Another phase III study showed that dual inhibition of HER2 in women with HER2 positive primary breast cancer with a combination of lapatinib and trastuzumab resulted in 51% of women achieving complete pathological response compared to 29% in the trastuzumab alone (Baselga *et al.,* 2012). These therapies are administered systemically, so are accompanied by a number of unfavourable side effects, which can result in cessation of treatment – much like chemotherapy. Furthermore identifying a target such as HER2 has not been possible for all cancers, in particular in PDAC. PDAC has a very low prevalence of HER2 upregulation, which was showing in a study of 469 patients with PDAC which found that 2% of patients had amplified HER2 (Chou *et al.,* 2013). Identification of druggable targets for PDAC are therefore required. This was explored in a study that utilised the results of genomic sequencing of PDAC as part of the International Cancer Genome Consortium. 76 PDAC biopsies were screened for

HER2 amplification, KRAS wild-type, BRCA-1, BRCA-2 PALB2 and ATM, and 22 samples were found to have eligible genetic signatures. This study aimed to determine the feasibility of procuring and processing biopsies for molecular profiling, and highlighted the associated challenges with the view to evolve into a clinically appropriate trial (Chantrill *et al.*, 2015).

This has led to research into local delivery of anti-cancer agents. The concept of local delivery of chemotherapeutics is growing, but very few implantable, localized treatment approaches have reached clinical trials and have been approved for clinical use. This chapter will discuss the current treatments available and the challenges faced when treating one of the deadliest cancers, PDAC. It will provide an overview of implantable drug delivery systems (DDS) that are currently undergoing preclinical and clinical development for a broad range of cancer types. The project rationale and objectives are also described.

1.1.1 Pancreatic Ductal Adenocarcinoma

PDAC is the 10th most commonly occurring cancer type, and is the 5th most common cause of cancer death in Australia with a 5 year survival rate of 9.8 % (Australian Institute of of Health and Welfare 2017). The aetiology of pancreatic adenocarcinoma is not well understood, however many environmental and genetic risk factors have been identified. Smoking is the most well established environmental risk factor, with a 2-fold increase in development of the disease, as well as heavy alcohol consumption and chronic pancreatitis also increasing risk. There is a 50 % greater risk of developing PDAC when individuals are recently diagnosed with type II diabetes (≤ 4 years), compared to patients who have had diabetes >5 years (Huxley *et al.,* 2005). More recently however, type II diabetes has been shown to be a risk factor, a manifestation and a prognostic factor for PDAC (De Souza *et al.,* 2016). Genetic factors such as family history of PDAC increase in chance of developing PDAC by 10-fold (Lowenfels and Maisonneuve 2006, Hassan *et al.,* 2007). BRCA1 and BRCA2 are the most common causes of familial PDAC. The lifetime risk of developing BRCA2-associated PDAC is estimated to be 5-10 %. BRCA1 mutations are estimated to lead to a 2-4 times increased risk of developing PDAC (Greer and Whitcomb 2007, Kowalewski *et al.,* 2018).

1.1.2 Symptoms

Seventy percent of pancreas tumours occur in the head of pancreas (Fig 1.2). However, depending on the location of the tumour, there are only few non-specific, early stage symptoms (Artinyan *et al.,* 2008). These include abdominal discomfort, nausea, or back pain, and approximately 50 % of patients will present with jaundice as tumours that develop in the head of the pancreas can cause biliary obstruction. Considering the average age of disease onset is 71 years old, these symptoms often go ignored until the cancer has progressed in to later stages (Oberstein and Olive 2013). Due to the deep location of the pancreas, tumours cannot be seen or felt by health care providers during routine health checks which also contributes to its late detection.

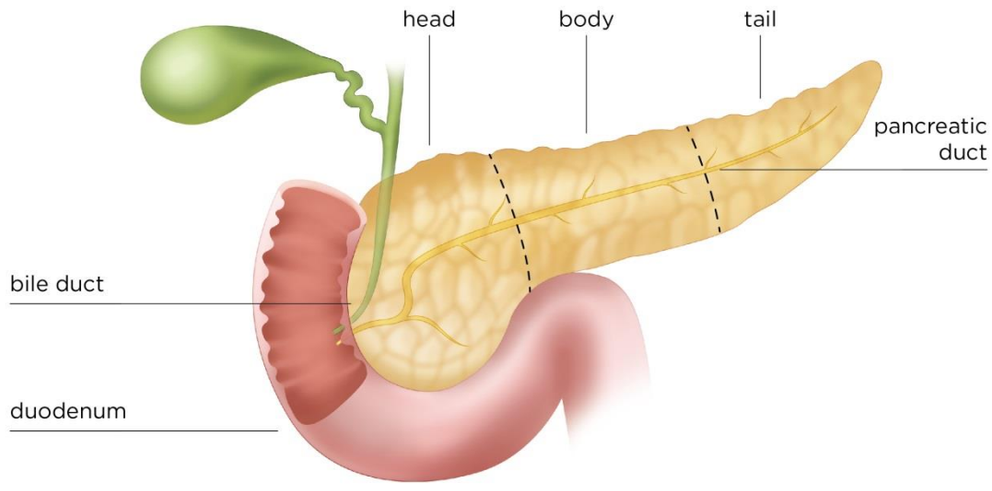

Figure 1.2: Schematic showing the anatomy of a pancreas. Taken from Hirshberg Foundation for Pancreatic Cancer Research

1.1.3 Early Detection

Advances in early screening tests for a number of cancer types (i.e. breast, colon, prostate) have seen dramatic decreases in mortality; however PDAC survival has remained largely unaffected by advances in science and technology. This is largely due to the typical late stage diagnosis and poor prognosis (Hassan *et al.,* 2007). Patients who are deemed high risk and who have had three blood relatives develop PDAC (with one being a first degree relative) are eligible for early screening options (Canto *et al.,* 2013). Screening methods such as magnetic resonance imaging (MRI) and helical computed tomography (CT) scans are highly utilised imaging options; however endoscopic ultrasound (EUS) fine needle aspiration (FNA) is the most superior of all early detection methods, with the highest sensitivity, specificity and accuracy (Hassan *et al.*, 2007, Kim and Ahuja 2015). EUS-FNA also has the added benefit of being able to take a histological sample for further diagnostic testing (Zhang *et al.*, 2018). All of these methods are time consuming, costly, and potentially invasive, so are not suitable for population screening and only those deemed to be at highest risk can access these tests, but as 90 % of PDAC cases are sporadic (non-hereditary), this results in majority of patients presenting with advanced disease (Chari *et al.*, 2015). A growing field in early cancer detection is the detection of specific cancer biomarkers in patients before they present with clinical

symptoms. A cancer biomarker is a "biological molecule found in blood, body fluids or tissue that is a sign of an abnormal process, or a condition or disease"[†]. Biomarkers such as carcinoembryonic antigen (CEA) and cancer antigen (CA) have been clinically used to monitor disease response in gastrointestinal cancers, with CA 19-9 identified for PDAC detection, however there are limitations of this biomarker (Acharya *et al.*, 2017). 10 % of the population do not secrete this specific antigen and it has a sensitivity and specificity of 81 % and 90 % respectively, which results in a large number of false positives and limits its practical applicability (Singh *et al.*, 2011, Swords *et al.*, 2016). The American Society for Clinical Oncology does not recommend CA 19-9 to be used for screening for pancreatic cancer, or for evidence of operability or recurrence. Monitoring response to therapy is not recommended on its own, however levels of CA 19-9 can be assessed at the start of treatment for locally advanced metastatic PDAC, and every 1-3 months throughout treatment, though any elevations of this biomarker indicating disease progression must be confirmed using other methods (Locker *et al.*, 2006).

[†] National Cancer Institute: Dictionary of Cancer Terms
https://www.cancer.gov/publications/dictionaries/cancer-terms/def/biomarker

1.2 Current Treatment Options

Following diagnosis, treatment for PDAC may include surgery, chemotherapy, radiotherapy or a combination of these therapies. Currently, the only treatment that has curative potential is surgery followed by adjuvant chemotherapy to kill residual cells and prevent metastasis (Conroy *et al.*, 2011). This has been proven to have the greatest increase in overall survival (OS) when compared to patients who had tumours that were deemed unresectable. Only around 20 % of patients are found to have resectable tumours however, leaving 80 % of patients to utilise the few therapeutics available. The advanced nature of the disease results in tumours that have involved critical blood vessels and surrounding organs such as the liver (Reynolds and Folloder 2014, Vincente *et al.*, 2014). The biggest challenge with systemically treating advanced PDAC is that the success of using whole body chemotherapy or radiotherapy treatment depends on the level a patient can attain before systemic dose limiting toxicity halts treatment. Many therapeutics have the ability to be effective, but at a concentration that is often too high for a patient to tolerate, which results in cessation of treatment which can lead to local recurrence and relapse. Treatments for PDAC (radio- and/or chemotherapy) can be administered in different settings dependant on the stage of the tumour. The definition of pancreatic tumour resectability as per the National Comprehensive Cancer Network (NCCN) and European Society of Medical Oncology (ESMO)[‡] are as follows; Tumours that are considered resectable have no contact with any arteries (superior mesenteric artery (SMA), common hepatic artery (CHA), coeliac axis (CA)) or veins (superior mesenteric vein (SMV), portal vein (PV)). Tumours are considered borderline resectable when there is <180° of solid tumour contact with SMA, or solid tumour contact to CHA without extension to the CA, or <180° contact with SMV or PV but with suitable vessels proximal or distal to the site to allow for safe resection and vein reconstruction. Tumours are considered unresectable when there is distant metastases, and when there is >180° of solid tumour contact with SMA, CHA or CA, or when the SMV/PV is un-reconstructible due to tumour involvement (Ducreux *et al.*, 2015).

Adjuvant therapy is the administration of treatment after the tumour resection, in order to kill residual cells that may

[‡] https://www.esmo.org/Guidelines/Gastrointestinal-Cancers/Cancer-of-the-Pancreas

cause tumour recurrence (Herreros-Villanueva *et al.*, 2012). Neoadjuvant therapy is the administration of treatment before surgery, and is administered to patients with borderline or non-resectable tumours, in order to shrink tumours to a size that can be surgically removed (Herreros-Villanueva *et al.*, 2012).

There are a number of treatment regimens for each stage of PDAC, however the choice is dependent on the patient's personal preference, comorbidities, toxicity profile and performance status (a score that estimates a patient's ability to perform normal daily tasks without the help of others.) Up until 1997, 5-fluorouracil (5FU) was extensively used, however had a consistently low response rate. In 1997, gemcitabine was introduced and was approved as a first line therapy, often administered in combination with drugs such as 5FU, cisplatin, docetaxel and irinotecan; however none had a statistically significant increase in survival compared to gemcitabine alone (Lee and Park 2016). Two treatment regimens have been clinically shown to be superior to gemcitabine alone in PDAC. The FOLFIRINOX regimen includes the drugs leucovorin, 5FU, irinotecan and oxaliplatin. A phase II/III study in patients with metastatic PDAC showed median survival increased from 6.8 months (gemcitabine alone) to 11.1 months (FOLFIRINOX), however the increase of adverse events and systemic toxicity was significantly higher in the FOLFIRINOX treated group (Conroy *et al.*, 2011). This led to FOLFIRINOX being administered only to patients with a good performance status. The FOLFIRINOX regimen is also administered to patients with resected PDAC in an adjuvant setting. A phase III study of 493 patients primarily compared the disease free survival of patients administered FOLFIRINOX or gemcitabine, with overall survival and safety being secondary endpoints. The median disease free survival of patients administered FOLFIRINOX was 21.6 months compared to 12.8 months in the gemcitabine group, while the median overall survival was 54.4 months in the FOLFIRINOX group compared to 35.0 months in the gemcitabine group (Conroy *et al.*, 2018).

The second regimen involves gemcitabine and nanoparticle albumin bound paclitaxel (*nab*-paclitaxel) administered in combination. This regimen was shown to have less treatment related toxicity than FOLFIRINOX and was an acceptable alternative. A phase III study was performed, in which the safety and efficacy was assessed in patients with advanced metastatic PDAC, who were treated with gemcitabine and *nab*-paclitaxel in combination, or

gemcitabine alone (Burris *et al.*, 1997). A total of 861 patients were enrolled, with 431 assigned the combination, and 402 receiving gemcitabine monotherapy. Overall survival increased from 6.7 months to 8.5 months with the combination therapy, with a progression free survival increasing from 3.7 to 5.5 months, and an increase in time to treatment failure of 3.6 to 5.1 months (Von Hoff *et al.*, 2013). A combination of gemcitabine and *nab*-paclitaxel is now the first line treatment for patients with advanced PDAC.

1.2.1 Gemcitabine

Gemcitabine (2',2'-difluoro-2'-deoxycytidine) is a nucleoside analogue that has been used as a chemotherapeutic for over 20 years to treat a number of solid tumours such as breast, ovarian, lung and PDAC (Fig. 1.3 A). It is a prodrug which requires cellular uptake and intracellular phosphorylation, where it is converted to gemcitabine monophosphate, then to gemcitabine di- and triphosphate – the active drug metabolites (Mini *et al.,* 2006). Gemcitabine has a number of mechanisms of action against cancer cells. DNA synthesis is inhibited when gemcitabine triphosphate is incorporated into the replicating DNA strand, allowing only one more deoxynucleotide to be incorporated after, which prevents chain elongation (de Sousa Cavalcante and Monteiro 2014). This prevents DNA polymerase from continuing DNA synthesis and results cell cycle arrest in S phase (Cappella *et al.,* 2001). Gemcitabine also acts to induce apoptosis in cells by activating p38 mitogen-activated protein kinase (MAPK) to trigger apoptosis in response to stress in tumour cells, but not normal cells (Habiro *et al.,* 2004).

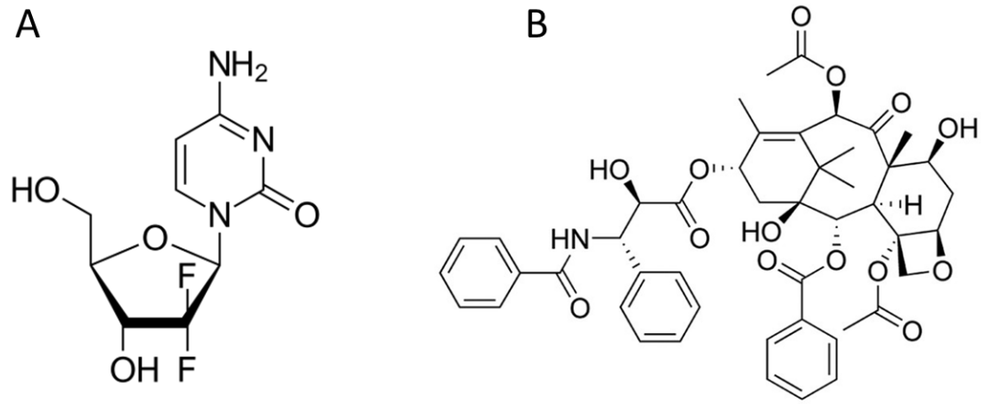

Figure 1.3: Structure of A: gemcitabine and B: paclitaxel

Upon treatment, PDAC cells initially show sensitivity to gemcitabine, however resistance rapidly occurs. Several genetic alterations have been associated with this resistance, including alterations in the nucleoside transporter-1, which is responsible for gemcitabine uptake into the cell and is involved with the phosphorylation events that convert the prodrug to its active metabolites (Kim and Gallick 2008). When gemcitabine was first introduced as a first line

therapy for PDAC, the one year survival rate increased from 2 % for patients on the gold standard 5FU regimen to 18 % (Burris *et al.*, 1997). This study significantly changed the way PDAC is treated, and the majority of clinical studies now use gemcitabine as a baseline for combinatorial treatment with an extensive list of chemotherapeutics drugs, as well as targeted therapies such as small molecule kinase inhibitors, nanoparticle albumin bound drugs, proteasome inhibitors and monoclonal antibodies (Tariman 2017).

1.2.2 Paclitaxel

Paclitaxel is a microtubule stabilizing drug that is used to treat ovarian, pancreatic, breast and lung cancer, and Kaposi's Sarcoma (Fig. 1.3 B). By promoting microtubule cytoskeleton stabilisation, polymerisation is inhibited and cells are arrested in the G2/M phase, resulting in apoptosis and inhibition of cell replication (Horwitz 1994, Kampan *et al.,* 2015). Paclitaxel has the ability to reduce the critical concentration of tubulin required to form a microtubule, and the resultant microtubules are resistant to depolymerisation by calcium and cold conditions, which destabilises normal microtubules. In order for microtubules to be involved in a variety of critical cell functions such as motility, maintenance of cell shape and mitosis, microtubules must be dynamic, and have the ability to switch between soluble tubulin and microtubule polymer, the function of which paclitaxel inhibits (Yang and Horwitz 2017).

Paclitaxel resistance also occurs in PDAC but the mechanisms are less well understood, and as PDAC cells are particularly susceptible to gemcitabine resistance, majority of published literature focuses on this (Gnanamony and Gondi 2017). One of the biggest problems with delivering paclitaxel is its hydrophobicity, which results in it being formulated with the micelle forming Cremaphor EL (CrEL) (polyoxyethylated castor oil). CrEL however, elicits acute hypersensitivity reactions (allergic reactions) characterised by chest pain, rash, shortness of breath, tachycardia and more, all of which can be life threatening (Gelderblom *et al.,* 2001). Premedication with high dose corticosteroids is the current treatment, and can reduce the incidence of hypersensitivity reactions from 30% down to 1-3% (Boulanger *et al.,* 2014). *Nab*-paclitaxel was developed to overcome the issues associated with CrEL administration, and is a water-soluble, CrEL free, albumin bound nanoparticle formulation of paclitaxel that is widely approved for use in many cancers, including PDAC (Reynolds *et al.*, 2009).

1.3 Biological Barriers to Effective Treatment

There is no one reason that makes PDAC hard to treat. In fact, a combination of an average elderly age at diagnosis, lack of early detection methods or early stage symptoms all pose significant problems. However the complex pathophysiology of PDAC compounds this issue. One of the hallmarks of PDAC is the fibrotic, stromal tissue that surrounds the tumour, otherwise known as desmoplasia. This desmoplasia creates a complex stromal microenvironment that is composed of extracellular matrix (ECM) components, activated fibroblast- and myofibroblast-like cells called pancreatic stellate cells (PSC), inflammatory cells, together with blood and lymph vessels, which provide a scaffold for the cancer cells to grow while providing growth factors and immune modulators (Pandol *et al.*, 2009, Neesse *et al.*, 2011). PSCs are the primary producer of ECM proteins (collagen, laminin, fibronectin, fibrin), as well as cytokines, chemokines and growth factors during progression of the disease (Fig. 1.4). PCS interact with PDAC cells and positively influence the progression of the disease (Vonlaufen *et al.*, 2008). Desmoplasia distorts the normal architecture of pancreatic tissue, inducing an abnormal configuration of blood and lymphatic vessels, which altogether results in a stiff matrix which compresses blood vessels, reducing tumour vascularity and impeding delivery of systemically administered chemotherapeutics.

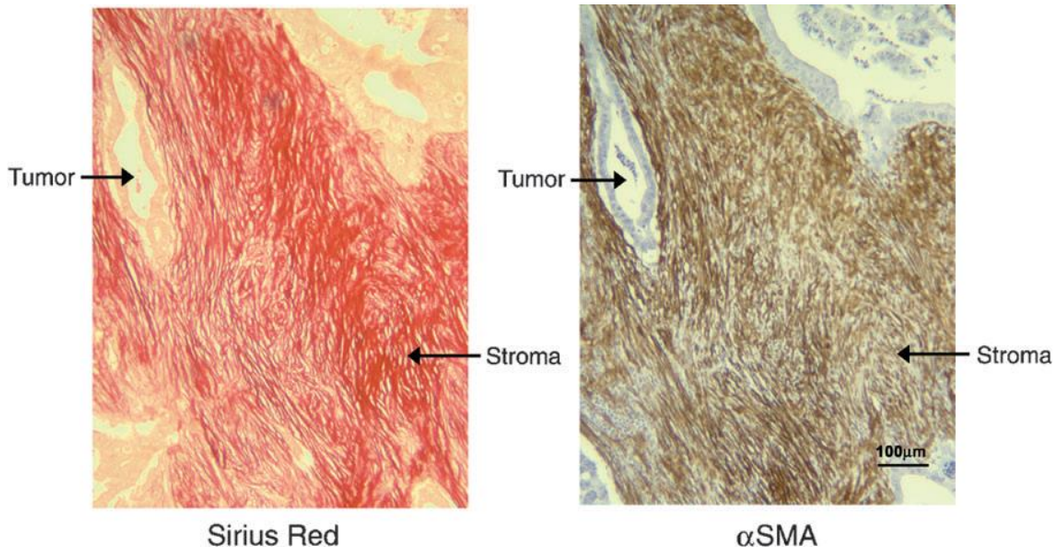

Figure 1.4: Co-localization of collagen and SMA staining in pancreatic cancer. A representative pair of serial paraffin sections of the pancreas from a patient with pancreatic cancer demonstrates that stromal areas (Sirius Red staining, left panel) exhibit strong positive staining for collagen as well as for alpha smooth muscle actin (αSMA staining, right panel), indicative of the presence of activated pancreatic stellate cells in the desmoplastic reaction in pancreatic cancer. Original magnification ×100. Taken from (Apte *et al.*, 2004)

Provenzano *et al.*, (2012) first showed that targeting the stromal fibroblasts using Pegvorhyaluronidase alfa (PEGPH20) breaks down intratumoural hyaluronic acid (HA) by disrupting the paracrine Hedgehog signalling in a preclinical orthotopic KPC PDAC mouse model. This led to an increase in tumour micro-vascularity, and systemic delivery of gemcitabine was therefore increased to the pancreatic tumour which resulted in an increase in overall survival to 91.5 days compared to 55.5 days in mice not treated with PEGPH20. The efficacy of PEGPH20 has now been assessed a phase II clinical trial in patients with previously untreated metastatic PDAC, in combination with the standard of care *nab*-paclitaxel and gemcitabine regimen. The combination of these treatments showed an overall survival increase from 8.5 months to 11.5 months, which is a clear demonstration of the inhibitory role that desmoplasia plays in drug perfusion (Hingorani *et al.*, 2018).

The stiff matrix further alters the cellular properties of PDAC cells by reducing polarity and disrupting tight junctions, and therefore increasing tumour proliferation, migration and invasion (Weniger *et al.*, 2018). As well as impeding drug perfusion, the stiff matrix also restricts oxygen and nutrient intake. As the proliferation of cancer cells require a source of nutrients, PDAC cells are able utilise micropinocytosis to acquire nutrients, and use the collagen rich tumour microenvironment as a source of energy (Weniger *et al.*, 2018). In addition to its unique microenvironment, PDAC is also characterized by having high interstitial fluid pressure due to its compressed and collapsed vasculature, which also acts as a barrier for drug perfusion (Provenzano *et al.*, 2012). The multiple biological barriers PDAC poses make it very difficult to treat systemically. While systemic treatment of this disease is the current gold standard, the abysmal survival rates of PDAC highlight the need for new therapies, or alternatively, new ways to deliver the current therapies.

1.4 Drug Delivery Systems

DDS are used to improve the pharmacological or therapeutic properties of chemotherapeutics that are traditionally administered systemically, but may have limitations with this route of delivery. DDS are beneficial for drugs that have poor solubility, high off target effects, unfavourable pharmacokinetics, low selectivity, poor biodistribution, and/or rapid breakdown *in vivo* (Allen and Cullis 2004). There are typically three types of plasma drug profiles – single dosing; in which the drug concentration in the blood plasma reaches a therapeutic level then drops rapidly, zero order sustained concentration; in which the level of drug remains in the therapeutic zone for an extended period of time, or oscillating concentration; which is achieved by multiple dosing (such as in the case of systemic chemotherapy), which can often go above the therapeutic zone into the systemic toxicity zone (Fig.1.5).

DDS in the form of nanoparticles dominate the drug delivery field, with the majority having applications in cancer therapy (De Jong and Borm 2008). Nanoparticle delivery systems are favoured for delivering many poorly soluble drugs, and are administered parenterally (Allen and Cullis 2004). Nanoparticles for cancer therapy are primarily designed to exploit the enhanced permeation and retention effect, in which the nanoparticles passively make their way to tumours relying on leaky vasculature. There are however many limitations to this type of DDS, with an average of only 0.7 % of the total injected dose of the nanoparticles reported to reach the tumour, and high rates of translational failure between animal and human experiments (Lammers *et al.*, 2016, Wilhelm *et al.*, 2016).

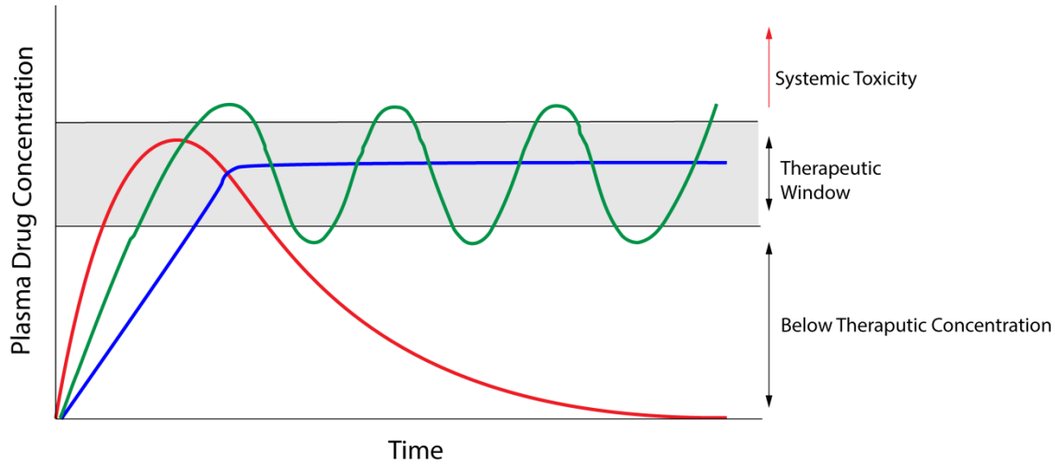

Figure 1.5: Plasma drug concentrations obtained by single dosing (red line), multiple dosing (green line) or zero order controlled release (blue line). Figure adapted from (Pekkari 2015).

Implantable DDS have emerged as an alternative to nanoparticles, and are designed to be specifically placed at the site of tumour growth or resection. The National Institute of Health (NIH) defines the term DDS as "engineered technologies for the targeted delivery and/or controlled release of therapeutic agents"[§]. They do not rely on the circulatory system for biodistribution, therefore avoiding unwanted biodistribution in any of the major clearance or off target organs. These can be fabricated in a number of forms, such as *in situ* forming structures, including; thermo- or pH sensitive gels, or solvent exchange gels, or as preformed structures, including; discs, wafers, fibres, rods, seeds, films or stents. This chapter will focus on preformed structures. These structures can be made from a very wide range of materials and in a number of different structural forms, which is dependent on the requirement and end goal of the implant.

While traditional chemotherapy delivers the drugs throughout the entire body (Fig. 1.6 A), DDS that are designed to be used in the neoadjuvant setting can be manufactured into a structure intended to cover the external surface of the tumour (Fig. 1.6 B) or to be implanted intratumorally (Fig. 1.6 C). In this way, the treatment becomes localised

[§] https://www.nibib.nih.gov/science-education/science-topics/drug-delivery-systems

to the tumour site with the goal of shrinking the tumour and enabling the patient to be eligible for surgical resection. DDS in the adjuvant setting are designed to be placed at the site of tumour resection to kill any residual cancer cells and prevent tumour recurrence (Fig. 1.6 D). Each structure has advantages and disadvantages that will be further discussed in Section 1.6.

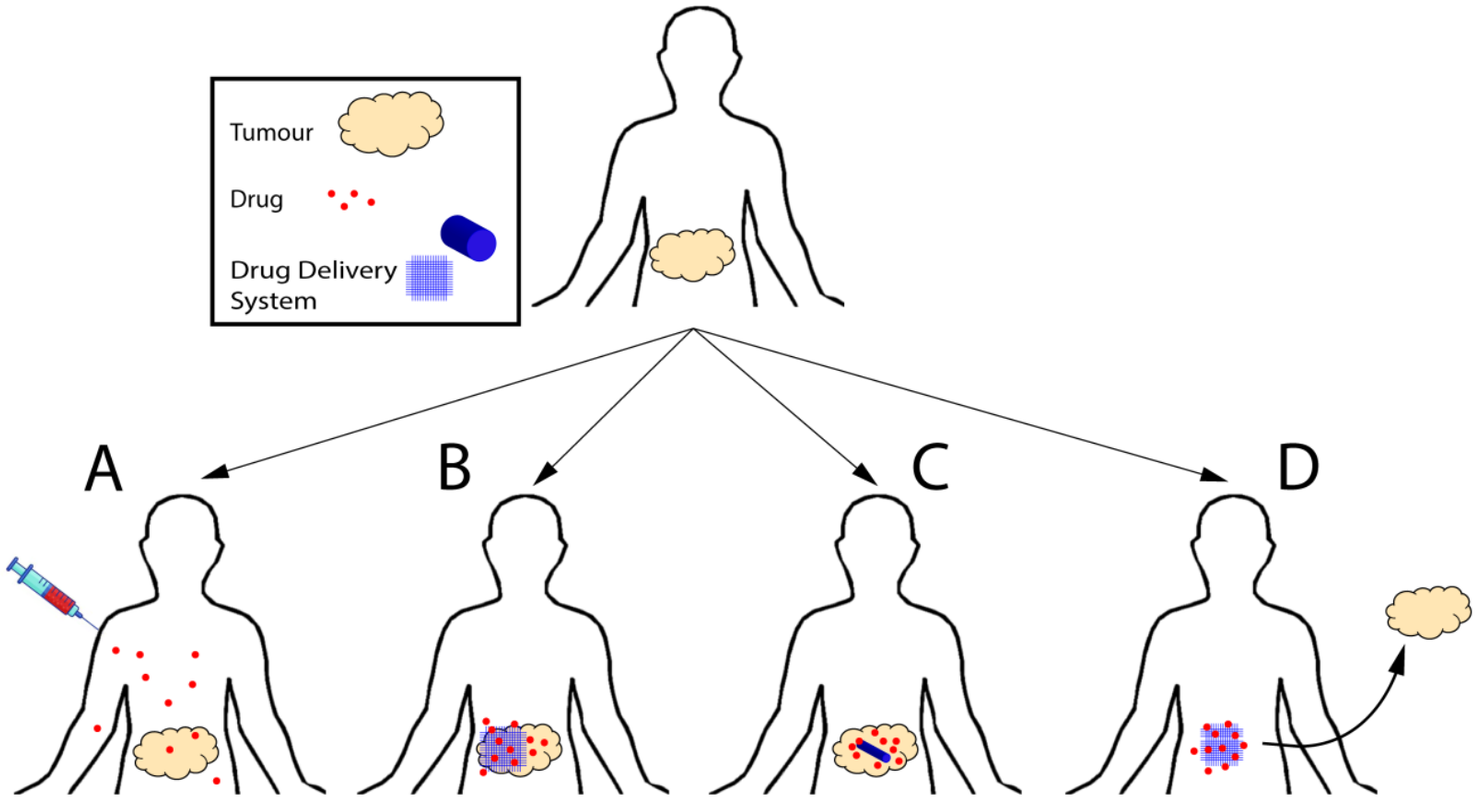

Figure 1.6: Modes of drug delivery. A) systemic drug administration, B) local drug delivery via placement of the DDS on the surface of a tumour, C) local drug delivery via placement of the DDS intratumorally, D) local drug delivery via placement of the DDS at the site of tumour resection therapy. Adapted from (Exner and Saidel 2008).

1.5 Polymers for Drug Delivery Systems

In order for a material to be suitable for forming a DDS, it must be biocompatible, biodegradable and have low immunogenicity. The type of material chosen will be heavily dependent on its properties, with each having its own limitations and special considerations. What type of drug, how much drug can be loaded, and the desired release profile are just some of the factors that need consideration before fabrication. The most common materials, both natural and synthetic, used in implantable DDS are summarised in Table 1.1. The polymers alginate, chitosan and poly-ε-caprolactone (PCL) are primarily used in the experimental chapters of this thesis, so there will be a particular focus on their properties. These polymers were selected based on their hydrophilic and hydrophobic properties, for example hydrophilic drugs (gemcitabine) can be loaded into the hydrogels alginate and chitosan, while the hydrophobic drug paclitaxel can be loaded into the hydrophobic PCL. These polymers are all already FDA approved for a number of applications, and this is envisioned to aid in the rapid clinical translation of the drug loaded implants.

Table 1.1: Polymers used in drug delivery systems and their properties

Polymer	Abbreviation	Natural/ synthetic	FDA Approval	Reference
Polyanhydride poly-[bis(p-carboxyphenoxy)propane-sebacic acid] copolymer	CPP/SA	Synthetic	Implantable DDS for delivery of carmustine to malignant glioma	(Westphal *et al.*, 2003, McGirt *et al.*, 2009, Mu *et al.*, 2015)
poly(lactic-co-glycolic acid)	PLGA	Synthetic	Injectable microsphere DDS	(Wang *et al.*, 2016)
Poly(lactic acid)/poly-lactide	PLA, PLLA	Synthetic	Injectable microsphere DDS	(Wang *et al.*, 2016)
Polyethylene glycol	PEG	Synthetic	Oral administration, drug conjugation	(Food and Drug Administration 2006)
Polyurathane	PU	Synthetic	Contraceptive device	(Kafka and Gold 1983)
Poly-ε-caprolactone	PCL	Synthetic	Suture, implant: bone healing, nerve conduit, hormonal contraceptive	(Arslantunali *et al.*, 2014, Dorati *et al.*, 2017, Manoukian *et al.*, 2018)
Pullulan	Pullulan	Natural	Dietary supplement	(Rekha and Sharma 2007)
Alginate	Alginate	Natural	Dietary supplement	(Food and Drug Administration 2019)
Chitosan	Chitosan	Natural	Dietary supplement, wound dressing	(Wedmore *et al.*, 2006)

1.5.1 Alginate

Alginate is a linear copolymer containing blocks of β(1-4) linked D-mannuronate (M) and α-L-gluronate (G) residues (Fig. 1.7) (Lee and Mooney 2012). Alginate is derived from brown seaweed by solubilising the alginic acid in seaweed by treating with an alkaline solution. The alginic acid can then be converted to sodium alginate, the form that is most currently used in drug delivery (Tønnesen and Karlsen 2002). Alginate is biocompatible, inexpensive and widely available in the food and medical grade form (Jain and Bar-Shalom 2014). It has the ability to form both reversible (can alternate between solid and liquid phases) and non-reversible hydrogels (once solidified cannot return to a solution) (Zhang 2007). Hydrated alginate in the presence of multivalent cations and gentle conditions (room temperature, neutral pH) can form reversible gels, while irreversible gels are formed when hydrated alginate is in the presence of polyvalent cations, with calcium being the main crosslinker of choice (Tønnesen and Karlsen 2002, Sachan *et al.,* 2009). Although other cations such as zinc have been used to produce alginate gels, calcium is primarily used due to its safety, accessibility and economic benefits (Jain and Bar-Shalom 2014).

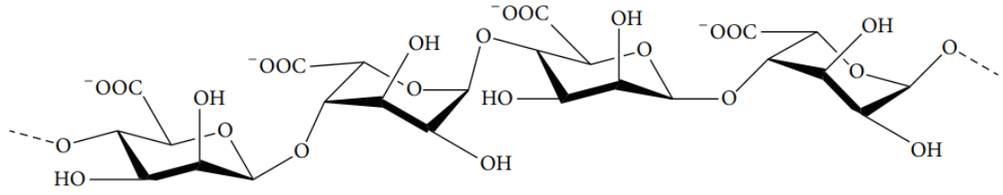

Figure 1.7: Structure of alginate. Taken from (Ahmadi *et al.,* 2015)

1.5.2 Chitosan

Chitosan is an cationic, linear, copolymer polysaccharide made up of random β(1-4) linked D-glucosamine and N-acetyl-D-glucosamine units (Fig. 1.8) and is the second most abundant naturally occurring polymer after cellulose. Chitosan is derived from chitin, a polysaccharide found in crustacean shells (Saikia *et al.*, 2015). Chitosan has a positive charge and mucoadhesive properties which allows it to adhere to soft tissue and makes it desirable as a drug delivery platform (Shaikh *et al.*, 2011). It is biocompatible and non-immunogenic, and breaks down in the body into non-toxic amino sugars, which can be easily cleared by the body without any side effects (Agnihotri *et al.*, 2004).

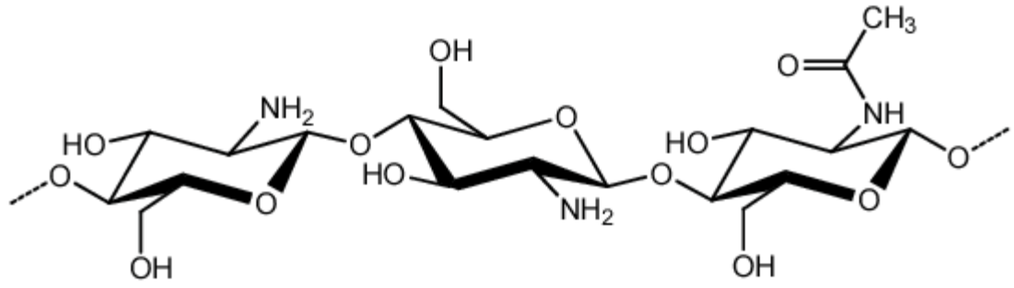

Figure 1.8: Chemical structure of chitosan. Taken from (Alvarenga 2012)

1.5.3 Poly-ε-caprolactone

PCL is a synthetic, hydrophobic polymer, synthesised by a ring opening polymerisation of ε-caprolactone (Fig. 1.9) (Mondal *et al.*, 2016). Unlike alginate and chitosan, PCL is not degraded by human enzymes, but by surface erosion, where the polymer backbone has ester linkages that can be hydrolysed and cleaved at the surface of the polymer. This happens when the rate of hydrolytic polymer breakdown is faster than the rate of water infiltration into the polymer bulk, which causes thinning of the polymer over time (Lam *et al.*, 2009). This rate of degradation however is dependent on its molecular weight (Mw), as higher Mw products degrade at a slower rate. PCL therefore has a longer degradation rate than chitosan and alginate (years rather than months) and therefore loaded drugs typically have a slower release profile (Kamaly *et al.*, 2016).

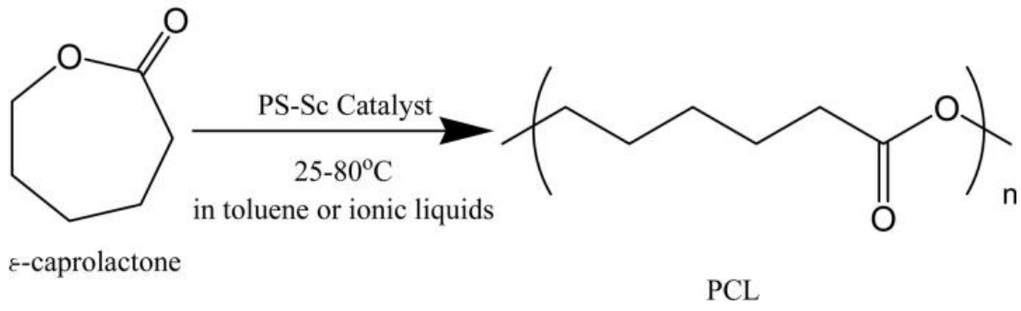

Figure 1.9: Ring opening polymerisation of PCL. Taken from (Oshimura *et al.*, 2009)

1.6 Chemotherapy Drug Delivery Systems for Cancer Treatment

The structure and function of DDSs are very broad and can be grouped into a number of categories. Some of these categories include; external pumps (pain management) (Yang *et al.,* 1996), topical delivery (local infection/pain control) (Hua 2014), transdermal delivery (microneedle array – vaccine delivery) (Kim *et al.,* 2012), intravenous (i.v.) nanoparticle delivery (liposomes/micelles), and macroscale polymer based delivery, to name a few. This section will focus on implantable, polymeric DDS for the delivery of chemotherapeutics and other anti-cancer agents for treatment of a number of cancer types, with a focus on PDAC where applicable. There are limited publications describing implantable, polymeric DDS for PDAC (including chemotherapy and non-chemotherapy DDS), and all have only been published within the last 5 years and are summarised in Table 1.2. Only publications with clinical or preclinical biological efficacy will be discussed. The review will also discuss the final 3D structure of the DDS and will include wafers, rods, films and fibres, which captures the majority of preformed implantable DDS for cancer therapy (Fig. 1.10).

Table 1.2: Drug Delivery Systems for Pancreatic Ductal Adenocarcinoma Treatment

Polymer	Therapeutic Approach	Type of Implant	Application	Stage	Model Details	Ref
PLGA	Chemotherapy (Ostelmativir)	Cylinder	Surgical implantation adjacent to tumour	Preclinical animal	RAGxCγ mice. PANC-1 subcutaneous xenograft	(Hrynyk *et al.*, 2015)
PLGA	Chemotherapy (Paclitaxel)	Polymer coated steel disk	Surgical implantation on tumour surface	Preclinical animal	NOD scid gamma. Patient derived orthotopic xenograft	(Indolfi *et al.*, 2016)
PLGA	Chemotherapy (Gemcitabine + osteltmativir)	Cylinder	-	Preclinical *in vitro*	PANC-1 2D cell culture	(Allison Logan *et al.*, 2017)
PLA/ hyularonin	Chemotherapy (Gemcitabine)	Electrospun fibre patch	Surgical implantation on tumour surface	Preclinical animal	BALB/c nude mice. PANC-1 subcutaneous xenograft	(Xia *et al.*, 2018)
PLGA+PCL	Chemotherapy (5FU)	3D printed patch	Surgical implantation on tumour surface	Preclinical animal	BALB/c nude mice. Mia-PaCa-2 subcutaneous xenograft	(Yi *et al.*, 2016)
Novel terpolypeptide	Chemotherapy (Gemcitabine)	pH responsive injectable hydrogel	Subcutaneously injected near tumour surface	Preclinical animal	NOD.CB17-Prkdc^{scid}/J mice. AsPC-1 subcutaneous xenograft	(Bilalis *et al.*, 2018)
PLGA	siRNA (siG12D)	Casted cylinder	EUS-FNI intratumoural implantation	Clinical human	Phase 1/2a	(Golan *et al.*, 2015)
Alginate	CAR T cells + STING agonist	15 mm x 2 mm disk	Surgical implantation on tumour surface	Preclinical animal	Albino B6 mice. KPC orthotopic transgenic model	(Smith *et al.*, 2017)

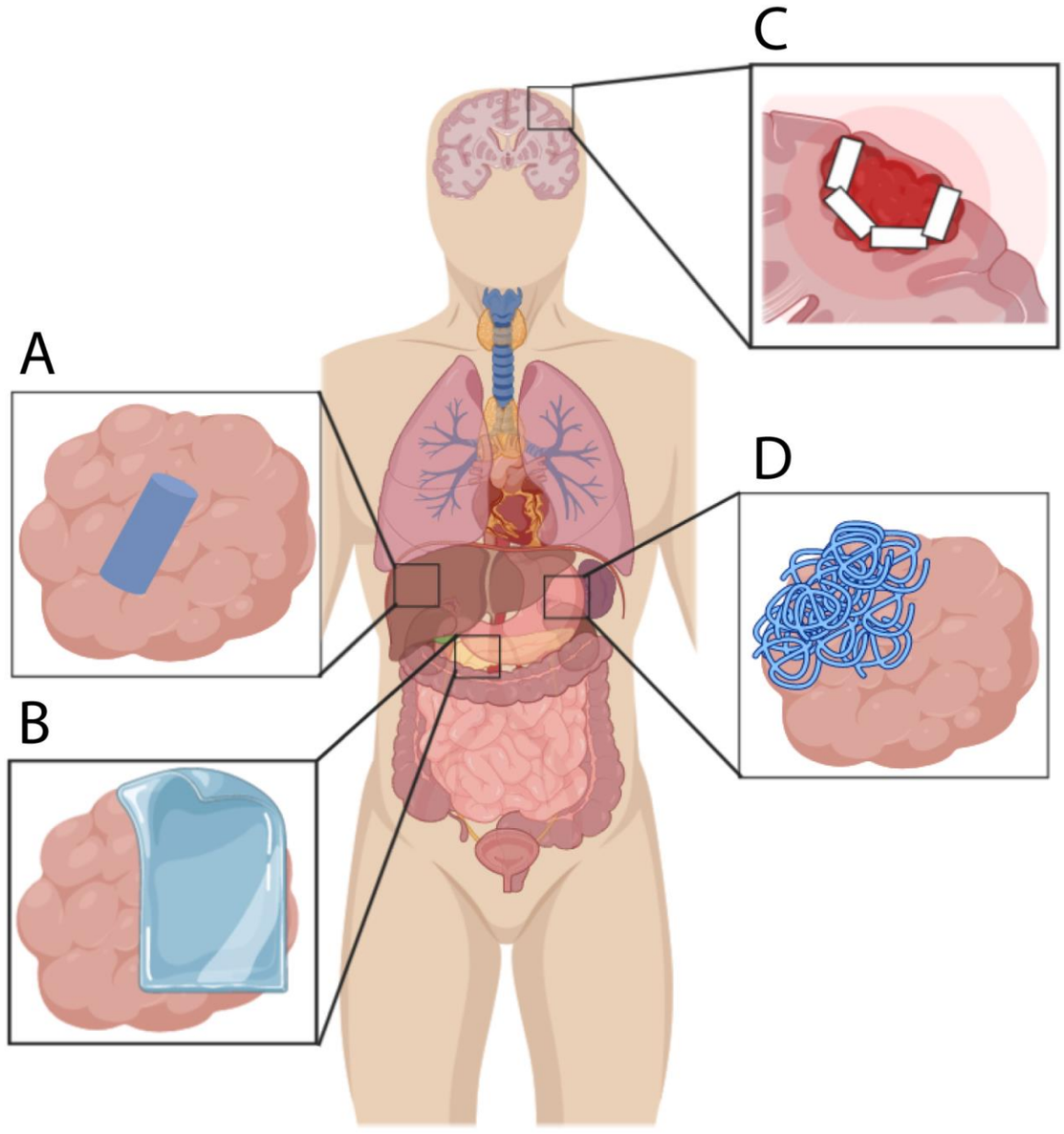

Figure 1.10: Examples of structure and form of localised chemotherapy drug delivery systems A) intratumorally implanted cylinders/rods, B) films placed on outside of tumour, C) wafers placed at site of resection, D) fibre mat placed on outside of tumour.

1.6.1 Wafers

Discs and wafers are non-woven structures that consist of layers of spray dried, compression moulded or electrospun biodegradable polymers that can be loaded with a number of anticancer drugs. While not used for PDAC treatment, wafers have gained the most recognition due to their commercialisation for the treatment of malignant glioma (brain cancer) (Ng and Jumaat 2014). Carmustine (CM) wafers (Gliadel®) are currently the only FDA approved implantable, degradable drug eluting polymeric structure for cancer therapy on the market.

Over 75 % of newly diagnosed primary brain tumours are malignant gliomas (Ray *et al.*, 2014). The current standard of care consists of surgical resection of the tumour followed by radiotherapy, while simultaneously treating with CM and temozolomide. Generally, treatment guidelines for newly diagnosed glioblastoma recommend maximal surgical resection, with or without Gliadel implantation (Fig. 1.11), followed by adjuvant radiotherapy and temozolomide. Gliadel wafers are formed by spray drying Polyanhydride poly-[bis(p-carboxyphenoxy)propane-sebacic acid] copolymer (pCPP/SA) microspheres with CM-polymer solution. The final formulation contains 3.85 % CM which is homogenously distributed within the pCPP/SA matrix (Nasongkla 2009). The first phase III study of Gliadel used on newly diagnosed malignant gliomas involved 32 patients in a randomised double blind trial of an active treatment group vs a placebo group. Survival was measured as time from surgery to death, with the Gliadel group having a median survival of 58.1 weeks vs 39.9 weeks for the placebo wafer group (Valtonen *et al.*, 1997). A larger phase III trial was subsequently performed; enrolling 248 randomized patients to receive either the Gliadel or placebo control. The survival for the patients receiving the Gliadel was 13.9 months vs 11.6 months for the placebo wafer group (Westphal *et al.*, 2003). Phase III trials were also conducted on patients with recurrent malignant glioma, with 222 enrolled patients in a randomized trial. The median survival for the patients receiving the Gliadel was 31 weeks compared to 23 weeks for the patients that received the placebo wafer control (Brem *et al.*, 1995). It was from these studies that FDA approval was granted for the use of Gliadel for the treatment of malignant glioma.

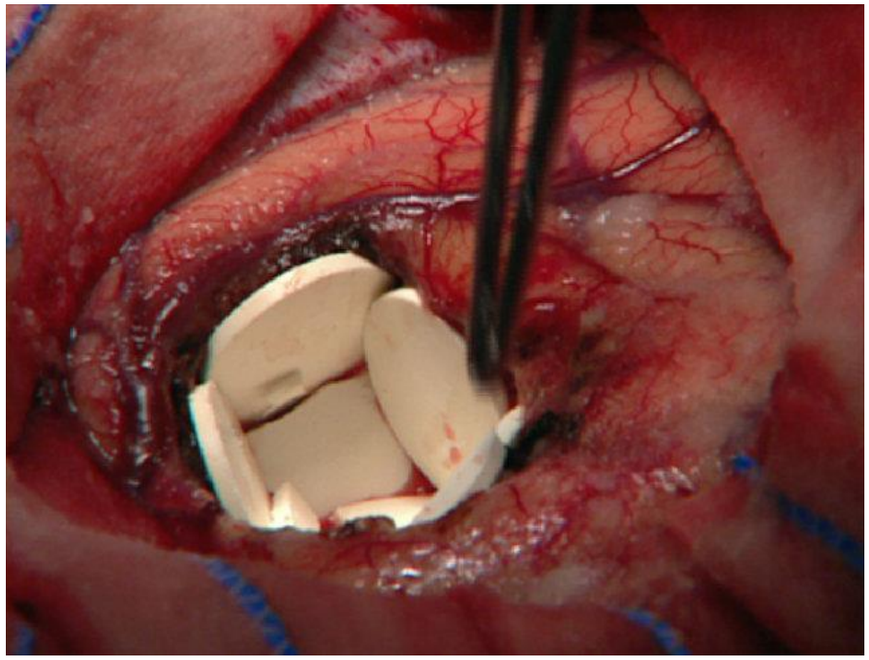

Figure 1.11: Gliadel placement at the site of tumour resection. Figure taken from (Kleinberg 2016).

A meta-analysis performed on the survival outcomes and safety of Gliadel wafers was performed on 62 publications, which reported data for 60 studies (Chowdhary *et al.*, 2015). The validity of many of these studies has been called into question. For example, randomised trials have only been conducted on patients that had accessible and completely resectable tumours, better performance status and therefore a better overall prognosis than patients who are not eligible for wafer implantation. Another issue with Gliadel implantation is that the wafers come with an exclusion criterion, in which patients are excluded from participating into further clinical trials, as the potential toxicity and possibility of adverse events of these new therapies with the wafers is unknown. Patients are also excluded from these trials as the issue of confounding results as the presence of the wafers may alter the reliability of imaging of the resection site (d'Avella and DellaPuppa 2012, Chowdhary *et al.*, 2015). The poor compliance and minimal survival benefits of the only FDA approved biodegradable polymeric implant for cancer therapy highlights the importance of further research and development of chemotherapy loaded DDS.

1.6.2 Rods

Rigid, rod shaped DDS are beneficial when intratumoural insertion is required, as the mechanical strength allows for higher pressure insertion techniques. There are currently no rods being developed for PDAC treatment. Millirods are small cylindrical rod shaped polymeric implants that are fabricated via compression moulding. Weinburg *et al.*, developed doxorubicin loaded PLGA millirods (1.6 mm height by 8.0 mm length) by the compression moulding technique (Weinberg *et al.,* 2007). The compression moulding involved mixing PLGA microspheres and a doxorubicin/NaCl powder together, and compressed in a Teflon tube, giving a final composition of 65 % PLGA, 21.5 % NaCl and 13.5 % doxorubicin. VX2 liver carcinomas were established in rabbits (adult New Zealand whites) and treatment commenced when the tumours reached a diameter of 8 mm (approx. 12 days). Radiofrequency (RF) ablation is a process by which heat is used to kill cancer cells, and is commonly performed in unresectable liver cancers. After RF was performed on the animals, a millirod with or without doxorubicin was inserted with the aim to kill residual cancer cells and prevent recurrence. At the conclusion of the study (4 or 8 days), it was found that the doxorubicin penetrated 3.7 mm and 80 % of the ablation zone, and had a concentration 10 × higher than the therapeutic dose, which then dropped to 40 % by day 8. Beyond the ablation boundary however, where the doxorubicin had not penetrated, tumour recurrence had begun to occur and the presence of viable tumour cells were detected. After 8 days of treatment, the treated tumours were on average 10 times smaller than the controls (non-drug loaded implants). This treatment was not compared to any systemically administered doxorubicin however, which questions the clinical significance of the study.

Another group designed and developed two-phase eluting millirods, in which the millirod displays an immediate burst and followed by sustained release (Qian *et al.,* 2002). An initial burst release immediately delivers the drug to the tumour, which is theorised might prevent tumour progression while the sustained release would ensure the level of drug remains high in the tumour – a release profile that is desirable for implantable DDS. Two phase release millirods were formed by dip coating a doxorubicin loaded PLGA millirod into a polyethylene glycol (PEG)/ polylactic acid (PLA) solution, then further dip coated with a doxorubicin/PEG suspension to form an even layer.

The drug release profile showed that *in vivo*, the dual-drug loaded millirods display a high burst of doxorubicin from the outer doxorubicin PEG layer, in order to get the drug level to a therapeutic concentration. The intermediate layer restrained the drug diffusion from the inner core, giving a sustained release over 8 days, at which time nearly all of the drug was released. The levels of drug remained at a similarly high level throughout the ablated liver region between 1 and 8 days when the millirods were inserted *in vivo*, demonstrating the effectiveness of the initial burst followed by sustained release and warrants further investigation.

1.6.3 Films

While rigid implants have a multitude of benefits, they are at a disadvantage when the site that a DDS is required is irregularly shaped – whether it is the site of tumour resection or the external surface of a tumour. This is where flexible film composites are advantageous – they are able to mould tightly around the area providing an even drug delivery distribution. Flexible drug eluting films have been explored as alternatives to the rigid Gliadel wafers (section 1.6.1), as coverings for non resectable tumours and as stent coverings.

One of the first implantable DDS for PDAC was developed by Indolfi *et al.*, who reported on the fabrication of a PLGA-based platform for local delivery of paclitaxel to non-resectable PDAC (Indolfi *et al.*, 2016). A paclitaxel loaded PLGA solution was cast onto a stainless steel disc, which was then sutured onto the tumour surface in a patient-derived xenograft mouse model of PDAC. Matrices of different thicknesses containing either 200 or 400 µg of paclitaxel were assessed, and results showed that the 400 µg loaded implant had up to 12 fold reduction in tumour volume, increased overall survival of mice, and reduced off target effects of paclitaxel in comparison to the group that received intravenous (i.v.) paclitaxel.

Paclitaxel loaded Poly(glycerol monostearate co-ε-caprolactone) polymer films were designed to prevent local recurrence after non-small cell lung cancer resection in mice bearing LLC1 mouse Lewis lung cell carcinomas (Liu *et al.*, 2010). The paclitaxel films were placed at the site of complete tumour resection, and tumour recurrence

was compared in animals treated with an empty film or systemic or intratumoural paclitaxel at the same concentration. Animals that received empty films, intraperitoneal (IP) or i.v. paclitaxel had recurrence rates over 80 %, while no animals in the paclitaxel film treated group experienced recurrence. This DDS, while not specifically assessed in PC, holds potential to be an effective way to prevent tumour recurrence in PDAC due to the paclitaxel loading.

The major advantage of films is their flexible nature for irregular surfaces. This however, often requires specific placement through surgical implantation. This makes them most useful at the time of tumour resection however it also restricts their use to patients with a high performance status. Due to the advanced nature of PDAC upon diagnosis, major abdominal surgery may not be possible and patients with non-resectable disease may be excluded from the benefits chemotherapeutic films. In addition to implantation of films over the site of the primary tumour and/or at the tumour resection site, they have also been developed for use as stent coverings, for local treatment of malignant tumours (for example gastrointestinal stents). Paclitaxel loaded polyurethane (PU) films have been developed for this purpose, as stents are often placed in vessels when tumours cause obstruction in areas such as colon, oesophageal and biliary. These malignancies however can further invade the stent, thereby causing re-obstruction. Paclitaxel films have been used to coat stents used in coronary artery obstruction, which has been shown to prevent cell proliferation and neointimal hyperplasia, which bought attention to their use in cancer therapy (Waugh and Wagstaff 2004).

1.6.4 Fibres

The morphology of fibres is of great importance for drug delivery applications, as their cylindrical shape, high surface area to volume ratio and tunable dimensions allows drug to be released in a controlled manner. Fibres can be fabricated in a number of different ways, which means they can be used to deliver drugs to a wide number of diseases. Two of the most common methods for fabricating fibres include electrospinning and wet spinning, which produce fibres in different configurations and for different applications.

1.6.4.1 Electrospun Fibres

Nanostructured polymeric fibres can be fabricated through electrospinning process using an electrical field to produce polymeric fibres with nanoscale diameters (Bhardwaj and Kundu 2010). This process involves charged polymer being ejected from a capillary spinneret, where the solvent evaporates as this jet moves through the air, leaving a charged fibre that can be collected on a grounded collector (often a metal screen or rotating drum) (Fig. 1.12) (Doshi and Reneker 1995). These consistently uniform fibres form a patch with a variety of applications. Some of the benefits of electrospun patches are the tuneable porosity - which is the ability to increase/decrease pore size to modulate drug release, the range of polymers and drugs that can be used, a high surface area and high malleability. For this reason, they have been explored in the field of drug delivery for a number of different conditions; they can be used as patches for implantation at the site of tumour resection (Ding *et al.*, 2016) or over an inoperable tumour (Jun *et al.*, 2017) or as a stent covering (Janjic *et al.*, 2017, Khashi *et al.*, 2018, Kuznetsov *et al.*, 2018). There is an abundance of literature on the use of electrospinning for the fabrication of drug eluting patches for cancer therapy; however, this section will only describe patches developed for PDAC therapy. Studies that did not report preclinical biological efficacy data have been excluded.

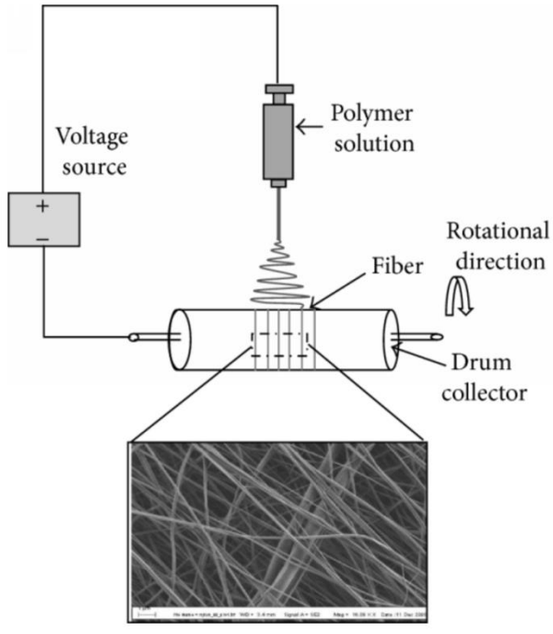

Figure 1.12: Schematic of electrospinning set up. Charged polymer solution is ejected from a syringe and collected on a grounded, rotating metal drum to form sheets of non-woven fibres. Taken from (Junoh *et al.*, 2015).

One study described the development of an electrospun scaffold made from polyglycolic acid-trimethylene carbonate (PGA-TMC) and gelatine and loaded with FOLFIRINOX for the post-surgical treatment of PDAC (Zhan *et al.*, 2013). In this study, pieces of resected PDAC tumours from patients were implanted into a mouse pancreas, along with a FOLFIRINOX loaded patch, or non-drug loaded patch. Mice with non-drug loaded patches were systemically administered either phosphate buffered saline (PBS) or FOLFIRINOX and all animals were treated for 3 weeks. The animals treated with the FOLFIRINOX patch had a 3.1 fold decrease in tumour volume at the end of the 21 day experiment compared to those treated with systemic FOLFIRINOX or PBS, respectively. Mice that received the FOLFIRINOX patch showed no metastasis, however the mice treated with systemic FOLFIRINOX showed minor hepatic metastasis, while the PBS treated mice had significant hepatic metastasis.

1.6.4.2 Wet Spun Fibres

Wet spinning is the oldest and simplest method to create monofilament or multiaxial fibres (see Section 1.6.4.3 for description of multiaxial fibres). It is a simple and scalable way to produce fibres using solvent based coagulation, in which the polymer is ejected from a spinneret and passed through a coagulation bath where it is crosslinked and solidified, before being washed and dried (Fig. 1.13) (Bao *et al.,* 2019, Rinoldi *et al.,* 2019). This method has benefits over electrospinning, such as low cost and gentle fabrication conditions that allow for the production of fibres containing sensitive biological material (Rinoldi *et al.,* 2019). This method produces fibres with a larger diameter compared to the electrospinning method, and typically undergo further fabrication processing in terms of knitting, weaving, coating or otherwise modifying the fibres to form an implantable structure. Fibres produced using this method have a wide variety of applications – including tissue engineering (Du *et al.,* 2019, Rinoldi *et al.,* 2019), supercapacitators (Park *et al.,* 2019, Zhang *et al.,* 2019), and even for wearable materials with improved textile properties (Cunha *et al.,* 2018). The focus in this thesis however is their use as DDS for cancer therapy. There is very little published literature on using wet spinning for fabrication of DDS. Gao *et al.,* reported wet spun single polylactic acid (PLLA) fibres, loaded with 5FU (Gao *et al.,* 2007). The fibres were tested for cytotoxicity *in vitro* against a human stomach cancer cell line (SGC-7901). The fibres were placed in PBS for 3 weeks, or in NaOH (to accelerate fibre degradation), and the solutions added to the cells for 44 h before an MTT cell viability assay was performed. This showed an 80 % reduction in cell viability; however a more rigorous *in vitro* and *in vivo* assessment is needed to assess its potential as a DDS.

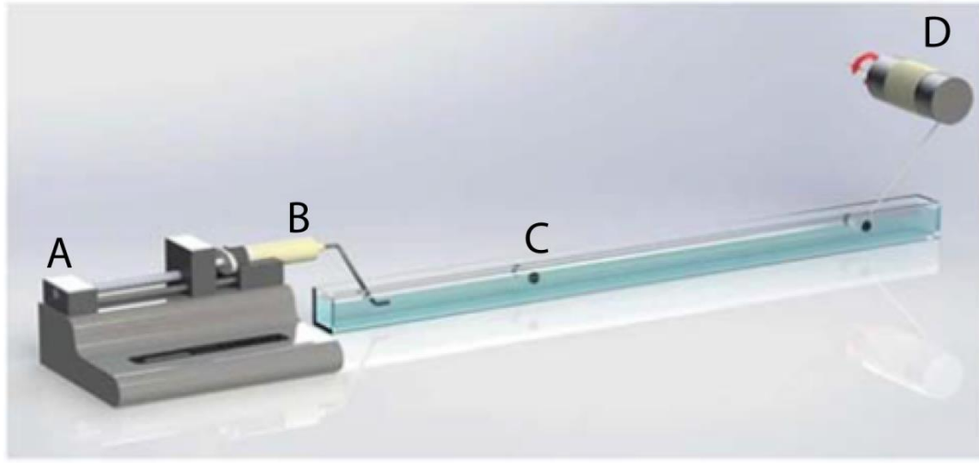

Figure 1.13: Schematic of a wet spinning set up.A) electronic programmable pump, B) syringe, C) coagulation bath, D) rotating collector. Taken from (Mirabedini *et al.*, 2016).

1.6.4.3 Multiaxial Fibres

A major advancement in drug release from fibres occurred when multiaxial fibre configuration was introduced. Fibres are versatile in their configuration – with single (Fig. 1.14 A), coaxial (Fig. 1.14 B) and triaxial (Fig. 1.14 C) fibres being reported. A coaxial fibre has a core-sheath configuration, in which two concentric layers are formed from different polymers. The spinning set up involves a needle inside another needle, each of which is connected to a reservoir of polymer dissolved in solvent (Lu *et al.*, 2016). Triaxial fibres are a modification of the coaxial structure, in which three concentric layers are formed – a core, an intermediate layer, and a sheath layer.

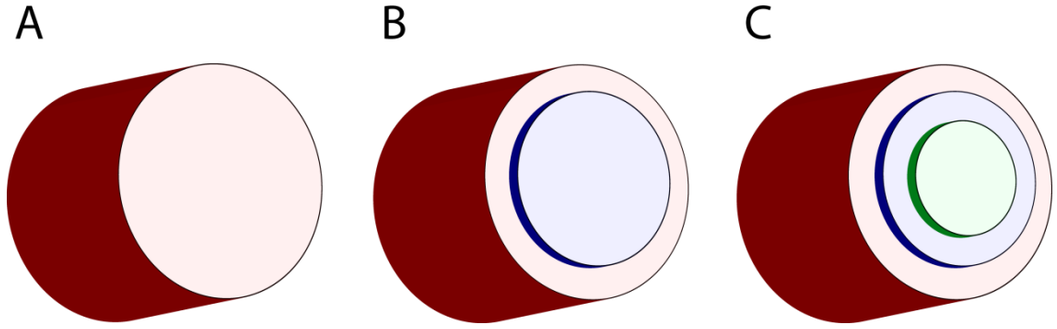

Figure 1.14: Schematic of fibre configurations.A) monofilament fibre, B) coaxial fibre, C) triaxial fibre.

Multiaxial fibre configurations are beneficial for a multitude of reasons. They can be fabricated from polymers with different properties, and thus can be tailored to load multiple drugs of choice. The outer sheath layer/s can act as a protective barrier; protecting it from both drug loss and degradation during the fabrication process. Modulation of drug release is also another potential benefit of a multiaxial structure – the shell hydrophobicity/hydrophilicity, thickness and porosity can be fine-tuned to release the core contents at a slower and more sustained rate. There are very few multiaxial fibre configurations for cancer therapy, with majority of publications still in the *in vitro* stages of pre-clinical testing. One study describes the use of electrospinning to form coaxial fibres consisting of a hyaluronic acid core which was loaded with gemcitabine, and a PLLA sheath for use in PDAC treatment (Xia *et al.*, 2018). Subcutaneous PANC-1 tumours were established in nude BALB/C mice and animals were treated with either a wet-spun gemcitabine loaded patch (2 cm × 2 cm) placed over the exposed surface of the tumour, or the equivalent amount of gemcitabine administered IP. No significant difference in tumour volume or weight was observed between treatment groups – which indicates that the patch and systemic gemcitabine have equivalent anti-tumour effects. There was however, a significant difference in animal weight, with the systemically treated animals experiencing significant and constant weight loss over the 32 day period, while the animals treated with the patch continued to gain weight throughout the study. Weight loss is the one of the biggest indicators of health decline in these experimental animals, which suggests the systemic toxicity in IP treated animals was significant while the locally treated animals had no apparent side effects from treatment – further emphasising the potential of local drug delivery.

Another coaxial electrospun fibre formulation was developed by Yan *et al.,* in which doxorubicin was loaded into a PVA core, surrounded by a chitosan sheath (Yan *et al.,* 2014). *In vitro* efficacy was assessed against a SKOV-3 human ovarian cancer cells which showed a 40-50 % reduction in cell viability, however further *in vivo* work should be performed in order to further assess their potential as successful DDS.

Coaxial wet spun fibres have been significantly underutilised in the field of DDS. To the best of our knowledge there are no publications describing dual-drug loaded, multiaxial fibres for use in cancer therapy. Majority of the literature on DDS describe the delivery of a singular drug, which, given the clinical use of combination chemotherapy regimens for cancer theory, is not the most relevant approach. The gold standard for many cancer treatments is a combination of chemotherapeutics, which is where the wet spinning technology is desirable due to its versatility in concomitant drug loading to create all-in-one formulation. Furthermore, each structure described in this chapter so far has been designed for a single application method. Wet spun fibres have the potential to be created into a 3D structure using conventional textile manufacturing such as knitting, weaving or braiding to create a surface covering for a tumour, coated to form a rigid implant for intratumoural implantation, or used as a suture like material.

This is therefore the focus of this thesis – to utilise the wet spinning method to create single (Chapter 3 and 6) and coaxial (Chapter 4 and 5) fibres for local delivery of single or dual anti-cancer agents for the treatment of PDAC.

1.7 Non Chemotherapeutic Delivery Systems for Cancer Treatment

While chemotherapy DDS are showing promise in treating PDAC, it is important to acknowledge that chemotherapy alone is unlikely to be the most efficacious treatment. Many cancer types are commonly treated with chemotherapy in combination with other anti-cancer agents such as radiation, and more recently immunotherapy. This section will describe the progress of non-chemotherapy DDS for PDAC where applicable and highlight the potential of implantable DDS to improve the way these therapies are delivered.

1.7.1 Immunotherapy

Immunotherapy for cancer therapy is a rapidly growing field and offers a new therapeutic approach outside of conventional radiotherapy, chemotherapy and surgery (Torphy *et al.*, 2018). Immunotherapy has evidence of success in melanoma, lung cancer, bladder cancer, kidney cancer, head and neck cancer, and liver cancer (Brahmer *et al.*, 2012). This has laid hope for success in cancers like PDAC, however to date immunotherapy in PDAC has been largely unsuccessful. This non-responsiveness is largely due to the low immunogenicity of pancreatic tumours. An immunogenic tumour is defined as a tumour that provokes an immune response – that is they have been infiltrated by high numbers of T cells. This means that the body has recognised the cancer and is already trying to fight it. Non immunogenic tumours are ones that fail to illicit an immune response, and therefore lack T cell activation. Pancreatic tumours fail to attract infiltrating T cells, and therefore administration of checkpoint inhibitors has shown to be unsuccessful, and this can be due to multiple reasons. PDAC has a low mutational load, and this means there are less neoantigens produced. Generally, cancers with high mutational load are more easily recognised by the immune system, as they produce more “foreign” antigens (Vogelstein *et al.*, 2013). It has been shown however, that PDAC sometimes elicits a small immune response in the body, with some patients often having increased levels of CD8+ and CD4+ T cells which normally would be associated with better prognosis, however as PDAC progresses so does the suppression of these cell types. Another problem lies in getting the T cells to infiltrate into the tumour (Fukunaga *et al.*, 2004, Liu *et al.*, 2016). As mentioned in Section 1.3, the dense desmoplasia surrounding pancreatic tumours prevents delivery of systemically administered chemotherapeutics to the tumour, and it is also thought to prevent T

cell infiltration in a similar way. In a study of T cell infiltration into lung tumours, the authors found that T cell concentration is directly correlated to the ECM structure (Salmon *et al.,* 2012). ECM's that display a dense accumulation of collagen and fibronectin were devoid of T cells, while ones that had been degraded showed improved T cell numbers. Many studies have focused on degrading the fibrotic stroma to assess the level of immunosuppression. A study by Jiang *et al.*, sought to observe the role of hyperactivated focal adhesion kinase (FAK) in the development of the immunosuppressive tumour microenvironment. They found that by inhibiting the FAK pathway in a KPC mouse model of PDAC, the previously unresponsive model became responsive to T cell immunotherapy and checkpoint agonists (Jiang *et al.,* 2016).

Immunogenic tumours have a higher predicted level of success in response to a checkpoint inhibitor (such as programmed cell death protein 1 (PD-1) or cytotoxic T-lymphocyte associated protein 4 (CTLA-4)). Tumours have immune checkpoints, which is a way the tumour can evade the immune system. These are inhibitory pathways that regulate the levels of infiltrating T cells, by causing them to "switch off" in order to control immune activation (Mahoney *et al.,* 2015). When checkpoint inhibitors are administered to immunogenic tumours, they block this inhibitory pathway, which allows T cells to "switch on" and attack the tumour (Mellman *et al.,* 2011). The development of checkpoint inhibitors has been revolutionary for many immunogenic cancers, and is best known for its role in treating melanoma. The two main checkpoints (and most extensively studied) in cancer therapy are PD-1 and CTLA-4. There have only been 4 checkpoint inhibitor clinical trials that include advanced PDAC patients; three PD-1/PD-L1 and one CTLA-4, all of which have been largely unsuccessful. In the one phase II CTLA-1 trial, none of the 27 PDAC patients showed any objective response. Of the three phase I studies which enrolled 1 PDAC patient (Brahmer *et al.,* 2012) (Herbst *et al.,* 2014) or 14 PDAC patients (Patnaik *et al.,* 2015), none showed any objective response.

There are currently no implantable DDSs for immunotherapy drug administration, which indicates that the local delivery of these agents has the potential to improve their efficacy, especially if combined with a compound such as

paclitaxel which is known to increase the immunogenicity of tumours (Bracci *et al.,* 2013, Park *et al.,* 2013, Hilmi *et al.,* 2018).

1.7.2 Radiation

External beam radiation is the most common form of radiation delivered to PDAC patients. It involves directing high energy radiation beams from outside the body through the skin and to the tumour. Radio- and chemotherapy administered in combination is a common treatment regimen for many cancers, PDAC included, which is commonly referred to as chemoradiation or chemoradiotherapy. As discussed in Section 1.2, chemoradiotherapy can be administered as an adjuvant therapy (after tumour resection) or as a neo-adjuvant therapy (before tumour removal) for borderline, non-resectable and palliative cases. A phase III study enrolled 449 patients with locally advanced PDAC who were randomised to receive either gemcitabine or gemcitabine and erlotinib, followed by a second randomisation to either continue on the same chemotherapy or receive administration of chemoradiotherapy (54 Gy plus capecitabine). There was no significant survival benefit between chemotherapy and chemoradiotherapy, as the median overall survival from the date of first randomisation was 15.2 vs 16.5 months in the chemoradiotherapy and chemotherapy groups respectively (Hammel *et al.,* 2016). Further to this, a systematic review and meta-analysis of chemoradiotherapy vs chemotherapy for locally advanced unresectable PDAC was performed which assessed 5 randomised and 3 observational studies that included 830 patients (Ng *et al.,* 2018). It was concluded that the addition of radiation to chemotherapy in the randomised trials did not improve overall survival or progression free survival, and the improvement in overall survival and progression free survival observed in the observational studies may have been from an imbalance in baseline characteristics.

Internal radiation treatment is termed brachytherapy, and is best known for its use in the treatment of prostate cancer. It involves insertion of high dose rate (HDR) or low dose rate (LDR) metallic radioactive implants (usually ^{125}I), placed into or next to a tumour. LDR are permanent implants, which are placed in the prostate, surrounding the tumour. The radiation penetrates only a small distance, so there is less damage to surrounding tissue. HDR is for

more locally advanced disease, and is removed after 1-2 days. Implantation of ^{125}I seeds for prostate cancer was first described in 1972, and is now common clinical practice (Holm 1997).

Currently, the majority of research into implantable brachytherapy devices for PDAC is in the form of micro/nano particles, and is often injected in a solution/gel form. While this form of DDS is not the focus of this thesis, there has been significant work published in the field of PDAC and warrants brief discussion. Beta emitting Phosphorus-32 (^{32}P) microparticles (Oncosil™) is a brachytherapy that is designed to treat unresectable, locally advanced PDAC. The ^{32}P is encapsulated in microspheres made from semiconducting silicone that has been porosified using electrochemical techniques. These particles are suspended in a solution of microcrystalline cellulose and sodium carboxymethycellulose, which is injected as a gel (Zhang *et al.*, 2005). Previous pre-clinical studies in PDAC xenograft nude BALB/c mice showed complete tumour response after 10 weeks following intratumoural injection of the Oncosil ^{32}P microspheres. This has resulted in pilot clinical studies being approved, which are currently in progress. A subsequent study was performed in which patients were treated with FOLFIRINOX or gemcitabine + *nab*-paclitaxel, in combination with Oncosil (Harris *et al.*, 2018). Oncosil was delivered using endoscope ultrasounded guided fine needle injection (EUS-FNI), using a fine needle injection technique, with each patient receiving a total dose of 100 Gy. The study involved 40 participants and to date no adverse events in relation to the implantation procedure have been reported. The study is ongoing.

1.8 Limitations and Future Directions

The benefits of local chemotherapy DDSs are numerous, a major advantage being the delivery of high concentrations of anti-cancer agents locally, thereby reducing systemic toxicity. This can significantly improve a patient's quality of life; however as with the majority of cancer treatments there are some limitations to implantable polymeric DDSs and these will be discussed below.

An important factor to consider for the success of implantable DDS is drug penetration, as the efficacy of these treatments depends heavily on their ability to deliver the therapeutic in adequate concentrations to the diseased tissue. One of the most significant downfalls of the Gliadel wafers for implantation at the site of glioma resection was the poor tissue penetration and rapid clearance of the drug. One of the most well cited studies into CM brain tissue penetration was by Fung *et al.,* in which CMW were implanted into the brain of a cynomolgus monkey (Fung *et al.,* 1998). It was discovered that CM penetrated 6.1 mm into the brain tissue from the implant site after 24 hours, but then dropped and fluctuated between 1.1 mm and 3.6 mm from day 3-30. This small penetration distance is not favourable, as recurrence of tumours is commonly observed within a 2 cm radius of the resection site (Torres *et al.,* 2011). This poor penetration was also observed in a study by Walter *et al.,* in which they measured paclitaxel concentration up to a 7 mm radius around the implant. Within 2-3 mm of the implant, the paclitaxel concentration was high - 100-1000 ng/mg brain tissue - but rapidly dropped to 1-10 ng/mg at 4 mm away (Walter *et al.,* 1994). Drug concentrations 2 cm from the implant were not reported, however it is possible that the concentration would fall below the limit of detection (0.2 ng/mg). Poor drug penetration into the tumour tissue plays a large role in the failure of implantable DDS, which highlights the importance of using combination treatment approaches together with systemic and localized drug delivery.

Implantable polymeric structures have also been utilised to deliver gene therapies. Gene therapy is a relatively new treatment modality for cancer, which involves altering the gene expression patterns of cancer cells. Khvalevskya *et al.,* developed a PLGA cylindrical implant containing siG12D (siRNA against mutated KRAS oncogene), for

delivery via EUS-FNI implantation into pancreatic tumours (Golan *et al.,* 2015). siRNA based therapeutics show great potential in sensitising cancer cells to chemotherapy by silencing the genes that are involved in drug resistance (Guo *et al.,* 2013). They found that siG12D was stable and active in the implant for 155 days in an *in vivo* PDAC SCID/bg mouse model, and was shown to reduce tumour volume and increase overall survival. A phase I/IIa clinical trial has been completed in 15 patients with unresectable locally advanced PDAC. The siG12D implants were inserted intratumorally in combination with systemic gemcitabine, gemcitabine + erlotinib + oxaliplatin or FOLFIRINOX. The median overall survival was 15.1 months. A review of the various gene therapies for PDAC describes the gene therapies and their progress and highlights the potential of these technologies to treat PDAC as a systemic disease with increased targeting, reduced side effects and increased tolerability (Sato-Dahlman *et al.,* 2018).

There has been a recent shift in the field of immuno-oncology; with adoptive cell therapy (ACT) causing a shift in the way the immune system can be harnessed to treat cancer. As mentioned in Section 1.7.1, current immunotherapy drugs (such as checkpoint inhibitors) display efficacy in a limited number of tumours. ACT involves identifying a patient's own anti-tumour lymphocytes, isolating them and growing them *ex vivo,* and infusing them back in to the patient along with additional vaccines/growth factors to increase the anti-tumour efficacy of the transferred cells (Rosenberg and Dudley 2009). The most clinically advanced ACT is chimeric antigen receptor (CAR) T cell therapy, which involves the use of peripheral blood T cells that have been genetically modified to express CAR genes (Newick *et al.,* 2017). The adoptive transfer of CAR T cells has had success in treating haematological cancers such as acute lymphoblastic leukaemia (ALL) and large B cell lymphoma, however show less efficacy in solid tumours. This is due to many solid tumours producing immunosuppressive signals that impedes CAR T cell recognition. Smith *et al.,* developed an implantable scaffold designed to co-deliver CAR T cells and a stimulator of IFN genes (STING) agonist to mice bearing KPC pancreatic tumours (Smith *et al.,* 2017). These scaffolds were made from alginate, and were manufactured to contain migration promoting macromolecules and stimulatory cues. Initially the scaffolds were loaded with CAR T cells and when implanted into a tumour the CAR T cells underwent significant

proliferation when compared to CAR T cells injected intratumourally. The authors found that while the scaffold reduced tumour growth and doubled the OS, they didn't clear the disease. STING agonists work to stimulate the immune response to eliminate tumour cells that are not recognised by the adoptively transferred lymphocytes. The scaffolds were then loaded with cyclic di-GMP (cdGMP) (STING agonist) to be co delivered with CAR T cells, and implanted in KPC tumour bearing mice and compared to scaffolds containing cdGMP alone, and intratumoural injections of cells + cdGMP or cdGMP alone. In the animals treated with dual loaded scaffolds, KPC tumours were eradicated completely in 4/10 mice, with the remaining 6 displaying substantial tumour regression, with no animals showing metastasis. They had a 4.6 fold increase in OS compared to the animals that received the dual injection. This work is outside the scope of this thesis, but was worth discussing due to the promising results and reported downfalls of other immunotherapy treatments (i.e. checkpoint inhibitors) in PDAC therapy.

1.9 Summary, Project Rationale and Thesis Aims

PDAC is a disease with a very high mortality rate, and while the incidence is relatively low compared to other cancer types, it is the 3rd leading cause of cancer related death in the developed world. It is one of the few cancers for which overall survival has not increased for over 20 years. PDACs unique tumour microenvironment, primarily the surrounding desmoplasia, is a large contributor to treatment failure. Poor drug perfusion of systemically administered chemotherapy has therefore highlighted the need for local drug delivery strategies to overcome such biological barriers and achieve therapeutic response. This thesis focuses on the development of single and dual-drug eluting DDS for the localized treatment of non-resectable PDAC. This thesis reports on the use of the wet spinning method to create single and coaxial fibres loaded with chemotherapeutics and immunotherapy agents. The biophysical characterisation of these fibres is also reported. Finally, *in vitro* efficacy is described using 2D PDAC cell monolayer and 3D PDAC tumour spheroid models, followed by the *in vivo* efficacy of coaxial dual drug loaded fibres using a human PDAC mouse model.

The specific aims were to:

1. Prepare and characterise gemcitabine-loaded alginate and chitosan monofilament fibres and assess their *in vitro* efficacy in 2D and 3D PDAC cell culture models (single-drug eluting fibres; Chapter 2).
2. Prepare and characterise gemcitabine and paclitaxel loaded coaxial fibres and assess their *in vitro* efficacy in 2D and 3D PDAC cell culture models (dual-drug eluting fibres; Chapter 3).
3. Assess the colony forming ability and survival of PDAC cells treated with gemcitabine and paclitaxel coaxial fibres with and without radiation (dual-drug eluting fibres; Chapter 3).
4. Assess the *in vivo* efficacy of gemcitabine and paclitaxel loaded coaxial fibres in a subcutaneous PDAC xenograft mouse model (Chapter 4).
5. Finally, in an effort to validate the versatility of the wet-spun DDS approach; prepare and characterise immunotherapy (nivolumab) loaded alginate fibres for the localised delivery of immunotherapy to pancreatic tumours in the future (Chapter 5).

Chapter 2: Fabrication and *In Vitro* Assessment of Wet Spun Gemcitabine Loaded Polymeric Fibres

Portions of this chapter have been published in the following work:

Wade SJ, Zuzic A, Foroughi J, Talebian S, Aghmesheh M, Moulton SE, Vine KL. Preparation and in vitro assessment of wet-spun gemcitabine-loaded polymeric fibers: Towards localized drug delivery for the treatment of pancreatic cancer. Pancreatology 2017, 17 (5), 795-804

Author contributions: Samantha J Wade and Kara L Vine designed the experiments; Samantha J Wade, Sepehr Talebian and Amanda Zuzic performed the experiments and analysed the data; Samantha J Wade, Kara L Vine and Simon E Moulton wrote the manuscript. All authors edited the manuscript for submission.

2.1 Introduction

PDAC has one of the lowest survival rates of all cancers, with a cumulative 5 year survival of 8.7 %. Gemcitabine was the first agent to have a significant impact on survival, however despite the emergence of new drugs and therapeutics there has been little improvement in overall survival in the last 20 years (Burris *et al.,* 1997). The lack of response of PDAC tumours to chemotherapeutics is in large due to the surrounding tumour microenvironment (TME), namely the desmoplastic tissue that surrounds the tumour, discussed in Chapter 1, Section 1.3. The stiff and hypovascular nature of the PDAC in combination with a high interstitial fluid pressure results in poor drug penetration and reduced efficacy of systemically administered therapies. Local DDS have the potential to overcome many of the shortcomings of conventional drug delivery, which requires repeated dosing and often has the negative side effect of off target systemic toxicity. DDS have the advantage of locally delivering toxic chemotherapy drugs, effectively dosing the site of disease with higher levels of the desired therapeutic than can be achieved with systemic delivery.

This concept of local drug delivery has been explored in PDAC, with a number of DDS being developed in the last 5 years, which show that the local delivery of chemotherapeutics has significant advantages in regards to tumour control over systemic delivery. This chapter describes the production of hydrogel fibres made from alginate or chitosan polymers, as a DDS for the delivery of the chemotherapeutic agent gemcitabine. A hydrogel is a network of hydrophilic polymers that swell when in contact with water while maintaining their structure (Qiu and Park 2001). Their ability to absorb water comes from the hydrophilic functional groups attached to the polymer backbone, such as –OH, -CONH, -$CONH_2$, -SO_3H , which allows them to swell up to 90 % wt, while their resistance to degradation arises from the interconnecting crosslinks (Hamidi *et al.*, 2008, Ahmed 2015). Their highly porous structure can be easily tuned by controlling the polymer crosslinking density and their affinity for the aqueous environments they swell in (Hoare and Kohane 2008). These crosslinks can be physical (including ionic, hydrogen bonding, polymer entanglement, hydrophobic/hydrophilic interactions), or covalent. Ionic crosslinking of chitosan occurs when the pH of chitosan in aqueous acidic solutions is raised above the pKa value. If the pH is high enough, gelation rapidly

occurs to form a physical hydrogel instead of a precipitate (Malaise *et al.*, 2014). Physical crosslinking is often used in reversible hydrogel systems, as it is non-permanent and the interactions between polymer chains are often in the form of hydrogen or electrostatic bonds (Ahmadi *et al.*, 2015). Ionic crosslinking is commonly used for alginate, with calcium crosslinking being the most common method. Calcium crosslinked alginate has been shown to be biocompatible and non-toxic, and is approved for use in food and pharmaceutical products (Jain and Bar-Shalom 2014). When sodium alginate containing drug is placed into a calcium solution, the calcium ions replace the sodium, and each calcium ion is able to attach to two of the polymer strands, thereby crosslinking the chains and trapping the respective drug (Fig. 2.1) (Smidsrød and Skja 1990).

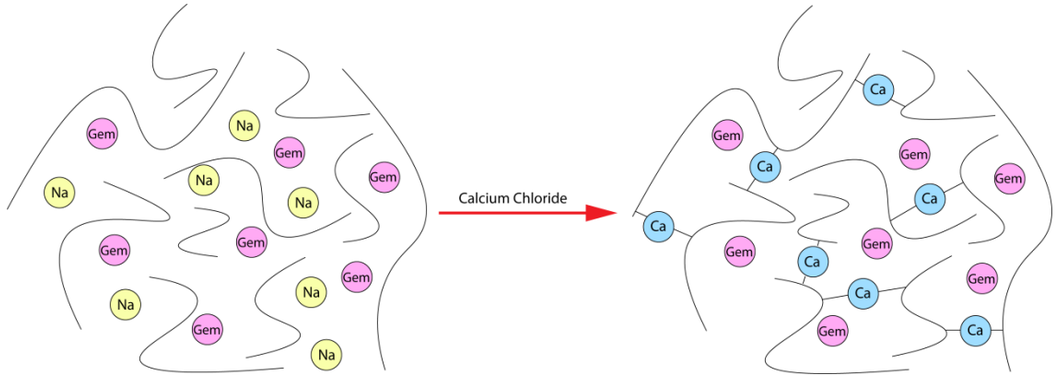

Figure 2.1: Schematic of the ionic crosslinking of sodium alginate with calcium chloride. Na: sodium, Ca: calcium, Gem: gemcitabine. Adapted from (Xu *et al.*, 2018).

The process of wet spinning was utilized in this chapter to produce continuous fibres that have a high surface area to volume ratio. Wet spinning is a gentle fibre fabrication method that involves pumping polymer solution at a controlled rate in to an coagulation bath, which causes the polymer to crosslink and solidify and is drawn off as a continuous fibre onto rotating rollers (Ozipek and Karakas 2014). The fascile nature of this fabrication process is advantageous when an active agent, sensitive to heat or pressure, is to be incorporated into the fibre. Wet spinning has been used in the applications in delivery of sensitive drugs, proteins or growth factors (Cronin *et al.*, 2004, Yilgor *et al.*, 2009). Wet spun fibres are able to be further processed after fabrication – whether it be through weaving or coating. Their final form is heavily dependent on their intended use. At sites where a flexible structure is required, the fibres can be woven into a mat like structure and placed over the site of disease whereas sites where a rigid

structure is required (e.g. intratumoural implantation) the fibres can be coated or encased in another polymer to improve the rigidity, a concept that is further discussed in Chapter 3.

The specific aims for this chapter were to:

1. Prepare gemcitabine-loaded alginate and gemcitabine-loaded chitosan fibres using the wet-spinning technique
2. Assess the following physical properties of gemcitabine-loaded alginate and chitosan fibres; morphology, diameter, tensile strength, drug loading capacity and drug release profile. Ascertain the biocompatibility of alginate/chitosan fibres and the cytotoxicity profiles of gemcitabine loaded alginate or chitosan fibres using *in vitro* cell based models of PDAC.
3. Compare the uptake of doxorubicin into 3D PDAC spheroids when delivered either as a free drug, or eluted from an alginate fibre.

2.2 Experimental

2.2.1 Materials

Gemcitabine hydrochloride, doxorubicin hydrochloride, sodium alginate (from brown algae), chitosan (medium molecular weight), calcium chloride ($CaCl_2$), sodium hydroxide (NaOH) and acetic acid were from Sigma-Aldrich Co. USA. Simulated biological fluid (SBF) was prepared using analytical grade reagents consisting of 5.403 g l^{-1} NaCl, 0.504 g l^{-1} $NaHCO_3$, 0.426 g l^{-1} $NaCO_3$, 0.225 g l^{-1} KCl, 0.230 g l^{-1} $K_2HPO_4 \cdot 3H_2O$, 0.311 g l^{-1} $MgCl_2.6H_2O$, 0.8 g l^{-1} NaOH, 0.293 g l^{-1} $CaCl_2$, 0.072 g l^{-1} Na_2SO_4 and 17.892 g l^{-1} HEPES as buffering agent. The pH was adjusted to 7.40 ± 0.05 using 1.0 M NaOH solution. The CellTiter 96® Aqueous One Solution Cell Proliferation Assay (MTS) was from Promega, Australia. DMEM-High glucose media was made in house. Foetal calf serum (FCS) was from Invitrogen, USA. Trypsin/EDTA, Penicillin/Streptomycin and doxorubicin hydrochloride were from Life Technologies, Australia.

2.2.2 Polymer Solutions for Fibre Spinning

Prior to spinning, alginate solutions were prepared at concentrations of 1 % or 2 % w/v by adding alginate powder to de-ionized water under stirring and heating to 50 °C for 1 h before being left mixing at room temperature overnight. Chitosan solutions (2 % or 3 % w/v) were prepared by dissolving chitosan powder in 3 % v/v acetic acid at 50 °C and stirring at 1000 rpm. The solutions were left stirring overnight at room temperature before being filtered through a 0.45 µm membrane. Gemcitabine hydrochloride powder (0.52 or 5.2 mg) was added to each spinning solution (10 mL) (1 % or 2 % alginate, and 2 % or 3 % chitosan) to give a final drug concentration of 200 µM or 2 mM respectively. Doxorubicin (10.8 mg) was added to 1 % alginate spinning solution (10 mL) to give a final drug concentration of 2 mM.

2.2.3 Coagulation Solutions

The coagulation solution used to cross-link alginate fibres was 2 % w/v $CaCl_2$ prepared in 20 % v/v ethanol solution. The coagulation solution used to cross-link chitosan was prepared using 1.0 M NaOH in a solution of 10 % v/v ethanol.

2.2.4 Wet Spinning of Fibres

Fibres were prepared using the wet spinning method. The spinning solutions (with or without gemcitabine or doxorubicin) were placed in a 10 ml syringe with an 18 gauge needle (alginate) or 21 gauge needle (chitosan) attached to the programmable syringe pump (kdScientific KDS100) and extruded at 60 ml/h (alginate) or 50 ml/h (chitosan) into a coagulation bath with its corresponding coagulation solution. The fibres were collected onto a rotating mandrel, rinsed with deionized water for approximately 30 seconds then left to air dry.

2.2.5 Fibre Morphology Analysis

Fibre morphology was assessed using optical microscopy and scanning electron microscopy (SEM). Fibre diameter was calculated using optical microscopy. The diameter was calculated at 9 points along each 1 cm fibre before taking an average. A total of 3 fibres were measured to calculate overall average diameter (total n = 27). Internal morphology was assessed using SEM. SEM images were acquired by Sepehr Talebian (University of Wollongong, Australian Institute for Innovative Materials) using a JEOL JSM-7500 FESEM at an accelerating voltage of 15 kV, a spot size of 60 and a working distance of 10 mm. Fibre cross sections were obtained by placing pieces of hydrated fibre into holes drilled into the surface of a brass block such that the fibres protruded approximately 1-2 mm above the surface. The block was then plunged into liquid nitrogen for approximately 45 sec and a liquid nitrogen cooled blade run over the surface of the block to obtain a cross section of the fibres. The block was then quickly transferred to the SEM for imaging. No coating of the fibres was required, as they remained conductive in the SEM vacuum for approximately 20 min due to their high water content. SEM images of dried fibres were obtained by Amanda Zuzic (University of Wollongong, Australian Institute for Innovative Materials) and were frozen with liquid nitrogen

before snapping and imaging.

2.2.6 Tensile Testing

Fibres were tested on an EZ-L Shimadzu Instron tensile tester with a load cell of 10 N, gauge length of 10 mm and an extension rate of 1 mm/min. The fibre sample is held between two clamps and slowly stretched until breaking point, giving a graph of distance (mm) vs force (N). Elongation at break (mm) and Young's Modulus (GPa) were then calculated using the obtained results. Elongation refers to the length to which a fibre was able to extend when a load was applied. Young's Modulus was calculated for the initial, linear period using the equation;

$$Young's\ Modulus\ (N/mm^2) = \frac{FL}{eA} \quad (1)$$

Where F is the force (N), L is the length of test sample (mm), e is the extension (mm) and A is the cross-sectional area of the fibre (mm^2). Four samples were run for each fibre and the results are the average.

2.2.7 Gemcitabine Release

Thirty centimeter lengths of gemcitabine loaded or empty fibre (in triplicate) were placed in 2 mL of SBF, and 200 µL aliquots removed at 10, 30, 60, 90 min, hourly for 10 h, and then daily for 3 weeks, followed by replacement of fresh buffer. The amount of drug released from alginate and chitosan fibres was assessed using high performance liquid chromatography (HPLC). HPLC is a technique that separates, identifies and quantifies components in a mixture. The basis of separation is the variation of in movement of components of a sample through a column, which is driven by solvents and pressure. This thesis uses reverse phase (RP) C18 system. In RP systems compounds are separated based on their hydrophobic character. The columns are packed with silica beads that can range from 3-50 microns with pores that range from 100-1000 angstroms. The stationary phase is made up of hydrophobic alkyl chains in lengths from C4-C18, with C18 being the most common and used for peptides and small molecules. The mobile phase consists of an aqueous buffer, solvent or a mixture of the two. The time taken for components in a

sample to separate and elute is known as the retention time, and depends on the samples interactions with both the stationary and mobile phase. The system comprised of a 600 controller pump, 717 plus autosampler and 2996 UV-Vis PDA detector. Samples were filtered through a 0.2 µm syringe membrane filter unit before being injected (10 µL) onto an Atlantis T3 C18 analysis column (4.6 × 250 mm, 5 µm particle size). Using an isocratic elution with a water/acetonitrile (95/5), flow rate 1 mL/min, pressure 100 bar, and gemcitabine was detected with the UV-Visible detector at 272 nm. A standard curve was prepared using gemcitabine concentrations ranging from 0.1 to 1000 µg/mL. The amount of gemcitabine released (µg) was calculated by interpolating AUC values from the standard curve using Empower Pro V2 (Waters) software.

2.2.8 Drug Loading

The theoretical drug loading in the fibres was calculated using the known concentration (µg/mL) of the drug in the polymer spinning solution, the spinning rate (mL/min) of the solution and the rate at which the fibre forms (m/min). Using these values and equation (2) it is then possible to determine the encapsulation efficiency using equation (3).

$$Theoretical\ Loading = \frac{C \times SR}{FF} = \ \mu g/m \qquad (2)$$

Where C is the concentration, SR is spinning rate and FF is fibre formation rate,

$$Encapsulation\ Efficiency\ (\%) = \frac{Actual\ Loading}{Theoretical\ Loading} \times 100 \qquad (3)$$

The actual loading (µg/m) of drug in fibres was determined by the cumulative release calculated from the release profiles.

2.2.9 Cell Lines and Culture Conditions

The Mia-PaCa-2 and PANC-1 human PDAC and MCF-7 breast cancer cell lines were purchased from the American Type Culture Collection (ATCC). All cell lines were authenticated using short tandem repeat (STR) profiling at the Garvan Institute of Medical Research. Cells were confirmed to be mycoplasma free. All cells were cultured in DMEM-high glucose media supplemented with 10 % foetal calf serum (FCS) at 37ºC, 95 % humidity, and 5 % CO_2 in a Heracell incubator (Kendor Laboratory Products, Germany)

2.2.10 Growth Inhibition of Cell Monolayers

Cells monolayers were generated by seeding (5000 cell/well) in a 96-well plate in a final volume of 100 uL 24 h prior to addition of empty or gemcitabine loaded alginate or chitosan fibres (5 cm lengths). Cell images were acquired at 10 × magnification using IncuCyte ZOOM real time quantitative live-cell imaging system (Essen Bioscience, USA) at 24, 48 and 72 h and cell confluency calculated using IncuCyte ZOOM software. The system resides within a standard cell incubator (37ºC, 95 % humidity, 5 % CO2) and all imaging is non-invasive and non-perturbing to cell health. Cell viability was assessed using the CellTitre® 96 AQ_{eous} One Solution Cell Proliferation Assay is a colorimetric assay used to determine the number of viable, proliferating cells in cytotoxicity assays. The assay kit contains MTS tetrazolium compound (Owens reagent) and will be hereforth referred to as an MTS assay. The MTS tetrazolium compound is reduced by viable cells into a coloured formazan product that is soluble in tissue culture medium, the conversion accomplished by NAHD/NADPH produced by dehydrogenase enyzmes in metabolically active cells (Fig 2.2). Small amounts of MTS reagent are added to cells at the endpoint of an experiment (20 µL MTS into 100 µL cell medium), the colour allowed to develop for 3 h before reading at 490 nm using a UV-Vis spectrophotometer.

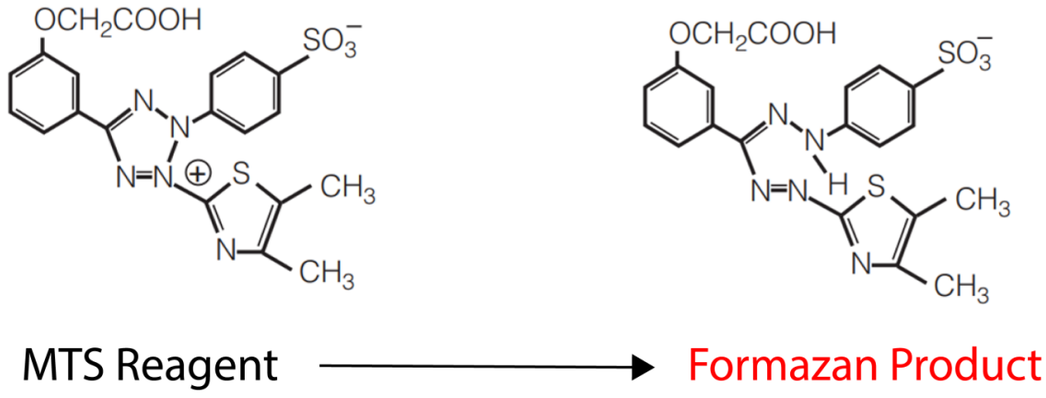

Figure 2.2: CellTitre 96 Aqueous One Solution Cell Proliferation (MTS) Assay.MTS tetrazolium reagent (3-(4,5-dimethylthiazol-2-yl)-5-(3-carboxymethoxyphenyl)-2-(4-sulfophenyl)-2H-tetrazolium) is metabolized and bioreduced by viable cells into a coloured formazan product.

2.2.11 UV-Visible Spectrophotometry

UV-visible (UV-vis) spectrophotometry is a technique used for quantitative determination of analytes. When a molecule absorbs a photon, it transitions from its ground state to a higher energy (excited) state. When in solution, some analytes absorb UV or visible light, and the light absorbed is directly proportional to the number of absorbing molecules (i.e. its concentration) according to the Beer Lambert law.

$$A=\varepsilon lc$$

Where A is the absorbance, ε is the molar absorptivity, l is the path length of the cell (in cm), and c in the concentration (in mol/L)

Unknown samples can be determined from a standard curve of known concentrations of the analyte, providing the unknowns falls within the linear range of the curve. The spectrophotometer used to measure colorimetric assays was Spectromax 250 UV plate reader in association with the Softmax Pro software (Molecular Devices, USA).

2.2.12 Growth Inhibition of Tumour Spheroids

PANC-1 and MCF-7 tumour spheroids were generated by seeding cells in Corning® Costar ® ultra-low attachment (ULA) U-bottomed plates (Sigma-Aldrich Co. USA) at 350 cell/well. MCF-7 cells were seeded in complete media (DMEM high glucose + 10 % FCS + 1 × PenStrep), while PANC-1 cells were seeded into media with reduced serum (1 % FCS). Spheroids spontaneously formed 4-7 days post seeding, and treatment began once spheroids reached a diameter of 200 – 400 µm in diameter. Following spheroid formation, spheroids were treated with empty or gemcitabine loaded alginate or gemcitabine loaded chitosan fibres. Spheroids were imaged twice weekly using the IncuCyte ZOOM software and spheroid diameter calculated using Image J software. Media was replaced weekly or as indicated by media colour change. All images were acquired at 10 × magnification. And endpoint viability acid phosphatase (APH) assay was performed at the conclusion of the experiment.

The acid phosphatase assay (APH) is a colorimetric assay used to quantify viability of cells by measuring the levels of acid phosphatase activity. The assay uses *p*-nitrophenyl phosphate as a substrate that turns yellow when dephosphorylated by acid phosphatase (Fig. 2.3). A modified method by Friedrich *et al*., allows for quantification of spheroid viability (Friedrich *et al.*, 2007). Using the ULA 96-well plate the spheroids were grown in, the media was removed and spheroid thoroughly washed with PBS before addition of 100 uL of fresh APH buffer (0.1 M sodium acetate (pH 5.5), 0.1 % (v/v) Triton-X-100, 2 mg/mL *p*-nitrophenyl phosphate) The plate was incubated at 37 ^{o}C for 90 mins, before addition of 10 µL of 1 M NaOH to stop the reaction. The absorbance was read using UV-Vis spectrophotometry at 405 nm.

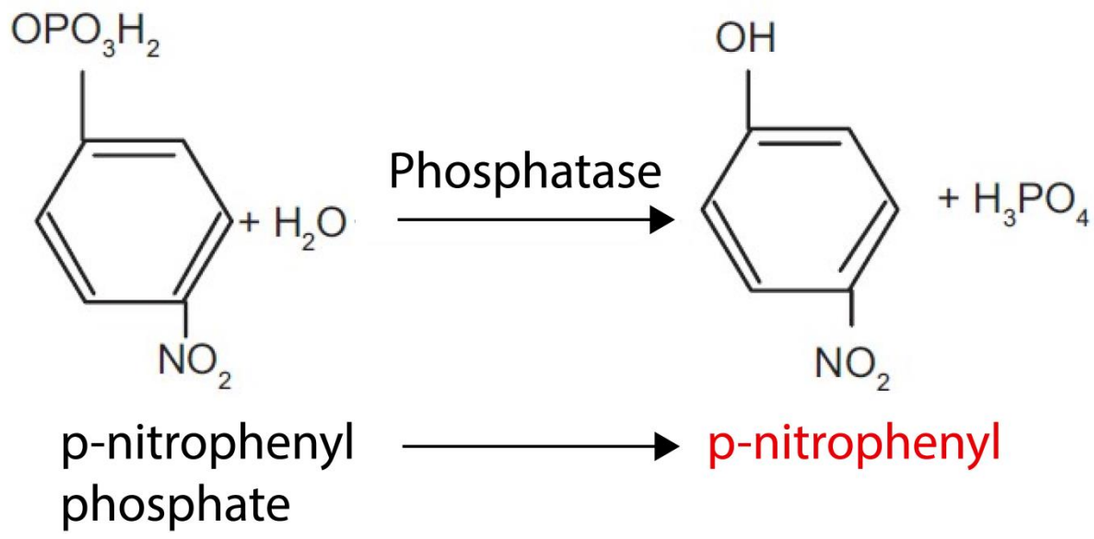

Figure 2.3: Acid Phosphatase Assay.*p*-nitrophenyl phosphate is dephosphorylated by acid phosphatases in viable cells into its product *p*-nitrophenyl, which turns yellow when dephosphorylated, then pink in alkaline solutions.

2.2.13 Drug Accumulation in Tumour Spheroids

A drug accumulation study was performed using MCF-7 tumour spheroids grown in DMEM high glucose + 10 % FCS + 1 × PenStrep after 14 days. Two centimetre lengths of 1 % alginate fibre containing doxorubicin (0.015 µg) were added to the spheroids, alongside free doxorubicin at the equivalent amount (0.015 µg), or 10 × the amount loaded in the fibre (0.15 µg). Cells were incubated with fibres/drug for 5, 20, 40, 90, 120, 180 min, washed at each time-point and imaged using IncuCyte ZOOM software at 10 × magnification.

A further accumulation study was performed to assess the effect of polymers (crosslinked and uncrosslinked) on drug uptake when co-administered with free doxorubicin.

Crosslinked polymer: Spheroids were treated with either 2 cm length of 1 % alginate doxorubicin loaded fibre (0.024 µg), 2cm of 1 % alginate fibre + 1 × equivalent free doxorubicin (0.024 µg), 2cm of 2 % alginate fibre + 1 × equivalent free doxorubicin (0.024 µg), 2 cm of 3 % chitosan + 1 × equivalent free doxorubicin (0.024 µg), 1 × equivalent free doxorubicin (0.024 µg), 10 × equivalent free doxorubicin (0.24 µg), 20 × equivalent free doxorubicin (0.48 µg). Spheroids were incubated for 4 hours, washed with phenol red free media and imaged using the IncuCyte

ZOOM at 10 × magnification. Corrected total cell fluorescence (CTCF) wa calculated using Image J software.

Uncrosslinked polymer: spheroids were treated with either a 2 cm length of 1 % alginate doxorubicin loaded fibre (0.024 µg), 1 × equivalent free doxorubicin (0.024 µg), 10 × equivalent free doxorubicin (0.24 µg), 3 µL of 1 % alginate solution + 1 × or 10 × equivalent free doxorubicin (0.024 or 0.24 µg). Spheroids were incubated for 4 hours, washed with phenol red free media and imaged using the IncuCyte ZOOM at 10 × magnification.

2.2.14 Statistical Analysis

Statistical significance of treatment groups as compared to control groups was determined using a two-way ANOVA with a Bonferroni post-test or unpaired students multiple t test (GraphPad Prism V 6.0; San Diego, CA, USA). *P* values < 0.05 were considered statistically significant. Values are reported as the average replicates ± standard error of the mean.

2.3 Results

The preparation of wet spun gemcitabine loaded fibres presents an attractive strategy for the local delivery of chemotherapeutics to non-resectable PDAC. PDAC is a disease that has an abysmal survival rate, and is notoriously difficult to treat. The difficulty in delivering chemotherapy to pancreatic tumours systemically has the potential to be overcome with a local DDS. We therefore sought to prepare gemcitabine loaded wet spun alginate and chitosan fibres to assess their preclinical efficacy in a number of *in vitro* human PDAC models.

2.3.1 Diameter and Morphology of Gemcitabine Loaded Fibres

The morphology and diameter of all fibre preparations was assessed using optical light microscopy (Appendix Fig. A1 a-d) and found that higher concentrations of hydrogel produced thicker fibres, as more monomer is able to be cross-linked per length of fibre. This was significant between 1 % and 2 % alginate but not 2 % and 3 % chitosan formulations. The addition of gemcitabine to the polymer solution before wet-spinning significantly decreased the final dried fibre diameter by up to 60 µm for 2 % and 3 % chitosan, while a change in diameter was not observed when gemcitabine was loaded into 1 % or 2 % alginate fibres (4 µm) (Fig. 2.4). SEM images of hydrated fibres revealed those prepared from alginate contained larger pores with a more “honeycomb” like structure (Fig 2.5 A and B), while chitosan fibres displayed smaller pores and a denser structure (Fig 2.5 C and D) that required increased magnification to resolve (Fig. 2.5 E and F).

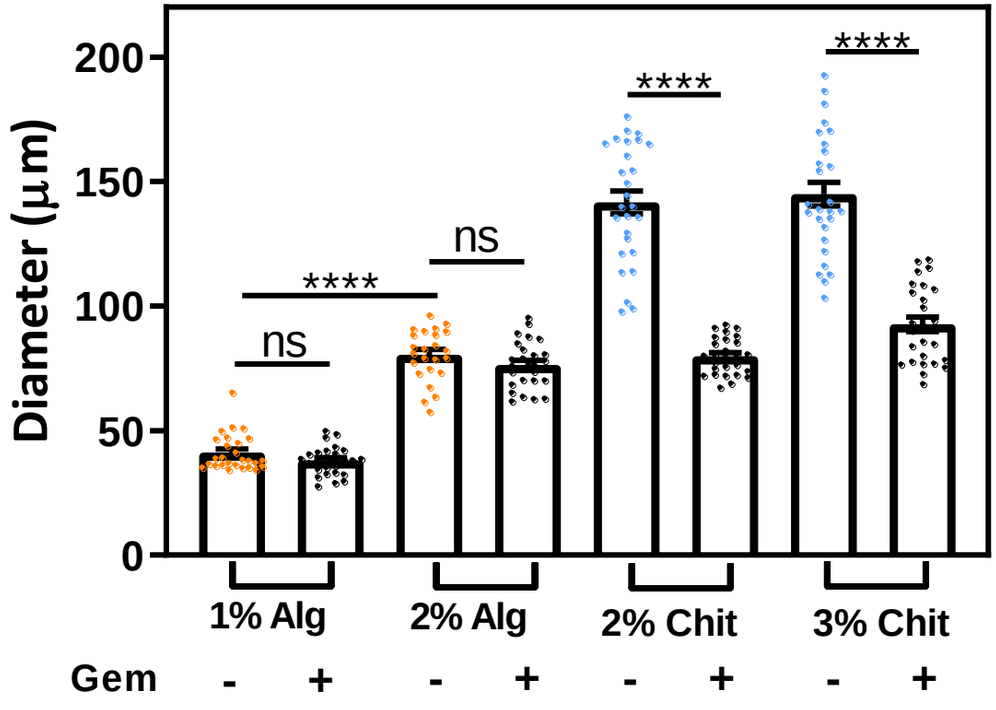

Figure 2.4: Chitosan diameter is reduced by addition of gemcitabine, while alginate was not. Dried fibre diameter was measured after wet-spinning then drying the fibres and obtaining images light microscopy. The values represent the mean of 27 measurements ± SEM. (p****<0.0001). Alg = alginate. Chit = chitosan. Gem = gemcitabine.

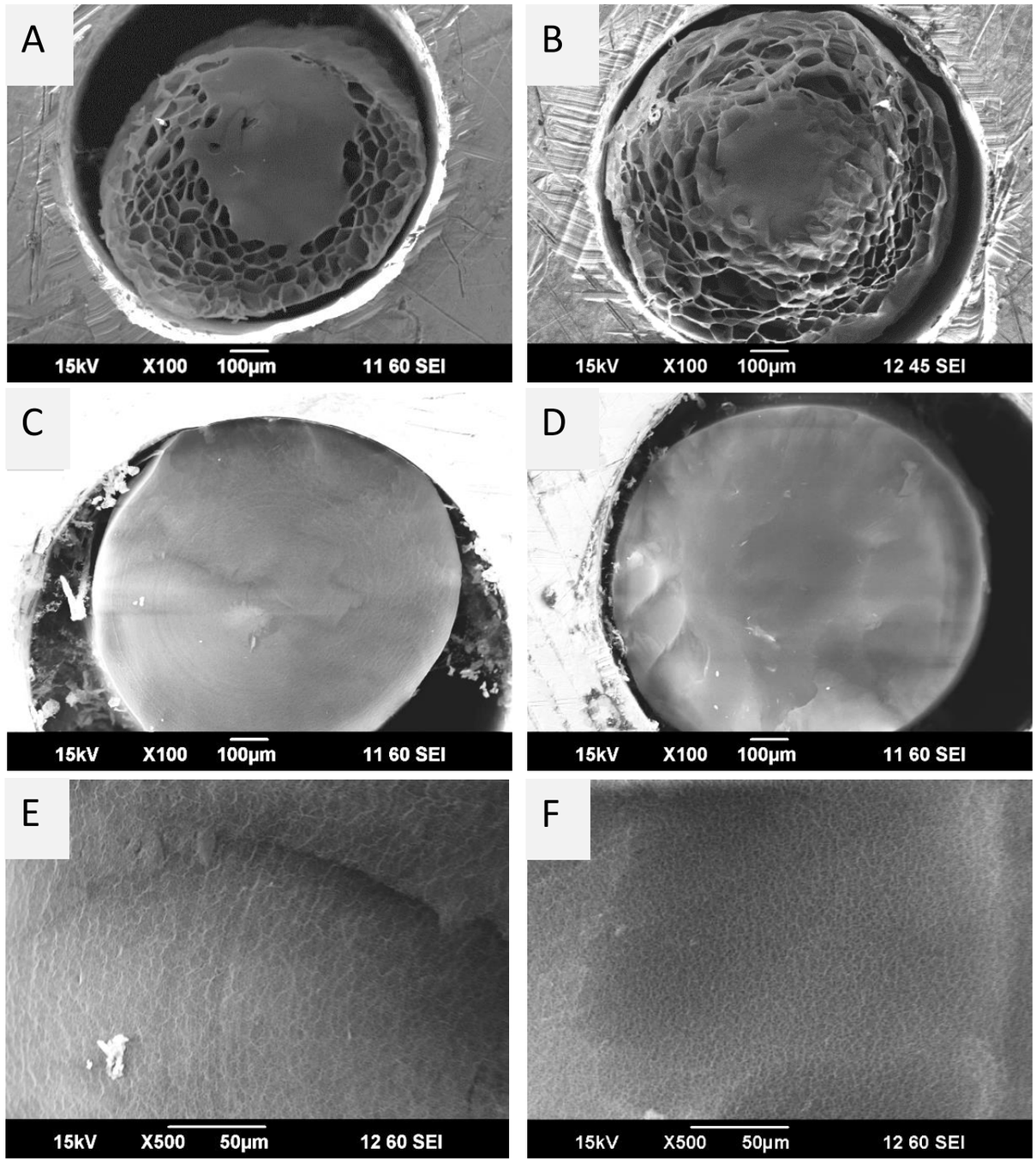

Figure 2.5: Cross section SEM images of each fibre formulation show variation in porosity between polymersSEM images showing cross sections at 100 × magnification of A) 1 % alginate, B) 2 % alginate C) 2% chitosan D) and 3 % chitosan fibres. 500 × magnification of E) 2 % chitosan and F) and 3 % chitosan fibres.

SEM images of the dried fibres revealed all fibres to have a uniform surface area with no apparent drug crystallisation on the surface and were the same size and shape. The chitosan fibres (with or without gemcitabine) appeared homogeneously smooth (Fig. 2.6 C, D, G, H). Conversely, alginate fibres, both with and without drug, contained small, raised ridges along the outer area (Fig. 2.6 A,B,E,F). The cross-sectional images show the internal morphology of the fibres to be homogeneous, with no observable traces of solid drug crystals or large pores. Lack of crystallized drug on the surface indicates that a maximum threshold of drug loading had not been reached when starting with 2 mM gemcitabine in the spinning solution (Fig. 2.6 E,F,G,H). This suggests gemcitabine concentration could be further increased in future studies without undue effects on the fibre structure, which is further explored in Chapter 3.

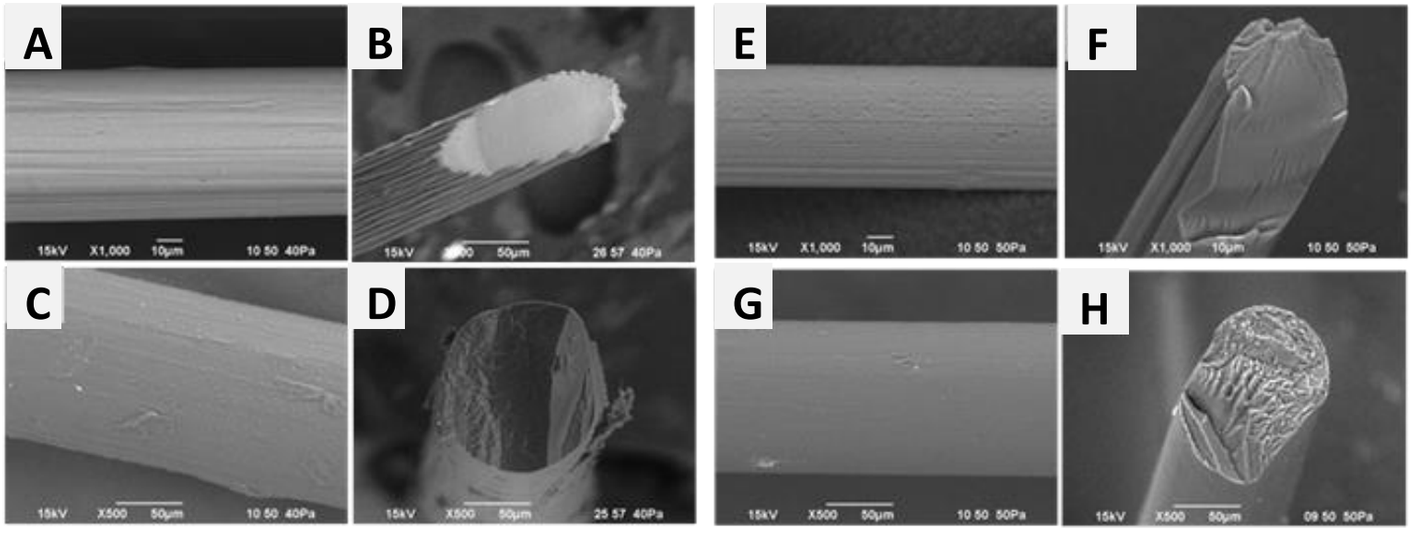

Figure 2.6: Addition of gemcitabine does not affect fibre morphologySEM images are of the surface or cross section of dried A) and B) 2 % alginate fibres, C) and D) 3 % chitosan fibres, E) and F) gemcitabine loaded 2 % alginate fibres, G) and H) gemcitabine loaded 3 % chitosan fibres. Images were acquired at 1000 × or 500 × magnification for alginate or chitosan fibres respectively.

2.3.2 Tensile Testing

In order for these fibres to be used as a DDS, it is important to ensure that when loaded with drug they possess suitable mechanical properties to be fabricated into a 3D structure. Mechanical properties were therefore assessed using tensile testing. The Young's modulus is the ratio of tensile stress to the corresponding strain produced, in order

to measure the elasticity of a material (Bansal 1996). It was calculated for the elastic (linear) period of the stress/strain curve, using equation 1 (Section 2.2.6). A fibre with a low Young's modulus will be relatively flexible and easier to manipulate into a 3D structure than a fibre with a higher Young's modulus. We found an increase in the Young's modulus when the concentration of alginate was increased from 1 % to 2 % in the empty fibres ($p < 0.05$), indicating that there was a slight loss in elasticity at the higher polymer concentration (Appendix Table A1). For the 1 % alginate, 2 % chitosan and 3 % chitosan samples the Young's modulus did not change significantly upon addition of gemcitabine at 2 mM ($p > 0.05$).

2.3.3 Gemcitabine Loading

The encapsulation efficiency of gemcitabine in 1 % and 2 % alginate fibres varied based upon the alginate concentration, with the lowest encapsulation coinciding with the lowest alginate concentration, 23.3 ±6.3 µg/m (12.7 %) and 139.7 ±21.3 µg/m (51.8 %), respectively (Table 2.1). Although 1.4 times more gemcitabine was loaded into 3 % chitosan fibres (118.3 ±20.3 µg/m) than 2 % chitosan fibres (85.3 ±1.7 µg/m), there was no significant difference in their encapsulation efficiency (32.3 % and 38.1 %, respectively), indicating that the degree of polymer chain crosslinking at these concentrations does not significantly affect drug entrapment.

Table 2.1: The encapsulation efficiency of gemcitabine in alginate and chitosan fibres was determined using a spinning solution containing 2 mM gemcitabine. Theoretical loading was calculated using equation (2) whilst the actual loading values were determined through complete degradation of the gemcitabine loaded fibres and quantification using HPLC. The values represent the mean actual loading value ± SD.

Fibre	Theoretical Loading (µg/m)	Actual Loading (µg/m)	Encapsulation Efficiency (%)
1 % alginate	183.3	23.3 ± 6.3	12.7
2 % alginate	269.7	139.7 ± 21.3	51.8
2 % chitosan	264.2	85.3 ±1.7	32.3
3 % chitosan	310.8	118.3 ± 20.3	38.1

2.3.4 Gemcitabine Release

Fig. 2.7 shows the cumulative, first-order release profile of gemcitabine from all four fibre formulations prepared from the same starting concentration of drug (2 mM) in the spinning solution. The 2 % alginate fibres released 5.8 times more gemcitabine by mass than the 1 % alginate fibres after 144 h (Table 2.1). However, given the initial drug loading of gemcitabine in the 2 % alginate fibres was 6-fold greater than the 1 % alginate fibres (Table 2.1), this difference was not surprising. When comparing the rate of gemcitabine released from 1 % and 2 % alginate fibres over the initial $t_{0\text{-}10h}$ and secondary $t_{24\text{-}114h}$ release phases (Fig. 2.7A, B, inset; Table 2.2), no significant difference was observed by 2-way ANOVA. Similarly, there was no significant difference in the rate of gemcitabine released from 2 % and 3 % chitosan fibres over $t_{0\text{-}10h}$ and $t_{24\text{-}114h}$ (Fig. 2.7C, D, inset; Table 2.2), despite differences in initial drug loading.

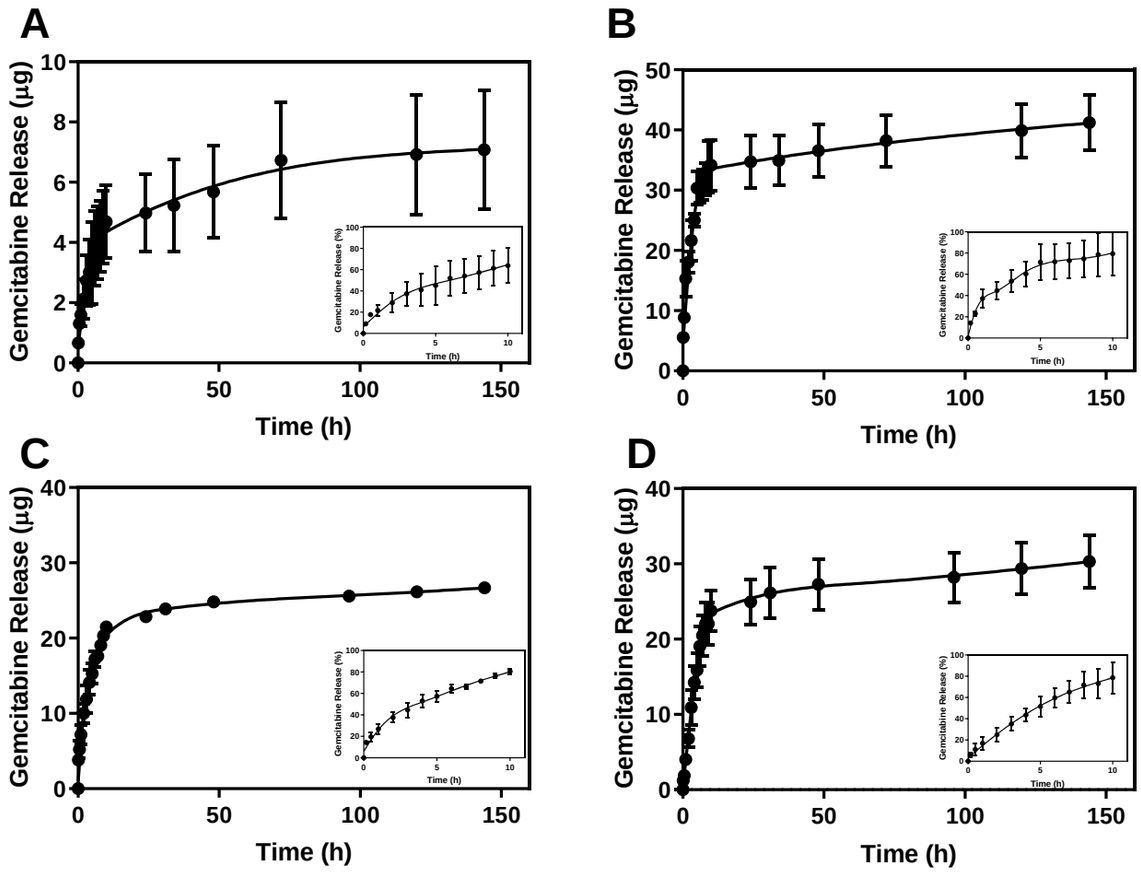

Figure 2.7: Burst release profile is observed in all fibre formulations A rapid release profile is observed for gemcitabine, in which ~80 % of drug is released in the first 10 h followed by a slower secondary release from 24-144 h. Cumulative release of gemcitabine was measured from (**A**) 1 % alginate, (**B**) 2 % alginate, (**C**) 2 % chitosan and (**D**) 3 % chitosan. The percentage of gemcitabine released in the first 10 h is shown in the embedded figures. Values are the mean (±SEM) of triplicates.

In this study, we found higher polymer concentrations led to longer time to total drug release (Table 2.2). The maximum time to total drug release was 336 h (14 days) for 2 % alginate fibres, 1.5-times that of the 1 % alginate fibres (9.5 days). A similar trend was observed between 2 % and 3 % chitosan fibres, where the 2 % chitosan took 6 days to release, while the 3 % fibres took 11 days to release all of the encapsulated gemcitabine.

Table 2.2: The amount and rate of drug released from 30 cm length of fibre and the time taken to reach equilibrium

Fibre	Total amount of drug released (µg)	Rate of release $t_{0\text{-}10h}$ (%/h)	Rate of release $t_{24\text{-}144h}$ (%/h)	Total Release Time*
1 % Alginate	7.0 ± 1.9	5.7 ± 0.9	0.24 ± 0.17	228 h (9.5 days)
2 % Alginate	41.9 ± 6.4	7.3 ± 0.7	0.13 ± 0.07	336 h (14 days)
2 % Chitosan	25.6 ± 0.5	7.1 ± 0.5	0.10 ±0 .02	144 h (6 days)
3 % Chitosan	35.5 ± 6.1	8.0 ± 0.5	0.13 ± 0.08	264 h (11 days)

* Total drug release time represents the time it takes before no further drug release is detected during the experimental period.

2.3.5 Biological Activity

The biological efficacy of the alginate and chitosan fibres was assessed using a number of *in vitro* cell based assays. This is an important step in developing DDSs, as it gives insight into the biocompatibility of the polymer and the cytotoxicity of the eluted drug. This section describes results using human cancer cells in 2D and 3D systems to assess the efficacy of gemcitabine loaded alginate and chitosan fibres.

2.3.5.1 Cell Confluency and Viability

Mia-PaCa-2 and PANC-1 human PDAC cell lines grown as monolayers were incubated with empty or gemcitabine loaded 1 % and 2 % alginate or 2 % and 3 % chitosan fibres and their effect on cell proliferation and viability assessed. Mia-PaCa-2 cells treated with 1 % or 2 % alginate fibres containing 1.2 µg and 7 µg of gemcitabine respectively, displayed a steady decrease in cell growth (as indicated by reduced cell confluency) over 72 h when compared to their respective empty fibre controls (Fig. 2.8 A, B). At 72 h gemcitabine-eluting 1 % and 2 % alginate fibres reduced the confluency of Mia-PaCa-2 cells to 37.8 ±1.1 % and 31.4 ±1.0 %, respectively, while PANC-1 cell confluency was on average 2-fold greater at 66.6 ± 2.7 % and 77.1 ±7.1 %, after 72 h (Fig. 2.9 A, B), likely owing

to the inherent resistance of the PANC-1 cells to gemcitabine (Hong *et al.*, 2009).

Mia-PaCa-2 cells treated with 2 % and 3 % chitosan fibres containing 4.3 µg and 5.9 µg of gemcitabine respectively, exhibited a time-dependent decrease in cell confluency similar to that of the alginate fibres (28.5 ±3.1 % and 40.7 ±9.0 %, respectively at 72 h), however, unlike alginate, this decrease in confluency was also observed for non-drug loaded 2 % and 3 % chitosan fibres (34.7 ±0.9 %) and 37.4 ±0.9 %, respectively), suggesting that the empty fibres were displaying non-specific inhibitory activity (Fig. 2.8 C, D). Non-drug loaded 2 % and 3 % chitosan fibres had less of a toxic effect on PANC-1 cells, while the gemcitabine eluting fibres reduced cell viability at 72 h by 18.6 ±6.5 % and 25.7 ±8.6 % respectively (Fig 2.9 C, D).

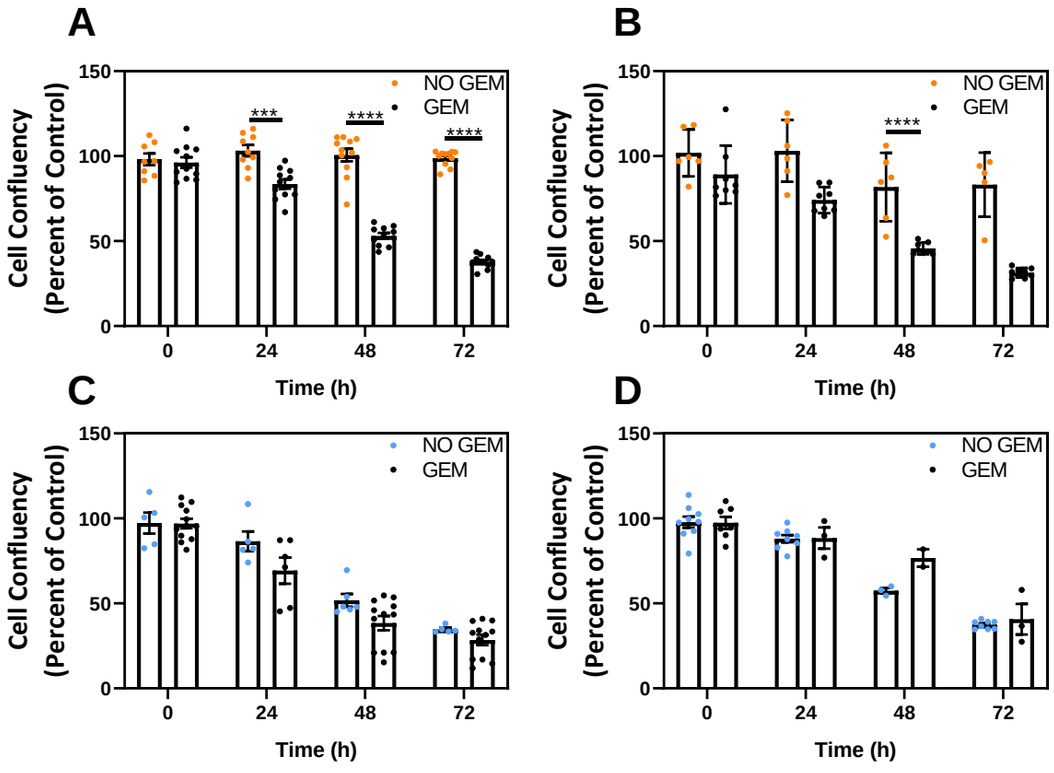

Figure 2.8: Gemcitabine loaded fibres show time dependant effect on cell confluency, while empty chitosan fibres cause reduction in confluency in Mia-PaCa-2 cells. Cell confluency of human PDAC (Mia-PaCa-2) cells after treatment with gemcitabine loaded A) 1 % alginate, B) 2 % alginate, C) 2 % chitosan or D) 3 % chitosan fibres over 72 h. 5 cm lengths of fibre were placed in wells of 96-well plates containing 5000 cells/well and incubated for 72 h. Results are displayed as IncuCyte ZOOM confluency as percent of cell only (no treatment) control. Orange data points represent treatment with empty alginate fibres, blue data points represent treatment with empty chitosan fibres, and black data points represent treatment with gemcitabine loaded fibres. **V**alues are the mean (±SEM) of 12 areas of interest. **** P ≤0.0001. GEM = gemcitabine.

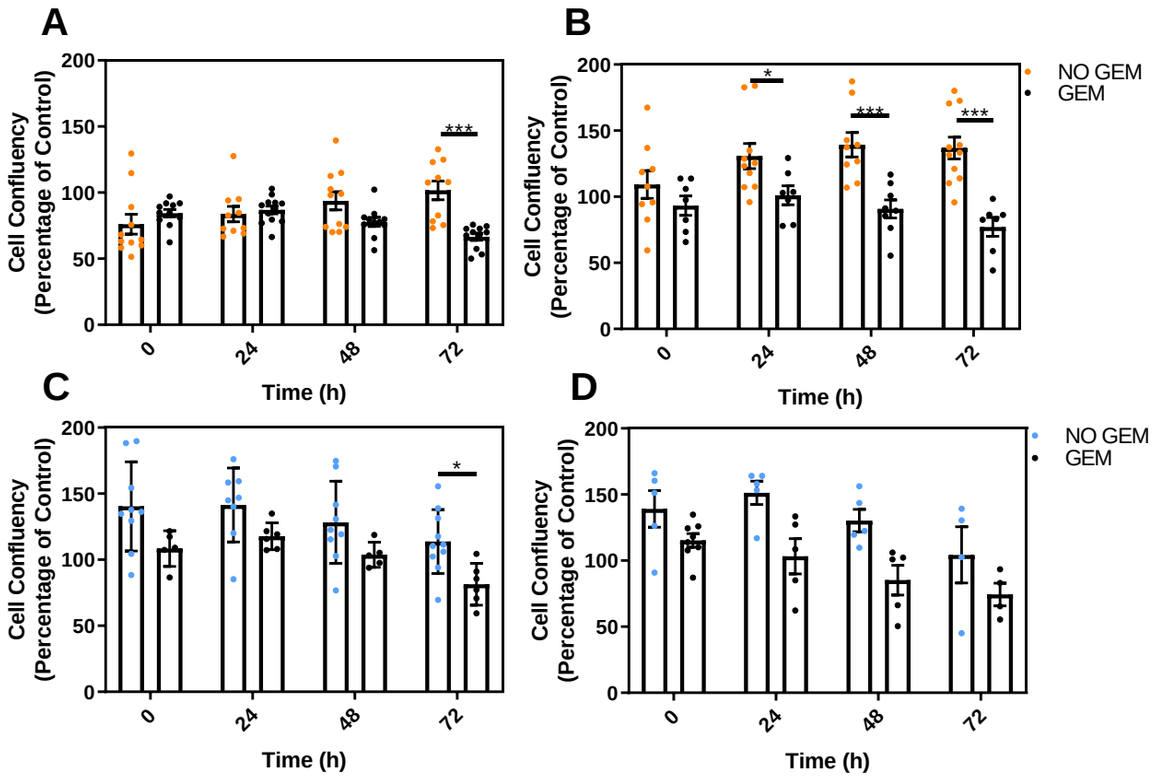

Figure 2.9: Gemcitabine loaded fibres show time dependant effect on cell confluency, while empty chitosan fibres cause reduction in confluency in PANC-1 cells. Cell confluency of human PDAC (PANC-1) cells after treatment with gemcitabine loaded A) 1 % alginate, B) 2 % alginate, C) 2 % chitosan and D) 3 % chitosan fibres over 72 h. 5 cm lengths of fibre were placed in wells of 96-well plates containing 5000 cells/well and incubated for 72 h. Results are displayed as percent of cell only (no treatment) control. Orange data points represent treatment with empty alginate fibres, blue data points represent treatment with empty chitosan fibres, and black data points represent treatment with gemcitabine loaded fibres. Values are the mean (±SEM) of 12 areas of interest. * P ≤0.05, *** P ≤0.001 GEM = gemcitabine.

To confirm decrease in cell confluency equates to reduced viability, a 72 h cell viability study was performed on both Mia-PaCa-2 and PANC-1 cell lines, in which the cells were incubated with each fibre formulation for 72 h before an endpoint MTS assay was performed. Mia-PaCa-2 cells treated with gemcitabine loaded 1 % and 2 % alginate fibres showed a 30.9 ±0.6 % and 53.4 ±2.5 % decrease in cell viability respectively, while the cells treated with the respective non-loaded fibres remained unaffected and had a viability equivalent to the untreated control (Fig 2.10 A). The gemcitabine loaded 2% and 3% chitosan fibre treated cells had a 52.6 ±2.6 % and 75.5 ±8.4 % reduction in cell viability respectively, however the cells treated with the non-loaded fibres displayed a 25.2 ±5.8 % and 35.0 ±6.3 % reductions in viability respectively (Fig. 2.10 B).

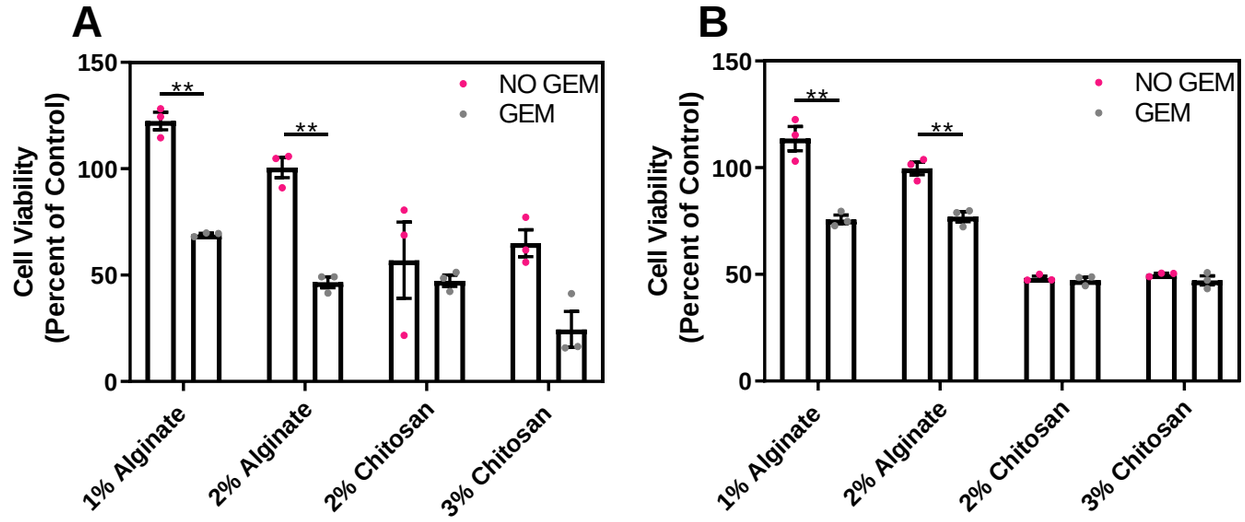

Figure 2.10: Endpoint cell viability assay shows empty chitosan fibres are toxic to cells. 5 cm lengths of fibre formulations of 1 % or 2 % alginate, and 2 % or 3 % chitosan (± gemcitabine) were incubated with A) Mia-PaCa-2 or B) PANC-1 cells for 72 h before an endpoint MTS assay was performed. Results are displayed as a percentage of an untreated control. Pink data points represent treatment with empty fibres; black data points represent treatment with gemcitabine loaded fibres. Values are the mean (±SEM) of triplicates. Experiment performed in triplicate, one representative result shown. ** $P \leq 0.01$. GEM = gemcitabine.

2.3.5.2 Growth Inhibition of Tumour Spheroids

In order to further assess the efficacy of our gemcitabine-eluting 1 % and 2 % alginate fibres and 2 % and 3 % chitosan fibres, we utilized a 3-dimensional (3D) tumour spheroid model. Given PANC-1 pancreatic spheroids spontaneously assemble into loose aggregate spheroids (Vinci *et al.*, 2012) and may not accurately represent the dense fibrotic tissue found in pancreatic cancer, we sought to primarily assess the efficacy of gemcitabine-loaded 1 % and 2 % alginate fibres in the well-studied MCF-7 tumour spheroid model prior to assessment in PANC-1 spheroids. MCF-7 cells form tight, compact spheroids where the diameter can be accurately measured. In addition, they form a clearly visible hypoxic core and act as a superior model to assess the response of drugs that are intended for use on solid tumours (Breslin and O'Driscoll 2013). MCF-7 tumour spheroids were incubated with 1 % and 2 % alginate fibres containing gemcitabine and their growth properties assessed over 17 days (Fig. 2.11).

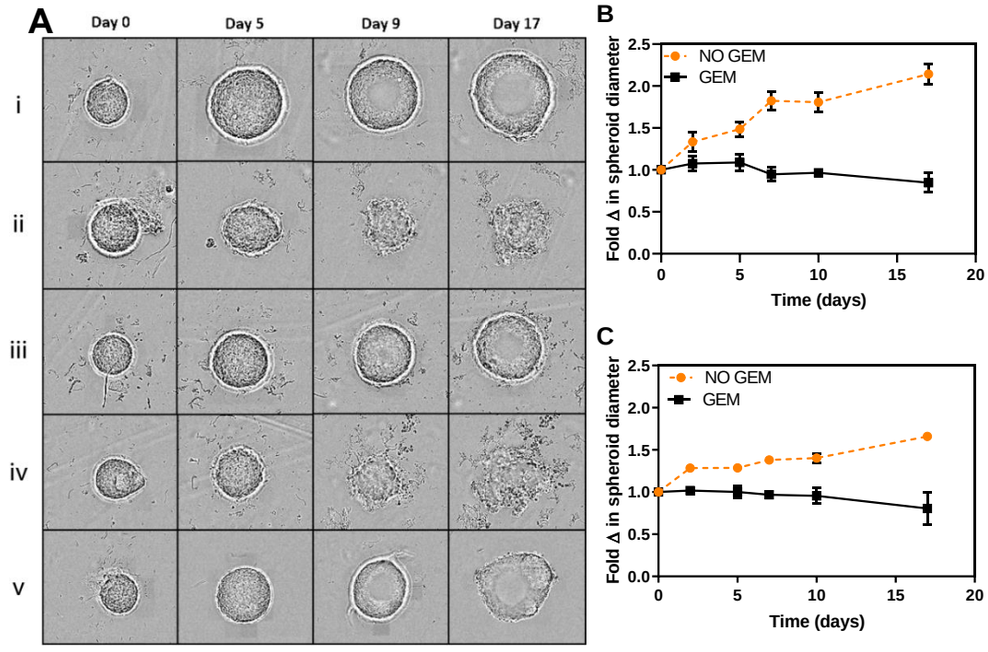

Figure 2.11: Gemcitabine loaded alginate fibres cause a reduction in spheroid diameter. A) Light microscopy images of MCF-7 tumour spheroids after treatment with 5 cm lengths of 1 % alginate fibre (i), 1 % alginate fibre loaded with gemcitabine (ii), 2 % alginate fibre (iii), 2 % alginate fibre loaded with gemcitabine (iv), or no treatment control (v). B) The fold change in spheroid diameter after treatment with 1 % alginate fibre (dashed orange line) or gemcitabine loaded 1 % alginate fibre (solid black line) and C) 2 % alginate fibre (dashed orange line) or gemcitabine loaded or 2 % alginate fibre (solid black line) was calculated from spheroid diameter determined from bright field images acquired at 10 × magnification and are expressed as a function of time. Values are the mean (±SEM) of triplicates. GEM = gemcitabine.

Both 1 % and 2 % gemcitabine-loaded alginate fibres significantly reduced the diameter of MCF-7 spheroids compared to their respective empty fibre controls (Fig. 2.11 A i-v). After 17 days, spheroids treated with empty 1 % or 2 % alginate fibres had a fold diameter change of 2.14±0.12 and 1.66±0, respectively, while spheroids treated with drug-loaded fibres were on average 2-times smaller (0.85±0.11 and 0.81±0.19 fold change in diameter, respectively) (Fig 2.11 B and C). Using an unpaired t test it was determined that the fold change difference in spheroid diameter at 17 days in the 1% and 2% alginate fibre treated groups (± gemcitabine) was significant ($p=0.016$ and $p=0.039$ respectively).

Spheroids treated with control fibres appeared morphologically similar to that of the no fibre control (Fig. 2.11 A v) and no significant difference in diameter was observed on day 17 by one-way ANOVA.

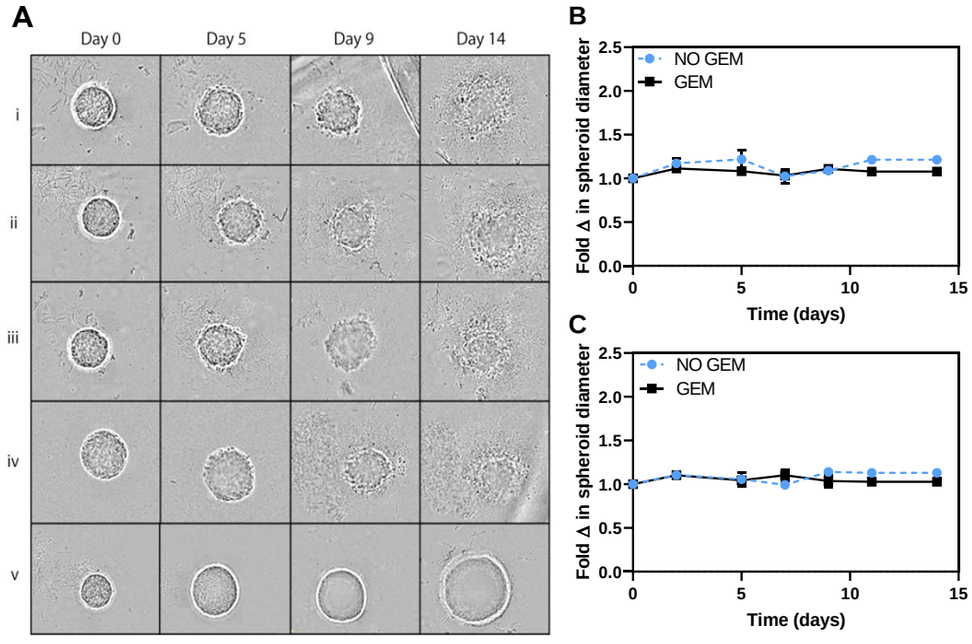

Figure 2.12: Empty chitosan fibres show similar reduction in spheroid diameter as the gemcitabine loaded formulations. A) Light microscopy images of MCF-7 tumour spheroids after treatment with 5 cm lengths of 2 % chitosan fibre (i), 2 % chitosan fibre loaded with gemcitabine (ii), 3 % chitosan fibre (iii), 3 % chitosan fibre loaded with gemcitabine (iv), or no treatment control (v). B) The fold change in spheroid diameter after treatment with 2 % chitosan fibre (dashed blue line) or gemcitabine loaded 2 % chitosan fibre (solid black line) and C) 3 % chitosan fibre (dashed blue line) or gemcitabine loaded or 3 % chitosan fibre (solid black line) was calculated from spheroid diameter determined from bright field images acquired at 10 × magnification and are expressed as a function of time. Values are the mean (±SEM) of triplicates. GEM = gemcitabine.

Spheroids treated with 2 % and 3 % chitosan containing gemcitabine were assessed over 14 days (Fig 2.12), a slightly shorter time as the spheroids reached the maximum size more quickly for accurate live cell imaging and measurement. Spheroids treated with gemcitabine-loaded 2 % and 3 % chitosan fibres showed similar effects over a 14 day period to that of the corresponding control fibres. The morphology of the spheroids treated with either empty 2 % or 3 % chitosan fibres of gemcitabine-loaded 2 % or 3 % chitosan fibres appeared similar (Fig 2.12 i-v). The fold change in diameter of 2 % chitosan with and without loaded gemcitabine was 1.08 ±0 and 1.21 ±0 respectively, while the fold change in the 3 % chitosan treated spheroids was 1.03 ±0.02 and 1.13±0, respectively (Fig 2.12 B and C).

An endpoint viability APH assay confirmed that tumour spheroids treated with gemcitabine-loaded 1 % and 2 % alginate fibres were significantly less viable (47.6 ±1.6 % and 51.4 ±6.1 %) than spheroids treated with corresponding empty fibres (Fig 2.13). Although it appears the empty 1 % and 2 % alginate fibres had a proliferative effect on the spheroids (131.4 % and 117.5 % viability, respectively), this effect was not statistically significant to the untreated control. The 2 % and 3 % chitosan fibres loaded with gemcitabine displayed a 48.6 % and 48.3 % decrease in cell viability, while their respective controls had a 58.3 % and 57.3 % decrease in cell viability (Fig. 2.13).

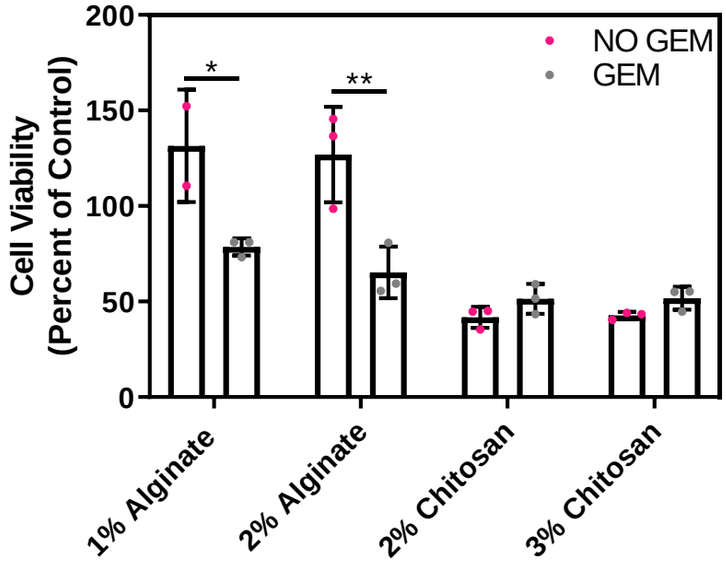

Figure 2.13: Empty chitosan fibres showed toxicity similar to that of gemcitabine loaded fibres on MCF spheroids. 5 cm lengths of fibre (all ± gemcitabine) were incubated with MCF-7 spheroid for 17 (alginate) or 14 (chitosan) days before an endpoint cell viability APH assay was performed. Results are displayed as percentage of untreated control. Pink data points represent treatment with empty fibres, black data points represent treatment with gemcitabine loaded fibres. Values are the mean (±SEM) of triplicates. Experiment performed in triplicate, one representative result shown. * $P \leq 0.05$, ** $P \leq 0.01$ GEM = gemcitabine.

Considering the toxicity displayed by the chitosan, the alginate fibres were selected for further characterisation. To ensure that the result the alginate formulations had on the MCF-7 line were not only limited to that line, loose tumour spheroids generated from the PANC-1 cancer cell line were incubated with alginate fibres containing 1.2 µg gemcitabine. Similarly, the drug-eluting fibres significantly inhibited the growth of PANC-1 spheroids compared to empty alginate control fibres, where inhibition was evident as early as day 3 (Fig. 2.14 A). By day 13, gemcitabine treated spheroids had significantly smaller diameter (Fig 2.14 B). An endpoint cell viability assay found only 6.9 ±0.2 % of the drug treated cells to be viable compared to 83.5 ±5.1 % for non-drug loaded fibre controls (Fig. 2.14 C). Notably, empty 1 % alginate fibres had no effect on the growth or viability of spheroids compared to untreated controls, further confirming biocompatibility in a pancreatic model. A comparison of PANC-1 spheroid growth after incubation with 5 µg/mL free gemcitabine or 5 µg/mL equivalent gemcitabine (1 µg/5cm/200 µL) in drug-loaded fibres found no significant difference in diameter at day 13, indicating bioequivalence (Fig. 2.15).

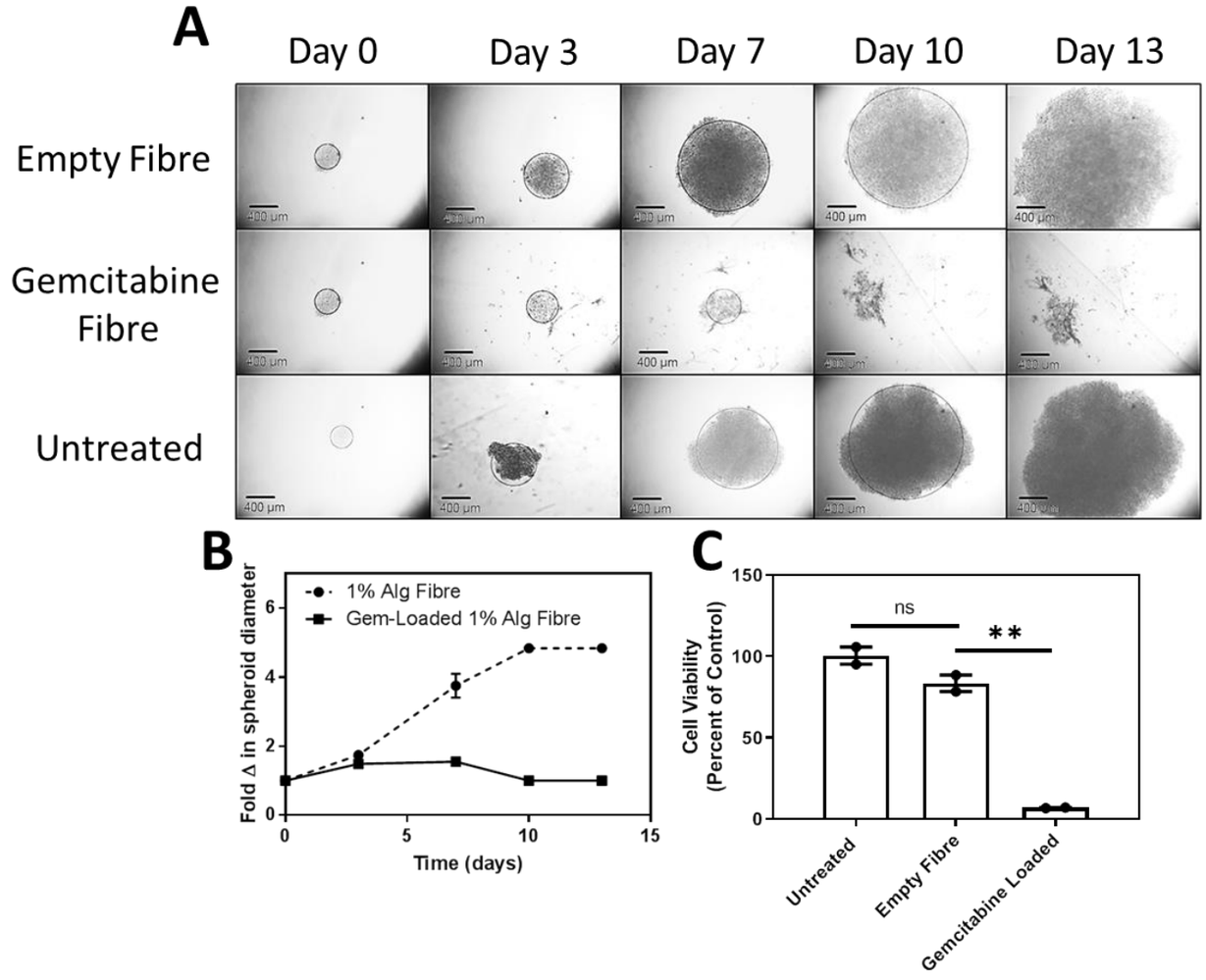

Figure 2.14: Gemcitabine loaded 1 % alginate fibres show significant cytotoxicity on PANC-1 spheroids Light microscopy images of PANC-1 tumour spheroids after treatment with 5 cm lengths of A) 1 % alginate fibre, B) 1 % alginate fibre loaded with gemcitabine (1.2 µg), C) or no treatment control. The fold change in spheroid diameter after treatment with 1 % alginate fibre (dashed line) or gemcitabine-loaded 1 % alginate fibre (solid line) (d), was calculated from spheroid diameter determined from light microscopy images acquired at 10 × magnification. Cell viability was determined at the end of the experimental period (day 13) by APH assay (e). Values are the mean (±SEM) of duplicates. ns = not significant, ** $P \leq 0.01$, Alg = alginate, Gem = gemcitabine.

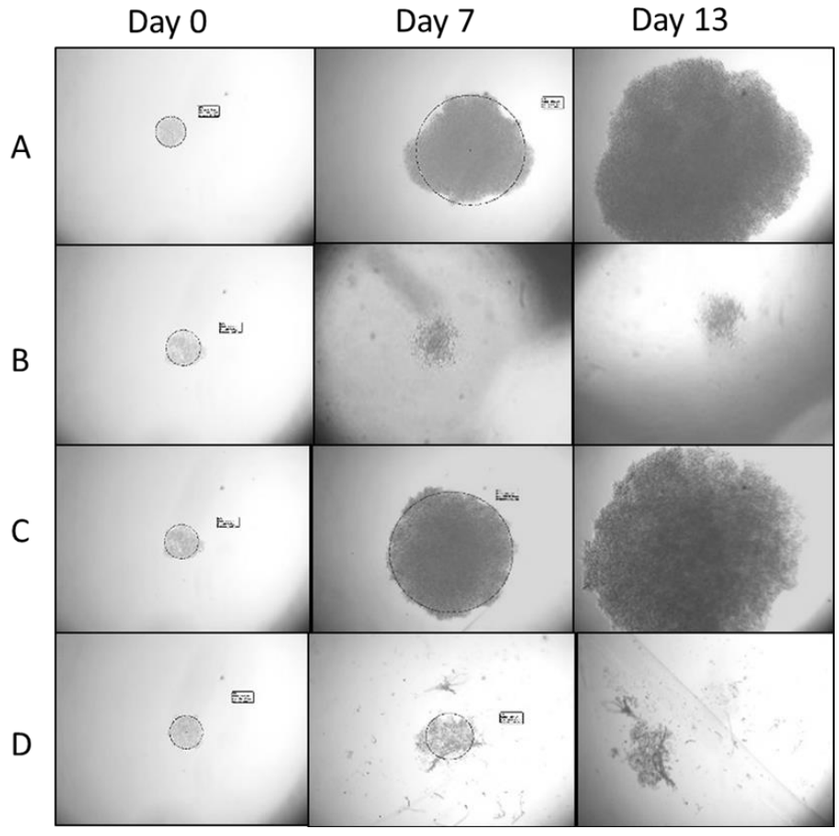

Figure 2.15: Gemcitabine eluted from 1 % alginate and free gemcitabine show bioequivalence when tested on PANC-1 spheroids. Light microscopy images of PANC-1 tumour spheroids treated with A) Untreated, B) free gemcitabine (1 µg/200 µL), C) 5cm 1 % alginate fibres, or D) 5cm 1 % alginate fibres loaded with 1.2 µg gemcitabine.

2.3.5.3 Drug Accumulation

We further utilized the MCF-7 tumour spheroid model to assess drug uptake when delivered continuously from alginate fibres. Doxorubicin as was used as our model drug due to its inherent fluorescent properties (Shen *et al.*, 2008, Boddu *et al.*, 2010, Mansoor *et al.*, 2015). Tumour spheroids were incubated with doxorubicin loaded alginate fibres or free doxorubicin at an equivalent amount (15 ng), or 10-folder higher amount (150 ng) than that encapsulated in fibres. Spheroids were washed at each imaging time point to simulate the clearance of extracellular fluid from the body. Greater accumulation, as indicated by higher fluorescence intensity, was observed for spheroids incubated with doxorubicin loaded 1 % alginate fibres, compared to free doxorubicin (Fig. 2.16 A,B,C). Doxorubicin delivered from alginate fibres demonstrated linear ($r^2 = 0.9952$) and homogenous uptake of the drug over 320 min,

while the free doxorubicin showed minimal uptake that remained static over time (data not shown). Interestingly, spheroids incubated with 10 × doxorubicin demonstrated heterogeneous uptake, with some regions of the spheroid accumulating greater amounts of drug than others. By 120 min, evidence of doxorubicin efflux from the tumour spheroid was observed, as indicated by the arrowhead in Fig. 2.16 C.

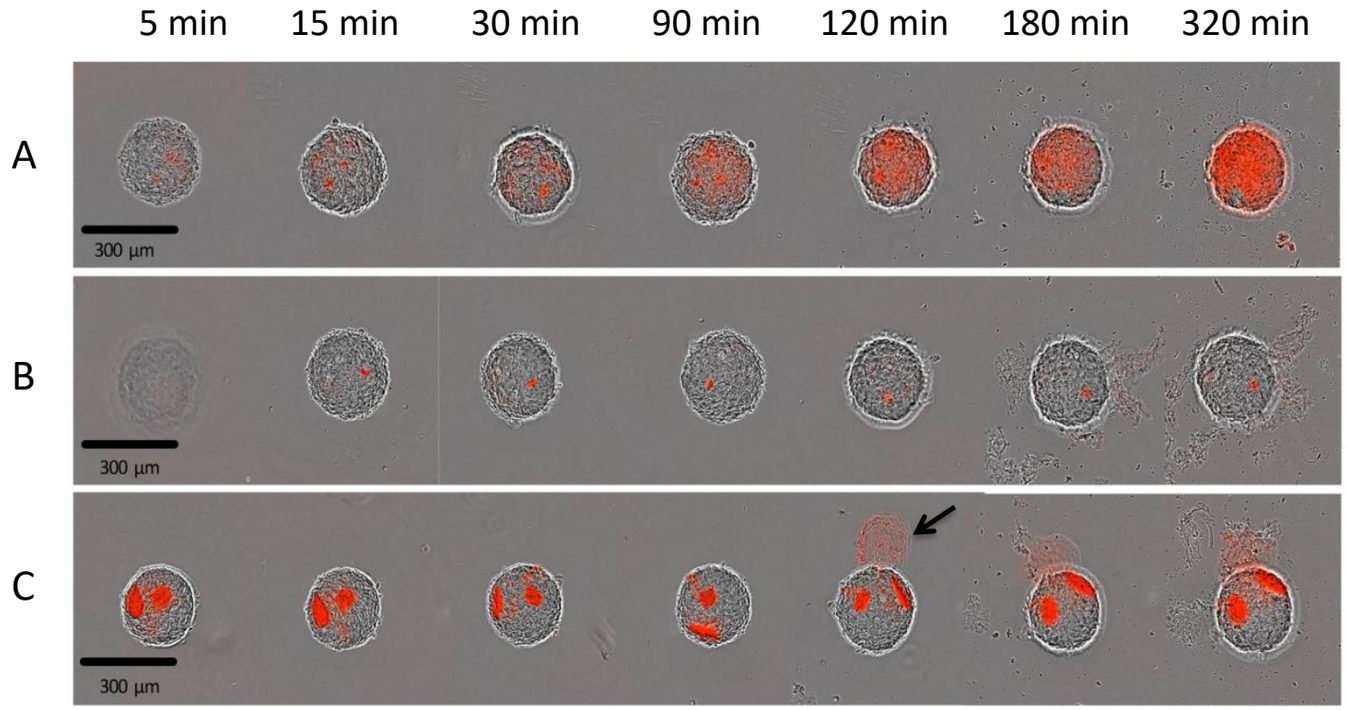

Figure 2.16: Doxorubicin uptake into MCF-7 spheroids is increased when eluted from alginate fibres. MCF-7 tumour spheroids were treated with A) 1 % alginate fibres containing doxorubicin (15 ng), B) equivalent amount of free doxorubicin (15 ng), or C) 10 × equivalent amount of free doxorubicin (150 ng) for 5 mins then washed prior to imaging at 10 × magnification at the indicated timepoints.

To assess any potential permeation effect of the alginate on drug uptake and accumulation, a study was performed over 4 h in which the uptake of free doxorubicin in the presence of a fully formed, crosslinked and dried 1 % alginate fibre was assessed. Spheroids incubated 1 × and 10 × free doxorubicin (24 ng and 240 ng respectively) (Fig. 2.17 A and B) had a corrected total cell fluorescence (CTCF) of 23,350 and 23,105 respectively, while the spheroids treated with a doxorubicin loaded fibre had a CTCF that was 30.7-31.2 fold higher at 718,595. (Fig. 2.17 C). Spheroids treated with free doxorubicin in the presence a 2cm length of 1 % alginate fibre (Fig. 2.15 D), 2 % alginate fibres (Fig. 2.17 E) or 3 % chitosan fibre (Fig. 2.17 F) showed CTCF of 37,782, 187,855, and 23,887 respectively

(Appendix Fig. A2). A further study was performed in which spheroids were incubated in the presence of uncrosslinked polymer solution with free doxorubicin. This was tested on both MCF-7 (Appendix Fig A3 A) and PANC-1 (Appendix Fig. A3 B) spheroids and imaged over a period of 30 h. There was no increase in drug uptake between the spheroids incubated with doxorubicin alone and those incubated with uncrosslinked polymer solution with equivalent amounts of free doxorubicin when co-administered.

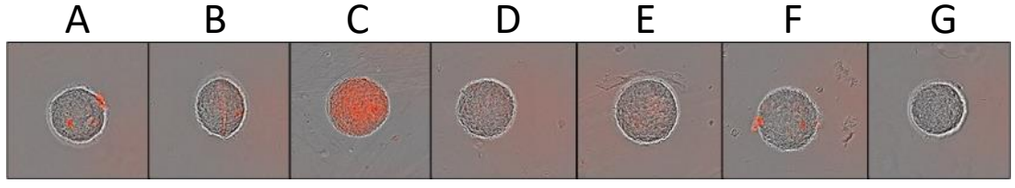

Figure 2.17: Three was no effect of crosslinked alginate when co-administered with doxorubicin on the uptake of doxorubicin. MCF-7 tumour spheroids were treated with A) 1 × free doxorubicin (24 ng), B) 10 × free doxorubicin (240 ng), C) 2 cm length of 1 % alginate doxorubicin loaded fibre (24 ng), D) 2cm length of 1 % alginate fibre + 1 × free doxorubicin, E) 2 cm length of 2 % alginate fibre + 1 × free doxorubicin (24 ng), F) 2 cm length of 2 % chitosan fibre + 1 × free doxorubicin or G) untreated for 4 hours before being washed and imaged at 10 × magnification using the IncuCyte ZOOM.

2.4 Discussion

This chapter focused on the development and preclinical assessment of gemcitabine loaded alginate and chitosan fibres. Gemcitabine has been part of the clinical standard of care for PDAC patients for over 20 years, however the difficulty in delivering adequate concentrations to the tumour has prompted the need for improved ways to deliver this drug (Neesse *et al.,* 2011, Dimou *et al.,* 2012). Here we discuss the physicochemical properties and *in vitro* efficacy results of alginate and chitosan fibres formulations loaded with and without gemcitabine.

2.4.1 Physicochemical Characterisation

Polymeric fibres were prepared from alginate or chitosan by taking advantage of ionic crosslinking. Alginate being a polyanoinic polymer, forms hydrogels in the presence of divalent cations (like Ca^{2+}) owing to ionic cross-linking via calcium bridges between the L-guluronic acid residues on adjacent chains (Berger *et al.,* 2004, He *et al.,* 2012). On the other hand, chitosan, being a polycationic polymer, forms hydrogels based on the reaction between the positively charged amino groups of chitosan and negatively charged ions (such as NaOH) (Berger *et al.,* 2004, Ventura *et al.,* 2011). Differences in morphology were observed between alginate and chitosan fibres when loaded with gemcitabine. SEM images of the surface morphology showed that alginate developed ridges along its surface, however this is most likely an artefact of SEM imaging, by which the fibre further dehydrates under vacuum and is not of concern for the final product. The internal porosity of the chitosan and alginate fibres was also very different – with the alginate displaying very large pores and the chitosan displaying very small pores. Smaller pores are advantageous for drug release, as it decreases the surface area of the fibre, and reducing the uncontrolled rapid release of drug (Sill and von Recum 2008). The fibres fabricated in this chapter have had their tensile strength assessed, in order to test their flexibility and the extent to which they can stretch before breaking. Higher polymer concentrations caused a loss of elasticity, which can be attributed to the increase in the G block content, a phenomenon previously shown to increase the Young modulus (Draget *et al.,* 1991). Overall however, there was no significant difference in the elasticity of the fibres after gemcitabine addition. These fibres therefore possess the properties to form a 3D structure by weaving or braiding into a patch for covering the outer surface of a tumour,

however this is not explored further in this thesis. Instead, the information gained from this chapter is utilised in subsequent chapters in fabrication of dual-drug loaded coaxial implant (Chapter 3 and 4), and for immunotherapy DDS proof of concept studies (Chapter 5).

The gemcitabine loading and release was assessed in order to get an indication of how the release profiles will look when performing *in vitro* cytotoxicity tests. The loading between formulations varied slightly, with the higher polymer concentrations having a higher drug loading. As the polymer concentration increases, as do the polymer chains that interlock, and more interlocking chains results in more area for drug to be trapped and incorporated into the fibre. Although the loadings were different between formulations, there was no significant difference in the release kinetics of gemcitabine. Gao *et al.*, reported an analogous trend in which the duration of 5FU release from poly(lactic acid) (PLLA) wet-spun fibres was increased from 5 to 20 days when the polymer concentration was doubled (Gao *et al.,* 2007). While promising, this is dependent not only on polymer type, but also polymer concentration. As concentration increases so too does viscosity and this can have a significant impact on the manufacturing process of the fibres. Thus suitable working concentrations of polymer must be carefully chosen to maintain optimum spinning conditions and continuous fibre formation, whilst minimizing negative impacts on drug-loading and release kinetics.

The release profile observed from both the alginate and chitosan formulations showed an initial burst release, in which over 80 % of the drug is released in the first 10 h. This is unsurprising, as chitosan and alginate are both hydrogels. Hydrogels are hydrophilic polymers that are able to hold large amounts of water within their 3 dimensional structure, and swell when placed in aqueous environments (Ahmed 2015). The swelling properties of hydrogels contribute greatly to the release of drug into solution (Siepmann and Peppas 2001, Lin and Metters 2006). As the dehydrated fibres begin to instantly swell when placed in aqueous solution, interstitial spaces become filled with water. At the same time, the dissolved drug diffuses through the swollen hydrated matrix into the external releasing medium. This simultaneous absorption of water and desorption of drug via a non-Fickian (swelling-

controlled) diffusion mechanism may be used to describe the biphasic release profiles exhibited by gemcitabine in Fig. 2.7. For example, as the swelling ratio becomes greater, the water imbibition into the hydrogel increases and as a result, the drug diffusion coefficient increases leading to greater release of drug from the fibres in the first 10 h.

Modulation of the burst release profile displayed by hydrogel materials is one of the biggest challenges facing their use in *in vivo* drug delivery applications. One way to improve their release profile would be to employ covalent crosslinking methods where the drug is attached to the polymer chains prior to gelation. This tethering method limits release of the drug which occurs only when the hydrogel breaks down or the molecular tether is broken (Hoare and Kohane 2008). Linkages between the drug and polymer that are susceptible to enzymatic degradation have been used to control the speed and timing of release of drugs from a number of different polymeric-based DDS (West and Hubbell 1995, Bhattarai *et al.,* 2010). If the delay of drug release using cross-linked hydrogels is not sufficient to slow the release rate for long-term applications, a secondary release system may be incorporated into the hydrogel, such as drug containing micro- or nano-capsules (Leach and Schmidt 2005). For example PVA-based hydrogels showed loss of the dexamethasone payload over 2 weeks, but when the steroid was loaded into encapsulated microspheres, drug release was slowed to ~6 %/month (Galeska *et al.,* 2005). For implantable devices, the ideal release profile would involve an initial release of drug at a therapeutic concentration, followed by a sustained release at this concentration (Fig 1.5). This is often difficult to predict *in vitro*, a concept which will be further discussed in Chapter 3.

2.4.2 Biological Evaluation

Following physicochemical characterisation, *in vitro* studies were performed to assess the biocompatibility of the polymer and the efficacy of the drug eluting polymers in 2D monolayer and 3D tumour spheroid models. Tumour spheroids provide an intermediate model between the oversimplified 2D monolayer cell culture models and more complex *in vivo* models (Hirschhaeuser *et al.,* 2010). Compared to cells grown in 2D, 3D spheroids more accurately recapitulate and maintain the functional phenotype and heterogeneity of human cancer cells found within tumour

tissues (Mehta *et al.,* 2012). For example, tumour spheroids develop many characteristics of an actively growing tumour, such as oxygen, nutrient and catabolite gradients when they reach a size of 200-500 μm in diameter (Hirschhaeuser *et al.,* 2010). A necrotic core begins to develop when the tumour spheroid reaches a size ~500 μm (McLeod *et al.,* 1997). The cells on the spheroid periphery reflect the *in vivo* characteristics of actively cycling tumour cells, while the inner cells are quiescent, display stem cell-like properties and are often chemoresistant (Hirschhaeuser *et al.,* 2010). Further, their 3D architecture can be used to better model the physical and physiological barriers impacting upon drug penetration, the latter of particular importance to PDAC.

The alginate polymer alone showed good biocompatibility, with no adverse effects on 2D or 3D systems, its gemcitabine loaded counterpart showed toxicity as was evidenced by reduction in cell proliferation, cell viability, and spheroid morphology and viability. The empty chitosan fibres however showed a toxic effect that was similar to that of the gemcitabine loaded fibres. It reduced confluency and viability in both 2D monolayer experiments, and also reduced spheroid diameter, structure and viability. While chitosan is approved for its use in wound healing applications, there are also reports detailing the cytotoxic activity of chitosan and chitosan nanoparticles (Hu *et al.,* 2011). This is largely dependent on the concentration of chitosan, its molecular weight and degree of deacetylation (Ma and Lim 2003, Huang *et al.,* 2004, Qi *et al.,* 2005, Loh *et al.,* 2010). For example, Huang *et al.,* found that the toxicity of both chitosan and chitosan nanoparticles to A549 cells was significant at concentrations above 0.741 mg/mL and was further increased when using chitosan with higher degrees of deacetylation. The chitosan used in our study has a high degree of deacetylation (75-85 %), this together with the high concentrations used in biological experiments (5 cm fibre/ 200 μL media; equiv. 6.26 mg/mL) may have played a role in the toxicity observed. In addition to this, Yan *et al.* formulated PVA/chitosan coaxial fibres, in which the PVA core was loaded with doxorubicin and the chitosan sheath was labelled with FITC. An internalization experiment performed with SKOV3 cells found doxorubicin to accumulate in the nucleus as expected, however uptake of FITC labelled chitosan into the nucleus was also observed (Yan *et al.,* 2014). This indicates as chitosan breaks down, polymer fragments may also be taken up by cells and have a similar toxic effect to that of chitosan nanoparticles at increasing concentrations. Another potential problem facing the use of chitosan fibres for *in vivo* applications is that the majority of the

crosslinkers and solvents used to form chitosan fibres using the wet spinning method leave residual toxic traces either inside, or on the surface of the fibre (Berger *et al.,* 2004). The inhibitory effect of the empty chitosan fibres observed in this study could also be attributed to residual NaOH from the coagulation solution or the acetic acid used to dissolve chitosan prior to spinning. Given the above results, and that any further wash steps to remove residual solvent would have resulted in significant hydrogel swelling, drug loss and a gel state unsuitable for *in vitro* applications, we chose to use alginate as the choice for gemcitabine and other hydrophilic drug encapsulation for all experiments in subsequent chapters.

The 3D architecture of an *in vivo* tumour with poor perfusion presents both physical and physiological barriers for drug penetration and accumulation (Minchinton and Tannock 2006). This is particularly problematic in PDAC where increased desmoplasia contributes to increased stromal stiffness and high interstitial fluid pressures. Together with significant hypo-vascularity this results in a low drug concentration at the target tumour site and invariably an incomplete response (Shepard 2015). When we performed a simple uptake study, it was observed that there was significantly more uptake of doxorubicin into spheroids that was eluted from the fibre compared to the free drug. The improved accumulation of encapsulated drug to free drug is likely due to sustained release from the fibre over time, but thought to potentially be attributed to the permeation enhancing effects of the polymer (Thanou *et al.,* 2001, Bernkop-Schnürch *et al.,* 2003, Di Colo *et al.,* 2008, Sadeghi *et al.,* 2008). Penetration enhancing polymers have primarily been explored in the context of drug delivery. The hydrogel chitosan is a well-known penetration enhancer, as it disrupts tight junctions which increases permeability due to its polycationic properties (Ranaldi *et al.,* 2002). This therefore led to a simple study to assess whether the alginate itself was having an effect on the uptake. The study in which an alginate fibre was added to the media at the same time as the free doxorubicin (Fig 2.17) confirms that the presence of the polymer or the polymeric fibres themselves are not acting as penetration enhancers. Alginate is not a reported penetration enhancer; which is unsurprising due to its anionic properties; however there is little evidence in the literature that this has been explored, so warrants further investigation.

2.4.3 Conclusions

This chapter described the feasibility of using the naturally derived hydrogels chitosan and alginate for the delivery of gemcitabine. The biocompatibility alginate was superior to that of chitosan which had significant non-specific toxicity to cells, while all drug loaded formulations showed efficacy on 2D and 3D *in vitro* cell models. The wet spinning method as a platform for fabrication of drug loaded fibres was validated as a simple and high throughput method for drug loaded fibre fabrication. This study has provided a basis for which further studies into fabrication of dual drug loaded fibres can be explored, as well as modifications of the flexible fibres into a 3D structure suitable for intratumoural implantation can be performed, which will be explored in the following chapters.

Chapter 3: Dual Delivery of Gemcitabine and Paclitaxel by Wet Spun Coaxial Fibres Induces Pancreatic Ductal Adenocarcinoma Cell Death and Sensitises Cells to Radiation.

Portions of this chapter have been prepared for publication in the following work:

Wade SJ, Piper, AK, Talebian S, Aghmesheh M, Foroughi J, Wallace GG, Moulton SE and Vine KL. Dual delivery of gemcitabine and paclitaxel by wet-spun coaxial fibres induces pancreatic ductal adenocarcinoma cell death and sensitises cells to radiation.

Author contributions: Samantha J Wade and Kara L Vine designed the experiments; Samantha J Wade, Sepehr Talebian and Ann-Katrin Piper performed the experiments and analysed the data; Samantha J Wade wrote the manuscript. All authors edited the manuscript for submission.

A provisional patent has been filed based on the work presented in this chapter

Wade SJ, Talebian S, Aghmesheh M, Foroughi, J, Wallace GG, Moulton SE, Vine KL. An Implantable Device and a Method for Implanting Said Device in a Subject. Patent number: 2018903570. Date filed: 23/09/2018

3.1 Introduction

It is common in the clinic to deliver multiple chemotherapeutic agents at different stages throughout PDAC treatment, with anywhere from 1-3 different agents used in combination to treat PDAC. Chapter 2 described the fabrication and characterisation of gemcitabine loaded wet spun 1 % or 2 % alginate and 2 % and 3 % chitosan fibres. This chapter will expand on, and further describe, the fabrication and *in vitro* cytotoxicity of a fibre loaded with two chemotherapy drugs: gemcitabine and paclitaxel. As discussed in Chapter 1, gemcitabine administered as a single agent was the gold standard for PDAC treatment for >20 years, however the development of drug resistance to this agent typically occurs in a number of weeks, despite initial sensitivity to treatment (Binenbaum *et al.*, 2015). This rapid resistance is a hallmark of PDAC, and is just one of the multitude of factors that leads to recurrence and poor survival outcomes (Amrutkar and Gladhaug 2017). The introduction of *nab*-paclitaxel to the gemcitabine regimen led to increased survival and quickly became the new standard of care for metastatic PDAC patients (Von Hoff *et al.*, 2013). The combination of *nab*-paclitaxel and gemcitabine was shown to increase the overall survival from 6.6 months when treated with gemcitabine alone, to 8.7 months. An extended follow up showed that 4 % of patients who received the *nab*-paclitaxel and gemcitabine regimen were alive at 36 months, and 3 % at 42 months, while no patients in the gemcitabine alone group survived past 36 months (Goldstein *et al.*, 2015). Ideally, chemotherapeutics delivered in combination will have different mechanisms of action which is important in preventing drug resistance. Drug resistance in cancer cells is complicated and involves many mechanisms such as alteration in drug transport and metabolism, mutation, amplification or reactivation of drug targets, microenvironment crosstalk, activation of alternative pathways, altered DNA response (Pan *et al.*, 2016). In addition, tumours are heterogeneous, so when treating them with a single chemotherapy drug, only a certain cell population may respond allowing the remaining cell population to continue proliferating and eventually render the monotherapy treatment ineffective (Pan *et al.*, 2016). Paclitaxel and gemcitabine disrupt the cell cycle in different stages, which reduces the risk of a singular cell subtype being eliminated while resistant cells continue to grow (Passacantilli *et al.*, 2018). Administration of a singular drug in different ways is another way to increase the effectiveness of a chemotherapeutic. A study with 92 patients with PDAC (91% who had metastatic disease) showed

that a fixed dose of gemcitabine which involves infusion of gemcitabine (1,500 mg/m^2 over 150 min) compared to the standard treatment (2,000 mg/m^2 over 30 mins) significantly improved overall survival (8 months in fixed dose arm vs 5 months in standard arm) (Tempero *et al.*, 2003). While this study showed that there was significantly higher levels of intracellular gemcitabine triphosphate (active form of gemcitabine), there was significantly higher grade 3 and 4 haematological toxicity in patients who received the fixed dose arm, and therefore a patient's performance status would need to be considered prior to starting fixed dose infusion.

Systemic administration of multiple chemotherapeutics is not without its disadvantages. While a combination approach may have therapeutic benefits, the side effects are often increased, especially when the drugs have similar toxicity profiles. This can rapidly lead to cessation of treatment. Furthermore, drug interactions need to be considered as this can lead to significant unwanted side effects, where for example, one drug may inhibit the metabolic process that allows the other drug to be cleared (Bayat Mokhtari *et al.*, 2017). A combinatorial approach is not limited to only chemotherapeutics however.

Currently, radiation in combination with chemotherapy has not shown significant survival benefit in patients with locally advanced PDAC (Hammel *et al.*, 2016, Ng *et al.*, 2018). There have been some recent phase I trials however that have shown indications of increased efficacy of radiation therapy with a combination of chemotherapy drugs that warrant further investigation and larger phase II and III trials (Shabason *et al.*, 2018, Takahashi *et al.*, 2018). With any potential increased survival benefits of multimodality therapy however, comes the potential for increased side effects of the treatments, which often results in cessation of treatment and disease progression.

These issues of toxicity from systemic delivery and multimodality treatments further highlight the importance of local drug delivery, where multiple drugs can be delivered directly to the site of disease, significantly reducing the chances of intolerable nonspecific toxicity. This chapter describes the fabrication of an alginate and PCL (Alg/PCL) coaxial fibre that has an internal core-sheath morphology that allows for the simultaneous loading and delivery of gemcitabine and paclitaxel (termed dual-drug loaded hereafter). This all in one formulation is beneficial over single

drug loaded implants, as both of the drugs can be released in the same location, reducing the risk of cancer cell resistance to a singular chemotherapeutic. This chapter describes the cytotoxic activity of this fibre formulation *in vitro*, as well as its efficacy in combination with radiotherapy. The hydrophobicity of paclitaxel meant that an equally hydrophobic polymer was required, and in this study PCL was the polymer selected, while alginate remained the choice of polymer for loading gemcitabine. These polymers are both FDA approved (PCL for sutures and implants for bone healing and hormonal contraception, alginate for dietary supplements) which can be beneficial at later stages of product testing as it may speed up the commercialisation and regularity processes.

The specific aims of this chapter were to:

1. Assess the ability of two different hydrophobic polymers, polycaprolactione and poly(lactic-co-glycolic acid) to be fabricated using the wet-spinning method and their suitability to dissolve the hydrophobic drug paclitaxel
2. Fabricate coaxial fibres from hydrophilic and hydrophobic polymers as the core and sheath that are simultaneously loaded with gemcitabine and paclitaxel, respectively, and assess their biophysical properties
3. Assess the biocompatibility and cytotoxicity profiles the dual-drug loaded coaxial fibres in *in vitro* cell based models of PDAC
4. Assess the efficacy of multimodality therapy of dual-drug loaded fibres in combination with radiotherapy using a clonogenic cell survival assay

3.2 Materials and Methods

3.2.1 Materials

Sodium alginate, polycaprolactone (PCL), poly(lactic-co-glycolic acid) (PLGA) calcium chloride ($CaCl_2$), calcium carbonate ($CaCO_3$), sodium hydroxide (NaOH), glucono delta-lactone (GDL), fluorescein sodium salt, absolute ethanol, crystal violet, sirius red, kolliphor EL, L-glutamine, penicillin/streptomycin (PenStrep), Tween-80, Tween-100, hydrocortisone, P-nitrophenyl phosphate and sodium acetate were from Sigma-Aldrich Co. USA. Gemcitabine hydrochloride was from Toronto Research Chemicals, CA. Paclitaxel was from FocusBio, Australia. Anzatax (Pfizer) was kindly supplied by Dr Morteza Aghmesheh (Illawarra Cancer Care Centre). Simulated biological fluid (SBF) was prepared using analytical grade reagents consisting of 5.403 g l^{-1} NaCl, 0.504 g l^{-1} $NaHCO_3$, 0.426 g l^{-1} $NaCO_3$, 0.225 g l^{-1} KCl, 0.230 g l^{-1} $K_2HPO_4 \cdot 3H_2O$, 0.311 g l^{-1} $MgCl_2.6H_2O$, 0.8 g l^{-1} NaOH, 0.293 g l^{-1} $CaCl_2$, 0.072 g l^{-1} Na_2SO_4 and 17.892 g l^{-1} HEPES as buffering agent. The pH was adjusted to 7.40 ± 0.05 using 1.0 M NaOH solution. Phospholipase D was from Sapphire Bioscience, Australia. The CellTiter 96® Aqueous One Solution Cell Proliferation Assay (MTS) was from Promega, Australia. DMEM-High glucose media and RPMI-1640 media were made in house. N2, EGF, bFGF and acetonitrile were from ThermoFisher, Australia. Foetal calf serum was from Bovogen Biologicals, Australia. Hematoxylin and eosin were from POCD Sciences, Australia. Picric acid, Trypsin/EDTA and dimethyl sulfoxide (DMSO) were from Life Technologies, Australia. Dimethylformamide (DMF), chloroform and N-Methyl-2-pyrrolidone (NMP) were from RCI Labscan, Thailand.

3.2.2 Spinning Solutions

A number of spinning solutions were prepared in order to determine the most biocompatible hydrophobic materials and the details summarised in Table 3.1. PCL was prepared at a concentration of 10 %, 15 % and 20 % w/v by adding PCL pellets to DMF or chloroform while stirring at 70 ^oC and mixed overnight. PLGA (75:25) was prepared at a concentration of 20 % w/v by adding PLGA pellets to NMP or DMSO while stirring at 50 °C and mixed overnight.

Alginate solution was prepared by using an optimised internal ionic crosslinking method (Kuo and Ma 2001, Jang *et al.*, 2014). Firstly, 15 mM $CaCO_3$ was added to water, before adding alginate powder to a final concentration of 3 % w/v. In gemcitabine loaded solutions, the gemcitabine was added at a final concentration of 50 mM to water, before adjusting the solution to pH=7, then $CaCO_3$ and alginate were added and stirred overnight. Immediately before spinning, glucono delta-lactone was added to a final concentration of 30 mM and stirred to dissolve. Paclitaxel for injection (Anzatax) or as a pure powder was added to PCL solution to give a final concentration of 15 mM and stirred until thoroughly mixed. Fluorescein spinning solution was prepared by dissolving 2 mM of fluorescein sodium salt into the alginate solution before spinning.

Table 3.1: Hydrophobic polymer conditions and pump rates

			Pump Rate (mL/h)	
Polymer	**Polymer concentration (% w/v)**	**Solvent**	**Empty**	**Drug loaded**
PCL	15	Chloroform	50	-
PCL	10, 15, 20	DMF	50	50
PLGA	20	DMSO	25	-
PLGA	20	NMP	25	-

DMF: Dimethyl formamide
DMSO: dimethyl sulfoxide
NMP: N-Methyl-2-pyrrolidone

3.2.3 Wet Spinning of Fibres

Spinning solutions were placed in 10 mL syringes and placed in a programmable syringe pump (kdScientific KDS100). Coaxial fibres were spun using a novel coaxial spinneret with two input ports (Mirabedini *et al.*, 2015). Solution injected through port A formed the shell layer, and solution injected through port B formed the core. Coaxial fibres were prepared with a 15 % PCL shell and 3 % alginate core, and with a 3 % alginate shell and 15 % PCL core for comparison. Both PCL and the alginate were extruded at 50 mL/h into a bath containing 2 % w/v $CaCl_2$ prepared in 20 % v/v ethanol solution, and collected on a rotating mandrel at a fibre formation rate of 65 cm/min.

3.2.4 Fibre Morphology

Scanning electron microscopy (SEM) was used to observe the internal morphology of hydrated fibres and were images as per Chapter 2, Section 2.2.5.

3.2.5 Fibre Diameter

Fibre diameter was measured as per Chapter 2, Section 2.2.5.

3.2.6 Fibre Echogenicity

1 OD 10 nm gold nanoparticles were mixed with 3 % alginate solution prior to spinning at a concentration of 2.8×10^{12} particles/mL. Coaxial fibres were fabricated with the AuNP 3 % alginate core, and 15 % PCL solution for the shell. Fibres were threaded through an ultrasound training model, and imaged using a clinical ultrasound machine by Verity Gotch (Illawarra and Shoalhaven Local Health District).

3.2.7 Drug Loading

The theoretical drug loading of gemcitabine and/or paclitaxel was calculated using the formula as per Chapter 2, Section 2.2.8. The actual loading of drug was determined by performing a drug release experiment with the endpoint defined by no further release, and measured using high performance liquid chromatography (HPLC). Gemcitabine release was performed in SBF, while paclitaxel release was performed in absolute ethanol for complete drug extraction.

3.2.8 Drug Release

3.2.8.1. Model Drug Release: Fluorescein

Before performing release studies using paclitaxel and gemcitabine, fluorescein loaded single 3 % alginate fibres and Alg/PCL coaxial fibres with a fluorescein loaded alginate core were fabricated. A release study was performed to give an indication of what the release would look like from the alginate core before performing the release using costly agents. Fluorescein release was performed on 30 cm lengths of fibre in SBF with 1× PenStrep at 37 °C. Media was refreshed at each timepoint, and release was studied over an 8 day period. Fluorescein release from fibres was assessed using UV-Vis at 490 nm.

3.2.8.2. Gemcitabine and Paclitaxel Release

Following the fluorescein release, thirty centimetres of each fibre were heat sealed and placed in a 2 mL Eppendorf tube in triplicate. The release medium for paclitaxel release contained PBS, containing 2.4 % (w/w) Tween-80 and 4 % (w/w) Kolliphor EL (Zentner *et al.,* 2001). As paclitaxel is a hydrophobic drug, it is made up for injection in a mixture of pegylated castor oil (Kolliphore) and ethanol to increase its solubility. In order to make up standards and see any release of paclitaxel, we needed to add in these agents that would encourage paclitaxel release. The release medium for gemcitabine contained SBF, containing 10^4 U.L lipase (Dufresne *et al.,* 2012) and 1 × Penicillin/Streptomycin. Lipase was added to increase physiological relevance as it is commonly found in high concentrations in pancreatic tumours (Cho and Han 2017). 1.5 mL of release medium was added to each tube, and incubated at 37 ºC. At each specified timepoint, the medium was removed and replaced with fresh medium. The amount of drug released from gemcitabine loaded fibres was assessed using Shimadzu HPLC system comprising of a UV-Vis detector (SPD-10AV), system controller (SCL-10A), auto injector (SIL-10AD), Liquid chromatograph (LC-10AT) and degasser (DGU-14A). All samples were filtered through a 0.22 µm syringe membrane filter prior to injection. Chromatographic analysis of gemcitabine was carried out using a mobile phase of ultra-pure water and ACN at a ratio of 95:5 using an isocratic elution. Injection volume was 10 µL on to a Grace C18 column (4.6 × 250 mm, 5 µm particle size) at a flow rate of 1 mL/min. Gemcitabine was detected by the UV-VIS detector at 272 nm.

A standard curve was prepared using gemcitabine concentrations ranging from 0.004 to 0.5 mg/mL. Paclitaxel detection was carried out at 272 nm using a mobile phase of ultra-pure water and ACN using gradient elution according to the following program: from 0 to 30 min, linear gradient of 50 % to 100 % ACN. From 30-38 min, hold at 100 % ACN. From 38-40 min, linear gradient from 100 % to 50 % ACN, followed by 40 to 60 min at 50 % ACN. The injection volume was 10 µL and flow rate was 1 mL/min. Mobile phase for both separations was prepared daily, and filtered and degassed using an ultra-sonicating water bath. Data acquisition was carried out using Class-VP software (V. 6.14 SP1).

3.2.9 Cell Lines and Culture Conditions

PANC-1 and Mia-PaCa-2 were cultured as described in Chapter 2, Section 2.2.9 Genetically engineered Kras(G12D);Trp53(R172H);Pdx1-Cre (KPC) mouse PDAC cell line and human skin-derived telomerase-immortalised fibroblasts (TIFs) were sourced from Dr Paul Timpson and the Kinghorn Cancer Centre, Australia (Hingorani *et al.*, 2005). BxPC3luc cells were sourced from Cellbank, Westmead Australia. KPC cells were cultured in DMEM-high glucose media supplemented with 10 % FCS. BxPC3luc cells were cultured in RMPI-1640 media supplemented with 10 % FCS. Mia-PaCa-2 and PANC-1 cells were all cultured as per chapter 2, section 2.2.9.

3.2.10 Growth Inhibition of 2D Monolayers

The cytotoxic effect of each fibre formulation was tested either by direct addition into the cell media, or by pre-incubation of the fibres in complete media, which was then later added to the cells.

3.2.10.1 Direct Incubation of Fibres with Cells

PANC-1 or Mia-PaCa-2 cells were seeded at 5000 cell/well in complete media (100 µL) containing 1 × Pen/Strep in 96-well flat bottomed plates 24 h prior to addition of fibres (empty, gemcitabine, paclitaxel, or dual-drug loaded (gemcitabine and paclitaxel)) (0.5 cm). Each fibre was heat sealed at each end to prevent the drug being released from the exposed ends. Images of cells were taken using the IncuCyte ZOOM real-time quantitative live-cell imaging system (Essen Bioscience, USA) at 10 × magnification. Cell viability was assessed at 24, 48 and 72 h using

the colourmetric MTS assay according to manufactures instructions. Briefly, at the end time point, fibre lengths were removed from each well and 20 µL MTS reagent added, and incubated for 3 h at 37ºC before being analyzed using UV-Vis at 490 nm. Cell viability was normalised as a percentage of untreated cells.

3.2.10.2 Effect of Direct Application of Different Materials on Cells

To assess whether co-incubation of fibres and cells has an effect on cell viability, Mia-PaCa-2 cells were seeded at 5000 cell/well, and 5 cm lengths of either a commercially available suture (Surgical Specialities Corp, nylon black monofilament non-absorbable suture, provided sterile by Dr Bruce Ashford of ISLHD), 2 % alginate fibre loaded with gemcitabine or 2 % alginate fibre with no drug loaded were incubated together for 72 h. Images were taken at 24, 48 and 72 h using IncuCyte ZOOM, and cell confluency was calculated using IncuCyte ZOOM software as per chapter 2 section 2.2.10.

3.2.10.3 Preincubation of Fibres

To better understand if the method of fibre incubation (described above) had an effect on cell viability, a pre-incubation experiment was performed. Mia-PaCa-2 and PANC-1 cells were seeded at 5,000 cell/well, while and BxPC3luc cells were seeded at 10,000 cell/well, all in complete media. 1, 2 or 3 pieces of 0.5 cm lengths of empty fibre and dual-drug loaded fibres were pre-incubated at 37 ºC in 100 µL of media for 72 h. Equivalent amounts of free gemcitabine and paclitaxel were added to compare the effect. Final drug concentration from 1 piece of fibre (and equivalent free drug) was 1.5 mM gemcitabine and 0.19 mM paclitaxel. The cell media was then completely replaced with 100 uL of pre-incubated release media, and cells incubated for a further 72 h before 20 µL MTS reagent added, and incubated for 3 h at 37 ºC before being analyzed using UV-Vis at 490 nm. Cell viability was normalised as a percentage of untreated cells.

3.2.10.4 Kolliphore EL dose Response

The cytotoxicity of Kolliphore EL concentration was assessed on PANC-1 cells, in order to determine whether it was viable to culture cells in the same conditions as the paclitaxel release was assessed in. PANC-1 cells were seeded at 5000 cell/well in complete media containing 1 × Pen/Strep in 96-well flat bottomed plates 24 h prior to addition of Kolliphore. Cells were then incubated with serial dilutions of Kolliphore EL (diluted in complete media) and incubated for 72 h, before an endpoint MTS assay was performed.

3.2.11 Growth Inhibition of Tumour Spheroids

The efficacy of the dual-drug loaded fibres was tested on 2 PDAC tumour spheroid models. Fibres were pre-incubated as per 3.2.9.3. KPC and BxPC3luc cells were seeded at 150 or 1500 cells/well (respectively) in a final volume of 200 µL in Corning Costar ultra-low attachment U-bottomed plates. KPC cells were seeded in DMEM high glucose + 10 % FCS, while BxPC3luc cells were seeded in a specialized media that was optimized in house by Dr Daniel Brungs (University of Wollongong), and consisted of DMEM high glucose media, N2 (1 ×), EGF (0.01 %), bFGF (0.005 %), PenStrep (1 ×), L-Glutamine (1 ×), hydrocortisone (50 nM). Cells spontaneously formed spheroids 4 days post seeding. 150 µL of media was removed from the established BxPC3luc spheroids, and replaced with 100 µL of the aliquots of complete media to a final volume of 150 µL, while a 0.5 cm length of fibre was added directly to the KPC cells. KPC spheroids were imaged daily for 5 days using fluorescence microscope (Leica DMi8, Leica Biosystems, Germany). BxPC3luc spheroids were imaged daily for 10 days using IncuCyte ZOOM. Spheroid diameter was measured using Image J software. APH assay was performed as per section 2.2.12. All images were acquired at 10 × magnification.

3.2.12 Clonogenic Survival Assay

In order to assess the benefit of treating cancer cells with both the dual-drug loaded fibres and radiotherapy, Mia-PaCa-2 cells were subjected to treatment and then the survival quantified using a clonogenic survival assay. This method is commonly used to assess cell survival post radiation based on the ability of single cells to divide to form

a colony (Munshi *et al.,* 2005, Buch *et al.,* 2012). Mia-PaCa-2 cells (500,000 cells) were seeded in a T12.5 flask (5 mL complete media final volume) and incubated for 24 h. Cells were then treated with free drugs; gemcitabine (0.5 µM), paclitaxel (0.15 µM), a combination of both gemcitabine and paclitaxel (0.5 µM and 0.15 µM respectively), or fibre eluted drug at equivalent concentrations, and compared to the controls of empty fibre or untreated cells. Cells were incubated for a further 24 h. Flasks were then completely filled with complete media, ensuring no air bubbles and cells exposed to 1 Gy radiation using a Varian 2100iX linear accelerator operated by Dr Martin Carolan (Illawarra Shoalhaven Local Health District (ISLHD)) at Wollongong Hospital. Flasks were located at mid-point in a 23 cm thick Solid Water phantom (Gammex Inc, USA) and surrounded with Super Flex bolus (Radiation Products Design Inc, USA) to ensure electronic equilibrium. A dose of 1 Gy was delivered using parallel opposed beam geometry, in a single fraction at room temperature. Cells were then harvested and plated into petri dishes (100 mm × 20 mm) in DMEM high glucose + 1 × Pen/Strep (final volume 13 mL) seeded at cell densities outlined in Table 3.2. Cells were incubated at 37 ^{o}C for 10 days. Plates were then rinsed with PBS (containing Mg^{2+} and Ca^{2+}), and the cell colonies fixed and stained with a solution of 1:3 (v/v) crystal violet:absolute ethanol. After 10 minutes incubation at room temperature, the stain was removed, cells washed with distilled water, and allowed to air-dry overnight. Plates were imaged using a BioRad gel imager. Colonies were manually counted the next day using Image J and were only considered if they consisted of ≥ 50 cells. The results were graphed as percentage cell survival which was a calculated as percentage of the normalised untreated control.

Table 3.2: Cell seeding densities of Mia-PaCa-2 cells that were pretreated with empty or gemcitabine ± paclitaxel loaded fibres and exposed to 1 Gy of radiation.

	Cell Seeding Density	
Pre-treatment	+ 1 Gy	- 1 Gy
Untreated	500, 1000	500, 1000
Empty Fibre	500, 1000	500, 1000
Gemcitabine loaded fibre (1 µM)	2000, 4000	1500, 2500
Free Gemcitabine (1 µM)	2000, 4000	1500, 2500
Dual-drug loaded fibre (1 uM gemcitabine, 0.3 uM paclitaxel)	1500, 3000, 4000	1500, 3000, 4000
Free gemcitabine (1 µM) and paclitaxel (0.3 µM)	1500, 3000, 4000	1500, 3000, 4000

3.2.13 Statistical Analysis

Statistical significance of treatment groups as compared to control groups was determined using a two-way ANOVA with a Bonferroni post-test or unpaired students multiple t test (GraphPad Prism V 6.0; San Diego, CA, USA). *P* values < 0.05 were considered statistically significant. Values are reported as the average replicates ± standard error of the mean.

3.3 Results

This chapter focuses on the development of coaxial fibres loaded with two chemotherapeutic drugs, paclitaxel and gemcitabine. Gemcitabine and *nab*-paclitaxel administered in combination are the current standard of care for patients with advanced PDAC and have shown significant survival increase in patients when compared to gemcitabine alone (Von Hoff *et al.,* 2013). The dual-drug loaded fibres were assessed for their biophysical properties, such as morphology, drug loading and release, for their cytotoxicity against multiple human PDAC lines in 2D and 3D *in vitro* cell based models. The efficacy of the dual-drug loaded fibres in combination with radiotherapy was also assessed as chemoradiation is a common treatment regimen for PDAC patients in both the neoadjuvant and adjuvant setting in patients with resectable or borderline resectable PDAC. It may also be administered as part of the main treatment for patients with non resectable PDAC, or for pain relief (American Cancer Society 2019). Radiation together with chemotherapy has been shown to increase overall survival, however many patients are unable to tolerate the complete treatment schedule due to the compounded side effects (Vincent *et al.,* 2011).

3.3.1 Hydrophobic Polymer Selection

Chapter 2 described the fabrication and characterisation of 2 % and 3 % (w/v) alginate fibres loaded with gemcitabine. The hydrophilic alginate polymer was successfully loaded with gemcitabine and showed efficacy *in vitro*, while alginate itself demonstrated biocompatibility with cells. As gemcitabine in combination with *nab*-paclitaxel is the gold standard treatment for PDAC, a polymer formulation that allowed the concomitant loading of both hydrophilic (gemcitabine) and hydrophobic (paclitaxel) drugs was necessary. PCL (dissolved in DMF or chloroform) and PLGA (dissolved in NMP or DMSO) fabricated as single fibres were assessed for their biocompatibility against PANC-1 cells. PCL dissolved in chloroform did not successfully form a fibre and instead pooled at the bottom of the coagulation bath, hence biocompatibility could not be assessed. The cells treated with PCL/DMF prepared fibres retained viability of 76.19 % after 72 h, while cells treated with PLGA/NMP prepared fibres or PLGA/DMSO fibres had a viability of 46.26 % and 65.95 % respectively compared to no treatment control (Fig. 3.1). The PCL/DMF fibre formulation was therefore selected as the lead polymer for further studies of coaxial

fibre fabrication and paclitaxel loading.

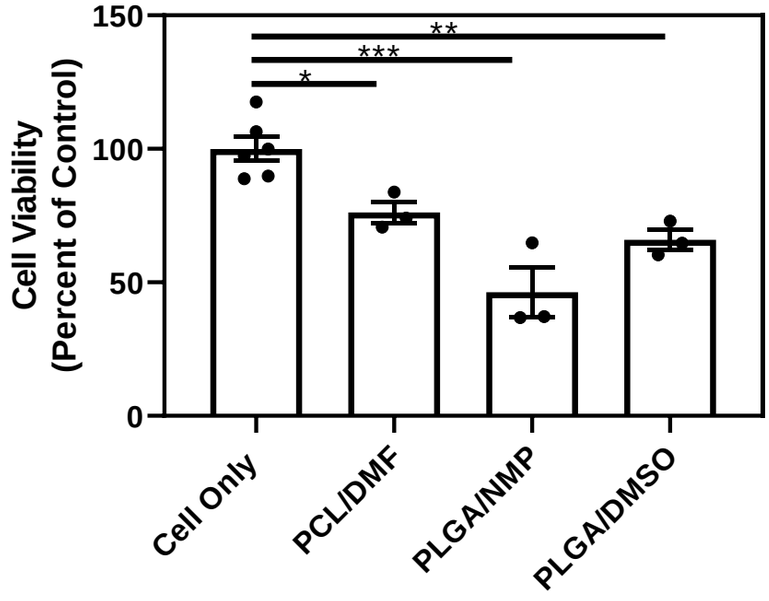

Figure 3.1: Fibres composed of PCL in DMF had the least toxicity towards cells. PANC-1 cells were incubated with 5 cm lengths of each fibre formulation for 72 h before an endpoint MTS assay was performed. Results are displayed as a percentage of an untreated control. Values are the mean (±SEM) of triplicates. * P≤0.05, ** P≤ 0.01 *** P ≤ 0.001

3.3.2 Fibre Morphology

Following the selection of polymers for forming a coaxial structure, in order to determine the lead formulation the polymer compositions, core shell arrangement, crosslinking, and drug loading needed to be optimised. Alginate remained the polymer of choice for gemcitabine delivery (as per Chapter 2). PCL dissolved in DMF was chosen as the superior polymer for paclitaxel loading. Alginate was initially spun as the shell material and PCL as the core, and hydrated SEM images showed even shell thickness and crosslinking (Fig 3.2 A). Upon drying however the alginate cracked and flaked away from the PCL core. The configuration was then reversed, with the PCL as the shell material and alginate as the core. When SEM images were taken, the “icy” appearance of the alginate and lack of visible porosity indicated lack of crosslinking (Fig 3.2 B). Therefore an internal crosslinking method was employed using $CaCO_3$ and glucono-delta lactone, to facilitate slow ionic crosslinking resulting in uniform crosslinking which

was observed by the presence of pores (Fig 3.2 C) (Kuo and Ma 2001, Jang *et al.*, 2014).

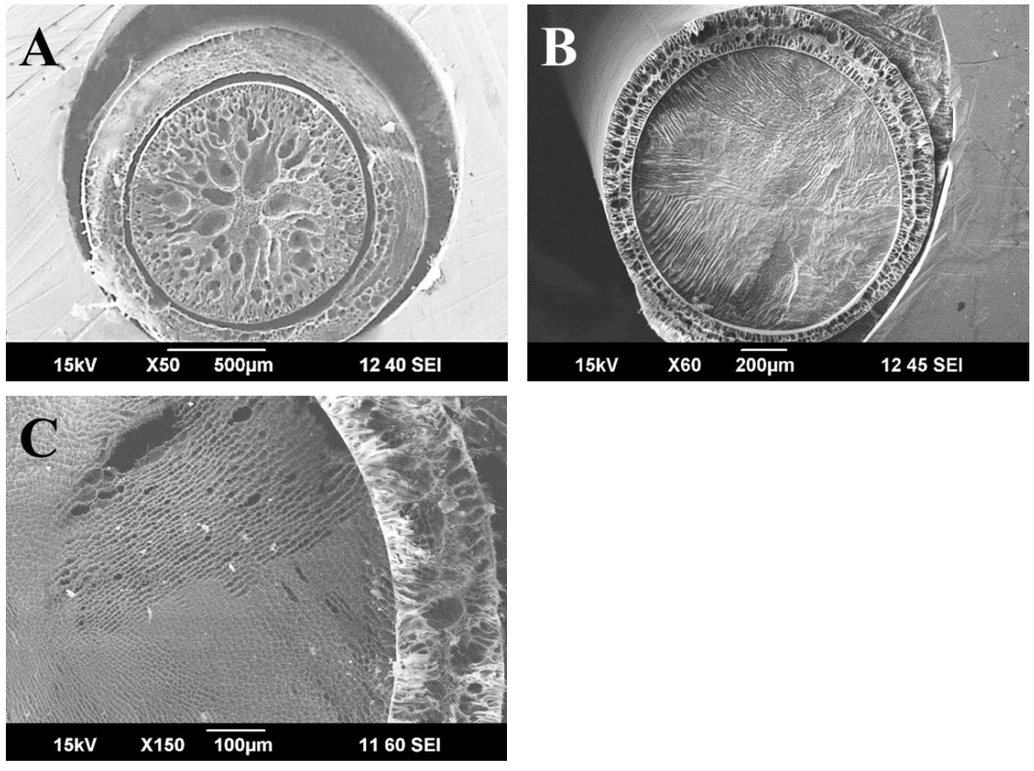

Figure 3.2: Coaxial cross sectional structures show the internal morphology and crosslinking of different coaxial fibre formulations. Scanning electron micrographs of cross sections of A) coaxial fibre consisting of a 3 % alginate shell and 15 % PCL core and B) coaxial fibres consisting of a 15 % PCL shell and 3 % alginate core (uncrosslinked). C) coaxial fibres consisting of a 15 % PCL shell and 3 % alginate core (crosslinked). No drugs were loaded into any fibre formulation.

Three concentrations of PCL were assessed for the shell material – 10, 15 and 20 %. Concentrations above 20 % did not completely dissolve in DMF, while concentrations below 10 % did not from a continuous fibre throughout the spinning process. SEM images showed the 10 % PCL formed a hollow shell (Appendix Fig A4 A,B), while the 15 % PCL formed pores throughout (Appendix Fig A4 C,D), and the 20 % PCL showed pore formation with a solid band down the centre (Appendix Fig A4 E,F). 15 % PCL was chosen for subsequent experiments as its viscosity was the most appropriate for wet spinning smooth fibres and is a commonly used concentration for electrospinning (Reneker *et al.,* 2002, Augustine *et al.,* 2017, Anindyajati *et al.,* 2018, Jiang *et al.,* 2018).

Paclitaxel formulated for injection (Anzatax^{TM}) was initially provided for loading into the PCL shell. The Anzatax/PCL shell was spinnable into long continuous fibres, but upon SEM imaging it was found that Anzatax significantly altered the internal morphology (Fig. 3.3 A). The outer PCL shell became hollow in the centre, and the alginate core lost the fine porosity observed in Fig 3.2 C. Anzatax is comprised of paclitaxel in castor oil (49.7 %) and ethanol (48.7 %), and it is clear that these excipients had a significant impact on the structure. Anzatax/PCL core with an alginate shell was also spun, and SEM images confirmed that the Anzatax had a significant effect on both the PCL and the alginate (Fig. 3.3 B). The alginate shell appeared very thin in sections, and the PCL core did not appear fully formed when compared to Fig 3.2 A when not loaded with any drug. Pure paclitaxel was obtained and loaded into the PCL and fibre successfully spun containing gemcitabine in the alginate core (Fig 3.4 C,D), and the SEM images show there is no visible impact on the morphology when compared to the non-drug loaded sample (Fig 3.4 A,B). Crosslinking was observed from the presence of pores in the alginate core in both the empty and gemcitabine loaded alginate which is consistent with Chapter 2.

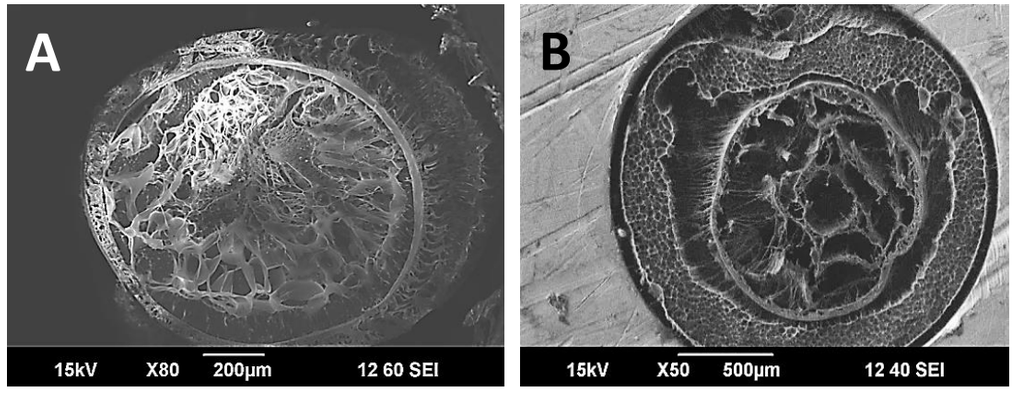

Figure 3.3 Scanning electron microscopy of Anzatax loaded coaxial fibres shows presence of Anzatax disrupts polymer structure.A) Coaxial fibre with a 3 % alginate core and 15 % PCL shell loaded with Anzatax. B) Coaxial fibre with 3 % alginate shell and 15 % PCL core loaded with Anzatax.

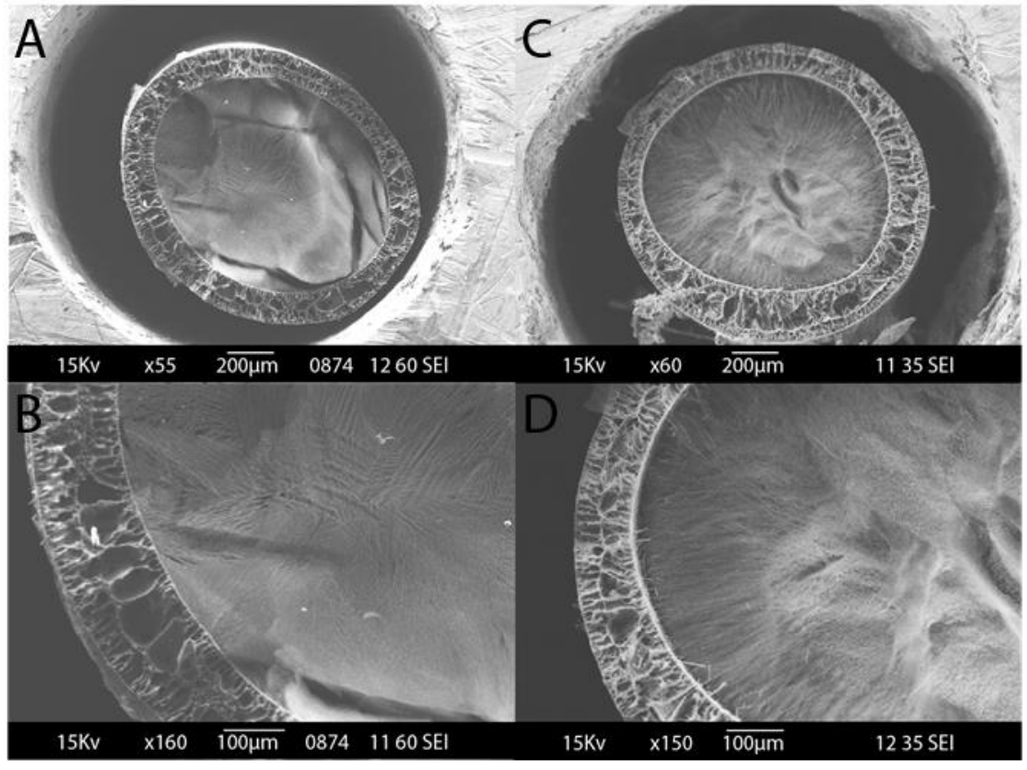

Figure 3.4: Scanning electron microscopy images of empty and dual-drug loaded fibres shows that the addition of paclitaxel and gemcitabine does not affect polymer structure.SEM images show the cross sections of empty fibres (A and B) and of dual drug loaded fibres (C and D). The shell material is polycaprolactone ± paclitaxel, and the core is alginate ± gemcitabine.

The diameter of the fibre in its dried state was not significantly different between empty fibres (1373.8 ±16.6 µm), gemcitabine loaded fibres (1382.8 ±12.9 µm), paclitaxel loaded fibres (1277.6 ±42.2 µm) and dual drug loaded fibres (1291.8 ±44.4 µm) (Fig 3.5).

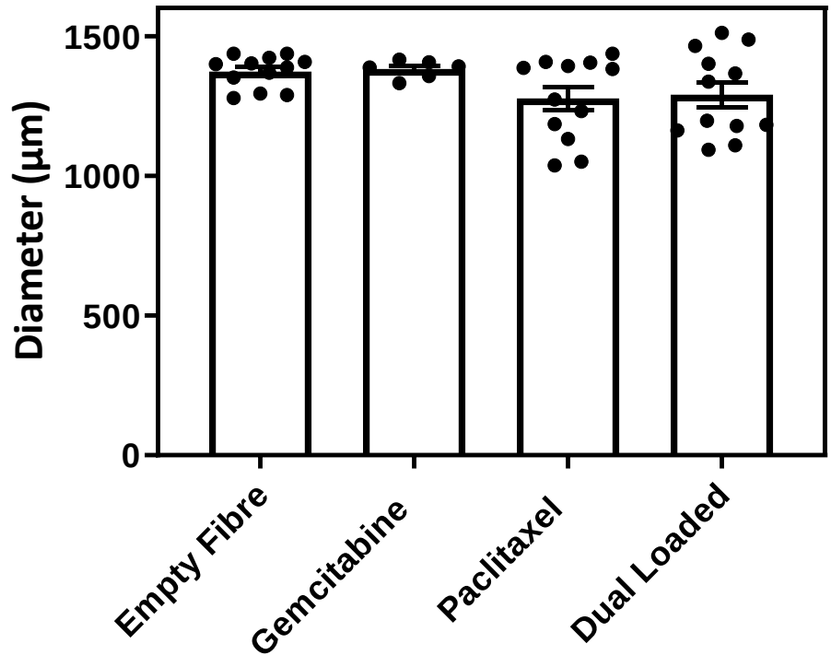

Figure 3.5: The addition of gemcitabine and/or paclitaxel did not significantly affect coaxial fibre diameter. Fibre diameter was measured after wet-spinning then drying the fibres. The bars represent the mean of n=6-12 measurements ± SEM. µ

3.3.3 Fibre Echogenicity

The 3 % alginate core of the coaxial fibres was loaded with gold nanoparticles to produce a coaxial fibre that is echogenic. This is an important aspect to consider when the intended implantation method is using EUS-FNI. The fibre was threaded through an ultrasound training block and imaged by a technician. The fibre was clearly visible under ultrasound (Fig 3.6), and further confirmed when slowly removed while imaging, which recorded the movement of the image.

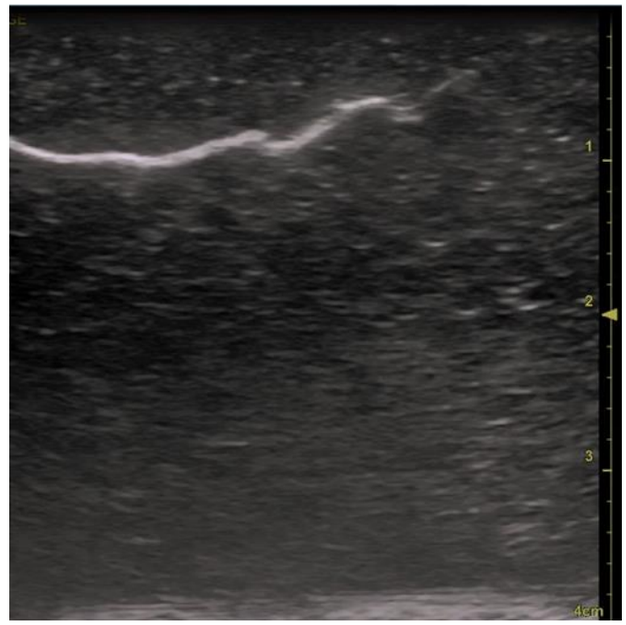

Figure 3.6: Gold nanoparticles allow for the coaxial fibre to be visualised under ultrasound. Gold nanoparticles OD 10 nm gold nanoparticles were mixed with 3 % alginate solution prior to fabrication of a coaxial fibre containing a 15 % PCL sheath.

3.3.4 Drug Loading and Release

It is important assess drug release in each newly fabricated DDS, as it gives an indication of subsequent drug release *in vivo*. Prior to performing release experiments with loaded gemcitabine and paclitaxel, fluorescein (a water soluble fluorescent dye) was loaded into the alginate core, and the release profiles compared to that of a single alginate fibre. This was explored in order to assess the ability of the PCL shell to impact release rate. In these studies, the coaxial fibres released 90.4 % of loaded fluorescein, while single alginate fibres released 100 % over 8 days (Fig. 3.7 A). Over the first 7 h 43.4 % and 70.9 % of fluorescein was released from coaxial and single fibres, respectively, which was significant (P=0.018) (Fig 3.7 B). There was a visual difference observed in the release of fluorescein into the coagulation bath during the spinning process, with the single fibre formulation appearing to release dye, while the coaxial formulation did not (Fig 3.8 A and B).

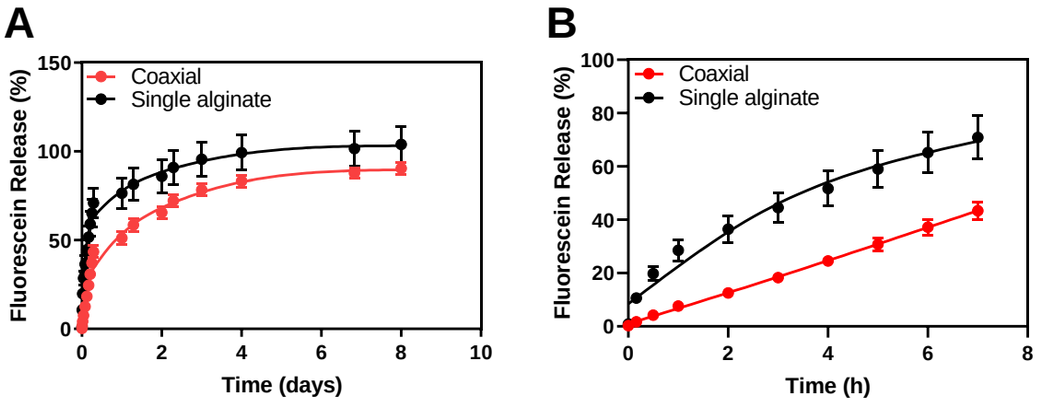

Figure 3.7: Fluorescein release profile is linear from coaxial formulations over the first 7 h. Percentage release of fluorescein from single 2 % alginate or coaxial fibres in simulated body fluid at 37 °C over A) 8 days and B) in the first 7 h. Values are the mean (±SEM) of quadruplicates.

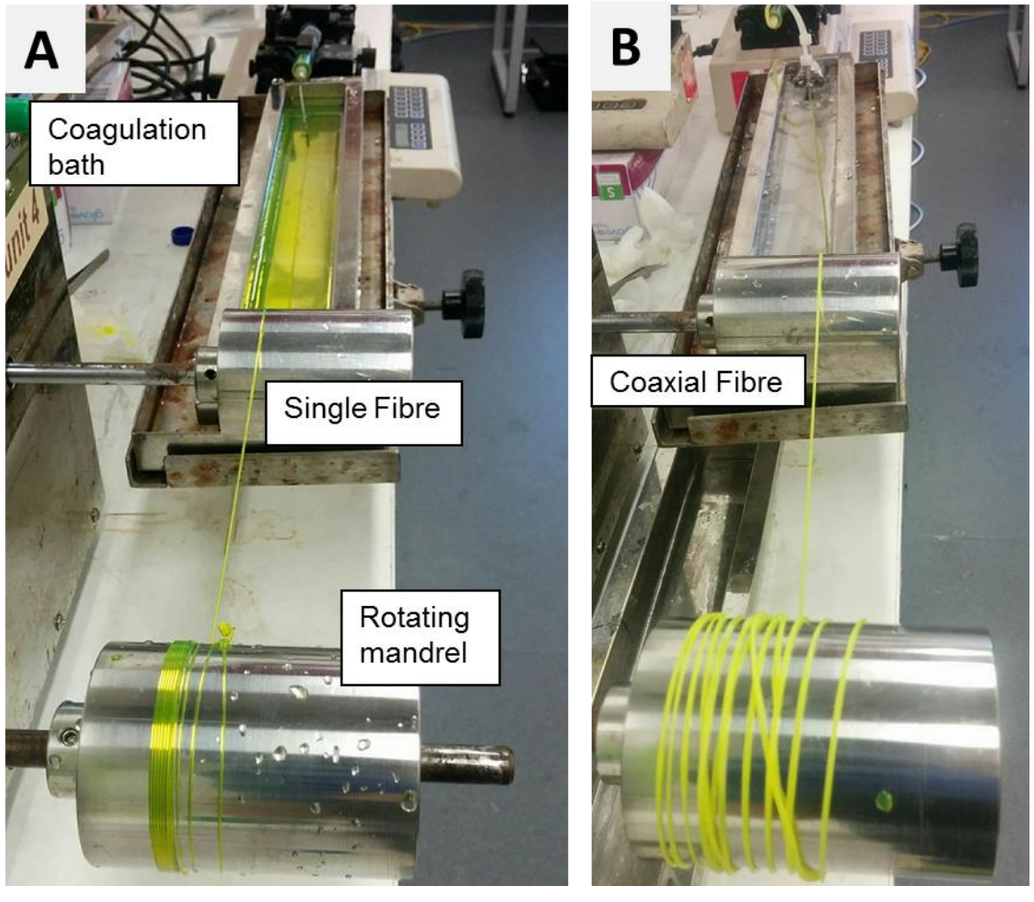

Figure 3.8: PCL shell of coaxial fibres prevents fluorescein loss into the wet spinning coagulation bath.A) wet spinning set up for fabrication of fluorescein loaded 3 % alginate fluorescein loaded fibres, and B) wet spinning set up for fabrication of coaxial fibres containing a 15 % PCL shell and 3 % alginate fluorescein loaded core**.** Polymer is extruded into the coagulation bath (pictured) and collected on the rotating mandrel (pictured).

Gemcitabine loading into fibres and release were assessed in an aqueous medium containing SBF and an enzyme commonly found in pancreatic tumours (phospholipase D) (Dufresne *et al.*, 2012). The drug loading of gemcitabine was determined when there was no further release of the drug from the fibre for 10 days. Gemcitabine loading was found to be 8.1 mg/m of fibre, which equated to an EE % of 48.5 % (Table 3.3). This is similar to that of the 2 % alginate single fibre described in Chapter 2 which had an encapsulation efficiency of 51.8 %. In order to determine total paclitaxel total loading, extraction of paclitaxel was performed in absolute ethanol to assess the total drug loading. Frequent replacement of the ethanol in the release study maximised paclitaxel release with 4.36 mg released over the first 7 hours, with no more drug released over the next 14 days (Appendix Fig. A5). This determined that paclitaxel had an EE % of 89.3 %.

Table 3.3: Drug loading and encapsulation efficiency of gemcitabine and paclitaxel in a polycaprolactone-alginate coaxial fibre. Theoretical loading was calculated using equation (2) whilst the actual loading values were determined through complete release of drug and quantification using HPLC. The values represent the mean actual loading value ± SEM.

	Theoretical Loading (mg/m)	Drug loading (mg/m)	Drug loading (µg/0.5 cm)	Encapsulation Efficiency (%)
Gemcitabine	16.7	8.1 ±0.80	40.5 ±4.0	48.5 ±4.78
Paclitaxel	14.89	14.5±0.95	72.5 ±4.75	89.3 ±5.85

Release experiments were performed using gemcitabine loaded alginate core and paclitaxel loaded PCL shell. HPLC analysis of gemcitabine determined that 2.43 mg was released from the coaxial fibre over a 14 day period (Fig. 3.9 A). The majority of gemcitabine, 2.31 mg (95.1 %), was released in the first 10 h (Fig. 3.9 B and F). This burst release is typical of hydrogels as explained in Chapter 2, Section 2.4.1. Although encased by a PCL shell, the rate of gemcitabine release was not restricted by the PCL (Table 3.4).

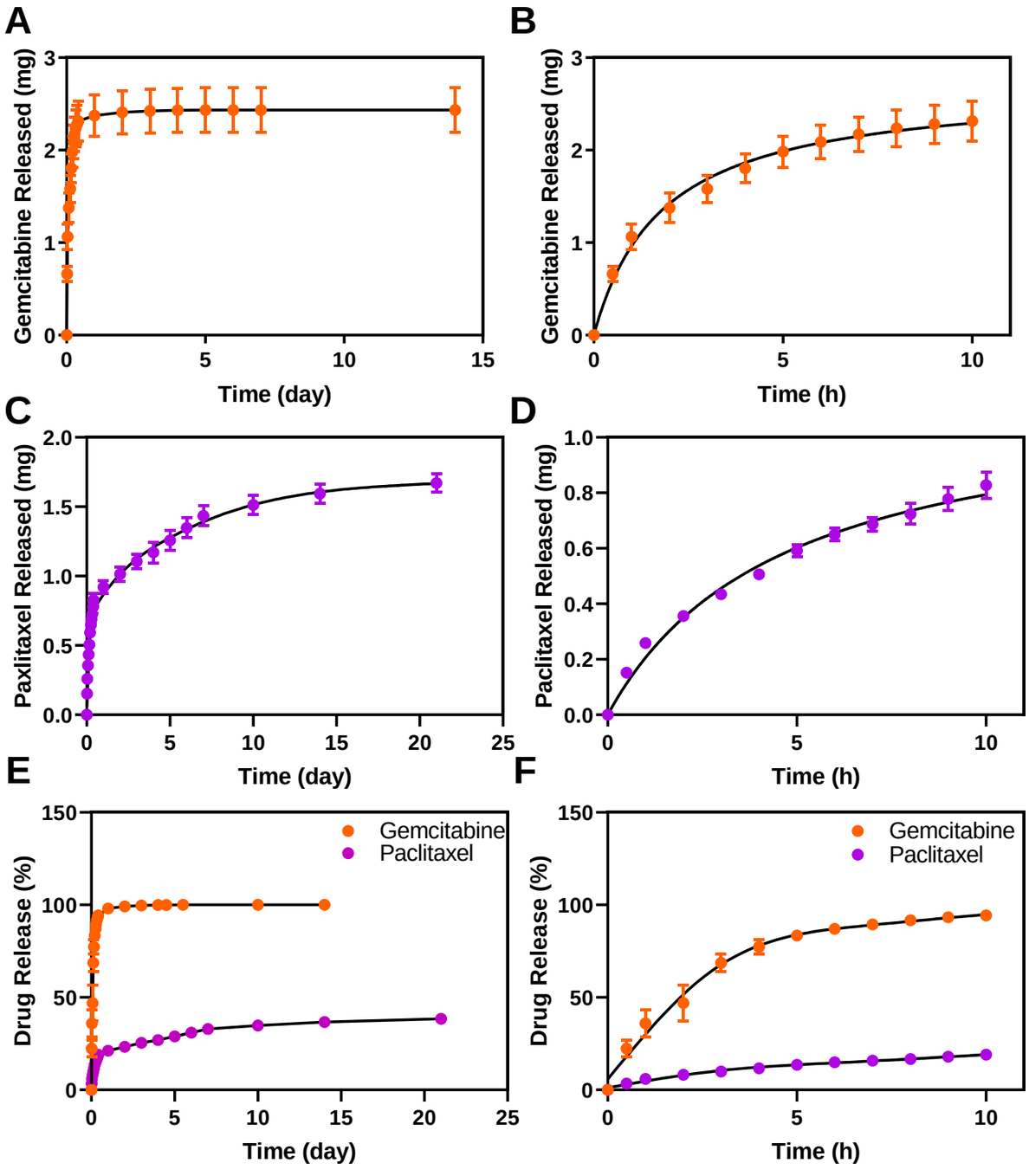

Figure 3.9: Gemcitabine release profile shows rapid burst release, while paclitaxel displays a more sustained release profile. Cumulative release of A) gemcitabine over 14 days, and B) the first 10, performed in a buffer containing SBF and lipase, C) Paclitaxel over 21 days and D) the first 10 h performed in a buffer containing PBS, tween-80, Kolliphor EL and ethanol, E) percentage release of both gemcitabine and paclitaxel over 14 and 21 days, respectively, and F) the percentage release of gemcitabine and paclitaxel over the first 10h All release studies performed at 37 ^{o}C over a period of 14-21 days. Values are the mean (±SEM) of triplicates.

Table 3.4: The amount and rate of drug released from 30 cm length of coaxial dual-drug loaded fibre

Drug	Total amount of drug released in 30 cm during experiment (µg)	Rate of release $t_{0\text{-}10h}$ (%/h)	Rate of release $t_{24\text{-}204h}$ (%/h)	Rate of release $t_{24\text{-}504h}$ (%/h)
Gemcitabine	2.43 ±0.41	9.52 ±0.87	0.56 ±0.055	-
Paclitaxel	1.67 ±0.07	1.90 ±0.11	-	0.08 ±0.003

The paclitaxel release in our study showed an initial burst, in which 0.8 mg (18.4 %) was released in the first 10 h (Fig 3.9 D and F), followed by a more sustained release over a 21 day period, releasing 1.67 mg (38.4 %) (Fig 3.9 C and E). This therefore showed that only 38.3 % of paclitaxel was released over 21 days, (18.3 % over the first 10 h) in the drug release study performed in the aqueous solution (Fig 3.9 E). The implication of the slow release rate (Table 3.4) is further explored in Sections 3.3.5 and 3.3.6 when the cytotoxic efficacy of the dual-drug loaded fibre is assessed in 2D and 3D cell based systems.

3.3.5 Growth Inhibition of 2D Monolayers

Coaxial fibres (0.5 cm) containing 40.5 µg and 72.5 µg of gemcitabine and paclitaxel respectively, were tested for their toxicity against Mia-PaCa-2 and PANC-1 cell lines over 72 h. The Mia-PaCa-2 cells treated with the dual-drug loaded fibres showed a reduction in cell viability equivalent to that of the gemcitabine and paclitaxel loaded fibres (45.8 % vs 46.2 % and 53.2 %, respectively) while the empty fibre showed a cell viability of 69.24 % (Fig 3.10 A). The PANC-1 cells treated with the dual-drug loaded fibres showed equivalent reduction in cell viability to the gemcitabine loaded, but still had a greater reduction than the paclitaxel (20.8 % vs 20.5 % and 33.3 % respectively), while the empty fibre treated cells had a viability of 57.1 % (Fig 3.10 B). Crystallisation of paclitaxel was observed in the culture media, indicating presence of released but unavailable paclitaxel (Appendix Fig A6).

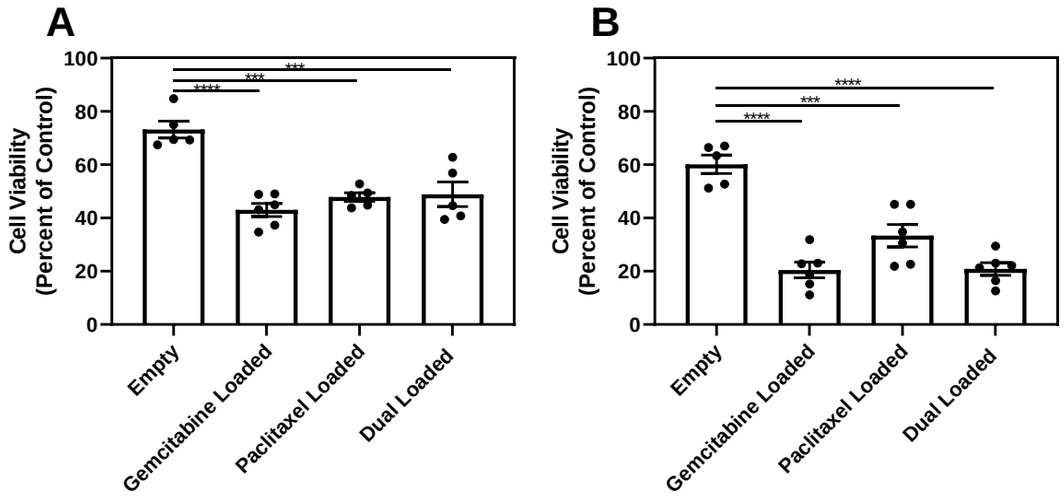

Figure 3.10: Presence of empty coaxial fibre reduces cell viability in two cell lines over 72 h A) Mia-PaCa-2 and B) PANC-1 cells were incubated with 0.5 cm lengths of each fibre formulation for 72 h before an endpoint MTS assay was performed. Results are displayed as a percentage of an untreated control. Values are the mean (±SEM) of sextuplicates. Experiment performed in triplicate, one representative result shown. *** $P \leq 0.001$ **** $P \leq 0.0001$

A dose response curve of Kolliphore EL was performed on PANC-1 cells, in order to see whether the *in vitro* efficacy studies could be performed in the same media as the release studies which contain 4 % Kolliphore EL. It was found that cells had an IC_{50} of 1.9 % w/v Kolliphor EL (Fig 3.11).

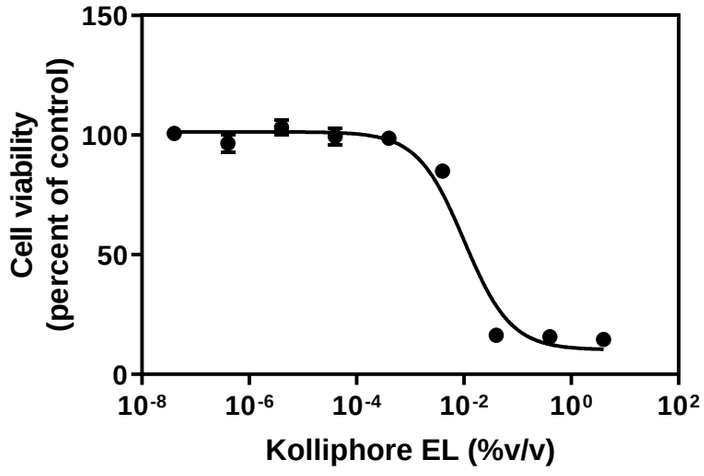

Figure 3.11: Dose response curve of Kolliphore EL. PANC-1 cells were treated with Kolliphore EL concentrations ranging from 4 - 4×10^{-8} % v/v and incubated for 72 h before an endpoint MTS assay was performed. Results are displayed as a percentage of an untreated control. Values are the mean (±SEM) of quintuplicates.

An additional study was performed to assess whether the presence of the fibre in the culture media with cells had an effect on cell growth. It was observed that the presence of an equivalent length of a surgical suture to that of empty fibre produced in this study inhibits cell confluency. Here the empty 2 % alginate fibres reduced confluency in Mia-PaCa-2 cells at a similar rate to that of the surgical suture (Fig 3.12).

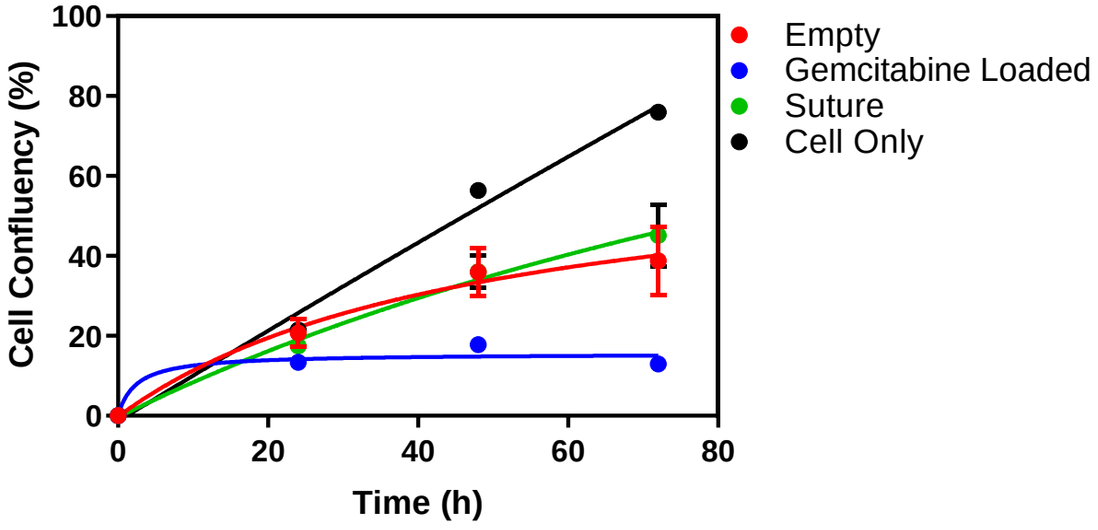

Figure 3.12: The presence of a suture decreases confluency similarly to that of an empty alginate fibre Mia-PaCa-2 cells were incubated with 5 cm lengths of either empty 2 % alginate fibres, gemcitabine loaded 2 % alginate fibres, a suture or untreated and their confluency determined from images obtained on IncuCyte ZOOM at 0, 24, 48 and 72 h. Values are the mean (±SEM) of triplicates.

In light of the results from the previous two studies, a cytotoxicity study was performed where the fibres were pre-incubated with media, and aliquots placed in with the cells. Different numbers of fibre pieces (1, 2 or 3) were incubated in order to see a dose dependant effect, and empty fibre and equivalent free drug were included as controls. Cells treated with the dual-drug loaded fibres (1, 2 and 3 pieces) showed a dose-dependent reduction in cell viability, with cells retaining 27.8 %, 28.4 % and 13.9 % viability (respectively) at endpoint (Fig 3.13). The cells treated with the empty fibres had an endpoint viability of 71.9 %, 73.8 % and 75.6 % respectively, and this did not significantly change with different numbers of fibre pieces. There was no significant difference in cell viability between the empty and untreated cells. The BxPC3luc (Appendix Fig A7 A) and PANC-1 (Appendix Fig A7 B) cells showed a greater sensitivity to the empty fibre aliquots. IncuCyte ZOOM images show that alginate from the core dissociates, and small pieces of alginate not visible to the naked eye are transferred over to the cells. Images of BxPC3luc wells show that in the areas that there is the presence of alginate no cells grow, while the spaces in between show cells with a healthy morphology (Appendix Fig A8 B).

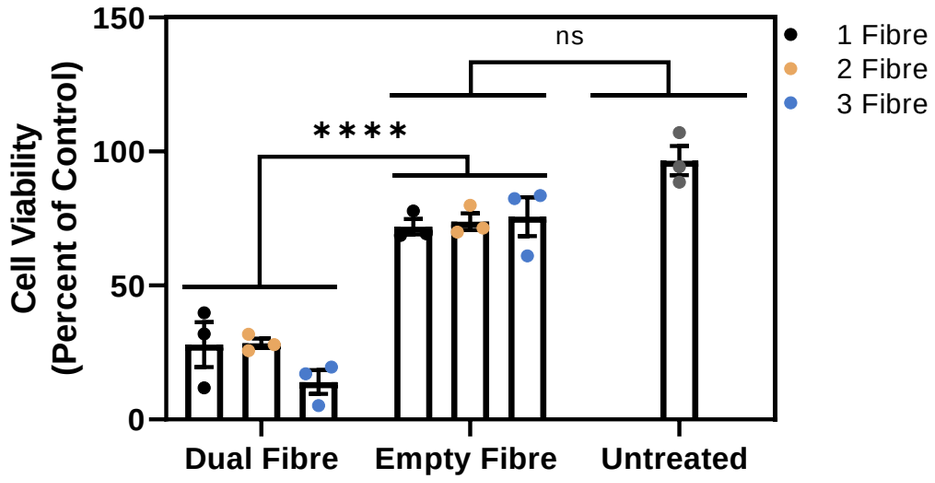

Figure 3.13: A dose dependant response is observed with increasing number of dual-drug loaded fibres. 1, 2 and 3 pieces of 0.5 cm length of fibre (dual or empty) were incubated in 100 uL of media for 72 h before addition to Mia-PaCa-2 cells. Cells were further incubated for 72 h before an endpoint MTS assay was performed. Results are displayed as a percentage of an untreated control. Values are the mean (±SEM) of triplicates. Experiment performed in triplicate, one representative result shown. ns = not significant **** P ≤0.0001

3.3.6 Growth Inhibition of 3D Tumour Spheroids

3D tumour spheroids were utilised for assessing the efficacy of coaxial fibres. KPC and BxPC3luc PDAC cell lines were chosen as the spheroid models as they form tight, compact spheroids (Longati *et al.*, 2013). BxPC3luc spheroids were treated with media containing eluted gemcitabine and paclitaxel. Live cell microscope images show BxPC3luc spheroids treated with a single dual-drug loaded fibre or the equivalent concentration of the free drugs in solution, cause dissociation of the spheroid after 5 days. The empty fibre and untreated spheroids maintain a spherical structure (Fig 3.14 A). Measurement of spheroid diameter revealed the empty fibre to have minimal impact on spheroid growth to that of untreated spheroids with 1.56 and 1.40 fold changes in diameter respectively after 10 days (Fig 3.14 B). The spheroids treated with dual-drug loaded fibre showed a 0.98 fold change, while the free drugs showed a 0.81 fold change, of which was not significant between treatments.

There was significant change in diameter between the empty and dual/free drugs, as well as the untreated and dual/free drug treated spheroids. An endpoint APH assay showed that the spheroids treated with the empty fibre had a final cell viability of 87.1 %, while the dual fibre and free drug treated spheroids had a viability of 68.3 % and 67.0 %, respectively. There was no significant difference between the dual and free drug treated spheroids, but there was significance between the empty fibre treated and both of the dual and free drug treatment groups.

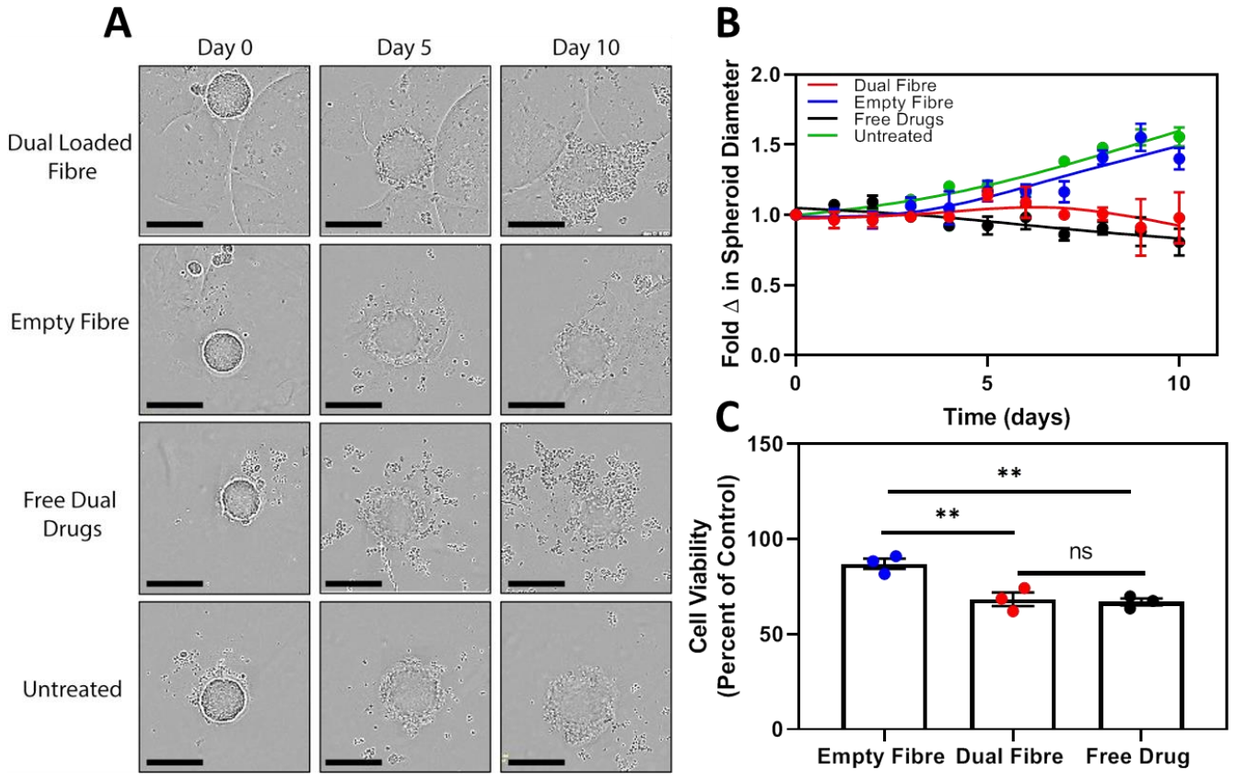

Figure 3.14: Drug eluted from the fibre has equivalent effect to that of free drug, while empty fibres have an effect equivalent to that of untreated spheroids. BxPC3luc tumour spheroids were treated with aliquots of media pre-treated with 0.5cm length of dual-drug loaded or empty fibre for 72 h. Spheroids were also treated with equivalent amount of free gemcitabine and paclitaxel as loaded in the fibre and results compared to untreated control. A) Microscopy images of BxPC3luc spheroids after a 10 day treatment, B) The fold change in spheroid diameter during the 10 day treatment time, diameter determined from IncuCyte ZOOM images acquired at 10 × magnification. C) Endpoint APH assay performed at the conclusion of the 10 day treatment time. Values expressed as a percentage of the untreated control. Data points are the mean of triplicate values ± SEM. **P≤0.01

KPC spheroids were treated over 5 days and were imaged daily and the diameter measured (Fig 3.15 A). There was an initial increase in diameter for all treatments, then a reduction or slowing in the dual-drug loaded fibre treated spheroids by day 5 (1.14 fold increase), and a steady increase in cells both untreated and treated with empty fibres (2.07 and 1.66 fold increase respectively) (Fig 3.15 B). An endpoint APH assay was performed, and cells treated with dual-drug loaded fibres retaining 17.5 % cell viability and the empty fibres retaining 59.0 % viability (Fig 3.15 C).

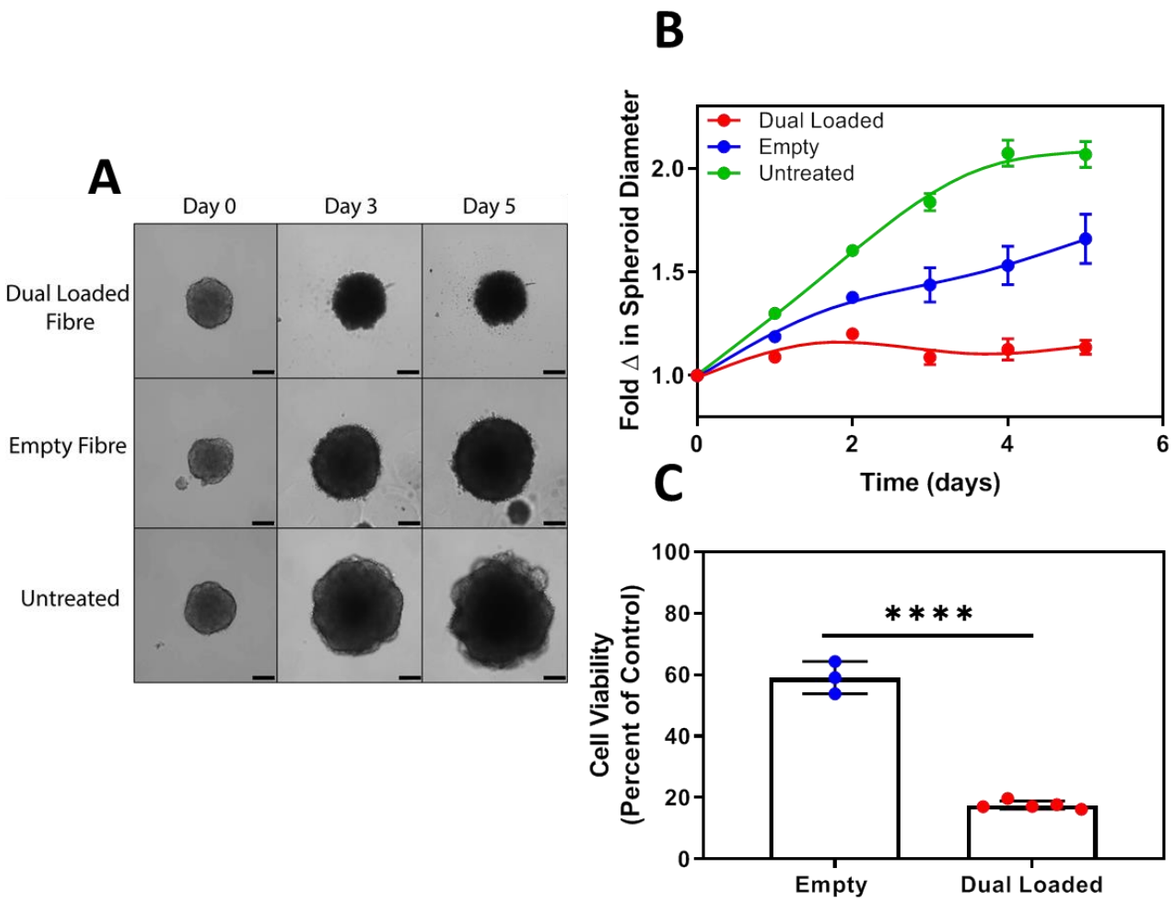

Figure 3.15: KPC cells show significant decrease in viability when treated with a dual-drug loaded fibre. A) Light microscopy images of KPC spheroids after a 5 day treatment with 0.5cm lengths of dual-drug loaded coaxial fibre, empty fibre, or no treatment control. B) The fold change in spheroid diameter during the 5 day treatment time, diameter determined from bright-field images acquired at 10 × magnification. C) Endpoint APH assay performed at the conclusion of the 5 day treatment time. Values expressed as a percentage of the untreated control. Data points are the mean of quintuplicate values ± SEM. *P=0.05, **P≤0.01, ****P=0.0001.

3.3.4 Clonogenic Assay

A clonogenic cell survival assay was used to assess the ability of gemcitabine and paclitaxel (free or fibre eluted) to exhibit a radiosensitising effect on cancer cells. Seeding densities were optimised so that there were minimal colonies in contact with each other (Fig 3.16), which increases the accuracy of colony counting.

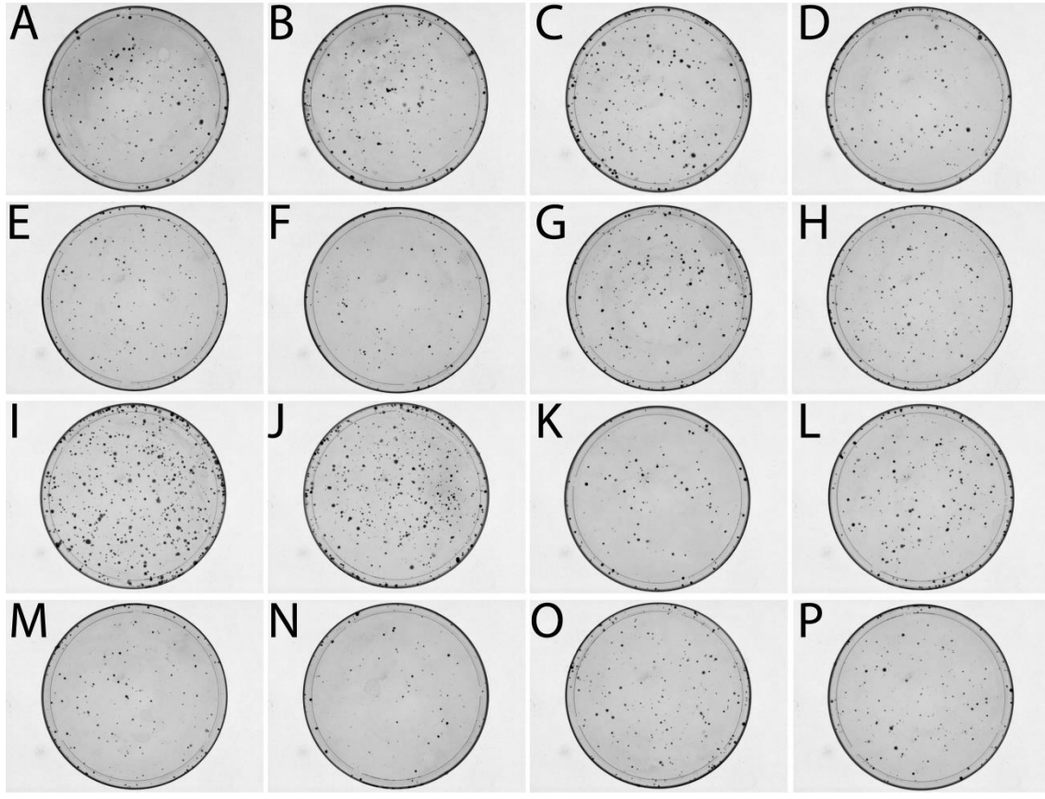

Figure 3.16: Crystal violet stained colonies of Mia-PaCa-2 cells.Mia-PaCa-2 cells were plated at the following densities and pre-treatments; A) untreated (500 cells), B) untreated + 1 Gy (500 cells), C) empty fibre (500 cells), D) empty fibre + 1 Gy (500 cells), E) gemcitabine fibre (1500 cells), F) gemcitabine fibre + 1 Gy (2000 cells), G) free gemcitabine (1500 cells), H) free gemcitabine + 1 Gy (2000 cells), I) paclitaxel fibre (1500 cells), J) paclitaxel fibre + 1 Gy (2000 cells), K) free paclitaxel (1500 cells), L) free paclitaxel + 1 Gy (2000 cells), M) dual-drug loaded fibre (1500 cells), N) dual-drug loaded fibre + 1 Gy (1500 cells), O) free dual drug (1500 cells), P) free dual drug (1500 cells). Gemcitabine concentration was 0.5 µM, and paclitaxel was 0.15 µM across every treatment. One of two seeding densities is shown as a representative image.

1 Gy radiation was chosen as the optimal radiation fraction, as initial studies where cells were irradiated with a 2 Gy fraction alone showed and 85 % cell kill, and with pre-treatment of gemcitabine loaded coaxial fibre a 100 % cell kill, which meant the study could not be quantified (Appendix Fig A9). Mia-PaCa-2 cells treated with 1 Gy alone or empty fibre retained a cell survival equivalent to that of untreated control, however a combination of both the empty fibre with 1 Gy radiation saw a significant reduction of colony formation, with 27.0 % reduction (Fig. 3.17). This suggests the empty fibre alone may be exhibiting radiosensitising effects. The cells treated with free gemcitabine and 1 Gy radiation had no significant difference in colony formation to that of cells treated with free gemcitabine only (25.7 % vs 16.8 % respectively). No significant difference in colony formation was seen between the cells treated with the gemcitabine loaded fibre with or without radiation (retaining 26.7 % vs 26.0 % respectively). This shows that the gemcitabine released from the fibre is bioequivalent to that of the free gemcitabine, as was expected. The paclitaxel from the fibre showed significantly less effect than that added as free drug, which again could be attributed to the poor solubility and release of paclitaxel in an aqueous system. The free paclitaxel was formulated for injection (Anzatax), as this was the most clinically relevant comparison, so is not surprising it has a greater effect *in vitro*. Interestingly, the paclitaxel fibre in combination and without 1 Gy showed significant difference in viability (52.7 % vs 88.2 % respectively).

The dual-drug loaded fibre in combination with 1 Gy radiation showed the greatest reduction in colony formation, with cells retaining only 12.9 % viability, which was found to be significant using a two-tailed t test compared to the no radiation control which retained 25.3 % viability. This has a greater cell killing ability than the free dual drugs, which retained 24.7 % and 31.4 % and viability with and without radiation, respectively.

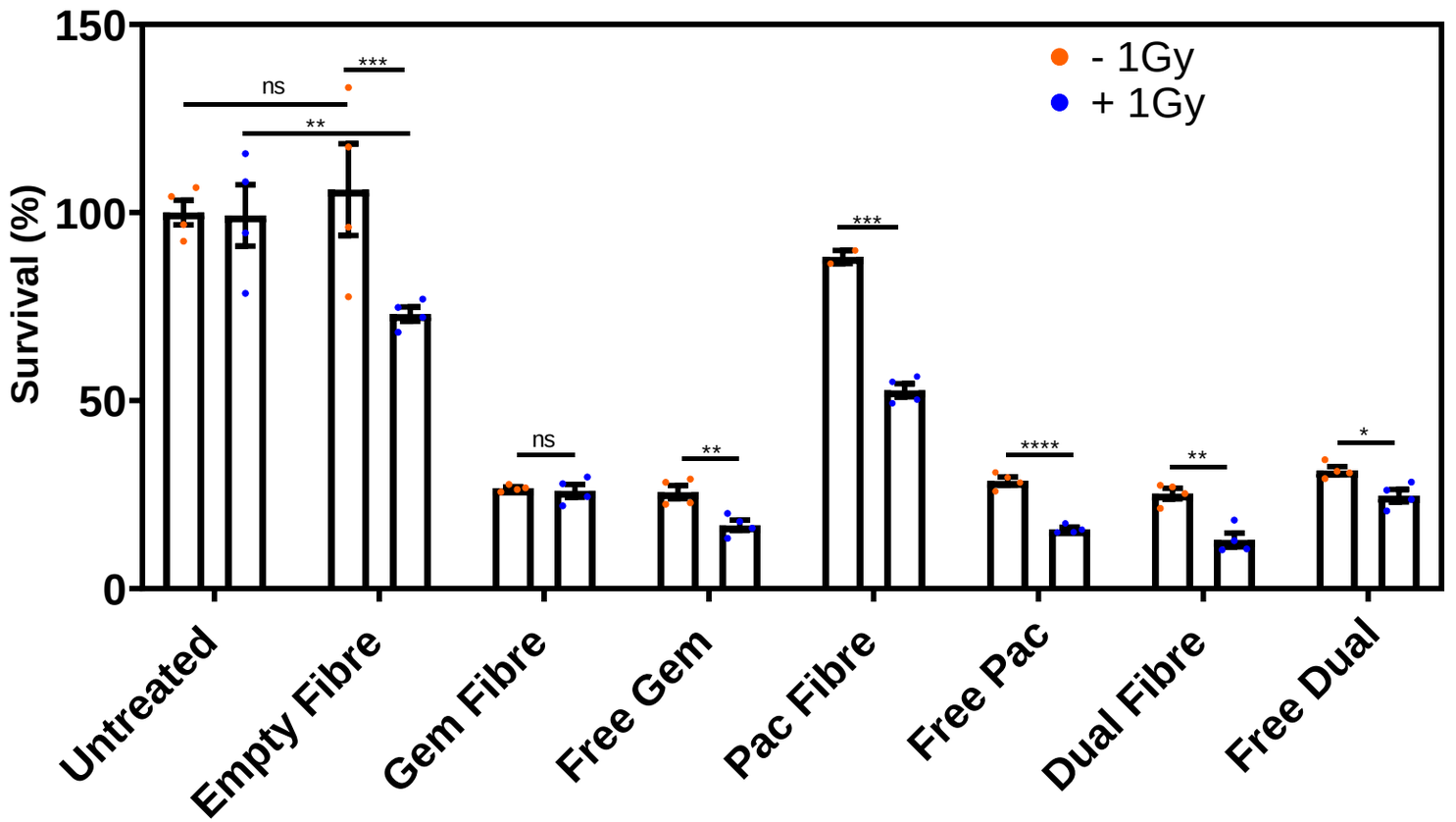

Figure 3.17: Percentage survival of Mia-PaCa-2 cells after exposure to various chemoradiotherapy treatments. Treatments included 0.5 µM gemcitabine (fibre/free drug), 0.15 µM paclitaxel (fibre/free drug), or a combination of the two, with or without 1 Gy radiation. Surviving fractions were normalized to the untreated control. Data points are the mean of quadruplicate values ± SEM. ns = $P > 0.05$, ** = $P < 0.01$, *** = $P < 0.001$, **** = $P < 0.0001$. Gem = gemcitabine, Pac = paclitaxel, dual = gemcitabine + paclitaxel.

3.4 Discussion

This chapter focused on the development of coaxial fibres loaded with two chemotherapeutic drugs paclitaxel and gemcitabine. These drugs administered in combination are the current standard of care for patients with advanced PDAC and have shown significant, but modest survival increase in patients when compared to gemcitabine alone (Von Hoff *et al.,* 2013). The dual-drug loaded fibres were assessed for their cytotoxicity against multiple human and mouse PDAC lines in 2D and 3D *in vitro* cell based models. Radiation with chemotherapy has been shown to increase overall survival, however many patients are unable to tolerate the complete treatment schedule due to the compounded side effects. The efficacy of the dual-drug loaded fibres in combination with radiotherapy was also assessed in a clonogenic cell survival assay.

3.4.1 Morphology

The structure of a coaxial fibre has two main components – the core and the sheath. These components can consist of polymers with different solubilities in organic and aqueous solvents (Saraf *et al.,* 2009). These differences are beneficial when developing multi-drug eluting structures, as the polymer chosen can be closely suited to the physicochemical properties required for solubility of the chosen drug. As gemcitabine and paclitaxel are the gold standard for PDAC treatment, suitable polymers needed to be chosen to allow maximal drug loaded with minimal morphological changes. Chapter 2 reported on the development of gemcitabine loaded alginate and chitosan fibres, and assessed their efficacy *in vitro*. Alginate was shown to be superior to chitosan, as the alginate polymer itself displayed no non-specific toxicity toward the cells, while the chitosan fibres did. In this chapter, alginate remained the polymer of choice for gemcitabine delivery. PCL and PLGA, both hydrophobic polymers, were selected for biocompatibility assessment, to determine which polymer was most suitable to form the shell structure of the coaxial fibre to allow for the loading of paclitaxel. PLGA is a co-polymer of PGA and PLA. Originally, the co-polymer was designed to overcome limitations of PLA and PGA alone, such as degradation control (Makadia and Siegel 2011). A 75:25 PLGA was chosen for use in this study as it has been reported to give a sustained release profile of hydrophobic drugs when modelled *in vitro* by Makadia and Seigel (2011), and the lower PGA concentration means

the polymer will have a slower degradation rate to that of a higher PGA content (Makadia and Siegel 2011). PCL is a commonly used polymer for drug delivery, and is known for its use in contraceptive implants and was discussed in Chapter 1, Section 1.4.3. In this study, PCL was the superior polymer, as it was the least toxic against cells when compared to PLGA, and was therefore selected for all further fabrication of coaxial dual-drug loaded fibres.

Initially alginate was spun as the shell material, and PCL as the core. Alginate has been reported to be successful in coating hydrophobic polymers in order to stabilise them and improve delay release from the core. The fibres formed during the spinning process and the SEM images showed alginate crosslinking and PCL coagulation. When the fibres dried however, the alginate began to crack and peel away from the PCL core. As alginate is a hydrogel which is comprised of up to 90 % water when in the hydrated state, this results in significant shrinkage upon drying (Wang *et al.,* 2005). Rapid dehydration and subsequent shrinkage is known to cause cracks so is the likely explanation for the flaking and cracking observed in this study (Matsukawa *et al.,* 2016). The cracking would be less likely to occur if the inner core material shrank at the same rate (i.e. was similarly a hydrogel), however PCL is reported to have very low shrinkage rates (Cheng *et al.,* 2014). Wanawananon *et al.,* performed a similar study in in which coaxial fibres were fabricated with a 1 % alginate shell and a 20 % PLGA core, however the final SEM images showed an uneven shell thickness, and apparent cracks throughout the alginate shell (Wanawananon *et al.,* 2016). It was therefore determined that the alginate was most suitable as the core material for this study and PCL the shell material.

There were no apparent problems with the fabrication and drying of this formulation. When the hydrated fibres were imaged however, the alginate core had an “icy” appearance. This is indicative that crosslinking has not properly occurred as there are no visible pores, and the frozen alginate/water mixture is thought to have given it the icy appearance. Even though the fibres were spun into a $CaCl_2$ coagulation bath, it is thought that the PCL coagulated too quickly for the $CaCl_2$ to properly crosslink the alginate. Therefore an internal crosslinking method was employed. $CaCl_2$ is commonly used when very rapid crosslinking is required, as it is soluble in water. When dissolved, the calcium ions are free to crosslink the alginate chains. An internal crosslinking method was then employed, using

$CaCO_3$ and glucono-delta lactone (Kuo and Ma 2001, Jang *et al.,* 2014). This is a slow crosslinking method, which is advantageous when the alginate structure is thick and even crosslinking throughout the structure is required. This is something that cannot always be achieved using $CaCl_2$, as the calcium will only penetrate a certain distance through the alginate, often leaving the centre uncrosslinked (Liling *et al.,* 2016). $CaCO_3$ is insoluble water at pH 7.4, so does not crosslink the alginate solution when added to the spinning solution. Glucono delta-lactone was added at the last step before spinning, where it slowly released H^+ ions, which causes decomposition of the $CaCO_3$. This decomposition results in calcium ions slowly being released and therefore available to successfully crosslink the alginate (Shchipunov and Postnova 2011).

It was clear that when the drug formulated for injection (in this case, paclitaxel formulated as Anzatax) is added to the polymer and a fibre fabricated, there is significant impact on the fibre morphology, which is likely from the presence of the oil in the excipients and observed by the lack of pore structure. Drugs for injection are not always the best to load into a polymeric DDS, so the addition of *nab*-paclitaxel was not assessed as it is also formulated for patients and contains excipients necessary for injection. Instead, pure paclitaxel was loaded, which resulted in no effect on polymer structure. This is in line with the literature, which primarily describes the loading of pure laboratory grade drugs into DDS. This result also agrees with previously published work in the area of electrospinning PCL fibres loaded with paclitaxel to form scaffolds for vascular grafts that showed that the addition of paclitaxel does not affect the final fibre morphology (Pektok *et al.,* 2008, Innocente *et al.,* 2009, Zhu *et al.,* 2013). Previous studies have shown that the addition of gemcitabine does not negatively impact the fibre morphology, which was also observed in Chapter 2.

The addition of gold nanoparticles was performed in order to increase the echogenicity. Echogenicity is the ability to reflect an ultrasound wave – and by increasing the echogenicity, the ability to be viewed under ultrasound is increased. This is important in this study, as EUS-FNI is the proposed technique for implantation. The importance of echogenicity when using EUS-FNI for implantation of DDS was identified in a study using OncoGel. OncoGel

is a thermosensitive gel carrier (ReGel) that is loaded with paclitaxel (Matthes *et al.*, 2007). It was injected as a solution into the pancreas of Yorkshire pigs, which solidified at physiological temperatures. The authors found difficult to clearly visualise the location of the EUS needle, and therefore found it challenging to inject the solution into the correct location of the pancreas. Further testing is still required on our formulation, as none of the drug loaded formulations in this study contained these gold nanoparticles. Although gold is inert, assessment of the impact on drug release, as well as cytotoxicity assessment is required (Elahi *et al.*, 2018). If drug release or fibre formations is found to be affected, gold sputtering is another technique that can be utilised, which involves sputtering a fine layer of gold on the outside of the implant. Future work should assess the effect of loading or sputtering with gold on the biophysical and biological aspects.

3.4.2 Drug Release

While hydrophobic, PCL has high drug permeability which makes it suitable for delivery of large drugs such as steroids, but therefore does not restrict gemcitabine release from the alginate core, resulting in a gemcitabine release profile similar to that of a single fibre (Pitt *et al.*, 1979, Coombes *et al.*, 2004). Release rate of gemcitabine from a coaxial fibre compared to the single fibre in Chapter 2 was actually increased, which was unsurprising as the increased drug loading (gemcitabine loading increased from 0.042 mg/30 cm in single fibres to 2.43 mg/30 cm in coaxial fibres) has been reported to increase the porosity of the polymer upon drug release, thus allowing more aqueous solution to enter the polymer, increasing the release rate (McConville *et al.*, 2015).

It was anticipated that the shell structure would have the effect of slowing the release of gemcitabine from the alginate core. Previous work by Mirabedini *et al.*, has shown that when a coaxial fibre that consisted of an alginate core loaded with a model dye (toluidine blue) and a chitosan shell, the release was significantly slowed when compared to a single alginate fibre. The burst release was reduced and the release more sustained from the coaxial structure. In a similar fashion, our study included fabrication of a coaxial fibre containing fluorescein loaded alginate core with a PCL shell, and compared the release to that of a single alginate fluorescein loaded fibre. It could be

observed that the PCL acted as a protective shell for the alginate core during spinning, with less of the fluorescent dye released in the bath compared to the single fibres (Fig 3.8). Furthermore, the release profile for the coaxial fibre showed a zero order release profile, while the single fibres displayed first order release profile. These results were not seen in release and loading studies using gemcitabine, and while model dyes are a cost effective way to estimate release profiles, it is clear that they do not accurately predict the release profiles of all hydrophilic, small molecule drugs and care must be taken when using dyes to model therapeutic DDS. The main stimuli that can trigger drug release from drug delivery devices are specific release media, temperature, hypoxia, presence of enzymes and pH (Iyer *et al.,* 2007, Shen and Burgess 2012, Chen *et al.,* 2017). We chose to use a simulated body fluid that is ionically similar to that of human blood plasma with the addition of phospholipase D, with release occurring at 37 °C. While this doesn't recapitulate the complexities of an *in vivo* solid tumour, it is more physiologically relevant than many systems that use only PBS solutions. In addition, there are currently no published *in vitro* release systems that describe an environment that is physiologically similar to that of a solid tumour for drug release studies.

PCL and paclitaxel are both soluble in many of the same organic solvents, such as DMF, chloroform and acetonitrile, however PCL is reported to be insoluble in alcohol, where paclitaxel has limited solubility in ethanol at 1.5 mg/mL. This allowed for extraction of paclitaxel in order to determine the total drug loading. A higher paclitaxel EE % compared to gemcitabine was expected due to the drugs hydrophobicity and the fact that the production method involves an aqueous bath, which theoretically should limit paclitaxel loss into the water bath by diffusion. Paclitaxel is a hydrophobic drug, which makes release into the same aqueous solution as gemcitabine difficult, and as a result a less physiologically relevant system was used. We chose to use a release method utilised by Zentner *et al.,* where paclitaxel release from a thermal gel (ReGel®) was studied (Zentner *et al.,* 2001). Due to the hydrophobic nature of the paclitaxel, and the drug release profile, we predicted that majority of the paclitaxel would remain in the fibre, unable to be released into the aqueous medium used in cell culture. It is known that paclitaxel solubility increases in Kolliphore EL (a main component of Anzatax), which was a component of the drug release medium. Cell viability tests were performed to test the tolerance of cells to Kolliphor EL, and found that the high toxicity meant that we

could not perform cell viability studies in a similar medium to that of the release studies, and is therefore possible the release profiles may be different.

3.4.3 Biological Studies

Before any DDS can progress into animal or human studies, vigorous *in vitro* assessment of their efficacy must be assessed. This is to minimise risk of adverse events occurring due to toxicity of the material and to prevent needless animal studies. This chapter describes the *in vitro* testing of the dual-drug loaded fibres in a 2D PDAC monolayer model and a 3D PDAC tumour spheroid model. 2D monolayer models are the most simple and high throughput cell based models and are often used as a starting point for *in vitro* drug testing. In this study, it was observed that both Mia-PaCa-2 and PANC-1 cells had a decrease in cell viability when treated with the empty fibre formulation after 72 h. While nonspecific toxicity from the polymer is undesirable in preclinical studies, it was considered that in this particular study, the physical presence of the coaxial fibre played a part in the reduction in cell viability. Coaxial fibre formulations absorb media (primarily the alginate core), and the implant frequently sinks to the bottom of the well, directly on top of the cells. This can cause cell shearing and damage, and therefore death or reduction in confluency. Studies into plasma membrane repair frequently use glass beads placed on top of cells to intentionally wound cells, it was therefore hypothesized that a similar phenomenon was occurring in this study (Reddy *et al.,* 2001, Defour *et al.,* 2014). This effect was further investigated by assessing cell viability after incubation of cells with a small length of clinically used, biocompatible surgical suture. Here the suture was placed in with the cells which after 72 h showed a reduction in cell confluency at a similar rate to that of an alginate fibre. As a nylon suture is assumed to be inert and lack cytotoxic properties, this confirms that the presence of the fibre itself is contributing to a reduction in cell viability. Such studies highlight both the advantages and disadvantages of using 2D monolayer cell culture for efficacy assessment of cancer therapeutics and devices/implants. 2D cell culture is a widely used and established method for further understanding cell biology, drug-cell interactions, mechanisms of disease and response to drug treatment. They are favoured for their high throughput, simple and cost effective nature and are the first line of testing for the majority of novel DDSs (Kapałczyńska *et al.,* 2018). The simplicity, however, of 2D cell

culture systems mean that the complexities of an *in vivo* tumour are not captured, and by altering the architecture of the cells the gene and protein expression may also be altered, as well as drug metabolism, cell differentiation and proliferation and is therefore a less accurate representation of the tumour and its microenvironment (Pampaloni *et al.*, 2007, Hickman *et al.*, 2014). Such simplified assays and false-hits contribute to the high translational failure of many cancer therapeutics. Realisation of the limitations that 2D monolayer assays have has resulted in the development of more advanced *in vitro* cell models, such 3D spheroid models of cancer.

In order to increase the physiological relevance of our *in vitro* systems, 3D spheroid models were utilised. As previously discussed in Chapter 2, Section 2.4.2, 3D cell culture models are superior to that of 2D cell models, due to their more relevant tissue architecture, nutrient and waste gradients, and cell interactions (Baker and Chen 2012). Cellular models that maintain a 3D architecture similar to that of an *in vivo* tumour are more physiologically relevant, and give a more realistic representation of drug-cell interactions (Nunes *et al.*, 2019). Like 2D monolayer experiments, 3D tumour spheroids experiments are performed in an aqueous environment which discourages hydrophobic drug (i.e. paclitaxel) release. The drug loading and release results described in performed in this chapter, Section 3.3.4 showed that only 25.4 % of paclitaxel is released after 72 h and 28.8 % is released after 5 days. This however was in a release medium that was different to the cell medium, as the release medium had been formulated to encourage drug release. Additionally, the crystallised paclitaxel present in the media may indicate that the all of the released paclitaxel is not available to the cells, and therefore is an underestimation of its efficacy in cell based studies. This further validates the need to perform these experiments *in vivo* for two main reasons. Firstly, the *in vivo* microenvironment is very different and complex compared to that of *in vitro*, and we do not yet have a system that accurately represents this complexity. Secondly, *in vitro* studies are typically short term which may not give these long term release implantable DDSs time to take full effect, whereas *in vivo* experiments commonly span over a longer period of time.

To further increase the relevance of the 3D tumour spheroid model, there have been studies which incorporate an

extracellular matrix surrounding the spheroids. One particular study combined pancreatic stellate cells with PDAC cells, and found that the spheroids formed with both cell types were smaller and had an increased optical density, indicating that the stellate cells and their production of ECM proteins such as collagen are creating a tightly bound matrix (Ware *et al.,* 2016). This increased density has implications in drug diffusion and drug resistance. This was further explored by Yip and Cho, in which a 3D tumour spheroid model was developed that closely mimics the *in vivo* tumour microenvironment in a liver carcinoma model (Yip and Cho 2013). A comparative study was performed using a hepatocellular liver carcinoma cell line, where a 2D monolayer, 3D tumour spheroids (± stromal fibroblasts) grown in media, and 3D tumour spheroids (± stromal fibroblasts) embedded in a collagen I gel (the main interstitial matrix component of solid tumours) were treated with doxorubicin at the same concentration. Their results showed a significant increase in drug resistance in the spheroids that were encapsulated within the collagen gel, and the greatest resistance increase in the collagen embedded spheroids co-cultured with fibroblasts. This is indicative that the stromal fibroblasts and a collagen hydrogel culture system (similar to that of a tumour extracellular matrix) provides more resistance to anticancer drugs, and therefore provide a model that is more relevant to an *in vivo* environment. While this type of system is classified as physiologically relevant, it still does not capture many aspects of the complex in vivo environment, such as the immune system and inflammation, however is something that would be useful in future work on this project (Froeling *et al.,* 2010). Organoids are another type of physiologically relevant *in vitro* model which involves taking cells from a tumour biopsy of a patient and growing them in a basement membrane matrix, which generates a patient specific organoid that can be used for diagnostic and therapeutic analysis (Aberle *et al.,* 2018). These organoids are able to incorporate aspects of the immune system, as was described in a study that generated patient derived PDAC organoids containing cancer associated fibroblasts (CAFs) and T cells (Tsai *et al.,* 2018). This study also described the activation of alpha smooth muscle actin (αSMA) which is indicative of a myofibroblast like phenotype, which was observed in the organoids grown with CAFs. It was also observed that the CAFs grown as a monolayer on plastic did not secrete αSMA, which is indicative of important paracrine signalling between cancer cells and fibroblasts in this organoid model.

Multimodality therapy is common in pancreatic cancer, and radio- and chemotherapy administered in combination is a common treatment regimen. Chemoradiation can be administered as an adjuvant therapy (after tumour resection) or as a neo-adjuvant therapy (before tumour resection) for borderline, non-resectable and palliative PDAC cases (Herreros-Villanueva *et al.,* 2012). Radiation therapy is often limited to the tolerance of the tissue surrounding the tumour to the radiation. Administration of gemcitabine and/or paclitaxel prior to radiation has been shown to sensitise cancer cells, resulting in no overlapping toxicities and requiring less radiation to achieve tumour shrinkage (Doyle *et al.,* 2001, Mierzwa *et al.,* 2010). It was observed in this study that cells pre-treated with empty fibres, followed by 1 Gy radiation had a radiosensitising effect, whereas the cells treated with the empty fibre alone had no effect on the survival (when compared to the untreated control). There are few papers describing the effect of polymers or polymer breakdown products on the ability to radiosensitise tumour cells. One study described the radiosensitising effects of some bioactive compounds isolated from marine sponges. Two isolated compounds showed minimal cytotoxicity against a human hepatocellular carcinoma (Hep3B) cell line, even at concentrations of 10 µg/mL (Choi *et al.,* 2018). Hep3B cells were then pre-treated with 1 µg/mL of these two compounds before exposure to increasing doses of radiation (0-8 Gy), and it was observed that the compounds had a significant radiosensitising effect at all radiation fractions after performing a clonogenic assay. This therefore warrants further investigation of our dual-drug loaded fibres to act as radiosensitising agents.

Gemcitabine is the most commonly administered agent for chemoradiation of pancreatic tumours prior to surgery, and has been shown to have more favourable outcomes compared to other agents such as 5FU and capecitabine (Peng *et al.,* 2019). It has also been shown that paclitaxel is an effective radiosensitiser for pancreatic cancer, with the added benefit that gastrointestinal mucosa are not radiosensitised (Safran *et al.,* 2001). The initial problems with paclitaxel treatment however, such as severe hypersensitivity reactions, were still an issue and resulted in cessation of treatment in a number of earlier studies (Safran *et al.,* 1997, Safran *et al.,* 2001, Chung *et al.,* 2004). A recent phase I dose escalation study was the first to clinically assess the efficacy of *nab*-paclitaxel administered prior to and concurrently with radiation in 9 patients with locally advanced PDAC (Shabason *et al.,* 2018). Of the 5 patients

that initially presented with non-resectable tumours, 2 underwent surgical resection, while of the 4 patients who initially presented with borderline resectable tumours, 2 underwent surgical resection, which indicates *nab*-paclitaxel is a promising radiosensitser and preferential to that of paclitaxel formulated with cremaphore. Another recent paper assessed the efficacy of concurrent administration of *nab*-paclitaxel, gemcitabine and radiation in 38 patients with borderline resectable PDAC (Takahashi *et al.*, 2018). Of the 29 patients who completed all of the chemoradiation, 24 received a total pancreatectomy while 5 did not receive subsequent surgery, with 3 patients achieving pathological complete response. 8 patients were unable to tolerate the chemotherapy prior to the radiation, and 1 patient was unable to tolerate the chemoradiation, which further highlights the potential benefit of local chemotherapy DDS in combination with radiotherapy as the systemic toxicity would potentially be significantly reduced.

3.5 Conclusions

This chapter describes the fabrication, biophysical characterisation and *in vitro* preclinical evaluation of coaxial fibres concomitantly loaded with gemcitabine and paclitaxel. The gemcitabine loaded alginate core displayed rapid drug release, whereas the paclitaxel release from the PCL shell was more difficult to model *in vitro*, as the hydrophobicity of paclitaxel meant that it was not fully soluble in aqueous media and therefore not all of the drug was released. A significant reduction in cell viability was observed upon treatment with dual-drug loaded fibres when PDAC cells were grown as 2D monolayers and 3D spheroids, which is promising for further studies. This chapter highlights the importance of using *in vivo* models for accurate assessment of the release properties of drugs, specifically hydrophobic drugs, as the majority of *in vitro* systems favour hydrophilic drug release media and for assessment of uptake into cells. Altogether this further highlights the importance of using *in vivo* animal models that recapitulate the *in vivo* environment for drug release studies. Data in this chapter also demonstrates that drug-loaded implantable delivery systems have potential application in the neoadjuvant setting as radiosensitiers for multimodality therapy where radiotherapy is required but combination treatment is not always tolerated due to the toxic side effects of systemic chemotherapy. More studies are therefore warranted.

Chapter 4: *In Vivo* Efficacy of Gemcitabine and Paclitaxel Loaded Implants

4.1 Introduction

Before any new therapeutic medical device can be entered into human clinical trials, and subsequently placed on to the market, rigorous preclinical studies must be performed. Strict guidelines for the approval of medical devices in Australia are described by the therapeutic goods administration (TGA), outlining the clinical evidence required before approval (Therapeutic Goods Administration 2017). This involves a number of steps, such as initial *in vitro* testing such as in Chapters 2 and 3, however the clinical significance of these tests requires further validation in more complex disease models. This is to assess the chemical, physical and biological properties of the device, which is just one of the 15 principles required by the TGA before approval (Therapeutic Goods Administration 2017). The bulk of preclinical testing is therefore performed in animal models before progression into clinical trials.

The majority of preclinical medical device testing is performed in mice, of which there are a number of models available for PDAC. Mice bearing human tumours are known as xenografts – of which there are two types. Cell line derived xenografts (generally referred to as just "xenografts") are established by injecting established and well validated cell lines into immunocompromised mice. This method has the advantage of being easily accessible and reproducible, however the cells may have lost some of their original characteristics through their *in vitro* growth conditions. Patient derived xenografts (PDX) are established by engraftment of a piece of a patient's original tumour directly into the mouse. This has the advantage of developing a tumour that retains its molecular signature, and original tumour heterogeneity and subpopulations. This can be further adapted to form what is known as an "avatar" model, in which immune cells and stromal components of the patient derived tissue is also transplanted into a mouse, allowing for facilitation of further studies into the interaction of stromal cells, cancer cells and immune cells (Zayed *et al.*, 2015). It is a useful way to predict drug responses in the patient, as samples of one tumour can be transplanted into a large number of mice, allowing for a very wide drug screen to be performed.

Limitations of this method include higher costs and skill levels required and longer establishment time. Additionally, the stromal cells that are of significant importance in human cancers cannot proliferate in mice,

limiting their usefulness as models to study the tumour microenvironment (Saluja and Dudeja 2013, Mazur *et al.*, 2015, Yada *et al.*, 2017).

Both cell line derived xenografts and PDXs must be established in an immunodeficient mouse – of which there are 3 main categories. "Nude" mice are homozygous for Foxn1^{nu} mutation, which results in a hairless, athymic mouse that is T cell deficient. Nude mice still retain natural killer (NK) and B cell function so cannot be used for models of blood cancers or slow growing primary tumour cells, however are useful for tumour development of rapidly growing tumour lines and fluorescence full body imaging due to their hairlessness (Yeadon 2013). This mouse model was therefore selected for our study.

Scid mice are homozygous for the *Prkdc*^{scid} mutation. *Prkdc* is required for DNA repair and sealing double stranded DNA breaks that occur during recombination of T cell receptor (TCR) genes and immunoglobulin (Ig) genes. Without *Prkdc*, TCR and Ig genes cannot rearrange which results in a mouse with no T or B cells. *Rag*-deficient mice fail to express *Rag1* or *Rag2*. The *Rag* genes function similarly to that of *Prkdc* genes and are important in recombination of TCR and Ig genes, and lack of either results in a mouse with a T and B cell deficiency (Yeadon 2013). These two latter strains of mice are useful when using slow growing primary cell lines, or blood borne cancers as they are more immunocompromised than nude mice. Finally, higher order multigenic mice are bred from either *scid* or *Rag*-deficient mice with additional immunodeficiency enhancing mutations. NSG mice, for example, are from the *scid* class (so therefore lack T and B cells), and additionally have null allele of the interleukin-2 (IL-2) receptor, which results in a NK cell deficient mouse. These are the most immunodeficient and are the most appropriate model for establishment of primary tumours (Yeadon 2013).

While human tumour bearing mice have their advantages, one significant downfall of those models is the lack of functioning immune systems. Syngeneic models are currently the backbone of pre-clinical immmuno-oncolgy studies, which involve transplanting murine derived cancer cell lines into a mouse of the same genetic origin. This

model allows for studies using an immunocompetent animal; however does not model tumour development and the induction of immune tolerance that occurs in humans (Lee *et al.*, 2016). Genetically engineered mouse models (GEMM) overcome this issue by developing spontaneous tumours in an immune proficient mouse. This model more accurately represents the tumour microenvironment, and the most extensively studied and utilised model for PDAC studies is the KPC mouse model (Lee *et al.*, 2016). This model mimics many of the immunologic features seen in human PDAC cases, such as an inflammatory reaction and exclusion of effector T cells. This model will be relevant for future testing of the implants prepared in in Chapter 5, where there is further discussion of immunotherapy treatments for PDAC.

Once the selection of the most appropriate host strain is selected, the tumour location needs to be determined, of which there are two main categories; ectopic (subcutaneous) or orthotopic. Ectopic PDAC models involve injection of cancer cells subcutaneously – often on the hind flank. This allows for development of a visible tumour that is easily accessible for confirmation of tumour development and subsequent calliper tumour volume measurements, and doesn't require surgery to establish (Richmond and Su 2008). This model is preferable when performing pilot studies, or when high throughput routine screening of therapeutics is required. This was therefore the location of choice for establishment of tumours in this study. An orthotopic model involves the establishment of a tumour in the tissue specific to the disease – for example injection of PDAC cells into the pancreas of a mouse. This is more clinically relevant as it provides more tissue specific pathology. However, there are some disadvantages to this model, as it is labour intensive and requires increased technical skill, the animals have a longer recovery time (as it requires open surgery), and produces a tumour with lower volume that is more difficult to measure and observe compared to the ectopic/subcutaneous model (Herreros-Villanueva *et al.*, 2012). Despite these issues, it is the preferred model for advanced testing of therapeutics and medical devices.

As animal studies are a critical step in the development of any new DDS, this chapter aimed to assess the *in vivo* tolerability and efficacy of dual-drug loaded fibres described in Chapter 3. A nude BALB/c mouse bearing human subcutaneous Mia-PaCa-2 PDAC tumour xenografts was utilised in this study.

This specific aims of this chapter were to:

1. Assess the tolerability of the implantation procedure (including the implant insertion procedure and mouse recovery from the procedure).
2. Assess the tolerability (including irritation or implant migration) of the implant (with and without gemcitabine and paclitaxel) *in vivo*.
3. Assess the tumour response and survival of mice treated with a dual-drug loaded implant compared to mice treated with an empty implant (with either i.v. saline or systemic gemcitabine and paclitaxel) or i.v. saline control.

4.2 Materials and Methods

4.2.1 Materials

Sodium alginate, polycaprolactone (PCL), calcium chloride ($CaCl_2$), calcium carbonate ($CaCO_3$), sodium hydroxide (NaOH), glucono delta-lactone (GDL), Gemcitabine hydrochloride was purchased from Toronto Research Chemicals, CA. Paclitaxel was purchased from FocusBio, Australia. 10 × Dulbecco's phosphate buffered saline (PBS) with $CaCl_2$/$MgCl_2$ and without $CaCl_2$/$MgCl_2$, endotoxin-free sterile water and Trypan blue were from Sigma-Aldrich. DMEM-High glucose medium was made in-house. Foetal calf serum (FCS) were purchased from Invitrogen, USA. Trypsin/EDTA was purchased from Life Technologies, Australia. Dimethylformamide (DMF) was purchased from RCI Labscan, Thailand. Insulin syringes (29 G) were from BD Biosciences. Needles for implantation were from Ebay, Aus. The isoflurane anesthetic, lignocaine and tissue glue was from Provet, Aus.

4.2.2 Spinning solutions

A higher level of sterility was required for the *in vivo* study, as the animals are immunodeficient and any potential endotoxins could skew results by causing an inflammatory response, and can lead to irreversible and fatal septic shock (Merck 2019). Spinning solutions were prepared as per *in vitro* studies (Chapter 3, Section 3.2.2) with the following changes: All bottles used to make the polymer/drug solutions were autoclaved before addition of polymers and water/solvents. Polymers (PCL and alginate) were UV sterilised for 20 min before dissolving in respective solutions. For the alginate spinning solution endotoxin free water was used to dissolve the alginate powder. Gemcitabine and paclitaxel solutions were filter sterilised through a 0.22 µm filter before addition to polymer solution.

For spinning procedure: all tools were submerged in 70 % ethanol before use, and spinning area and equipment were thoroughly wiped down with 70 % ethanol. No other people were allowed to enter the room during the spinning process. Immediately after spinning, fibres were rinsed in Milli-Q water, sprayed with 70 % ethanol and UV sterilised for 1 h, and allowed to completely dry for 72 h in BSC before being stored in sterile containers.

4.2.3 Capsule Fabrication

In order to make the coaxial fibres suitable for implantation a rigid capsule was fabricated for the fibre to be inserted in to, as the fibres themselves are too soft and flexible for implantation. With assistance from Dr. Sepidar Sayaar (University of Wollongong), PCL sheets were formed by melting PCL and pressed into a film at 120 °C using a heated press (Carver Bench Top Heated Presses, USA). Laser engraving (Univeral Laser Systems, PLS6MW, USA) was employed to create holes that were 100 µm in diameter, and 250 µm apart from each other. The sheets were cut into widths of 5.3 mm, in order to be molded around a metal rod with a circumference of 5.2 mm. Using a heat source, the sheets were warmed until the edges became transparent, and then were molded around the rod until sealed. Once cooled, the PCL molds were removed from the rod and the cut to lengths of 0.5 cm to form rigid capsules. Molds were submerged in ethanol for 10 sec and UV-sterilised for 1 h before use.

4.2.4 Implant toxicity *In Vitro*

To ensure the PCL capsule was biocompatible, the cell viability of Mia-PaCa-2 and PANC-1 cells was measured over time using the colorimetric MTS cell proliferation assay. The implant which consisted of the PCL capsule with 0.5 cm empty fibre loaded inside, or the PCL capsule with 0.5 cm dual-drug loaded fibre loaded inside were placed in in 600 µL of media (DMEM high glucose with 10 % FCS and 1 × PenStrep) and incubated at 37°C. At the following timepoints 24, 48 and 72 h 200 µL was removed and added to adherent cells in a 96-well plate. Cells were incubated for a further 48 h before MTS reagent was added to assess cell viability as described in chapter 2, Section 2.2.10.

4.2.5 Implant Formation for *In Vivo* Study

The implants were assembled just prior to implantation into mice in a BSC, so that they could be sterilised and properly dried before commencement of the study. Coaxial fibres (0.5cm) were cut, heat sealed and briefly dipped in 70 % ethanol, before being placed inside the pre-sterilised PCL capsule. The entire implant was then briefly

submerged in 70 % ethanol before being UV sterilised for 1 h and allowed to dry in the BSC hood and stored in a sterile container ready for use.

4.2.6 Preparation of Cells for *In Vivo* Study

The cells were prepared on the day of the experiment as previously described (Vine *et al.*, 2015). Mia-PaCa-2 cells were cultured in DMEM-High glucose containing 10 % FCS and cultured for 3 weeks before being expanded up into T-175 flask. Cells were confirmed mycoplasma free before injection. Cells were at passage 11 on the day of injection and were harvested in two separate batches. Cells viability and number were assessed using the Trypan blue exclusion method, with viable cells counted using a haemocytometer. On the day of inoculation, cells were detached using PBS/EDTA (5 mM in PBS without $MgCl_2$/$CaCl_2$) and the reaction stopped by adding PBS containing $CaCl_2$/$MgCl_2$. Cells were then pelleted by centrifugation (1200 rpm for 5 min), supernatant discarded, and cells resuspended in ice cold PBS to a final concentration of 1×10^7 cell/ml (1×10^6 cells/100 µL).

4.2.7 *In Vivo* Studies

Animal experiments were performed at the University of Wollongong with approval from the UOW AEC (ethics number AE18/13). Twenty four 4-5 weeks old nude BALB/c mice (12 male and 12 female) were purchased from the Animal BioResourses (Mossvale, NSW, Australia) and were housed in autoclaved individual ventilator cages in groups of 2 or 3. Animals were acclimatised for one week before they were subcutaneously inoculated with 100 µL suspension of 1×10^6 Mia-PaCa-2 cells in PBS by Dr Kara Vine-Perrow (University of Wollongong) using a 29 gauge insulin syringe in the right hind flank. Mice were injected one at a time, with the order of cages randomised. Mice were under isoflurane anesthesia for injections to ensure correct cell placement. Mice were weighed daily for the first week, then 3 times/week following. When tumours were palpable, they were measured 3 times/week until the treatment commenced. Treatment began when tumours reached a volume of 200 mm^3 using the following equation:

$$volume = a \times \frac{b^2}{2}$$

where a is the longest and b is the shortest tumour measurement along a perpendicular axis. All treatments were blinded, and mice were weighed and the tumour volume measured daily for the duration of treatment. The treatment cohorts contained n= 4- 6 mice per cohort (3 male, 3 female) and are as follows:

Cohort A: saline control (1 x 100 µL i.v. injection) 4 mice

Cohort B: 0.5 cm non-drug loaded (empty) implant (s.c. injection adjacent to the tumour) + saline (1 x 100 µL, i.v. injection) 6 mice

Cohort C: 0.5cm non-drug loaded (empty) implant (s.c. injection adjacent to the tumour) + 2 mg/kg gemcitabine and 0.2mg/kg paclitaxel (dose equivalent that that in the implant) in 1 x 100 µL i.v. injection) 5 mice

Cohort D: 0.5 cm dual drug-loaded implant* (s.c. injection adjacent to the tumour) + saline (1 x 100 µL, i.v. injection) 6 mice.

* containing 40 ug or 2 mg/kg gemcitabine and 27 ug or 1.35 mg/kg paclitaxel

The i.v. injections were performed on the lateral tail vein, immediately prior to the implantation procedure. Both procedures were performed by Dr Kara Vine-Perrow. For the implantation, mice were anesthetised under isoflurane, and once the animal was no longer responsive (toe pinch test), 20 µL lignocaine (2.5-4 mg/kg) was injected at the implant site for post implantation pain relief. Implants were inserted subcutaneously using a 13-gauge piercing needle and a titanium plunger, and implants placed above and adjacent to the tumour. Mice were recovered in an oxygen chamber and monitored for 15 min post procedure. Mice were checked twice more on day of procedure, and daily until endpoint.

4.2.8 Endpoint

Humane experimental endpoints in animal studies are put in place prior to the study's commencement. They are designed to terminate, minimise or decrease the pain and/or distress an animal experiences throughout the study while ensuring the scientific goal of the study is reached (Three Rs Microsite 2019). Experimental endpoints in this

study were when tumour reached a volume of 4000 mm^3 (2 cm × 2 cm), or when the treatment time reached 42 days, or if the tumour impeded hind leg movement or if there were any adverse effects from the implant. Upon sacrifice via CO_2 asphyxiation, the tumour, major clearance organs (kidneys, spleen, liver), auxiliary and inguinal lymph nodes, skin, lungs, and blood were collected. Blood was collected via cardiac puncture using a 25-gauge needle and placed in MiniCollect K3EDTA tubes (Greiner). Blood was centrifuged at 20,000 rpm for 20 min, the plasma collected and frozen at -20 °C. Tissue was weighed and washed in PBS before being placed in 10 % formalin (neutral buffered). Tumours were cut in half before addition to formalin. Tissues were fixed in formalin for 24 h, before being stored in 70 % ethanol until they were further processed for histopathology. The implant was recovered from all mice and stored at -20 °C until imaging by SEM.

4.2.9 Histopathology

All tissues that were fixed and stored in 70 % EtOH were processed for histopathology. Fixed tumour and major organs were processed overnight (ASP200 Vacuum Tissue Processer, Leica Biosystems, Germany), and embedded into paraffin blocks (EG1150 Modular Tissue Embedding Centre and EG1150 Cold Plate, Leica Biosystems, Germany) for histological analysis. Paraffin-embedded tissue blocks were sliced to a thickness of 5 µm (RM2255 Fully-Automated Rotary Microtome, Leica Biosystems, Germany) and transferred onto glass slides by floating sectioned tissue in a dH_2O water-bath at 37 °C. Slides were allowed to dry overnight prior to histological staining. Haematoxylin and eosin (H&E) staining was performed on a small linear stainer (Lecia ST4020, Leica Biosystems, Germany). Slides were imaged using a bright field microscope (Leica DM4000, Leica Biosystems, Germany). Stained tissue sections were examined for evidence of metastasis or histopathological changes associated with treatment.

4.2.10 Morphology of Implants Post Study

Morphology of the implants was assessed after removal from the animal, to observe any changes or degradation to the implant. Cross sections and the surface of the implants were assessed using SEM. Implants were cut in half and

placed in a brass block that contained predrilled holes and ridges for holding the implant in different configurations. Implants were imaged without freezing or coating and secondary electron images were taken at 5 or 10 kV operating voltage.

4.2.11 Cytokine Assay

A 13-panel cytokine assay was performed to determine whether there was any innate immune reaction to the implants. Serum concentrations of IL-1b, IL-6, IL-10, IL-18, IL-23, IL-12p40, IL-12p70, CCL17, CCL22, CXCL1, G-CSF, TFN-A, TGF-B1 were assessed using a BioLegend legendPLEX mouse macrophage/microglia 13-plex cytokine panel (Biolegend, USA). The assay was performed as per the manufacturer's instructions. Briefly, the serum was diluted 1:1 with assay buffer and incubated with the antibody coated beads for 2 h. After washing the beads, biotinylated detection antibodies were added and incubated for 1 h at room temperature. Streptaviden-phytoerythrin (SA-PE) was added and incubated at room temperature for a further 30 min. The beads were then analysed using flow cytometry (BD LSR Fortessa X-20). Concentrations of each cytokine were derived from standard curves using LEGENDplex analysis software.

4.2.12 Cell viability assay

In order to assess whether there was residual drug remaining in the implants after the animal study, implants that had been recovered from mice were incubated in 350 µL of complete media with 1 × Pen/Strep at 37 °C for 24, 48 or 72 h. At each timepoint, 100 µL of media was removed and placed in a 96-well flat bottom plate containing Mia-PaCa-2 cells that had been seeded at 4000 cells/well. Cells were incubated at 37 °C for 72 h before an MTS endpoint assay was performed as per Chapter 2, Section 2.2.10. Cell viability was normalised as a percentage of untreated cells.

4.2.13 3D printed capsule

The hand rolled capsules used in the *in vivo* study were a proof of concept, designed to show that housing the fibre in a rigid implant was a viable way to achieve successful implantation. To refine this process for future studies and upscaling, 3D printing was employed to fabricate capsules in an accurate, reproducible and scalable manner with equivalent strength to the handrolled capsules. 3D printing of capsules was performed by Dr Sepidar Sayyar (AIIM, UOW) using a KIMM SPS1000 bioplotter extrusion system. Melted PCL (> 60 °C) was printed through a 100 µM nozzle on to a rotating rod (1 mm diameter) to the length of 0.5 cm.

4.2.14 Mechanical Testing

Assessment of the strength of the 3D capsules compared to the hand-rolled capsules was assessed by Dr Sepidar Sayyar (University of Wollongong). Mechanical properties of the 3D printed capsules compared to the handrolled capsules and the fibre alone were compared using EZ-L mechanical tester (Shimadzu, Japan) and measured using a cyclic compression test. The samples were compressed by 30 % for 10 cycles. Compression strength is an important property as these capsules need to withstand pressure upon implantation.

4.3 Results

This *in vivo* study was performed to assess the tolerability of the implant procedure, the tolerability of the polymer implant in *vivo*, and the efficacy of the dual drug loaded implant when compared to empty implants and systemically administered drug. This study was performed over 6 weeks in immunocompromised nude BALB/c mice with ectopic human PDAC tumours, a popular animal model for PDAC efficacy studies. This model was selected due its ability to establish tumours from rapid growing cell lines and the animal's lack of hair, which made tumour measurement and implant insertion and observation easier.

4.3.1 Implant Cytotoxicity

The proposed future method of implanting the dual drug eluting implants developed in this thesis is by the use of endoscopic ultrasound guided fine needle injection (EUS-FNI), by which the implants are injected through the stomach wall and into the tumour. As discussed in Chapter 1, Section 1.3, pancreatic tumours are stiff due to their high intratumoural pressure and the surrounding desmoplastic stromal tissue. The fibres themselves were flexible and therefore not suitable for high pressure implantation as they were. We therefore fabricated a rigid hollow PCL capsule that the fibre could be housed in to form the final implant. To assess the biocompatibility of the implants, were performed a cell viability study using Mia-PaCa-2 cell lines grown as 2D monolayers to ensure that the capsules did not have any cytotoxic effect on cells before implantation into animals. Mia-PaCa-2 cells treated with empty implant aliquots taken at time 24, 48 and 72 h showed no decrease in cell viability compared to untreated cells, while cells treated with dual drug loaded implant aliquots taken at 24, 48 and 72 h showed an 18.8 %, 18.4 % and 30.3 % decrease in cell viability, respectively (Fig 4.1 A). PANC-1 cells were also unaffected by the empty implant aliquots, however showed a clear time dependent decrease in cell viability at 24, 48 and 72 h when treated with the dual-drug loaded implant aliquots, with an 11.1 %, 22.5 % and 37.8 % decrease in cell viability, respectively (Fig 4.1 B).

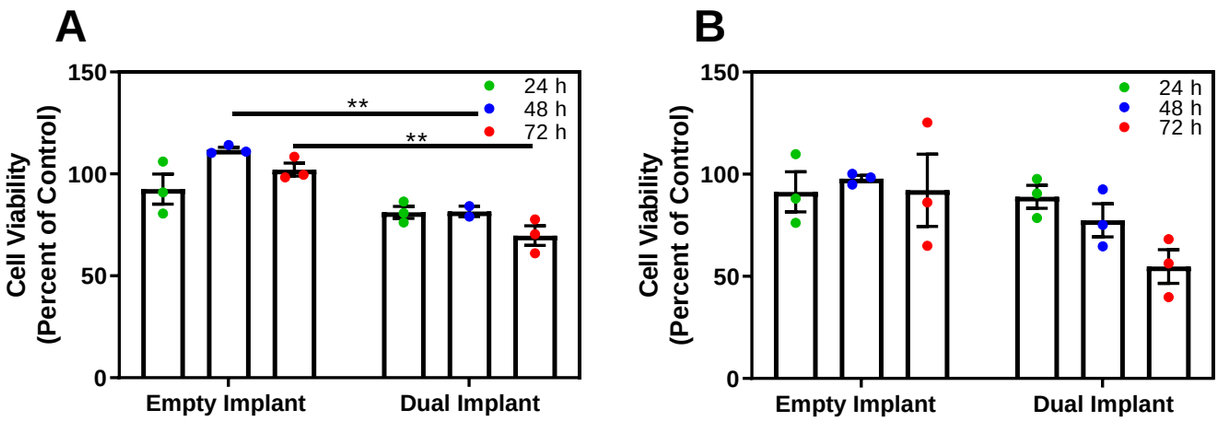

Figure 4.1: Dual-drug loaded implant consisting of a coaxial fibre housed in a rigid PCL capsule showed time dependant cytotoxicity. Cell viability after exposure to pre-incubated implant aliquots was assessed. Lengths of fibre (0.5 cm) encased in a PCL capsule were incubated in 600 µL of media, with 200 µL removed at 24, 48, and 72 h. The aliquots were placed in with A) Mia-PaCa-2 and B) PANC-1 cells and incubated for 48 h before an endpoint MTS assay was performed. Results are displayed as a percentage of an untreated control. Values are the mean (±SEM) of triplicates. **P≤0.01

4.3.2 Tumour Development and Treatment Toleration

Of the 24 mice injected with Mia-PaCa-2 cells (12 male, 12 female), 23 developed subcutaneous tumours (11 male, 12 female). Of the 23 tumour bearing animals, 21 were randomly assigned a treatment (11 male, 10 female). Two mice were excluded from treatment: one animal had a slow growing tumour that remained under the treatment start volume (200 mm^3) 90 days post tumour cell injection, while the other tumour bearing animal was sacrificed due to acute weight loss (16.3 % over 2 days) with no apparent cause identified. All animals tolerated the implantation procedure, with no animals experiencing any adverse side effects from the implantation (such as infection, inflammation or irritation) or the isoflurane anaesthesia (Gargiulo *et al.*, 2012). The implant is pictured in Fig 4.2, although the implants inserted into the animal were not gold sputtered as pictured. The implantation procedure used in this study was developed in house with the aid of animal welfare officer and veterinarian. The treatments were tolerated well with no reduction in animal weight over the treatment time in any treatment group (Fig 4.3). All cohorts gained weight over the study period and there was no significant difference between the start weights of the animals which were on average 24.2 ±1.9 g or the endpoint weights, which were on average 35.9 ±1.9 g between

cohorts. There were no side effects such as infection, irritation, inflammation, redness or swelling of the site of implantation or implant location (Fig 4.4 A). The implant did not migrate throughout the study and remained adjacent to the tumour in all treated animals, as can be seen in Fig 4.4 B after 14 days.

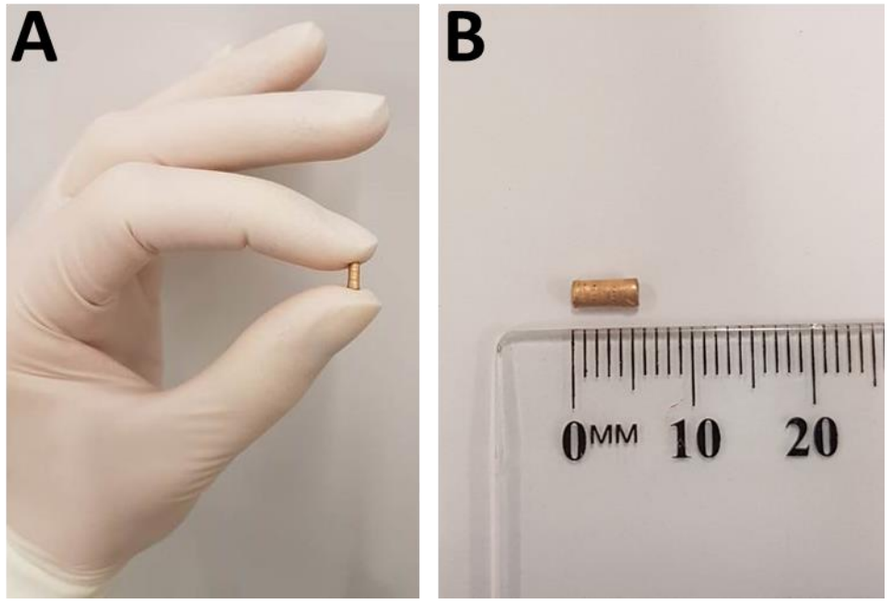

Figure 4.2: Photographs of gold sputtered, dual-drug loaded implant consisting of a coaxial fibre housed in a rigid PCL capsule.A) An implant relative to a human hand, and B) against a ruler showing the length (0.5 cm).

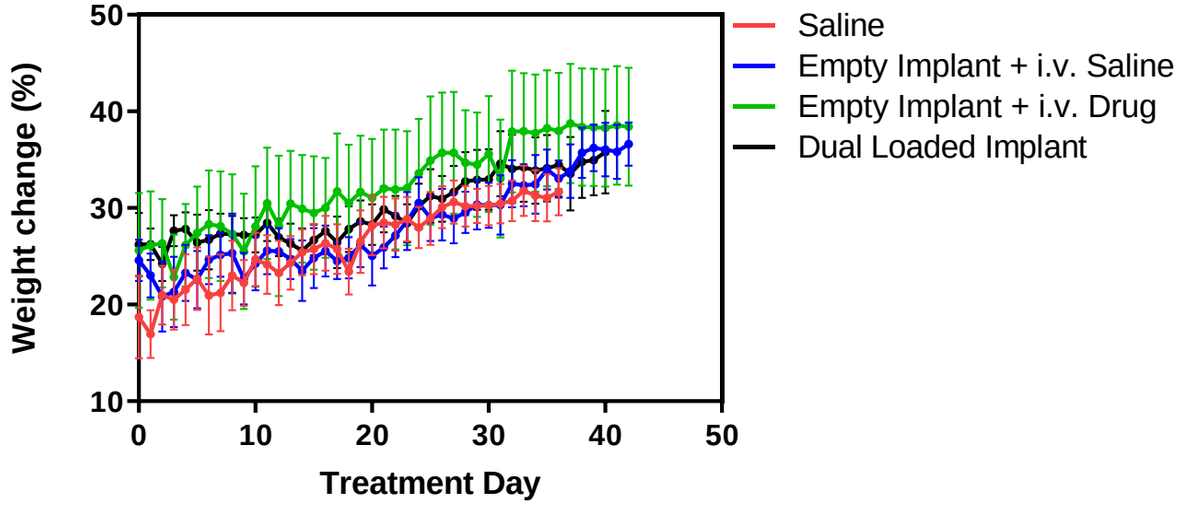

Figure 4.3: Percentage weight change over the treatment period. The percentage body weight change was calculated from the first time the animals were weighed before treatment had begun and is presented as the mean weight change +/- SEM. Data was pooled across male and female mice for all treatment cohorts.

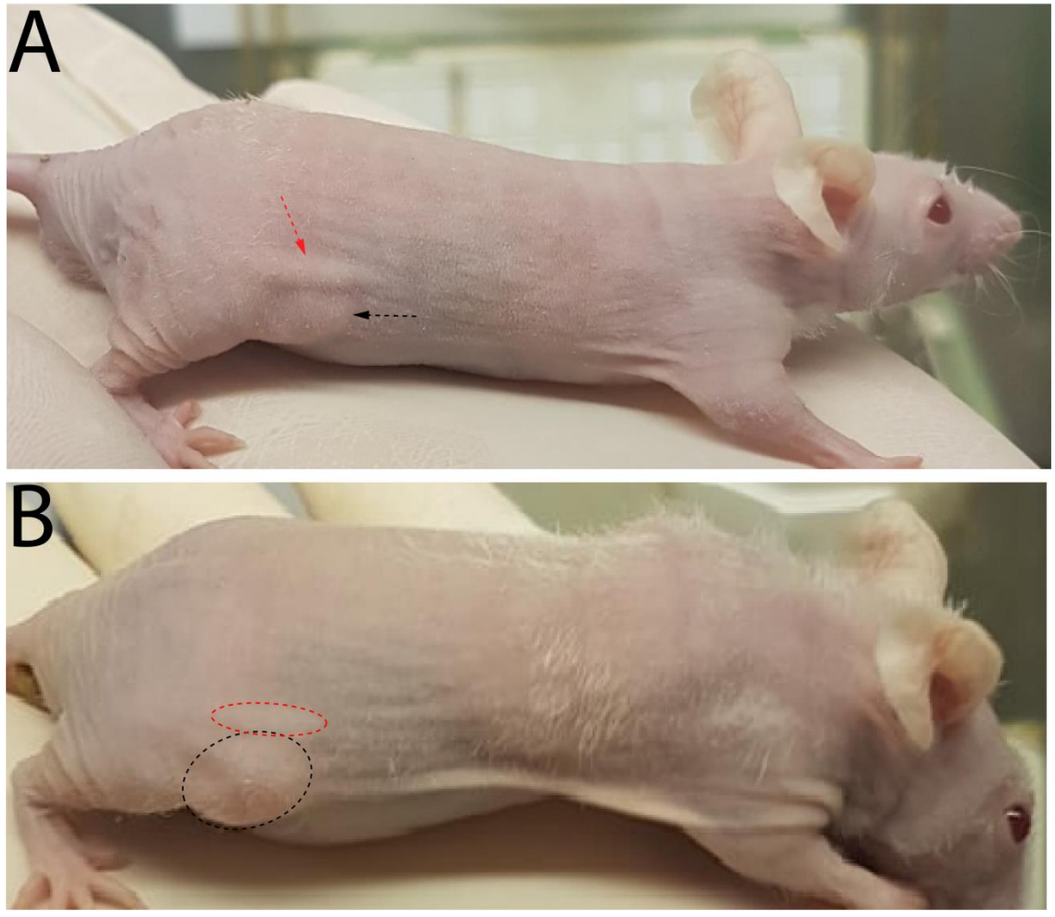

Figure 4.4: All mice tolerated the implantation procedure and implants did not migrate during study period. Photographs of a representative nude BALB/c mouse bearing subcutaneous Mia-PaCa-2 tumours implanted with an empty implant on A) day of implantation and B) 14 days after implantation. The red arrow and circle indicate placement of the implant, black arrow and circle indicates placement of the tumour. Representative image of male mouse from dual-drug loaded implant + i.v. saline cohort.

The time taken to reach the tumour start volume between the 4 different cohorts and across both sexes was also assessed. Following cell injection, the time taken for tumours to reach their starting volume of 200 mm^3 ranged from 29 – 87 days although was not statistically different between cohorts (Fig 4.5 A). On average, it took the male mice 56 days from cell injection to treatment, while the female mice took 67 days, although this was not statistically significant (Fig 4.5 B). The overall tumour growth between males and females was not deemed significant by one

way ANOVA (Fig 4.6).

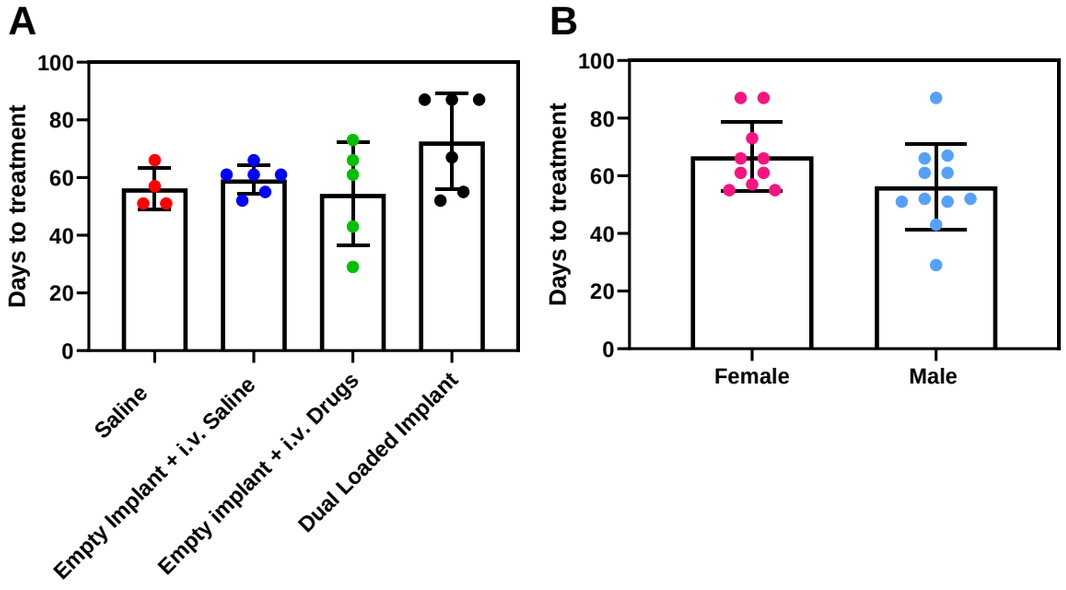

Figure 4.5: There was no significant difference in time to treatment start volume between cohorts or sex. The time taken to treatment start day was analysed for differences in A) cohort, B) sex. Values are the mean of 4-12 mice (cohort/sex dependant) ± SEM.

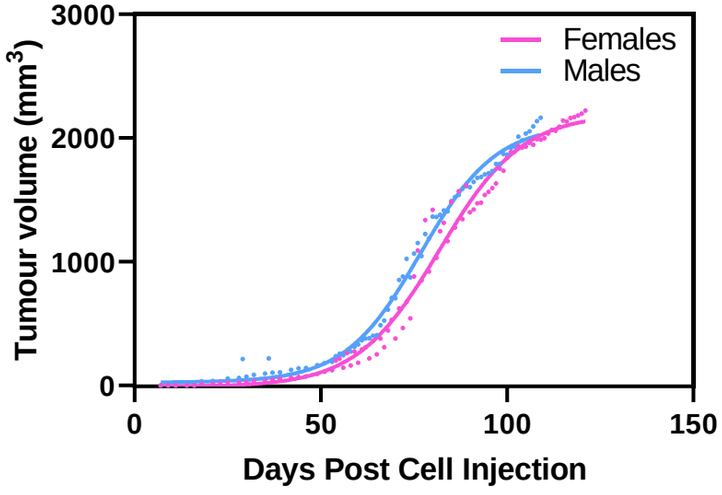

Figure 4.6: Tumour growth between male and female mice from day of Mia-PaCa-2 cell injection were not significantly different. Values are the mean of 12 mice per cohort.

4.3.3 Tumour Growth and Overall Survival

Tumour volume was measured 3 times weekly until start of treatment, and then daily until study endpoint. When measured from the treatment day zero, Cohort A (saline control) showed a 14.8 fold increase in tumour volume over the 42 day period (Fig 4.7 A). Mice treated with the empty implant, receiving either i.v. saline or i.v. gemcitabine and paclitaxel, or dual drug-loaded implants showed a 6.7, 12.0 and 12.1 fold increase in tumour volume over the 42 day study respectively. When the tumour growth was not normalised to treatment start day and instead from the day the Mia-Paca-2 cells were injected mice treated with the dual-drug loaded implant had a slower overall tumour growth compared to all other treatments (Fig 4.7 B). Four animals were sacrificed due to tumour involvement with the hind leg; one from the saline group (36 days after treatment), one from the empty implant + i.v. saline (41 days after treatment) and two from the dual-drug loaded implant cohort (12 and 40 days after treatment).

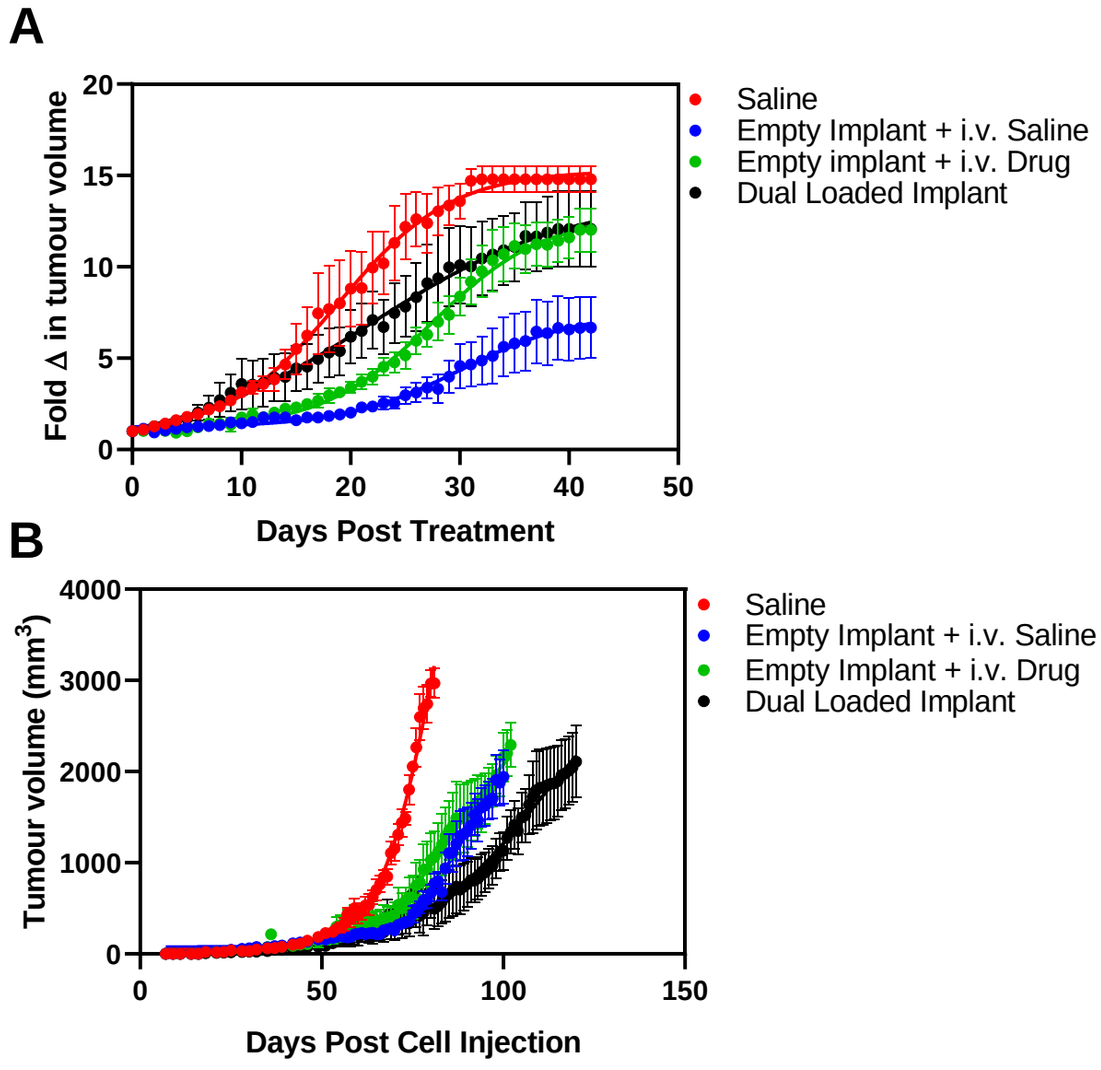

Figure 4.7 Tumour volume measurements. Tumour volume was measured from A) treatment day zero, B) from day of injection of cells. Measurements are the mean of 4-6 mice (cohort dependant) ± SEM.

The tumour growth curves were further plotted for each individual mouse per cohort (Fig 4.8). it was observed that there was a variation in tumour response in the animals treated with the dual-drug loaded implants, as can be observed by the bimodal growth curves (Fig 4.8 D). The tumour doubling time in dual-drug loaded implant treatment group was 13.47 (Fig 4.8 D) was comparable to the empty implant + saline group of 12.52 (Fig 4.7 B), while the doubling time in the saline treatment group was 9.97 (Fig 4.8 A) which was comparable to the empty implant + i.v. saline group of 10.70 (Fig 4.8 C).

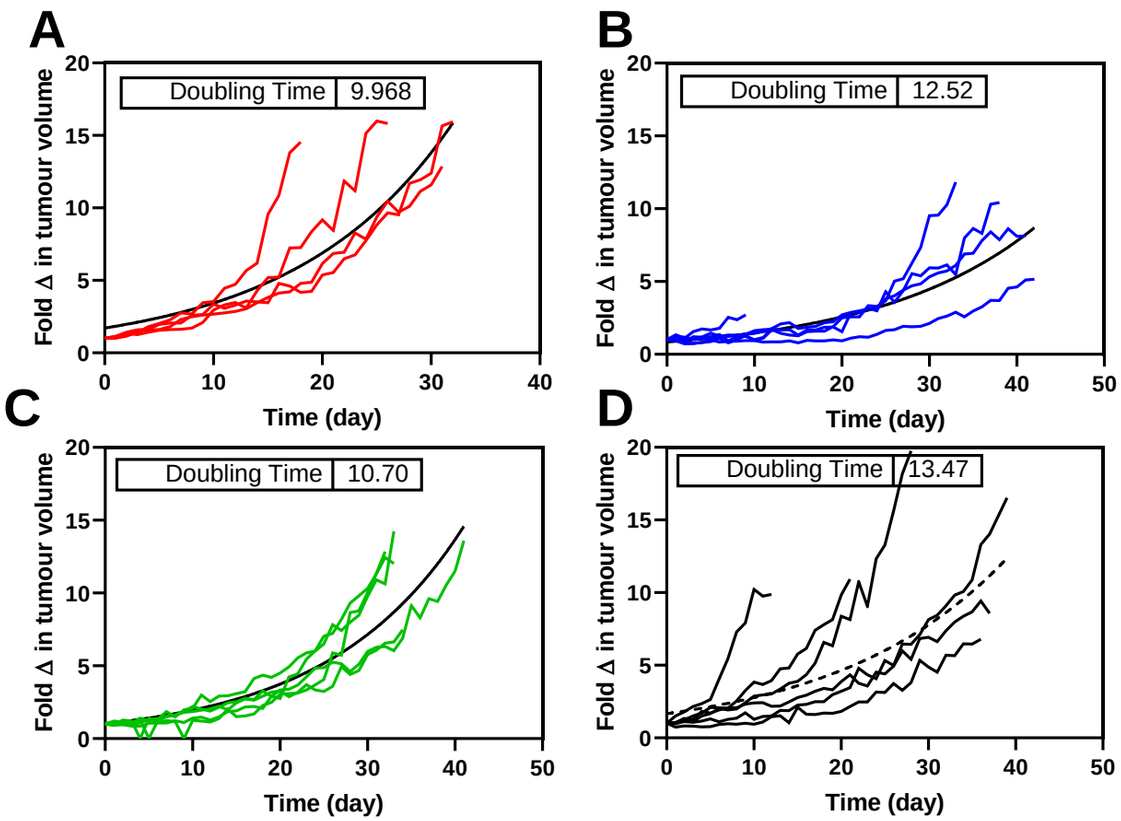

Figure 4.8: Variation of tumour growth was observed between animals in the cohort treated with the dual-drug loaded implants. Subcutaneous Mia-PaCa-2 tumour volume was measured from treatment day zero and the fold change in tumour volume calculated for animals treated with A) saline, B) empty implant + i.v. saline, C) empty implant + i.v. gemcitabine and paclitaxel, or D) dual-drug loaded implant

At the conclusion of the study, the tumours were excised, weighed and photographed (Fig 4.9). The average weight of the saline treated tumours was 2.3 ±0.3 g, the empty implant + i.v. saline was 1.3 ±0.2 g, the empty implant + i.v. gemcitabine and paclitaxel was 1.6 ±0.2 g and the dual-drug loaded implants was 1.4 ±0.2 g. There was no significant difference in the weight of the tumours between treatment cohorts at the conclusion of the study (Fig 4.10).

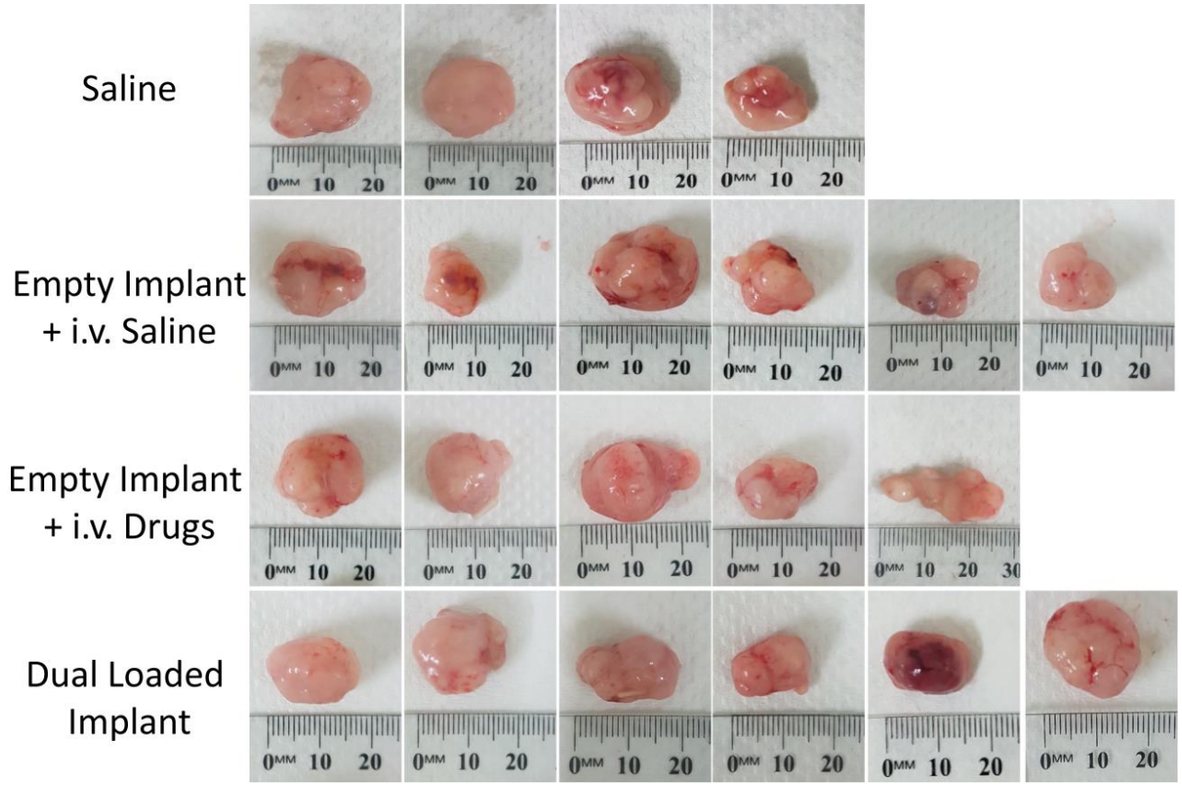

Figure 4.9: Photographs of tumours from each cohort at endpoint showed size variation. Mia-PaCa-2 subcutaneous tumours were excised from BALB/c nude mice at the conclusion of the study and photographed fresh before formalin fixation.

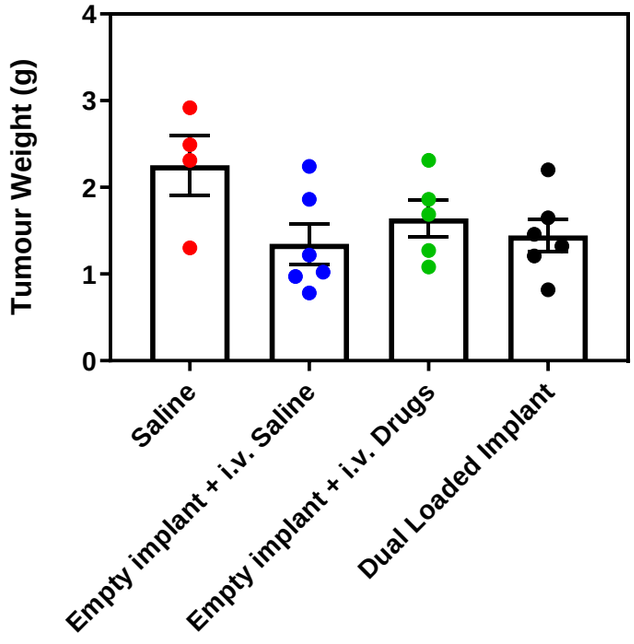

Figure 4.10: There was no significant difference in tumour weight between cohorts at the conclusion of the study. At endpoint, subcutaneous Mia-PaCa-2 tumours were excised and weighed. Measurements are the mean of 4-6 mice (cohort dependant) ± SEM.

The overall survival of animals in each treatment cohort was calculated using a Kaplan-Meier survival graph (Fig 4.11). Animals treated with saline had a median survival of 31 days, while empty implant + i.v. saline was 42 days, empty implant + i.v. gemcitabine and paclitaxel was 42 days and dual-drug loaded implants was 39 days. There was there was no significant difference determined by one-way ANOVA in survival however between treatment cohorts.

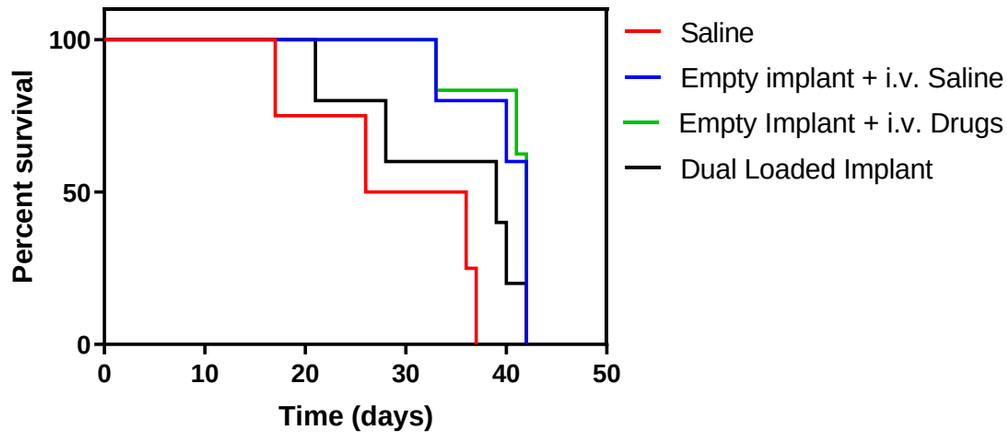

Figure 4.11: There was no significant difference in survival between any of the treatment cohorts. A Kaplan Meir survival curve was created to plot animal survival in each treatment cohort over 42 day study period.

Upon sacrifice, it was noted that the spleens of tumour bearing mice were enlarged, with the largest spleen weighing in at 1.00 g, non-tumour bearing mice have a spleen size of ~0.09 g, although overall there was no statistical difference between weights of the spleens in any treatment group (Fig 4.12 A). There was no significant difference in the weights of the lungs (Fig 4.12 B), liver, (Fig 4.12 C) kidney (Fig 4.12 D) between any treatment groups. H&E staining of paraffin embedded sections showed no signs of toxicity or metastasis to the liver or lungs (Appendix Fig A10 and A11).

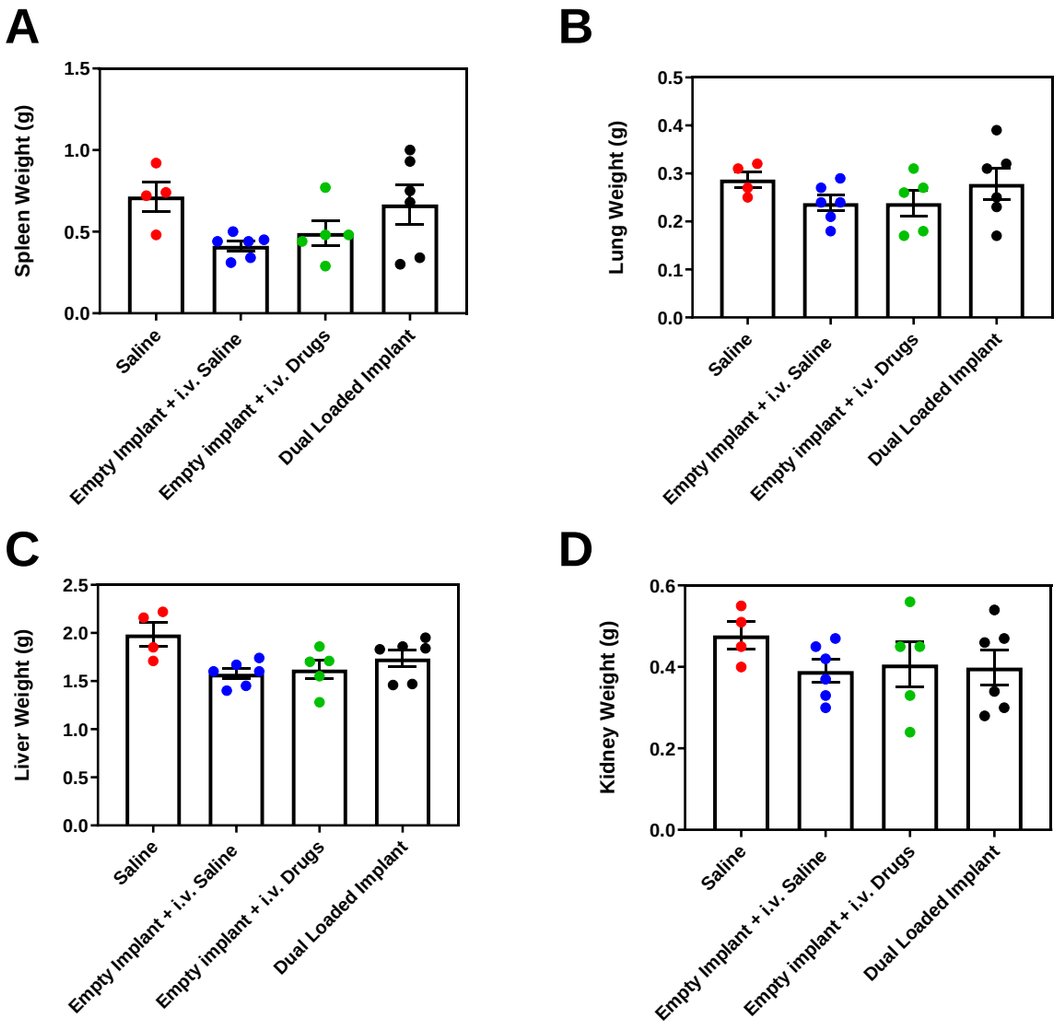

Figure 4.12: Excised tissue weights at the conclusion of the study. A) spleen, B) lungs, C) liver, D) kidneys . Measurements are the mean of 4-6 mice (cohort dependant) ± SEM.

4.3.4 Cytokine Profile

Cytokine levels in the blood of treated mice were assessed at the end of the experiment using a 13-plex macrophage/microglia cytokine panel (Fig 4.13). The data is summarized in Table 4.1. There was no significant difference between treatment cohorts in any of the 13 cytokines assessed.

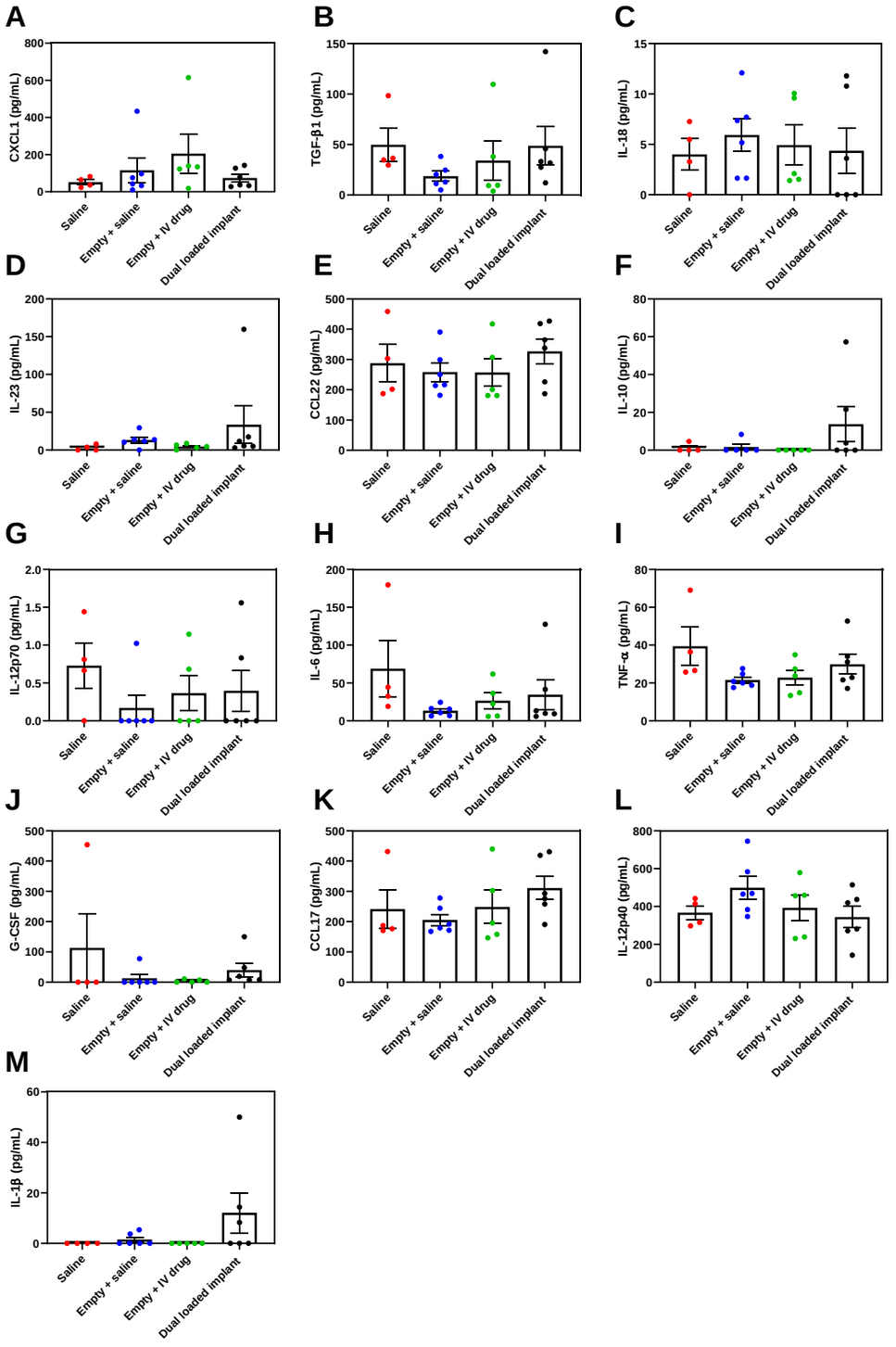

Figure 4.13: 13-plex cytokine panel showed no indication of an innate immune response toward the implants. Biolegend LEGENDplex 13-plex mouse macrophage/microglia cytokine panel. A) CXCL1, B) TGF-β1, C) IL-1β, D) IL-23, E) CCL22, F) IL-10, G) IL-12p70, H) IL-6, I) TNF-α, J) G-CSF, K) CCL17, L) IL-12p40, M) IL-1β. Data expressed as mean of 4-6 samples (cohort dependant) ± SEM.

Table 4.1 Mean cytokine concentration (±SEM) and fold change compared to saline only control

Cytokine	Saline	Empty Implant + i.v. saline		Empty Implant + i.v. Drugs		Dual-drug loaded Implant	
	Mean (pg/mL)	Mean (pg/mL)	Fold change	Mean (pg/mL)	Fold change	Mean (pg/mL)	Fold change
CXCL1	51.75±7.13	138.21±3.23	2.67	252.76 ±56.23	4.88	66.68 ±11.41	1.29
TGF-β1	49.81±8.72	13.46±2.92	0.27	40.24±11.18	0.81	62.18±11.21	1.25
IL-1β	4.00±0.91	4.58±1.04	1.14	5.64±1.22	1.41	3.84±1.28	0.96
IL-23	2.89±1.26	12.91±2.50	4.46	4.65±1.56	1.60	45.40±14.05	15.67
CCL22	287.66±33.54	250.82±17.62	0.87	276.53±23.69	0.96	329.06±26.73	1.14
IL-10	1.15±1.16	2.09±1.40	1.81	0	0	20.65±5.20	17.82
IL-12p70	0.72±0.31	0.25±0.17	0.35	0.45±0.26	0.63	0.59±0.29	0.82
IL-6	68.90±19.54	14.45±1.60	0.21	31.62±5.86	0.46	40.04±10.61	0.58
TNF-α	39.45±5.45	21.00±1.13	0.53	24.85±2.71	0.63	35.18±3.90	0.89
G-CSF	113.53±59.39	19.40±7.36	0.17	4.55±2.54	0.04	43.23±13.27	0.38
CCL17	241.43±33.76	204.22±10.51	0.85	261.71±32.07	1.08	285.94±23.14	1.18
IL-12p40	367.37±22.57	445.05±34.98	1.21	448.86±41.38	1.22	378.47±33.13	1.03
IL-1β	0	1.51±1.06	-	0	0	12.12±4.41	-

4.3.5 Residual Cytotoxicity of Extracted Implants

Following removal of implants from sacrificed mice, each implant was assessed for residual cytotoxicity. Drug release using HPLC analysis was unable to be performed, as previous assessments of the drug release of a 0.5 cm implant showed that the eluted amounts were too low to detect. The empty implants showed no cytotoxicity to the cells (Fig 4.14). The cells treated with the dual-drug loaded implants however showed 55.7 %, 56.2 % and 61.4 % of the cells remained viable after incubation with the implant for 24, 48 or 72 h, respectively (Fig. 4.14).

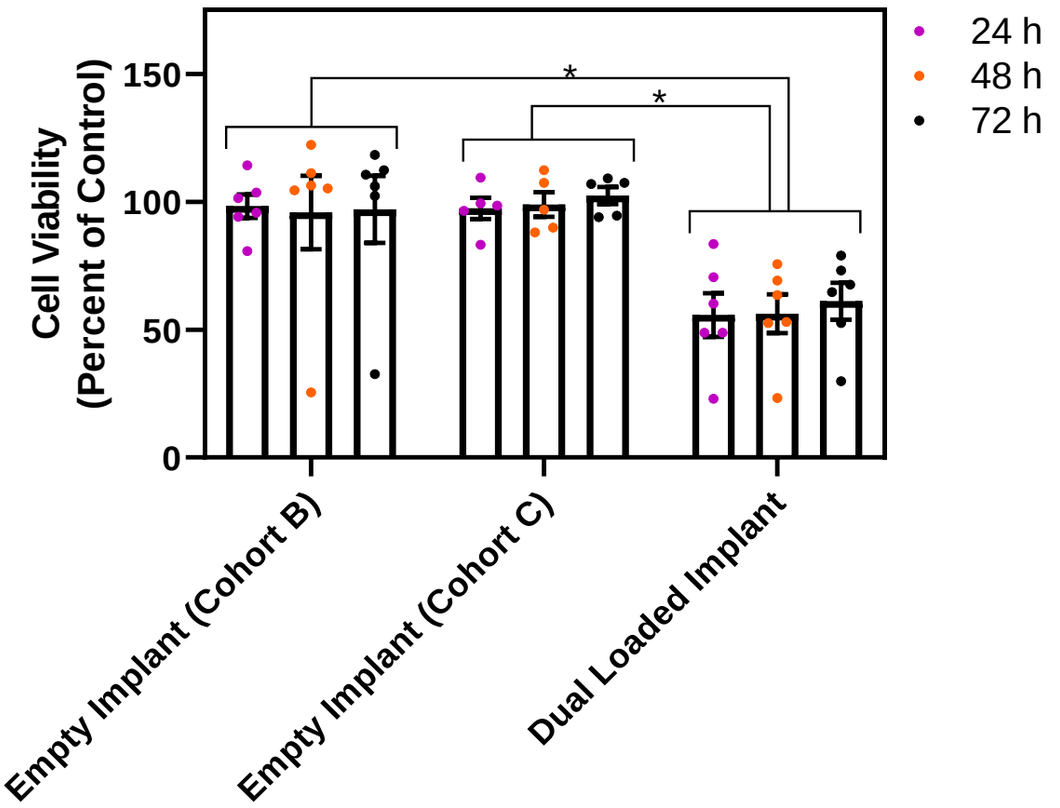

Figure 4.14: Dual-drug loaded implants retained loaded drug/s at the conclusion of the study and had a cytotoxic effect on cells. Implants were incubated in media and aliquots taken at 24, 48 and 72 h. Aliquots were placed in with Mia-PaCa-2 cells were incubated for a further 72 h before an endpoint cell viability MTS assay was performed. Results are displayed as a percentage of an untreated control. Values are the mean (±SEM) of sextuplicates. * $P \leq 0.01$

Cross sectional SEM images of the implants recovered from mice at the end of the experiment showed that the

fibre inside the implant was not fully hydrated (indicated by the blue arrow) (Fig 4.15 B,D,F). In addition, inspection of the surface morphology by SEM found many of the implants to be covered in a layer of connective tissue that appeared to have grown over the holes in the capsules, (indicated by the black arrows). Uncovered hole is indicated by red arrow as a comparison (Fig 4.15 A,C,E).

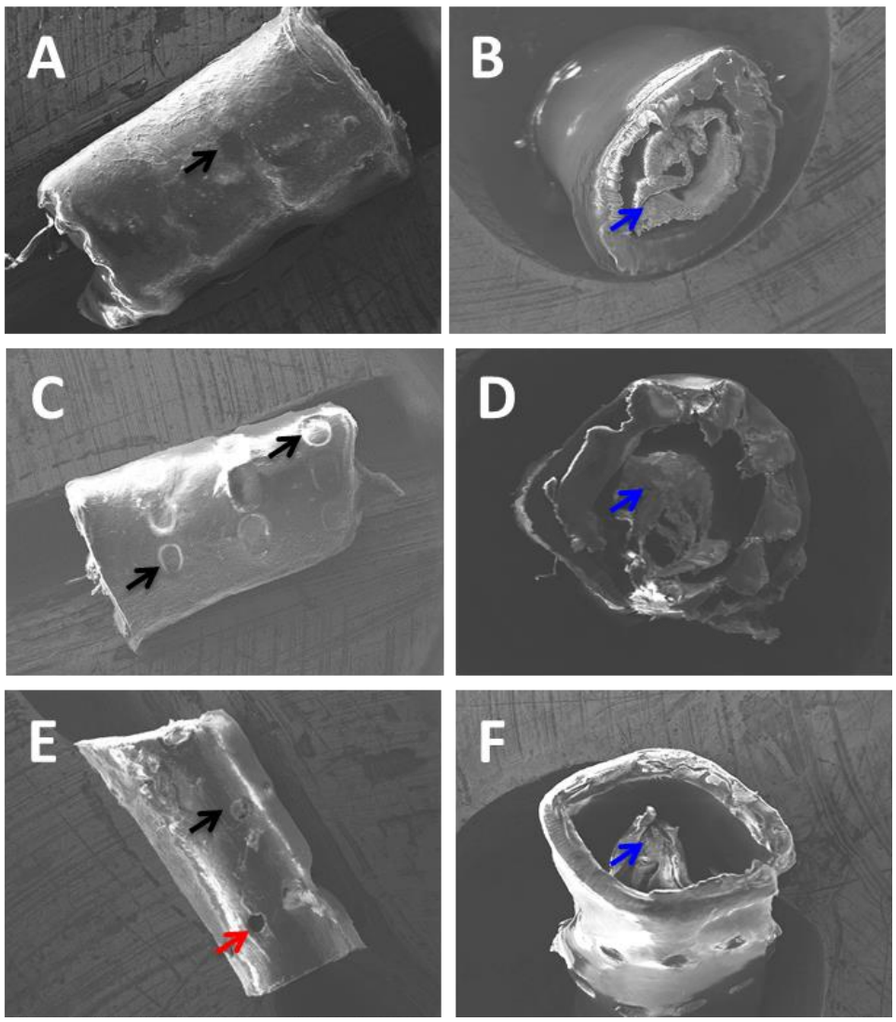

Figure 4.15: SEM images of implants from each cohort show that tissue has grown around the implant, and that the fibre within the implant appears dehydrated after removal from the animal. Representative SEM micrographs of implants after removal from animals after 42 days of treatment from each treatment cohort. A) external surface of an empty implant that was administered with i.v. saline, and B) its respective cross section. C) external surface of empty implants that was administered with i.v. gemcitabine and paclitaxel and D) its respective cross section. E) External surface of a dual-drug loaded implant and F) its respective cross section. Black arrows indicate holes in the implant that have been overgrown with tissue from the animal. Red arrow indicates presence of an uncovered hole. Blue arrows indicate presence of fibre (± drug) within the implant.

4.3.6 3D Printed Capsules

In order to progress these implants to further preclinical stages (e.g. larger animal models in rats and pigs), a

more reproducible and scalable method of capsule fabrication is required. Cross-sectional SEM imaging showed the hand rolled capsules to have an uneven wall thickness at the point where the polymer connects as indicated by the red arrow (Fig 4.16 A). The surface morphology was also imaged and showed location of the laser cut holes (green arrow) (Fig 4.16 B). We therefore used 3D printing as a method for specific and reproducible production of PCL capsules. SEM images showed an even wall thickness (Fig 4.16 C), and an outer exterior in a coil formation (Fig 4.16 D).

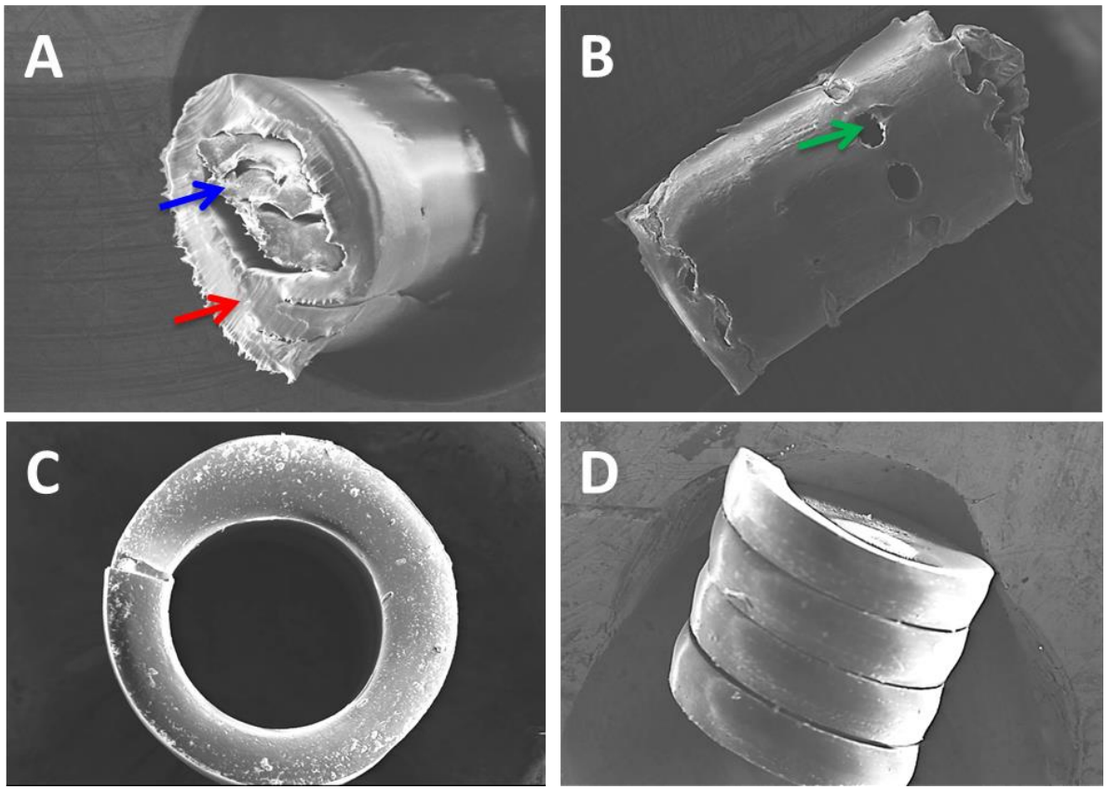

Figure 4.16: 3D printed capsules have a more consistent and uniform structure compared to handrolled capsules. A) cross section of handrolled capsule. Red arrow indicates position of the seam, blue arrow indicates presence of dehydrated fibre, green arrow indicates presence of laser cut hole B) external morphology of handrolled capsule. C) cross section of 3D printed capsule and D) external morphology of a section of a 3D printed capsule.

The implants are designed to be compatible with the EUS-FNI procedure for future implantation into tumours, so compression testing was performed to assess whether the mechanical strength of the 3D printed capsules was equivalent or better than the hand rolled capsules. The compression strength of the hand rolled and printed capsules was higher than the fibre alone (Fig 4.17). The force required to compress the fibre alone by 30 % was 0.2 N (Fig 4.17 C), whereas it took 7.4 N for the handrolled (Fig 4.17 A) and 9.5 N for the 3D printed capsules (Fig 4.17 B). The greater force required to compress the 3D printed capsules shows that it has superior strength and stiffness compared to the fibre and handrolled capsules. Due to the small sample size (n=2) of this proof of concept study, stastisitcal significance could not be calculated.

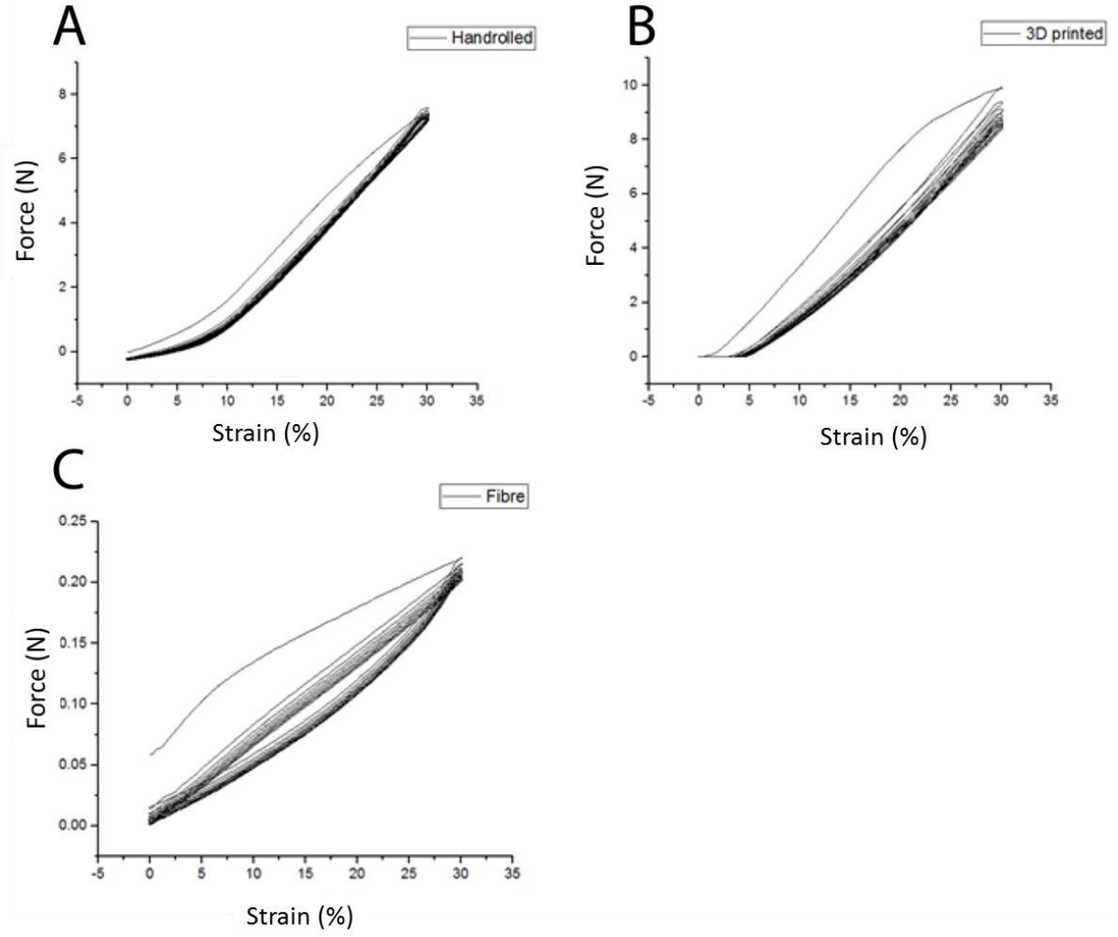

Figure 4.17: Compression strength of 3D printed capsules is higher than that of handrolled capsules or the fibre alone. The force (N) required to compress A) handrolled capsules, B) 3D printed capsules or C) fibre alone to 30 % was calculated. Values are the mean of 2 replicates.

4.4 Discussion

Mouse models of cancer are extensively used to assess the efficacy of new therapeutic devices before translation into human clinical trials. While use of these models does not assure translation into humans, it is a standard step in the pathway to larger animal studies and clinical trials. This chapter described the first efficacy study of gemcitabine and paclitaxel loaded coaxial fibres (described in Chapter 3) formed into an implant with a PCL capsule. These were implanted into a subcutaneous human xenograft mouse model of PDAC, and the efficacy of the implants (with and without gemcitabine and paclitaxel loading) was assessed over a 6 week period.

The tumour volume was measured externally using digital vernier callipers when the tumours became palpable. There was a difference in the time that it took the tumours to become established and the tumour growth across all mice. It was observed that the tumours in the male mice reached the 200 mm^3 implantation volume on average 11 days earlier than female mice and that could potentially be due to influence of male hormones, as the Mia-PaCa-2 cell line that was used in this study was originally derived from a male patient (American Type Culture Collection 2019). However although this was the trend, this was not significant. Sex differences in tumour establishment has previously been shown in sex dependent cancers such as prostate cancer (Namekawa *et al.*, 2019), however this has also been observed in other animal cancer models. For example, in one study, male mice established colon cancers more severely in males than in females (Lee *et al.*, 2016). This shows that while our results are not significantly different between sexes, it is something to note in future studies using different cell lines that are reported to be hormone dependent. The spleens of tumour bearing mice in this study were significantly larger than the non-tumour bearing mouse. This is likely due to the presence of the tumour, which is known to illicit an immune response and has been observed previously in KPC immunocompetent syngeneic tumour models (Bayne *et al.*, 2012), as well as in an animal model of breast cancer (Visonneau *et al.*, 1998). One study found that splenomegaly increased with tumour burden, but decreased with gemcitabine administration and subsequent reduced tumour burden (Le *et al.*, 2009). While nude mice are athymic and therefore T cell

deficient, they still have robust NK cells and B cell populations and display T cell leakage with age, and therefore can illicit an innate and a limited adaptive immune response (Belizário 2009, Okada *et al.,* 2019).

A surprising observation in this study was that the tumour volume was reduced in mice even in the presence of the empty implants. Initial *in vitro* studies performed prior to *in vivo* studies showed that the empty implant had no toxicity toward the cells (Section 4.3.1, Fig 4.1), as did post *in vivo* cell toxicity tests (Section 4.3.5, Fig 4.14). It is also widely published in the literature that PCL is biocompatible and FDA approved for implants (i.e. bone healing) (Roland *et al.,* 2015, Wu *et al.,* 2016), and although alginate has been shown to be biocompatible for implantable scaffolds, (de Vos *et al.,* 2002, Nunamaker *et al.,* 2007) it is currently FDA approved for dietary supplements. Hrynyk *et al*., observed a similar phenomenon in a subcutaneous PDAC xenograft mouse model in which non-drug loaded PLGA implants inhibited tumour growth and significantly reduced tumour volume compared to a saline only control after implantation (Hrynyk *et al.,* 2015). Implants containing oseltamivir phosphate showed initial tumour regression, but when the drug was depleted the tumour volume initially increased but then plateaued to have the same final tumour volume as the empty capsule – again indicating that the polymer was having an effect on the tumour. There are a number of potential reasons that this tumour inhibition from empty implants could be occurring. Hrynyk *et al.*, hypothesised that the presence of the implant adjacent to subcutaneously growing tumours prevented establishment of tumour vasculature, which in turn could impact the tumour growth rate. While we did not look at the relationship between tumour volume and vasculature on histological examination in this study, future studies could include injection of tracers that allow imaging of endothelial cell vessels in mice which will allow for high resolution observation of subtle changes in tumour vascularization upon treatment with implants (Eklund *et al.,* 2013).

Another reason for the observed tumour growth inhibition may be associated with a foreign body reaction (FBR) to the implant. A risk with implanting any foreign material is the activation of a local or systemic immune response. A FBR is the response of biological tissue to any foreign material in the tissue, despite it often being

inert and nontoxic. The response is characterised by macrophages and/or foreign body giant cells (FBGC) that persist at the biomaterial interface (Rodriguez *et al.*, 2009). A FBGC is a collection of fused macrophages which are generated in the response to a FBR. The reaction occurs in multiple phases; initially, following implantation of a biomaterial, blood/biomaterial interaction begins and a matrix forms around the biomaterial that is rich in cytokines, growth factors and chemo attractants that recruit cells of the innate immune system to the implantation site (Sheikh *et al.*, 2015). Following this, acute and chronic inflammation occurs in a sequential fashion, with the extent of this dependent on the degree of injury from implant insertion (Anderson *et al.*, 2008). The acute inflammatory response involves the infiltration of polymorphonuclear and mast cells, and is a short lived reaction that normally passes over a week, or progresses into chronic inflammation (Klopfleisch and Jung 2017). Degranulation of mast cells releases interleukin 4 and 13, which play a role in determining the extent and degree of the FBR (Sheikh *et al.*, 2015). Chronic inflammation lasts over a period of up to 2-4 weeks post implantation, and involves the infiltration of monocytes and lymphocytes at the implant site. Following this, FBGC develop which is a hallmark of FBRs and is what separates a FBR to chronic inflammation. Studies have shown that there are alternate FBR pathways that do not require T lymphocytes, and that nude mice are capable of eliciting a normal FBR in the absence of these cells (Rodriguez *et al.*, 2009). FBGC are a collection of fused macrophages that develop when a foreign body persists in the tissue. It is thought that failed or “frustrated” macrophages fuse to try increase their effectiveness (Klopfleisch and Jung 2017). Persistent presence of the implant may then lead to the formation of a fibrous capsule. Capsule formation is influenced by a number of pro-fibrotic and angiogenic growth factors such as platelet-derived growth factor (PDGF) and vascular endothelial growth factor (VEGF). Matrix metalloproteases (MMPs) are secreted by macrophages. These factors activate and attract fibroblasts and endothelial cells to the implant surface, which deposit collagen and ECM proteins to form granulation tissue. This capsule can then lead to implant failure, as the fibrous tissue surrounding the implantable DDS can hinder drug release and penetration (Klopfleisch and Jung 2017).

To further understand this phenomenon and assess whether a FBR was indeed involved, a mouse macrophage cytokine assay was performed using mouse plasma to assess up or down regulation of factors associated with the

innate immune system. Macrophages are derived from monocytes in response to tissue damage or infection and play an important role in modulating the host response. Macrophages also secrete a range of cytokines to aid in the wound healing process, as well as immunoregulation (Krzyszczyk *et al.*, 2018). In this study, no significant difference in the plasma levels of 13 cytokines was observed between the 4 treatment groups, indicating that an innate immune response was unlikely responsible for the reduced tumour volume observed in mice treated with the implants compared to saline only treated mice. This has highlighted the importance of looking at the immune system in studies using long term implants, and while not performed in this study, future work should include immunohistochemistry assessment of immune markers in tumours.

Over the course of the study, there was no significant difference in the tumour volume of mice treated with dual drug loaded implants compared to all other treatment groups. This is could be due to insufficient drug loading to elicit a therapeutic response, but also may be due to insufficient drug release. The implant was placed subcutaneously, between the skin and facia, as per other studies using implantable DDS (Hrynyk *et al.*, 2015), however upon recovery of the fibres at the study endpoint and subsequent morphology analaysis by SEM, did not appear hydrated. The primary release mechanisms of the drugs from these fibres is 1) swelling of the hydrogel 2) passive diffusion down a concentration gradient out of the polymer matrix and 3) polymer degradation. It is likely that the *in vitro* release profiles obtained in Chapter 3, Section 3.3.4, Fig 3.9 are considerably different to drug release occurring *in vivo*. Such a phenomenon has been previously reported (Abazinge *et al.*, 2000, Zolnik and Burgess 2008, Kau and Liu 2012). For example, one study compared the degradation of PLGA microspheres, and found that the *in vitro* release experiment displayed a triphasic release, starting with an initial burst release, followed by a lag period and then secondary zero order profile (Zolnik and Burgess 2008). The *in vivo* release profile however, displayed a biphasic release profile and did not exhibit a lag phase. The release was therefore significantly faster *in vivo*, thought to be potentially due to the presence of enzymes, fluid volume and local pH. We could not determine how much of each drug remained in each implant at the conclusion of this study due to the limits of HPLC detection of drug from 0.5 cm lengths of fibre, however previous studies assessing

cytotoxicity of implants in Chapter 3 (Section 3.3.5, Fig. 3.10 A) showed that when treated with fresh drug loaded implants, Mia-PaCa-2 cells retained 62.3 % viability after 72 h of treatment, which is similar to the viability observed from the implants recovered from our *in vivo* study (Fig 4.12). This therefore suggests that a significant portion of gemcitabine and paclitaxel must have remained within the implant and why an anti-tumour response was not observed. Future studies utilising hydrated implants may overcome this issue.

The SEM images of extracted implants from the *in vivo* study also showed that tissue had grown over the holes of the implants. This may have contributed to insufficient drug release, as the PCL outer capsule itself did not contain any drug to prevent this tissue overgrowth. Future studies should look at loading this PCL capsule with either an anti-inflammatory drug or a chemotherapeutic like paclitaxel, in order to increase the delivered dose of drug while preventing tissue growth over the implant.

Ideally, these implants would be implanted intratumorally as they are intended to be administered directly into the tumour by ESU-FNI in humans. However the large size of implants compared to the size of the small Mia-PaCa 2 tumours in mice meant that this route of delivery was not feasible (Hrynyk *et al.*, 2015). Indolfi *et al.*, who developed a paclitaxel loaded PLGA patch designed to be placed over the exterior of a tumour, specifically downscaled their device to suit the biology of a mouse, in order to overcome those size related barriers. This difference in placement (subcutaneously versus intratumourally) also means that the drug release properties may be significantly altered. Future studies should address this by either 1) downscaling the implant to a size that is appropriate for intratumoural implantation in mice or 2) using a larger animal for orthotopic tumour placement and treatment such as a rat or pig (Bailey and Carlson 2019). The majority of implants that are intratumorally implanted in mice are fabricated via melt moulding or melt extrusion. For the most, they contain only a single drug, as that particular fabrication method is easiest to make very small rigid cylinders (Belz *et al.*, 2017, Gao *et al.*, 2017). Melt moulding or melt extrusion however is not suitable for fabrication of implants with a coaxial morphology or for all drugs, as the high temperature required to liquefy the polymer has the potential to degrade sensitive agents. Hence, the choice of loaded drug and polymer composition needs to be carefully considered.

The capsules surrounding the coaxial fibres were fabricated to increase the rigidity for implantation, as the fibres themselves had poor rigidity and compression strength (Section 4.3.6, Fig 4.17). Each capsule was individually assembled by hand. This was shown to be successful and of acceptable strength for the *in vivo* study, but it was also identified that this process needed refining for scale up as required for the potential future commercialisation of this therapeutic device. The hand-made fabrication method means that there is variation between capsules, and as was observed in Fig 4.15 it also posed the problem of uneven wall thicknesses within the same sample. Thicker wall areas could potentially hinder the release of the drug in that area, resulting in an uneven distribution. Perhaps this resulted in the variable tumour response observed for the dual drug loaded implants. We therefore sought to fabricate a capsule fabricated via 3D printing for future work in this area. 3D printing was explored due to its ability to reproduce structures accurately, speed of fabrication, cost effectiveness and ability for customisation (Ventola 2014). While the handrolled capsules required holes to be laser cut in order to facilitate drug release from the fibre, the 3D printed layers were not fused. This resulted in gaps between each layer, which could allow for the even diffusion of drug from the implant. Most importantly, the compression strength of the proof of concept 3D printed capsules was superior to that of the hand-rolled capsules, with more force required to compress the capsule, therefore indicating superior strength and stiffness. 3D printing has shown applications in implantable drug delivery and will be further explored in future studies surrounding this work, but further assessment of the properties of these capsules is outside the scope of this thesis.

4.5 Conclusions

This chapter described the fabrication and the first *in vivo* safety and efficacy study of gemcitabine and paclitaxel loaded coaxial fibres formed into a rigid implant. This study found that the presence of the implants did not cause any adverse effects, such as weight loss, or redness, irritation or infection at the implant site at any time over the 6 week study period. The dual drug-loaded implants did not significantly reduce the tumour volume compared to the empty implants, which may be due to insufficient drug loading or drug release. The empty implants showed a delay in tumour growth when compared to saline only treated mice, a phenomenon that has previously been reported when implants are placed adjacent to the tumour. Ideally, future work will look at downscaling the implants so that they are able to be intratumorally implanted in small animal models. This will also allow us to utilise orthotopic models (such as a rat model, xenograft and KPC syngeneic model described in Section 4.1), which are more clinically relevant than subcutaneous models. Such implant placement within the orthotopically grown tumour may also change the way the drug is released, as it was observed that not all of the drugs had been released when implanted between the skin and facia. This lack of drug release is hypothesized to be due to the low fluid volume in that area, and may differ intratumorally, therefore altering the tumour response. Altogether, this points to the need for superior *in vitro* drug release models to better mimic drug release at the intended implant site. There was no evidence of metastasis of the tumour to the lungs or liver at the conclusion of the study, nor were there any signs of toxicity or metastasis in any of the other major organs and lymph nodes. Overall, this study was a useful evaluation of these implants, and will lead to further studies using more refined implant structures using 3D printed capsules and optimised drug loaded formulations.

Chapter 5: Feasibility of the Wet Spinning Method for the Fabrication of Anti-PD1 Monoclonal Antibody Loaded Alginate Fibres

5.1 Introduction

Chemotherapy is well known to significantly reduce tumour volume, and in some haematological cases can cure the disease. It is also well known that it often comes with high levels of systemic toxicity. It is when this toxicity outweighs the anti-cancer benefit that treatment ceases, and cancer often progresses. Chemotherapy is one of the most commonly associated cancer treatments, however the above limitations of chemotherapy has led to significant research into the harnessing of a patient's own immune system to fight the cancer – known as immunotherapy. Immunotherapy is a broad term, and encompasses a number of different subcategories. This chapter will focus on one type of immunotherapy called checkpoint inhibition. The development of checkpoint inhibitors has been revolutionary for many immunogenic cancers, and is best known for its role in treating melanoma. As described in Chapter 1, Section 1.7.1, checkpoint inhibitors are used to "switch on" T cells, which activate them to attack the tumour. The two main checkpoints (and most extensively studied) in cancer therapy are cytotoxic T lymphocyte antigen 4 (CTLA-4) and programmed cell death protein 1 (PD-1).

CTLA-4 is a homologous cell receptor that functions as an immune checkpoint to downregulate immune response (Rowshanravan *et al.,* 2018). It was the first checkpoint inhibitor to be targeted, and is expressed solely on the surface of activated T cells and regulatory T (Treg) cells and is a well-known down regulator of T cell function. Like CTLA-4, PD-1 is another immune checkpoint, which inhibits T cell activity and is expressed by activated T-cells. PD-1 is a down regulator of TCR signalling events, and while CTLA-4 down regulates at the priming phase of an immune response, PD-1 works at a later stage – in peripheral tissues and at the time of an inflammatory response to infection (Jin *et al.,* 2010, Quezada and Peggs 2013, Rausch and Hastings 2017). PD-1 has 2 ligands; PD-L1 and PD-L2, which are expressed on the surface of tumour and stromal cells. When T cells become activated, PD-1 is expressed on their surface, and when they engage with either PD-L1/2, inhibition of kinases that are involved in T cell proliferation occurs (Fig. 5.1) (Pardoll 2012). There are a number of PD-1 checkpoint inhibitors on the market, the three which have been used in PDAC clinical trials being nivolumab, pidilizumab and pembrolizumab. Nivolumab is the checkpoint inhibitor that was selected for loading into wet

spun fibres. The gentle fabrication method prevents inactivation of the antibody, and nivolumab was selected for use in this chapter for reasons described below. There have been no PDAC specific clinical trials to test the efficacy of anti PD-1 therapeutics, however there have been three large multicentre phase I trials that have included PDAC patients. A multicentre phase I trial was performed in which 207 patients with advanced cancer (including 14 PDAC patients) were treated with escalating doses of an anti-PD-1 antibody BMS-936559. BMS-936559 is a high affinity human PD-L1 specific IgG4 monoclonal antibody. Results showed a complete or partial response in patients with melanoma, renal cell cancer, non-small cell lung cancer and ovarian cancer, and no objective response in any patients with PDAC at the highest dose (Brahmer *et al.*, 2012). Another phase I first in human study assessed pembrolizumab (MK-3475) in 30 patients with advanced cancers, which included only one PDAC patient, who experienced stable disease as their best response, with disease free progression for 20 weeks (Patnaik *et al.*, 2015). Another large phase I trial in 277 patients with advance incurable cancer (including one PDAC patient) assessed the efficacy of MPDL3280A – a high affinity human monoclonal immunoglobulin-G1 antibody (Herbst *et al.*, 2014). The PDAC patient had no objective response over the course of treatment.

While immunotherapy as a monotherapy has largely been unsuccessful in the area of PDAC, recent studies have assessed the efficacy of immunotherapy in combination with other therapeutics, which have shown promising results. However due to the relative infancy of immunotherapy in the PDAC field, there are a large number still in clinical trials, with outcomes likely to be reported over the coming years (Henriksen *et al.*, 2019). A phase II study in 10 patients with metastatic PDAC was performed in which nivolumab, *nab*-paclitaxel, paricalcitol (vitamin D analogue), cisplatin and gemcitabine were administered in combination (Borazanci *et al.*, 2018). While this trial is still in progress, it has shown a high overall response rate of 80 % which is encouraging. Other studies still in progress that include anti-PD-1 therapeutics include a phase II trial of nivolumab in combination with GVAX (comprised of allogenic PDAC cells that express GM-CSF) with cyclophosphamide (which inhibits regulatory cells) and CRS-207 (which stimulates NK and T cells) (Le *et al.*, 2016). A phase II study of ipilimumab, nivolumab and radiotherapy in patients with metastatic PDAC is also being undertaken (Parikh *et*

al., 2019). The combination of radiotherapy in combination with immunotherapy is gaining increased interest, as it had been shown that radiotherapy has the ability to boost the effects of immunotherapeutics at abscopal sights – that is, in satellite tumours that weren't the primary radiation target (Walle *et al.,* 2018). Radiation has been shown to induce priming of tumour antigen specific T cells, attract leukocytes into the tumour and increase tumour cell susceptibility to lymphocyte mediated cytotoxicity, (Kwilas *et al.*, 2012, Klug *et al.*, 2013, Twyman-Saint Victor *et al.,* 2015). These changes in the immune environment caused by radiotherapy therefore increase the efficacy of immune checkpoint blockade therapy, warranting further investigation into this combination therapy (Wang *et al.*, 2018).

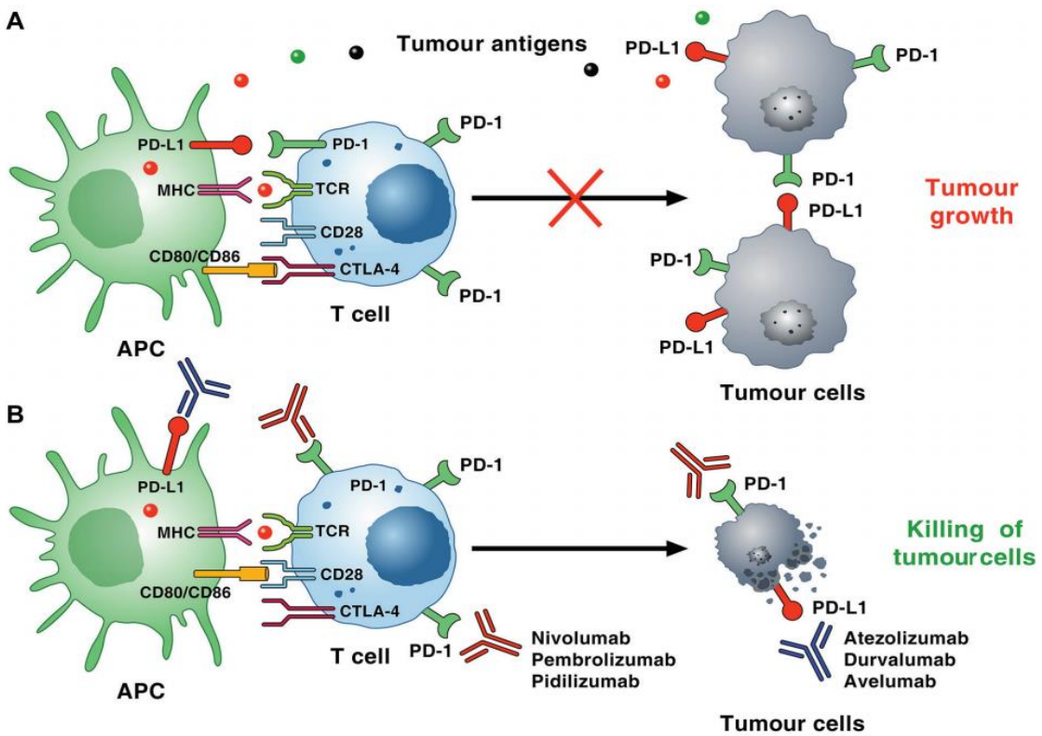

Figure 5.1: Mechanism of PD-1/PD-L1 pathway-induced immunosuppression within the tumour microenvironment.A) Tumour neoantigens (dots of different colours) released by cancer cells are captured by APCs. These cells present peptides in the context of MHC molecules/TCRs on the surface of $CD8^+$ cytotoxic T cells. PD-1 is induced on T cells on activation through the TCR and through several cytokines. Tumour cells and other cells in the tumour microenvironment (eg, endothelial cells, mast cells) can express high levels of PD-L1 and/or PD-L2 that binds to PD-1 on T cells, resulting in inhibitory checkpoint signalling that decreases cytotoxicity and leads to T cell exhaustion. Recent evidence suggests that murine and human cancer cell subpopulations can express PD-1 and promote tumour growth. B) PD-1 blocking antibodies (nivolumab,

pembrolizumab, pidilizumab and so on) inhibit the interaction of PD-1 with both PD-L1 and PD-L2, resulting in enhanced T cell cytotoxicity, TAM activity, increased cytokine production, and ultimately killing of tumour cells. PD-L1^{+} tumour cells can also induce T cell apoptosis, anergy, functional exhaustion and interleukin-10 production. Anti-PD-L1 antibodies (atezolizumab, durvalumab, avelumab) have similar effects, but only inhibit the interaction between PD-L1 and PD-1. PD-1, programmed cell death 1; PD-L1, programmed cell death ligand 1; TAM, tumour-associated macrophage; TCR, T cell receptor. Taken from (Varricchi *et al.,* 2017)

Checkpoint inhibitors administered as a monotherapy have been largely unsuccessful in treating PDAC, which is due in part to PDACs low immunogenicity and failure to attract immune cells. Combination of checkpoint inhibitors with immune stimulators (i.e. chemotherapy and radiotherapy) however are showing promise with increased overall response rates, yet many clinical trials are still in progress. In a similar fashion to systemically administered chemotherapeutics, the stromal tissue making up the tumour microenvironment prevents infiltration of checkpoint inhibitory drugs or T cells into the tumour (Salmon *et al.,* 2012). There are limited publications describing checkpoint inhibitor DDS in the literature, and none in the context of PDAC. We therefore sought to develop and characterise the first anti-PD-1 (nivolumab) loaded alginate fibre for PDAC therapy, with a view to further develop it for combination therapy with locally delivered chemotherapy and/or radiotherapy in the future.

The specific aims for this chapter are to:

1. Fabricate nivolumab loaded 3 % alginate fibres using the wet-spinning method
2. Assess the morphology and drug release profile of nivolumab-loaded alginate fibres
3. Assess PD-1/PDL-1 inhibitory activity of nivolumab after it is released from an alginate fibre in comparison to free nivolumab subjected to a number of storage conditions, to assess whether the fabrication and/or storage conditions affects antibody activity.

5.2 Materials and Methods

5.2.1 Materials

Sodium alginate (from brown algae) and calcium chloride ($CaCl_2$) were from Sigma-Aldrich Co. USA. Nivolumab (Opdivo) (10 mg/mL) for injection (containing the following excipients: sodium citrate, sodium chloride, mannitol, pentetic acid, polysorbate 80, sodium hydroxide and hydrochloric acid) was kindly supplied by Prof Morteza Aghmesheh (Illawarra Shoalhaven Local Health District, Illawarra Cancer Day Care Centre). The Pierce™ BCA assay used to determine nivolumab concentration was from Life Technologies. PD-1/PD-L1 activity assay was from Promega.

5.2.2 Fibre Fabrication

Alginate spinning solution was prepared at a concentration of 3 % (w/v) by adding alginate powder directly into nivolumab solution (10 mg/mL). Empty fibres were prepared by dissolving alginate powder into Milli-Q water. Solution was stirred at room temperature until dissolved. Single fibres were spun as per Chapter 2 Section 2.2.4. Fibres were dried and stored at 4 °C in the dark until used. Two separate batches of fibres were fabricated to ensure reproducibility.

5.2.3 Fibre Morphology

In Chapter 3, it was observed that the addition of polymer to the Anzatax solution (formulated for injection) had an negative effect on the polymer structure. To assess the effect of nivolumab on fibre morphology, nivolumab loaded fibres and empty fibres were imaged by SEM using parameters outlined in Chapter 2 Section 2.2.5.

5.2.4 Drug Release

It is important to assess the release profile each time a different therapeutic is loaded into a polymer, as factors such as size, hydrophilicity and charge may influence how the therapeutic is released. Release studies were performed as per Chapter 2, Section 2.2.7, with the following changes: Aliquots were collected hourly for 10

hours, then daily for 14 days. Aliquots were stored at 4 ºC. Amount of nivolumab released was determined by interpolating values from a standard curve generated using a Pierce™ BCA protein assay kit as per the manufacturer's instructions. Aliquots (25 µL) of BCA standards ranging from 0-2000 µg/mL and unknown samples were added to wells of a 96-well microtitre plate in triplicate (standards) and sextuplicate (unknowns). In each well 200 µL of working reagent (50:1 Reagent A:B) was added, and plate mixed for 30 sec. The plate was covered and incubated at 37 ºC for 30 min, allowed to cool to RT and then absorbance read at 562 nm using a spectrophotometer plate reader. A standard curve was generated using GraphPad Prism (v. 7.02) to calculate protein (nivolumab) concentration.

5.2.5 *In Vitro* Activity Assay

Monoclonal antibodies are known to be sensitive to degradation via thermal, pH or mechanical stresses (Jaccoulet *et al.*, 2019). The activity of nivolumab from two separate batches of fibres (batch 1: prepared and stored at 4 °C for 6 weeks, or batch 2: prepared and used within 1 week) was assessed following the spinning procedure. A PD-1/PD-L1 blockade bioassay (Promega) was performed as per the manufacturer's instructions. The assay contains two cell types: a Jurkat T-cell line that expresses human PD-1 and NFAT induced luciferase and CHO-K1 cells that expresses PD-L1 and a cell surface protein designed to activate cognate TCRs in an antigen dependant manner. When these cells are cultured together, the PD-1/PD-L1 interaction inhibits TCR signalling, and NFAT-mediated luciferase activity. Addition of an antibody that blocks PD-1 (i.e. nivolumab) releases the inhibitory signal and results in TCR signalling and NFAT-mediated luciferase activity (Fig. 5.2).

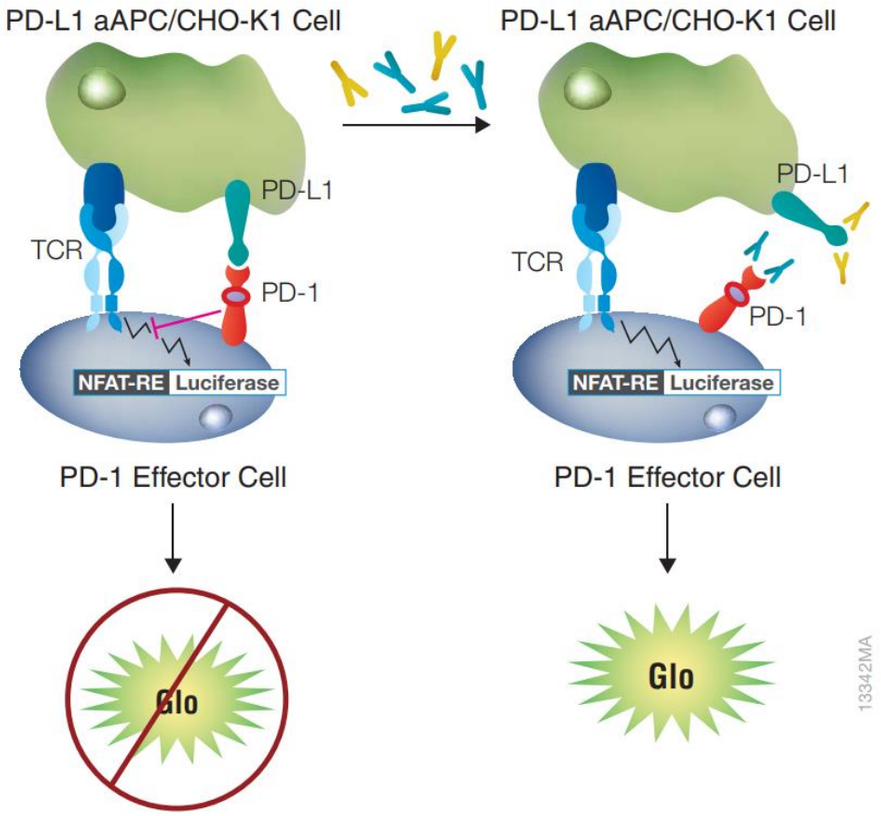

Figure 5.2: PD-1/PD-L1 blockade bioassay. The bioassay consists of two genetically engineered cell lines, PD-1 Effector Cells and PD-L1 aAPC/CHO-K1 Cells. When co-cultured, the PD-1/PD-L1 interaction inhibits TCR-mediated luminescence. When the PD-1/PD-L1 interaction is disrupted, TCR activation induces luminescence (via activation of the NFAT pathway) that can be detected by addition of Bio-Glo™ Reagent and quantitation with a luminometer. Taken from Promega PD-1/PD-L1 blockade assay specification sheet.

5.3 Results

5.3.1 Fibre morphology

In order to assess the effect of loading the nivolumab formulated for injection into the alginate fibres, cross sectional SEM images of the fibre were taken and compared to empty alginate fibres. The nivolmab fibres showed the alginate had been tightly crosslinked as indicated by the very small pores which required increase zoom (× 230) to visualize (Fig 5.3 A,B). This appeared very different from the typical non-drug-loaded alginate morphology showing large open pores (Fig 5.3 C,D). As the nivolumab used was for injection, it contained excipients (listed in Section 5.2.1).

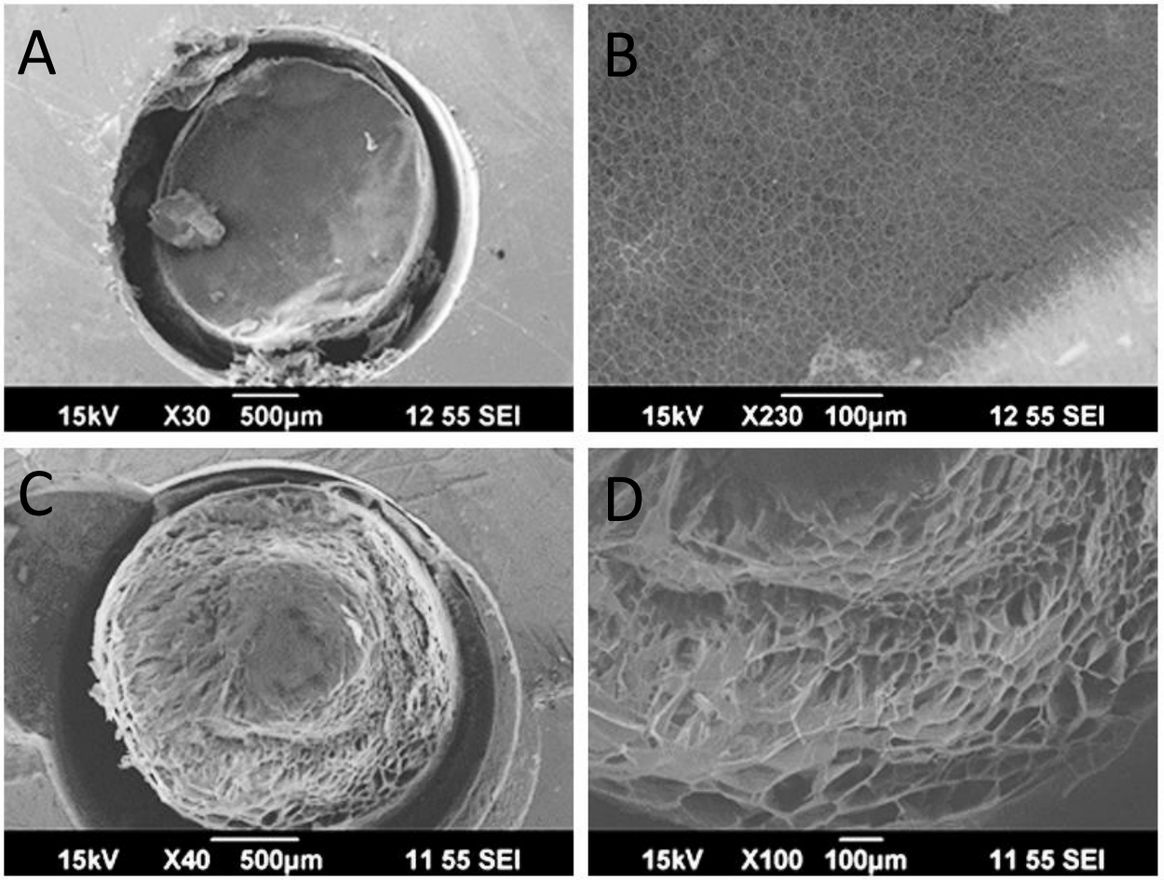

Figure 5.3: Scanning election microscopy images of nivolumab loaded alginate fibres show smaller pores indicative of greater crosslinking density of the polymer. Images show cross sections of 3 % alginate fibres that were loaded with A) and B) nivolumab or C) and D) unloaded

Next the diameter of empty and nivolumab loaded fibres was assessed in order to ascertain if there was any effect on the fibre diameter from nivolumab loading. The mean diameter of nivolumab-loaded fibres (237.5 ±3.6 µm) was 1.2 times larger than the empty fibres (196.9 ±5.8 µm) (Fig. 5.4), indicating nivolumab-loading has a significant ($P<0.0001$) impact on fibre diameter.

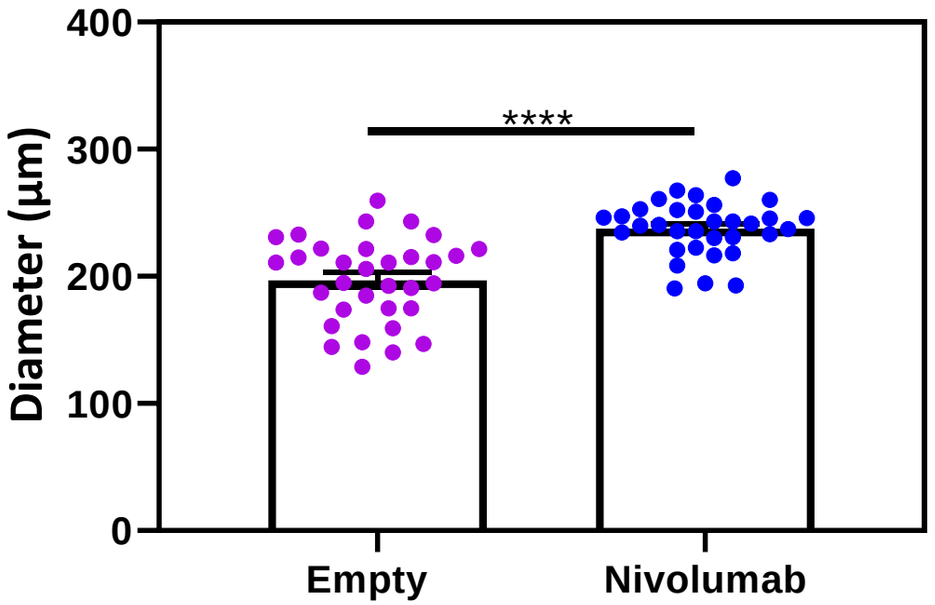

Figure 5.4: Nivolumab loading increases alginate fibre diameter. Fibre diameter was measured in 3 % alginate fibres loaded with or without nivolumab. The bars represent the mean of n=33 measurements ± SEM. **** $P\leq0.0001$

5.3.2 Nivolumab release

Release of nivolumab was detected and quantified using a BCA protein assay. Observation of the drug release curves revealed a burst release within 10 h, with 7.4 mg of nivolumab (88.8 %) nivolumab released into solution (Fig 5.5 B). Of the 15 mg of nivolumab loaded, a total of 9.51 mg was released (Fig 5.5 A) over the 14 day study period, which equates to an encapsulation efficiency of 61.26 % (Table 5.1).

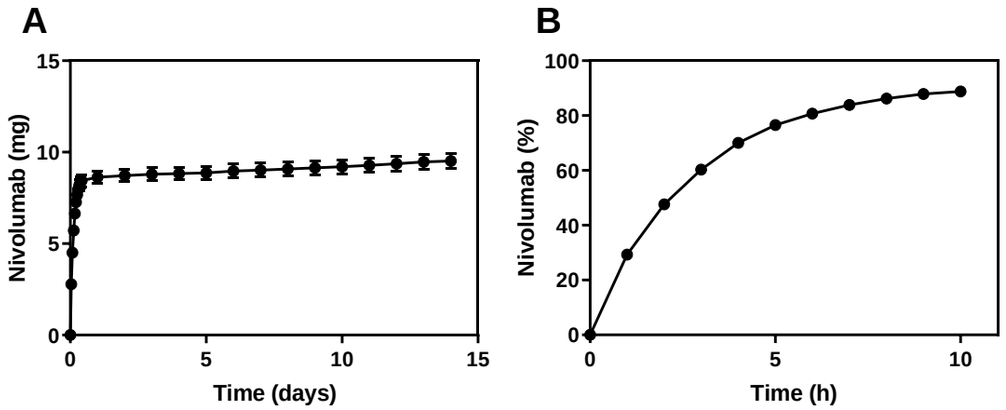

Figure 5.5: Nivolumab displays initial burst release profile over the first 10 h, followed by a slower, sustained release over 14 days. Cumulative release of nivolumab was measured from 3 % alginate fibres. A) amount of nivolumab released over 14 day period, B) percentage of nivolumab released over the first 10 h. Values are the mean (±SEM) of sextuplicates.

Table 5.1: Drug loading and encapsulation efficiency of nivolumab in a 3 % alginate single fibre. Theoretical loading was calculated using equation (2) whilst the actual loading values were determined through complete release of drug and quantification using HPLC. The values represent the mean actual loading value ± SEM.

Theoretical Loading (mg/m)	Actual Loading (mg/m)	Encapsulation Efficiency (%)
15.37	9.51	62.16

5.3.3 *In Vitro* Nivolumab Activity

The activity of nivolumab eluted from the alginate fibre was assessed using a cell based PD1/PD-L1 blockade assay, and compared to that of encapsulated nivolumab. Aliquots of release medium collected from 2 separately prepared batches of nivolumab loaded fibres were also compared. Nivolumab eluted from Batch 1 fibres retained 84.0 % of activity at the highest concentration compared to free nivolumab, while nivolumab eluted from Batch 2 fibres retained 88.1 % of activity. There was no significant difference in activity at the highest concentration (25 µg/mL) between nivolumab eluted from Batch 1 and Batch 2 fibres and free nivolumab (Fig 5.7). The empty fibre showed no inhibitory activity as expected (Fig 5.6). In addition, the activity of nivolumab heated at 37 °C for 7 and 14 days was assessed, to determine whether the release conditions had an effect on antibody activity (Fig 5.7 A). After 14 days the nivolumab eluted from the Batch 1 fibre appeared to lose its activity at the highest concentration; however this was not significantly different to that of the free nivolumab. The nivolumab incubated for 7 days showed a higher activity than that of the free nivolumab, however was not statistically significant. A further release experiment was performed on Batch 2 of fibres 8 weeks apart to assess whether storage of the fibres in the dark at 4 °C had an effect on activity. Here no significant difference in nivolumab activity was observed in either batch compared to the free nivolumab (Fig 5.7 B).

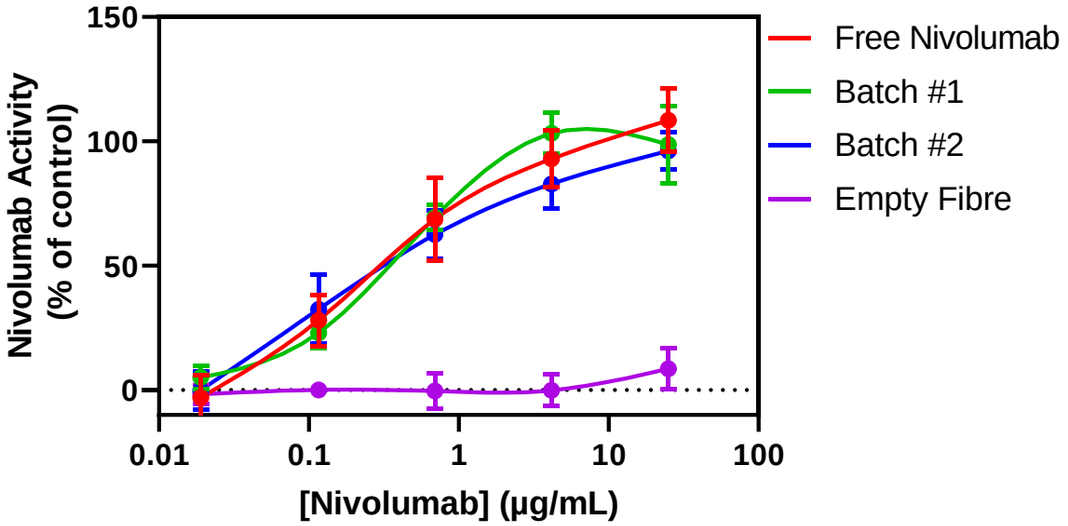

Figure 5.6: Fibre eluted nivolumab retains its activity. PD-L1 aAPC/CHO-K1 Cells were plated and incubated at 37 °C for 16–20 hours prior to the addition of increasing concentrations of nivolumab and PD-1 Effector Cells. After 6 hours, Bio-Glo™ Reagent was added and luminescence measured using the GloMax® Discover System.

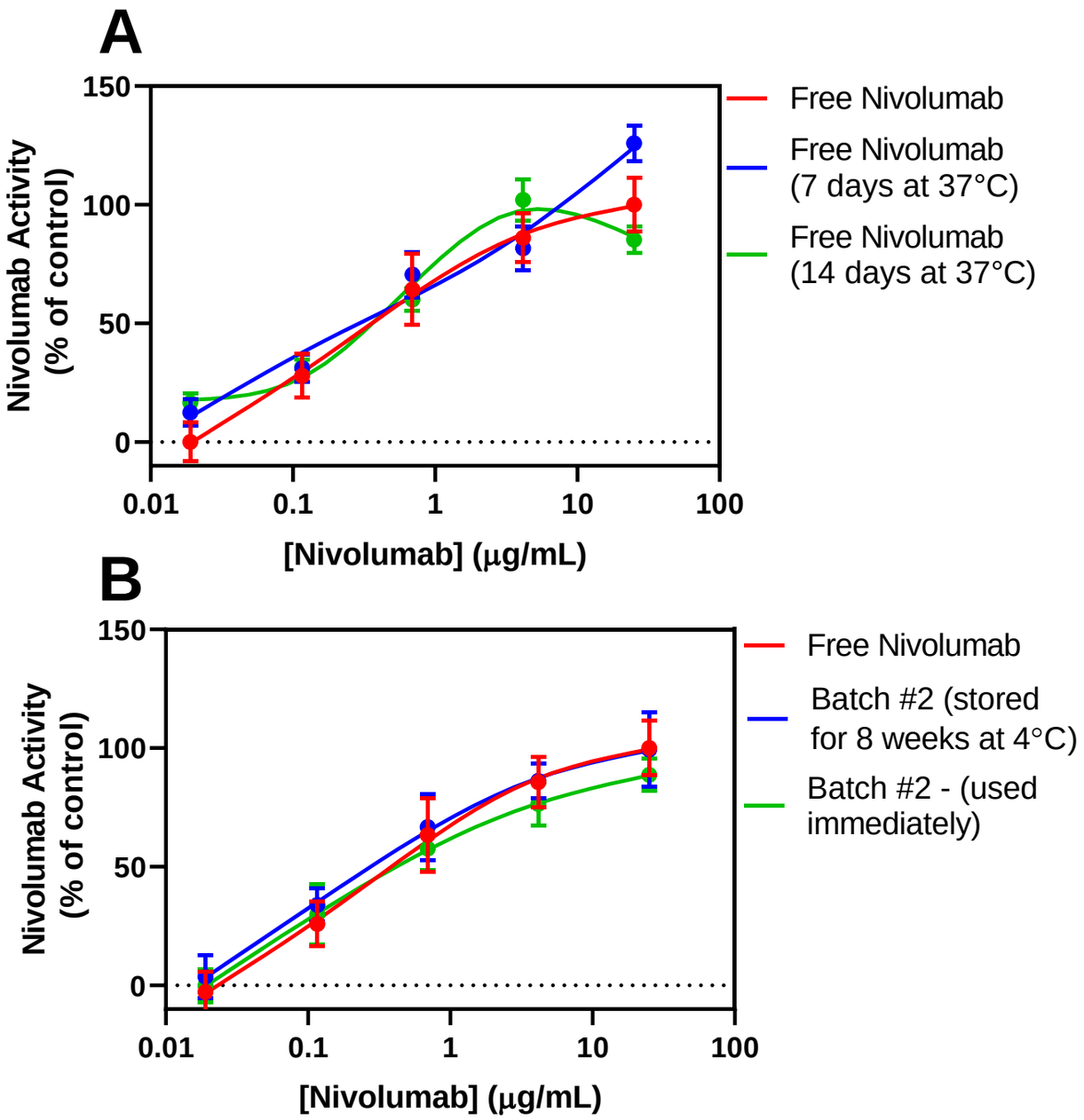

Figure 5.7: Activity of nivolumab is not affected by the time incubated at 37 °C or by 6 week storage time. PD-L1 aAPC/CHO-K1 Cells were plated and incubated at 37 °C for 16–20 hours prior to the addition of increasing concentrations of nivolumab and PD-1 Effector Cells. After 6 hours, Bio-Glo™ Reagent was added and luminescence measured using the GloMax® Discover System.

5.4 Discussion

This chapter sought to assess the feasibility of using the wet spinning method to fabricate fibres loaded with nivolumab, a PD-1 checkpoint inhibitor. Checkpoint inhibitors are used in cancer immunotherapy, but to date have shown poor efficacy in PDAC. Furthermore, there are limited publications describing DDSs for the localised delivery of checkpoint inhibitors such as nivolumab.

Cross sectional images of nivolumab-loaded fibres showed that the internal morphology was different to that of empty fibres in which the porosity was markedly reduced. Nivolumab loading also led to increased diameter compared to empty fibres. This was a different trend to that observed in gemcitabine loaded alginate fibres. It is known that drug-polymer interactions can influence pore size and crosslinking density (Shekunov *et al.*, 2007). When drugs interact and tether to the polymer, they can act as crosslinks, which may be why the porosity of nivolumab loaded fibres had a greater crosslinking density (Li and Mooney 2016). It was expected the excipients in the nivolumab solution would have a degree of an effect on the morphology, as was observed in Chapter 3 when paclitaxel formulated for injection (Anzatax) was used to fabricate PCL fibres caused significant structural damage. SEM is predominantly qualitative, so cannot determine the effect of drug release and nivolumab activity of an altered morphology by observation alone. In Chapter 2, Section 2.3.1, Fig 2.4 the addition of gemcitabine had no effect on alginate fibre diameter, however, antibodies are large (150 kDa) and at high concentrations, may impact upon fibre diameter. Despite these structural differences in the nivolumab fibres, there was no significant effect on the activity of nivolumab once released from the fibre. An important aspect of this chapter was to determine the *in vitro* activity of the nivolumab after encapsulation into the alginate fibre. Many implant fabrication methods involve high heat, pressure and/or harsh solvents (eg melt extrusion, solvent extrusion), so was thought that using the gentle wet spinning process this activity could be maintained. It was confirmed that this was the case, and concluded that neither the fabrication method nor the 6 week storage of fibres or *in vitro* release conditions significantly affects the activity of the anti-PD-1 drug nivolumab eluted from alginate fibres. This further validates the wet-spinning method for the production of immunotherapy DDS in the future. Other

solvent free hydrogel DDS have reported this retention in activity. An agarose hydrogel *in situ* forming depot loaded with gold nanoparticles and bevacizumab (a monoclonal antibody that targets VEGF-A) showed retention of activity in the bevacizumab under release conditions up to 50 °C (Basuki *et al.,* 2017). The majority of DDS used for the release of antibodies are *in situ* forming and are therefore aqueous at room temperature, many of these being hydrogels. This further supports our choice of alginate, but it also highlights the lack of solid DDS for the delivery of antibodies. It also emphasises the advantage of using the wet spinning method over other fabrication methods for loading of antibodies into a solid DDS.

The majority of commercially available therapeutic antibodies on the market are designed for systemic administration, which is beneficial for a disseminated disease, but undesirable for local disease, such as a solid tumour. Currently, checkpoint inhibitors are administered systemically. There is currently no clear dose response relationship for checkpoint inhibitors, with nivolumab showing similar response rates in a wide range of doses. This is likely due to the fact that the PD-1 reaches maximum occupancy at low doses – which means that increasing the dose doesn't necessarily increase the tumour response (Renner *et al.,* 2019). Systemic administration of checkpoint inhibitors however does come with adverse side effects such as diarrhoea, pneumonitis, body rashes, hormone imbalances and kidney infections due to excessive immune activation (Bajwa *et al.,* 2019). Investigation into DS for immunotherapies is therefore being explored in a number of ways, and have the added benefit of increasing cost saving for checkpoint blockade therapy. Systemic therapy will require higher doses of immunotherapeutic, in order to reach a therapeutic level in the tumour while taking into account the off target effects. Local therapy therefore will reduce the total amount administered to a patient, which can have a significant financial impact due to the current high costs per milligram of these drugs (Renner *et al.,* 2019). The use of delivery methods such as microneedle patches for melanoma have been described showing success, however this is limited to superficial tumours so is not relevant in cancers like PDAC. Nanoparticle delivery has also been explored, however the low percentage of accumulation in tumours poses a significant problem (Riley *et al.,* 2019). Intratumoural injections of immunotherapy drugs have been described, however leakage of the drug

back out of the tumour and into surrounding tissues is reported to be a significant problem, particularly when multiple punctures are required for adequate dispersion of the drug (Marabelle *et al.*, 2018). Alginate based delivery of monoclonal antibodies have been described, such as an injectable *in situ* alginate depot for the sustained delivery of IgG in mice. An internal crosslinking method (similar to that of Chapter 3, Section 3.2.2) was employed using glucono-delta lactone and $CaHPO_4$ (Schweizer *et al.*, 2013). The alginate gelated *in vivo* following injection as a liquid. None of the animals experienced any reaction to the depot, and the serum levels of IgG were more sustained in the depot treated mice. In mice with the depot, maximum IgG serum levels were reached at 4 days, compared to 2 days with the systemic injection. This was a small study performed on 3 mice only and despite promising results, warrants a more robust investigation.

This chapter has provided the basis for further work in to development of nivolumab DDSs, however it is unlikely that this type of therapy will have a therapeutic benefit in isolation. As previously mentioned, a characteristic of pancreatic tumours is their low immunogenicity, and therefore in the presence of immunotherapy fail to illicit an adequate immune response and attract T cells (Fukunaga *et al.*, 2004). While the fibre loaded nivolumab in this study is designed to be released at the site of the tumour, it needs T cells to be present in order to be effective. Some chemotherapeutics are known to increase tumour immunogenicity, with paclitaxel being a well-known immunostimulator. Recently, it has been shown that paclitaxel is able to convert macrophages from one an M2 phenotype to M1 (Wanderley *et al.*, 2018). M1 macrophages are pro-inflammatory and immunogenic, while M2 macrophages are anti-inflammatory and have pro-tumour effects. As with many cancer treatment regimens, combination therapy is often proven to be advantageous over treatment with a single agent. A recent phase I study sought to assess the safety and tolerability of nivolumab in combination with the current standard of care gemcitabine and *nab*-paclitaxel in 50 patients with advanced PDAC (locally advanced or metastatic) (Wainberg *et al.*, 2019). Of the 50 patients, 1 had complete response, 8 had a partial response, 23 had stable disease (≥6 weeks), and 10 had progressive disease. There were no unexpected adverse events, and is a feasible treatment option for patients with advanced PDAC.

Combination treatment has also been explored in the context of implantable DDS. Wang and team synthesised a ROS-responsive *in situ* forming hydrogel that was loaded with gemcitabine and anti-PD-L1 (Wang *et al.*, 2018). Initial *in vivo* experiments on mice bearing B16F10 melanoma tumours, administration of gemcitabine only loaded hydrogel showed that a high concentration of gemcitabine (25 mg/kg) depleted tumour infiltrating lymphocytes and had no significant effect survival. When the dose was lowered to 5 mg/kg, they found that the tumour infiltrating lymphocyte level increased, while also reducing other immunosuppressive cells such as M2 macrophages and myeloid derived suppressor cells. One interesting finding with the gemcitabine loaded hydrogel was that treatment increased PD-L1 expression on cancer cells. This was something that was also observed *in vitro* in poorly immunogenic 4T1 breast cancer cells, which holds promise for patients with poorly immunogenic cancers like PDAC. When the dual-drug loaded hydrogel containing both gemcitabine and anti-PD-L1 was administered in mice bearing melanoma tumours, tumour weights in the combination treated mice were significantly lower, but more importantly showed a significant increase CD8+ and CD4+ T cells, with a 20-fold increase in T cells per gram of tumour compared to the untreated control. In the poorly immunogenic T41 breast cancer model, the survival was significantly increased from 22 days untreated to 40 days with treatment.

This study shows promise in the area of localised immunotherapy treatment, and paves the way for further characterisation of our fibres. Future work should include *in vivo* efficacy assessment using an immunocompetent PDAC mouse model (such as a KPC model discussed in Chapter 4, Section 4.1), and efficacy assessed in combination with other therapies such as chemotherapeutics (gemcitabine and paclitaxel), radiotherapy or other immune stimulating agents (for example interleukin-2) (Bachmann and Oxenius 2007).

5.5 Conclusions

This chapter has shown that wet spinning is a viable method for the production of anti-PD1 monoclonal antibody-loaded fibres. This is important when preparing DDS containing sensitive biological agents. The checkpoint inhibitor nivolumab was successfully loaded into alginate fibres and the activity of the drug was maintained throughout the fabrication process, short term storage and upon release from the fibre. This proof of concept study has provided the basis for further investigation into the therapeutic efficacy of immunotherapy loaded fibres in order to increase the limited treatment options currently available for PDAC patients.

Chapter 6: Conclusions and Future Directions

6.1 Introduction

PDAC has a notoriously low survival rate, due to the advanced stage upon diagnosis, a stiff desmoplastic ECM that limits drug uptake and a rapid development of drug resistance. The non-specific toxicity caused by chemotherapy treatment can affect the treatment regimen, resulting is dose reductions, supportive measures and if treatment is ceased can result in disease progression. Typically, the therapeutic level of chemotherapy a patient requires is accompanied by very high levels of systemic toxicity, which leads to treatment cessation and disease progression. Development of an implantable, local DDS has the potential to overcome the issues with drug perfusion through the ECM, to deliver the required high concentrations of the drug directly to the tumour, while simultaneously avoiding the systemic toxicity. This thesis aimed to develop, characterise and preclinically assess polymeric DDSs in the form of fibres that were able to deliver commonly used chemotherapy (gemcitabine and paclitaxel) and immunotherapy (nivolumab) drugs for PDAC.

6.2 Gemcitabine Loaded Fibres are Cytotoxic to PDAC Cells and Show Improved Uptake into Spheroids Compared to Free Drug.

Single fibres were initially fabricated from the hydrogels alginate and chitosan and were loaded with the chemotherapy drug gemcitabine. These fibres were fabricated using the wet spinning method, of which is subsequently used in each chapter for development of different fibre formulations. The polymers were selected for fibre fabrication based on the current literature describing their biocompatibility, versatility and hydrophilic properties. They were loaded with gemcitabine due to the drugs long history of being used for PDAC treatment. Both alginate and chitosan fibres loaded with gemcitabine showed efficacy in 2D monolayer and 3D spheroid PDAC models however, a high level of non-specific toxicity was displayed by the empty chitosan fibres. This resulted in alginate being selected as the superior polymer for further use in the following chapters.

A drug uptake study using 3D spheroids further highlighted the benefit of a slow release system compared that of a single dose of free drug. Tumour spheroids treated with doxorubicin loaded alginate fibres showed a steady

uptake and homogenous drug distribution over 320 min, while spheroids treated with a single dose of free drug showed uneven uptake, and drug efflux back out of the spheroid. The development, characterisation and preclinical assessment of these successfully fabricated gemcitabine loaded alginate fibres then allowed for expansion of the project into a number of different applications.

6.3 Dual-Loaded Fibres are Cytotoxic to PDAC Cells and are Effective Radiosensitisers

It was identified that loading of a single drug into single alginate fibres was not in line with the current standard of care for PDAC. This lead to the fabrication of a coaxial fibre consisting of PCL for the shell, and alginate for the core. The selection of these polymers allowed for the loading of paclitaxel into the PCL shell, and gemcitabine into the alginate core as these drugs in combination are the current gold standard treatment for PDAC patients and provide a 1.8 month increase in overall survival (from 6.7 to 8.5 months) when compared to gemcitabine alone, justifying their use in this study (Von Hoff *et al.*, 2013). These dual-drug loaded fibres showed efficacy *in vitro* in a number of high throughput 2D monolayer experiments, but also in 3D culture experiments. It was observed that the dual-drug loaded fibres reduced cell viability by up to 86.1 % after 72 h in a 2D monolayer human PDAC cell line (Mia-PaCa-2). When assessed in two 3D PDAC tumour spheroid models, it was observed that the dual-drug loaded fibres decreased spheroid diameter over time comparable to the equivalent amount of free drugs which indicated bioequivalence, while the empty fibre treated spheroids showed increased spheroid diameter over the study period comparable to that of the untreated BxPC3luc spheroid control. The dual-drug loaded fibres showed a 31.7 and 82.5 % reduction in cell viability in BxPC3luc and KPC spheroids, respectively. This chapter also explored the potential of the dual-drug loaded fibres to be used in combination with radiotherapy, as gemcitabine and paclitaxel are known to sensitise cancer cells to radiation. Although there is no current evidence to show that there is a significant overall survival benefit of combining radiation and chemotherapy, emerging phase I trials of *nab*-paclitaxel and gemcitabine in combination with radiation show promise and warrant further trials.

The dual-drug loaded fibres in combination with radiation showed the greatest reduction in cell viability, even when compared to the equivalent free drug control with radiation. An interesting finding in this study was the radiosensitising properties the empty fibre had in combination with 1 Gy fraction of radiation, which decreases cell viability by 27 %. Animal studies utilising radiotherapy in combination with the chemotherapy loaded implants have been extensively assessed in glioma (utilising Gliadel wafers) and has been shown to increase overall survival, but has not yet been assessed using implantable polymeric chemotherapy DDS in PDAC. One study used ionotropic delivery (which utilises electric felids to drive drugs into tissues) of cisplatin into a PDX mouse model of breast cancer in combination with external beam radiation. This form of local chemotherapy delivery in combination with radiation therapy showed significant reduction in tumour volume when compared to i.v. cisplatin and radiotherapy (Byrne *et al.,* 2015). In addition, further exploration into the radiosensitising effect of the empty polymer observed in Chapter 3 is warranted and will be interesting to observe whether the same phenomenon also occurs *in vivo*.

6.4 Dual-Drug Loaded Implants are Well Tolerated *In Vivo*

A nude BALB/c Mia-PaCa-2 subcutaneous PDAC mouse model was utilised to test the *in vivo* efficacy of the dual-drug loaded fibres that were characterised in Chapter 3. The dual-drug loaded fibres were formed into an implant by inserting them into a rigid PCL shell to improve the mechanical properties for implantation into the animal, as the fibres were too flexible on their own. This study showed that the implantation procedure and the treatment were well tolerated, and there were no adverse effects of the implant itself over 42 days. No redness, irritation, or infection was observed at the implant site, there was no implant migration or weight loss in the animals in any treatment group. It was observed that there was no significant difference in tumour volume growth between the dual-drug loaded implant and the empty implant treated animals, potentially due to the lack of hydration of the implants and therefore insufficient drug release. A significant decrease in tumour volume of all implant treated animals compared to the saline control was observed, potentially due to the disruption of tumour vasculature development due to implant placement which future studies should further investigate.

The difference in the level of response of PDAC cells to treatment between *in vitro* and *in vivo* tests was remarkable. The dual-drug loaded implants that showed significant efficacy *in vitro*, had no significant effect on tumour growth *in vivo* when compared to the empty implants. This highlights the importance of using clinically relevant animal models, in order to minimise the chance of translational failure, which is a common outcome for many DDS (Park 2016).

A big challenge for the development of new DDS is the lack of correlation between *in vitro* and *in vivo* drug release. The majority of drug delivery devices fail in humans, as the extensive *in vitro* characterisation and small animal disease models cannot accurately recapitulate the individuality and complexity of the tumour microenvironment and how this impacts upon drug release each in each individual patient. As a result, many novel and promising DDS are not effectively translated into humans which is very costly and time consuming in regards to research time and funding (Park 2016). Mathematical modelling of *in vivo* drug release is a steadily increasing field and has significant future potential for predicting how the drug will release (i.e. rate of release) and the rates and concentration of drug uptake into the tumour (Siepmann and Siepmann 2008). For example, Indolfi *et al.*, used computational modelling to predict levels of systemically administered paclitaxel to pancreatic tumours, guided by the current standard of care treatment regimen (Indolfi *et al.*, 2016). The model predicted limited spatial distribution with a peak drug concentration at 12 μM and rapid capillary clearance. It predicted that the IC_{50} levels of paclitaxel would only reach the region immediately surrounding the tumour vasculature. In order to confirm these predications, a study was performed in mice, and levels of paclitaxel were assessed in the tumour and surrounding tissue. They found results to be consistent with the model predictions, with paclitaxel only penetrating 10 μm from the vasculature source, and very limited amounts in the tumour itself. This was effective at highlighting both the issues with treating PDAC systemically, but also the predictive power of computational modelling and is something that future work on this project should involve.

6.5 Nivolumab Retains its Activity When Loaded Into Alginate Fibres

The versatility of wet spinning was assessed for its suitability for the fabrication of fibres containing sensitive biological material. Chapter 5 looked at loading the immunotherapy agent nivolumab into single alginate fibres, as Chapter 2 had already demonstrated the success of loading the hydrophilic chemotherapeutic gemcitabine. Many fabrication platforms are unable to form DDS containing sensitive biological material, as many require high heat, pressure or solvents for successful fabrication (Patil *et al.*, 2016). It was shown that nivolumab can be successfully loaded and released from alginate fibres over 2 weeks without any significant effect on its biological activity. This is promising considering the high rates of failure in immunotherapy trials for PDAC. The next steps in validating nivolumab loaded fibres is designing and performing appropriate *in vitro* and *in vivo* studies. The PDAC mouse model used to assess the safety and efficacy of the dual drug loaded implants described in Chapter 4 is unable to be utilised, due to the lack of an adaptive immune system (i.e. lacks functional T cells) in that particular strain. As the mechanism of checkpoint inhibition is dependent on T cell activity, an immunocompetent strain bearing KPC tumours is the standard model for PDAC immunotherapy evaluation. This animal model expresses mutant p53 and *Kras* in the pancreas and develops premetastatic lesions which then further develop into metastatic disease, which closely mimics human disease. In addition, this model shows leukocyte invasion, but this is dominated by immunosuppressive cells such as TAMs, Treg cells, and myeloid derived suppressor cells), which indicates an immunosuppressive environment upon PDAC development (Torphy *et al.*, 2018). This effect is also commonly observed in humans, so is a valid model for preclinical assessment of novel immunotherapy treatment regimens.

The nivolumab loaded fibres developed here are not intended as a monotherapy in PDAC, as there is still the standard issue of low immunogenicity and poor levels of infiltrating macrophages. Ideally, these DDS will be used in combination with other therapies such as stimulator of interferon genes (STING) agonist cancer vaccines (Fu *et al.*, 2015). STING agonists have been shown to be critical for mounting an adaptive immune response and detection of tumour cells by the immune system (Barber 2014). Fu *et al.*, 2015 showed that mice treated with

STING agonist vaccines showed significant PD-L1 upregulation, which was associated with increased tumour infiltration of T cells. It also showed regression in PDAC tumours and improved overall survival compared to anti- PD-1 blockade alone.

6.6 Future Directions: Modulation of Drug Release

As was observed in Chapters 2, 3 and 5, where the *in vitro* drug release from single or coaxial fibres was assessed, the burst release from hydrogels such as alginate is rapid, with approx. 90 % of the drug content released within the first 10 hours *in vitro*. This is well documented in the literature, which has led to studies that look at modulating this release using a variety of methods. Polymer selection is a simple way to modulate release, as hydrophobic polymers are known to have slower release profiles (Talebian *et al.,* 2018). Encapsulation of drug inside nanoparticles such as liposomes, prior to loading into the hydrogel scaffold has also been shown to reduce this burst release. The drug is then either released by diffusion out of the nanoparticle and through the scaffold, or by release of the particle from the scaffold. A study of vascular endothelial growth factor (VEGF) loaded PLGA loaded nanoparticles that were embedded into a pluronic F127 hydrogel found the burst release was significantly minimised, with 25 % of VEGF released over the first 10 days. The PLGA nanoparticles alone released approx. 43 % after 10 days, while the VEGF loaded directly into the gel released close to 100 % after 10 days (Geng *et al.,* 2011).

Another way of modulating the burst release is by modification of the polymer backbone. This is known as affinity-based release which utilises the interactions between the drug and the polymer (Li and Mooney 2016). There are a number of physical and chemical interactions that can be exploited in order to increase affinity, including incorporation of covalent bonds, electrostatic interactions or introducing hydrophobic associations (Wang and von Recum 2011, Li and Mooney 2016). Increasing the affinity of the drug to a hydrogel polymer changes the way the drug is released. Rather than by swelling and diffusion which is often rapid, introducing a cleavable covalent bond such as an ester or disulfide bond for example immobilises the drug until the specific enzymes cleave the drug, making it available. This was shown in a study where enzymatically degradable peptide

bonds were used to tether a peptide based drug to a poly ethylene glycol gel (Van Hove *et al.,* 2014). Release studies showed a significant increase in drug released when proteases (in particular metalloproteinases) were added to the release medium, which demonstrated the enzymatically responsive nature of the gel, and is something that has the potential to be explored further in this work to increase the effectiveness of our dual drug loaded DDS.

6.7 Conclusions

The data presented in this thesis has provided a basis for further development of single and dual drug loaded implants for cancer therapy. The data presented provides a foundation for the development of implants loaded with a range of chemotherapeutics both hydrophobic and hydrophilic, but also other sensitive biological therapeutics, which traditionally have not been able to be successfully loaded and delivered using an implantable DDS. Improving the way current drugs are delivered to hard-to-treat cancers will shift the treatment paradigm, and remove the association of pain and suffering that traditionally accompanies chemotherapy treatment. Improved drug delivery will not only increase the overall survival of PDAC patients, but also significantly increase the quality of the extended survival time.

List of References

Abazinge, M., T. Jackson, Q. Yang and G. Owusu-Ababio (2000). "Comparison of in vitro and in vivo release characteristics of sustained release ofloxacin microspheres." Drug delivery **7**(2): 77-81.
Aberle, M. R., R. A. Burkhart, H. Tiriac, S. W. M. Olde Damink, C. H. C. Dejong, D. A. Tuveson and R. M. van Dam (2018). "Patient-derived organoid models help define personalized management of gastrointestinal cancer." The British journal of surgery **105**(2): e48-e60.
Acharya, A., S. R. Markar, M. Matar, M. Ni and G. B. J. A. o. s. o. Hanna (2017). "Use of tumor markers in gastrointestinal cancers: surgeon perceptions and cost-benefit trade-off analysis." **24**(5): 1165-1173.
Agnihotri, S. A., N. N. Mallikarjuna and T. M. Aminabhavi (2004). "Recent advances on chitosan-based micro- and nanoparticles in drug delivery." Journal of Controlled Release **100**(1): 5-28.
Ahmadi, A., S. Zorofchian Moghadamtousi, S. Abubakar and K. Zandi (2015). "Antiviral potential of algae polysaccharides isolated from marine sources: a review." BioMed research international **2015**.
Ahmadi, F., Z. Oveisi, S. M. Samani and Z. Amoozgar (2015). "Chitosan based hydrogels: characteristics and pharmaceutical applications." Research in pharmaceutical sciences **10**(1): 1-16.
Ahmed, E. M. (2015). "Hydrogel: Preparation, characterization, and applications: A review." Journal of Advanced Research **6**(2): 105-121.
Allen, T. M. and P. R. Cullis (2004). "Drug Delivery Systems: Entering the Mainstream." Science **303**(5665): 1818.
Allison Logan, S., A. J. Brissenden, M. R. Szewczuk and R. J. Neufeld (2017). "Combinatorial and sequential delivery of gemcitabine and oseltamivir phosphate from implantable poly(d,l-lactic-co-glycolic acid) cylinders disables human pancreatic cancer cell survival." Drug Design, Development and Therapy **11**: 2239-2250.
Alvarenga, E. S. d. (2012). Characterization and Properties of Chitosan.
American Cancer Society (2019). Radiation Therapy for Pancreatic Cancer.
American Type Culture Collection. (2019). "MIA PaCa-2 (ATCC® CRL-1420™)." from https://www.atcc.org/Products/All/CRL-1420.aspx#characteristics.
Amrutkar, M. and I. P. Gladhaug (2017). "Pancreatic Cancer Chemoresistance to Gemcitabine." Cancers **9**(11): 157.
Anderson, J. M., A. Rodriguez and D. T. Chang (2008). "Foreign body reaction to biomaterials." Seminars in immunology **20**(2): 86-100.
Anindyajati, A., P. Boughton and A. J. Ruys (2018). "Modelling and optimization of Polycaprolactone ultrafine-fibres electrospinning process using response surface methodology." Materials **11**(3): 441.
Apte, M., S. Park, P. Phillips, N. Santucci, D. Goldstein, R. Kumar, G. Ramm, M. Buchler, H. Friess and J. McCarroll (2004). "Desmoplastic reaction in pancreatic cancer: role of pancreatic stellate cells." Pancreas **29**(3): 179-187.
Arslantunali, D., T. Dursun, D. Yucel, N. Hasirci and V. Hasirci (2014). "Peripheral nerve conduits: technology update." Medical devices (Auckland, N.Z.) **7**: 405-424.
Artinyan, A., P. A. Soriano, C. Prendergast, T. Low, J. D. I. Ellenhorn and J. Kim (2008). "The anatomic location of pancreatic cancer is a prognostic factor for survival." HPB : the official journal of the International Hepato Pancreato Biliary Association **10**(5): 371-376.
Augustine, R., S. K. Nethi, N. Kalarikkal, S. Thomas and C. R. Patra (2017). "Electrospun polycaprolactone (PCL) scaffolds embedded with europium hydroxide nanorods (EHNs) with enhanced vascularization and cell proliferation for tissue engineering applications." Journal of Materials Chemistry B **5**(24): 4660-4672.
Australian Institute of of Health and Welfare (2017). Cancer in Australia 2017. Canberra **Cancer Series No. 101**.
Bachmann, M. F. and A. Oxenius (2007). "Interleukin 2: from immunostimulation to immunoregulation and back again." EMBO reports **8**(12): 1142-1148.
Bailey, K. L. and M. A. Carlson (2019). "Porcine Models of Pancreatic Cancer." Frontiers in Oncology **9**(144).

Bajwa, R., A. Cheema, T. Khan, A. Amirpour, A. Paul, S. Chaughtai, S. Patel, T. Patel, J. Bramson, V. Gupta, M. Levitt, A. Asif and M. A. Hossain (2019). "Adverse Effects of Immune Checkpoint Inhibitors (Programmed Death-1 Inhibitors and Cytotoxic T-Lymphocyte-Associated Protein-4 Inhibitors): Results of a Retrospective Study." Journal of clinical medicine research **11**(4): 225-236.
Baker, B. M. and C. S. Chen (2012). "Deconstructing the third dimension–how 3D culture microenvironments alter cellular cues." J Cell Sci **125**(13): 3015-3024.
Bansal, R. K. (1996). Textbook Strength of Materials
Bao, Y., Q. Zhou, M. Zhang, H. Zhang, Q. Luan, W. Zhou, H. Tang and F. Huang (2019). "Wet-spun nanoTiO2/chitosan nanocomposite fibers as efficient and retrievable absorbent for the removal of free fatty acids from edible oil." Carbohydrate Polymers **210**: 119-126.
Barber, G. N. (2014). "STING-dependent cytosolic DNA sensing pathways." Trends in immunology **35**(2): 88-93.
Baselga, J., I. Bradbury, H. Eidtmann, S. Di Cosimo, E. de Azambuja, C. Aura, H. Gómez, P. Dinh, K. Fauria, V. Van Dooren, G. Aktan, A. Goldhirsch, T.-W. Chang, Z. Horváth, M. Coccia-Portugal, J. Domont, L.-M. Tseng, G. Kunz, J. H. Sohn, V. Semiglazov, G. Lerzo, M. Palacova, V. Probachai, L. Pusztai, M. Untch, R. D. Gelber and M. Piccart-Gebhart (2012). "Lapatinib with trastuzumab for HER2-positive early breast cancer (NeoALTTO): a randomised, open-label, multicentre, phase 3 trial." The Lancet **379**(9816): 633-640.
Basuki, J. S., F. Qie, X. Mulet, R. Suryadinata, A. V. Vashi, Y. Y. Peng, L. Li, X. Hao, T. Tan and T. C. Hughes (2017). "Photo-Modulated Therapeutic Protein Release from a Hydrogel Depot Using Visible Light." Angewandte Chemie International Edition **56**(4): 966-971.
Bayat Mokhtari, R., T. S. Homayouni, N. Baluch, E. Morgatskaya, S. Kumar, B. Das and H. Yeger (2017). "Combination therapy in combating cancer." Oncotarget **8**(23): 38022-38043.
Bayne, Lauren J., Gregory L. Beatty, N. Jhala, Carolyn E. Clark, Andrew D. Rhim, Ben Z. Stanger and Robert H. Vonderheide (2012). "Tumor-Derived Granulocyte-Macrophage Colony-Stimulating Factor Regulates Myeloid Inflammation and T Cell Immunity in Pancreatic Cancer." Cancer Cell **21**(6): 822-835.
Belizário, J. E. (2009). "Immunodeficient mouse models: an overview." The open immunology journal **2**(1).
Belz, J. E., R. Kumar, P. Baldwin, N. C. Ojo, A. S. Leal, D. B. Royce, D. Zhang, A. L. van de Ven, K. T. Liby and S. Sridhar (2017). "Sustained release talazoparib implants for localized treatment of BRCA1-deficient breast cancer." Theranostics **7**(17): 4340.
Berger, J., M. Reist, J. M. Mayer, O. Felt, N. Peppas and R. Gurny (2004). "Structure and interactions in covalently and ionically crosslinked chitosan hydrogels for biomedical applications." European Journal of Pharmaceutics and Biopharmaceutics **57**(1): 19-34.
Bernkop-Schnürch, A., C. Kast and D. Guggi (2003). "Permeation enhancing polymers in oral delivery of hydrophilic macromolecules: thiomer/GSH systems." Journal of Controlled Release **93**(2): 95-103.
Bhardwaj, N. and S. C. Kundu (2010). "Electrospinning: A fascinating fiber fabrication technique." Biotechnology Advances **28**(3): 325-347.
Bhattarai, N., J. Gunn and M. Zhang (2010). "Chitosan-based hydrogels for controlled, localized drug delivery." Advanced Drug Delivery Reviews **62**(1): 83-99.
Bilalis, P., D. Skoulas, A. Karatzas, J. Marakis, A. Stamogiannos, C. Tsimblouli, E. Sereti, E. Stratikos, K. Dimas and D. Vlassopoulos (2018). "Self-Healing pH-and Enzyme Stimuli-Responsive Hydrogels for Targeted Delivery of Gemcitabine To Treat Pancreatic Cancer." Biomacromolecules **19**(9): 3840-3852.
Binenbaum, Y., S. Na'ara and Z. Gil (2015). "Gemcitabine resistance in pancreatic ductal adenocarcinoma." Drug Resistance Updates **23**: 55-68.
Boddu, S. H., J. Jwala, M. R. Chowdhury and A. K. Mitra (2010). "In vitro evaluation of a targeted and sustained release system for retinoblastoma cells using Doxorubicin as a model drug." Journal of Ocular Pharmacology and Therapeutics **26**(5): 459-468.
Borazanci, E. H., G. S. Jameson, M. J. Borad, R. K. Ramanathan, R. L. Korn, L. Caldwell, K. Ansaldo, K. Hendrickson, K. Marceau and D. D. Von Hoff (2018). A phase II pilot trial of nivolumab (N)+ albumin bound paclitaxel (AP)+ paricalcitol (P)+ cisplatin (C)+ gemcitabine (G)(NAPPCG) in patients with previously untreated metastatic pancreatic ductal adenocarcinoma (PDAC), American Society of Clinical Oncology.

Boulanger, J., J. Boursiquot, G. Cournoyer, J. Lemieux, M. Masse, K. Almanric, M. Guay and C. d. l. é. d. p. e. o. J. C. Oncology (2014). "Management of hypersensitivity to platinum-and taxane-based chemotherapy: cepo review and clinical recommendations." **21**(4): e630.
Bracci, L., G. Schiavoni, A. Sistigu and F. Belardelli (2013). "Immune-based mechanisms of cytotoxic chemotherapy: implications for the design of novel and rationale-based combined treatments against cancer." Cell Death And Differentiation **21**: 15.
Brahmer, J. R., S. S. Tykodi, L. Q. Chow, W.-J. Hwu, S. L. Topalian, P. Hwu, C. G. Drake, L. H. Camacho, J. Kauh and K. Odunsi (2012). "Safety and activity of anti–PD-L1 antibody in patients with advanced cancer." New England Journal of Medicine **366**(26): 2455-2465.
Brem, H., S. Piantadosi, P. Burger, M. Walker, R. Selker, N. Vick, K. Black, M. Sisti, S. Brem and G. Mohr (1995). "Placebo-controlled trial of safety and efficacy of intraoperative controlled delivery by biodegradable polymers of chemotherapy for recurrent gliomas." The Lancet **345**(8956): 1008-1012.
Breslin, S. and L. O'Driscoll (2013). "Three-dimensional cell culture: the missing link in drug discovery." Drug discovery today **18**(5): 240-249.
Buch, K., T. Peters, T. Nawroth, M. Sänger, H. Schmidberger and P. Langguth (2012). "Determination of cell survival after irradiation via clonogenic assay versus multiple MTT Assay-A comparative study." Radiation oncology **7**(1): 1.
Burris, H. r., M. J. Moore, J. Andersen, M. R. Green, M. L. Rothenberg, M. R. Modiano, M. Christine Cripps, R. K. Portenoy, A. M. Storniolo and P. Tarassoff (1997). "Improvements in survival and clinical benefit with gemcitabine as first-line therapy for patients with advanced pancreas cancer: a randomized trial." Journal of clinical oncology **15**(6): 2403-2413.
Byrne, J. D., M. N. Jajja, A. T. O'Neill, L. R. Bickford, A. W. Keeler, N. Hyder, K. Wagner, A. Deal, R. E. Little and R. A. Moffitt (2015). "Local iontophoretic administration of cytotoxic therapies to solid tumors." Science translational medicine **7**(273): 273ra214-273ra214.
Canto, M. I., F. Harinck, R. H. Hruban, G. J. Offerhaus, J.-W. Poley, I. Kamel, Y. Nio, R. S. Schulick, C. Bassi and I. Kluijt (2013). "International Cancer of the Pancreas Screening (CAPS) Consortium summit on the management of patients with increased risk for familial pancreatic cancer." Gut **62**(3): 339-347.
Cappella, P., D. Tomasoni, M. Faretta, M. Lupi, F. Montalenti, F. Viale, F. Banzato, M. D'Incalci and P. Ubezio (2001). "Cell cycle effects of gemcitabine." International journal of cancer **93**(3): 401-408.
Chantrill, L. A., A. M. Nagrial, C. Watson, A. L. Johns, M. Martyn-Smith, S. Simpson, S. Mead, M. D. Jones, J. S. Samra and A. J. J. C. c. r. Gill (2015). "Precision medicine for advanced pancreas cancer: the individualized molecular pancreatic cancer therapy (IMPaCT) trial." **21**(9): 2029-2037.
Chari, S. T., K. Kelly, M. A. Hollingsworth, S. P. Thayer, D. A. Ahlquist, D. K. Andersen, S. K. Batra, T. A. Brentnall, M. Canto, D. F. Cleeter, M. A. Firpo, S. S. Gambhir, V. L. W. Go, O. J. Hines, B. J. Kenner, D. S. Klimstra, M. M. Lerch, M. J. Levy, A. Maitra, S. J. Mulvihill, G. M. Petersen, A. D. Rhim, D. M. Simeone, S. Srivastava, M. Tanaka, A. I. Vinik and D. Wong (2015). "Early detection of sporadic pancreatic cancer: summative review." Pancreas **44**(5): 693-712.
Chen, B., W. Dai, B. He, H. Zhang, X. Wang, Y. Wang and Q. Zhang (2017). "Current multistage drug delivery systems based on the tumor microenvironment." Theranostics **7**(3): 538.
Cheng, D., X. Cao, H. Gao, X. Ye, W. Li and Y. Wang (2014). "Engineering PLGA doped PCL microspheres with a layered architecture and an island–sea topography." RSC Advances **4**(18): 9031-9038.
Cho, J. H. and J.-S. Han (2017). "Phospholipase D and Its Essential Role in Cancer." Molecules and cells **40**(11): 805-813.
Choi, C., A. Son, H.-S. Lee, Y.-J. Lee and H. C. Park (2018). "Radiosensitization by marine sponge Agelas sp. extracts in hepatocellular carcinoma cells with autophagy induction." Scientific reports **8**(1): 6317.
Chou, A., N. Waddell, M. J. Cowley, A. J. Gill, D. K. Chang, A.-M. Patch, K. Nones, J. Wu, M. Pinese, A. L. Johns, D. K. Miller, K. S. Kassahn, A. M. Nagrial, H. Wasan, D. Goldstein, C. W. Toon, V. Chin, L. Chantrill, J. Humphris, R. S. Mead, I. Rooman, J. S. Samra, M. Pajic, E. A. Musgrove, J. V. Pearson, A. L. Morey, S. M. Grimmond and A. V. Biankin (2013). "Clinical and molecular characterization of HER2 amplified-pancreatic cancer." Genome medicine **5**(8): 78-78.

Chowdhary, S. A., T. Ryken and H. B. Newton (2015). "Survival outcomes and safety of carmustine wafers in the treatment of high-grade gliomas: a meta-analysis." Journal of neuro-oncology **122**(2): 367-382.
Chung, H. W., S. M. Bang, S. W. Park, J. B. Chung, J. K. Kang, J. W. Kim, J. S. Seong, W. J. Lee and S. Y. Song (2004). "A prospective randomized study of gemcitabine with doxifluridine versus paclitaxel with doxifluridine in concurrent chemoradiotherapy for locally advanced pancreatic cancer." International Journal of Radiation Oncology* Biology* Physics **60**(5): 1494-1501.
Conroy, T., F. Desseigne, M. Ychou, O. Bouché, R. Guimbaud, Y. Bécouarn, A. Adenis, J.-L. Raoul, S. Gourgou-Bourgade, C. de la Fouchardière, J. Bennouna, J.-B. Bachet, F. Khemissa-Akouz, D. Péré-Vergé, C. Delbaldo, E. Assenat, B. Chauffert, P. Michel, C. Montoto-Grillot and M. Ducreux (2011). "FOLFIRINOX versus Gemcitabine for Metastatic Pancreatic Cancer." New England Journal of Medicine **364**(19): 1817-1825.
Conroy, T., P. Hammel, M. Hebbar, M. Ben Abdelghani, A. C. Wei, J.-L. Raoul, L. Choné, E. Francois, P. Artru and J. J. J. N. E. J. o. M. Biagi (2018). "FOLFIRINOX or gemcitabine as adjuvant therapy for pancreatic cancer." **379**(25): 2395-2406.
Coombes, A., S. Rizzi, M. Williamson, J. Barralet, S. Downes and W. Wallace (2004). "Precipitation casting of polycaprolactone for applications in tissue engineering and drug delivery." Biomaterials **25**(2): 315-325.
Cronin, E. M., F. A. Thurmond, R. Bassel-Duby, R. S. Williams, W. E. Wright, K. D. Nelson and H. R. Garner (2004). "Protein-coated poly (L-lactic acid) fibers provide a substrate for differentiation of human skeletal muscle cells." Journal of Biomedical Materials Research Part A: An Official Journal of The Society for Biomaterials, The Japanese Society for Biomaterials, and The Australian Society for Biomaterials and the Korean Society for Biomaterials **69**(3): 373-381.
Cunha, A. G., M. Lundahl, M. F. Ansari, L.-S. Johansson, J. M. Campbell and O. J. Rojas (2018). "Surface Structuring and Water Interactions of Nanocellulose Filaments Modified with Organosilanes toward Wearable Materials." ACS applied nano materials **1**(9): 5279-5288.
d'Avella, D. and A. DellaPuppa (2012). "Safety and efficacy of Gliadel wafers for newly diagnosed and recurrent glioblastomas." Acta Neurochirurgica **154**(8): 1379-1381.
De Jong, W. H. and P. J. A. Borm (2008). "Drug delivery and nanoparticles:applications and hazards." International journal of nanomedicine **3**(2): 133-149.
de Sousa Cavalcante, L. and G. Monteiro (2014). "Gemcitabine: Metabolism and molecular mechanisms of action, sensitivity and chemoresistance in pancreatic cancer." European Journal of Pharmacology **741**: 8-16.
De Souza, A., K. Irfan, F. Masud and M. W. Saif (2016). "Diabetes Type 2 and Pancreatic Cancer: A History Unfolding." JOP : Journal of the pancreas **17**(2): 144-148.
de Vos, P., C. G. Hoogmoed and H. J. Busscher (2002). "Chemistry and biocompatibility of alginate-PLL capsules for immunoprotection of mammalian cells." Journal of Biomedical Materials Research: An Official Journal of The Society for Biomaterials, The Japanese Society for Biomaterials, and The Australian Society for Biomaterials and the Korean Society for Biomaterials **60**(2): 252-259.
Dean-Colomb, W. and F. J. Esteva (2008). "Her2-positive breast cancer: Herceptin and beyond." European Journal of Cancer **44**(18): 2806-2812.
Defour, A., J. H. Van der Meulen, R. Bhat, A. Bigot, R. Bashir, K. Nagaraju and J. K. Jaiswal (2014). "Dysferlin regulates cell membrane repair by facilitating injury-triggered acid sphingomyelinase secretion." Cell death & disease **5**(6): e1306-e1306.
Di Colo, G., Y. Zambito and C. Zaino (2008). "Polymeric enhancers of mucosal epithelia permeability: synthesis, transepithelial penetration-enhancing properties, mechanism of action, safety issues." Journal of pharmaceutical sciences **97**(5): 1652-1680.
Dimou, A., K. N. Syrigos and M. W. Saif (2012). "Overcoming the stromal barrier: technologies to optimize drug delivery in pancreatic cancer." Therapeutic advances in medical oncology **4**(5): 271-279.
Ding, Q., Z. Li, Y. Yang, G. Guo, F. Luo, Z. Chen, Y. Yang, Z. Qian and S. Shi (2016). "Preparation and therapeutic application of docetaxel-loaded poly (D, L-lactide) nanofibers in preventing breast cancer recurrence." Drug delivery **23**(8): 2677-2685.

Dorati, R., A. DeTrizio, T. Modena, B. Conti, F. Benazzo, G. Gastaldi and I. Genta (2017). "Biodegradable Scaffolds for Bone Regeneration Combined with Drug-Delivery Systems in Osteomyelitis Therapy." Pharmaceuticals (Basel, Switzerland) **10**(4): 96.
Doshi, J. and D. H. Reneker (1995). "Electrospinning process and applications of electrospun fibers." Journal of Electrostatics **35**(2): 151-160.
Doyle, T. H., F. Mornex and W. G. McKenna (2001). The clinical implications of gemcitabine radiosensitization, AACR.
Draget, K. I., S. T. Moe, G. Skja˚k-Bræk and S. Olav (1991). Alginates. Food Polysaccharides and their Applications. T. a. F. Group, CRC Press. **67:** 289-328.
Du, L., Q. Yang, J. Zhang, M. Zhu, X. Ma, Y. Zhang, L. Wang and B. Xu (2019). "Engineering a biomimetic integrated scaffold for intervertebral disc replacement." Materials Science and Engineering: C **96**: 522-529.
Ducreux, M., C. Caramella, A. Hollebecque, P. Burtin, D. Goéré, T. Seufferlein, K. Haustermans, J. Van Laethem, T. Conroy and D. Arnold (2015). "Cancer of the pancreas: ESMO Clinical Practice Guidelines for diagnosis, treatment and follow-up." Annals of Oncology **26**(suppl_5): v56-v68.
Dufresne, M.-H. l. n., E. Marouf, Y. Kränzlin, M. A. Gauthier and J.-C. Leroux (2012). "Lipase is essential for the study of in vitro release kinetics from organogels." Molecular pharmaceutics **9**(6): 1803-1811.
Eklund, L., M. Bry and K. Alitalo (2013). "Mouse models for studying angiogenesis and lymphangiogenesis in cancer." Molecular oncology **7**(2): 259-282.
Elahi, N., M. Kamali and M. H. Baghersad (2018). "Recent biomedical applications of gold nanoparticles: A review." Talanta **184**: 537-556.
Exner, A. A. and G. M. Saidel (2008). "Drug-eluting polymer implants in cancer therapy." Expert opinion on drug delivery **5**(7): 775-788.
Food and Drug Administration. (2006). "Drug Approval Package: MiraLax (Polyethylene Glycol 3350) Powder."
Food and Drug Administration (2019). "CFR - Code of Federal Regulations Title 21."
Friedrich, J., W. Eder, J. Castaneda, M. Doss, E. Huber, R. Ebner and L. A. Kunz-Schughart (2007). "A reliable tool to determine cell viability in complex 3-d culture: the acid phosphatase assay." Journal of biomolecular screening **12**(7): 925-937.
Froeling, F. E. M., J. F. Marshall and H. M. Kocher (2010). "Pancreatic cancer organotypic cultures." Journal of Biotechnology **148**(1): 16-23.
Fu, J., D. B. Kanne, M. Leong, L. H. Glickman, S. M. McWhirter, E. Lemmens, K. Mechette, J. J. Leong, P. Lauer and W. Liu (2015). "STING agonist formulated cancer vaccines can cure established tumors resistant to PD-1 blockade." Science translational medicine **7**(283): 283ra252-283ra252.
Fukunaga, A., M. Miyamoto, Y. Cho, S. Murakami, Y. Kawarada, T. Oshikiri, K. Kato, T. Kurokawa, M. Suzuoki and Y. Nakakubo (2004). "CD8+ tumor-infiltrating lymphocytes together with CD4+ tumor-infiltrating lymphocytes and dendritic cells improve the prognosis of patients with pancreatic adenocarcinoma." Pancreas **28**(1): e26-e31.
Fung, L. K., M. G. Ewend, A. Sills, E. P. Sipos, R. Thompson, M. Watts, O. M. Colvin, H. Brem and W. M. Saltzman (1998). "Pharmacokinetics of interstitial delivery of carmustine, 4-hydroperoxycyclophosphamide, and paclitaxel from a biodegradable polymer implant in the monkey brain." Cancer Research **58**(4): 672-684.
Galeska, I., T.-K. Kim, S. D. Patil, U. Bhardwaj, D. Chatttopadhyay, F. Papadimitrakopoulos and D. J. Burgess (2005). "Controlled release of dexamethasone from PLGA microspheres embedded within polyacid-containing PVA hydrogels." The AAPS journal **7**(1): E231-E240.
Gao, H., Y. Gu and Q. Ping (2007). "The implantable 5-fluorouracil-loaded poly(l-lactic acid) fibers prepared by wet-spinning from suspension." Journal of Controlled Release **118**(3): 325-332.
Gao, L., L. Xia, R. Zhang, D. Duan, X. Liu, J. Xu and L. Luo (2017). "Enhanced antitumor efficacy of poly (D, L-lactide-co-glycolide)-based methotrexate-loaded implants on sarcoma 180 tumor-bearing mice." Drug design, development and therapy **11**: 3065.

Gargiulo, S., A. Greco, M. Gramanzini, S. Esposito, A. Affuso, A. Brunetti and G. Vesce (2012). "Mice anesthesia, analgesia, and care, Part I: anesthetic considerations in preclinical research." ILAR journal **53**(1): E55-E69.
Gelderblom, H., J. Verweij, K. Nooter and A. Sparreboom (2001). "Cremophor EL: the drawbacks and advantages of vehicle selection for drug formulation." European Journal of Cancer **37**(13): 1590-1598.
Geng, H., H. Song, J. Qi and D. Cui (2011). "Sustained release of VEGF from PLGA nanoparticles embedded thermo-sensitive hydrogel in full-thickness porcine bladder acellular matrix." Nanoscale research letters **6**(1): 312.
Gnanamony, M. and C. S. Gondi (2017). "Chemoresistance in pancreatic cancer: Emerging concepts." Oncology letters **13**(4): 2507-2513.
Golan, T., E. Z. Khvalevsky, A. Hubert, R. M. Gabai, N. Hen, A. Segal, A. Domb, G. Harari, E. B. David and S. Raskin (2015). "RNAi therapy targeting KRAS in combination with chemotherapy for locally advanced pancreatic cancer patients." Oncotarget **6**(27): 24560.
Goldstein, D., R. H. El-Maraghi, P. Hammel, V. Heinemann, V. Kunzmann, J. Sastre, W. Scheithauer, S. Siena, J. Tabernero, L. Teixeira, G. Tortora, J.-L. Van Laethem, R. Young, D. N. Penenberg, B. Lu, A. Romano and D. D. Von Hoff (2015). "nab-Paclitaxel Plus Gemcitabine for Metastatic Pancreatic Cancer: Long-Term Survival From a Phase III Trial." JNCI: Journal of the National Cancer Institute **107**(2).
Greer, J. B. and D. C. Whitcomb (2007). "Role of BRCA1 and BRCA2 mutations in pancreatic cancer." Gut **56**(5): 601-605.
Guo, W., W. Chen, W. Yu, W. Huang and W. Deng (2013). "Small interfering RNA-based molecular therapy of cancers." Chinese journal of cancer **32**(9): 488-493.
Habiro, A., S. Tanno, K. Koizumi, T. Izawa, Y. Nakano, M. Osanai, Y. Mizukami, T. Okumura and Y. Kohgo (2004). "Involvement of p38 mitogen-activated protein kinase in gemcitabine-induced apoptosis in human pancreatic cancer cells." Biochemical and biophysical research communications **316**(1): 71-77.
Hamidi, M., A. Azadi and P. Rafiei (2008). "Hydrogel nanoparticles in drug delivery." Advanced Drug Delivery Reviews **60**(15): 1638-1649.
Hammel, P., F. Huguet, J.-L. van Laethem, D. Goldstein, B. Glimelius, P. Artru, I. Borbath, O. Bouché, J. Shannon, T. André, L. Mineur, B. Chibaudel, F. Bonnetain and C. Louvet (2016). "Effect of Chemoradiotherapy vs Chemotherapy on Survival in Patients With Locally Advanced Pancreatic Cancer Controlled After 4 Months of Gemcitabine With or Without Erlotinib: The LAP07 Randomized Clinical Trial." JAMA **315**(17): 1844-1853.
Harris, M., D. Croagh, M. Aghmesheh, A. Nagrial, N. Nguyen, H. Wasan, T. Ajithkumar, A. Kraszewski, T. Maher and P. Ross (2018). "P-141 PanCO: An open-label, single-arm pilot study of Oncosil™ in patients with unresectable locally advanced pancreatic adenocarcinoma in combination with FOLFIRINOX or gemcitabine+ nab-paclitaxel chemotherapies." Annals of Oncology **29**(suppl_5): mdy151. 140.
Hassan, M. M., M. L. Bondy, R. A. Wolff, J. L. Abbruzzese, J.-N. Vauthey, P. W. Pisters, D. B. Evans, R. Khan, T.-H. Chou, R. Lenzi, L. Jiao and D. Li (2007). "Risk Factors for Pancreatic Cancer: Case-Control Study." The American Journal Of Gastroenterology **102**: 2696.
He, Y., N. Zhang, Q. Gong, H. Qiu, W. Wang, Y. Liu and J. Gao (2012). "Alginate/graphene oxide fibers with enhanced mechanical strength prepared by wet spinning." Carbohydrate polymers **88**(3): 1100-1108.
Henriksen, A., A. Dyhl-Polk, I. Chen and D. Nielsen (2019). "Checkpoint inhibitors in pancreatic cancer." Cancer Treatment Reviews **78**: 17-30.
Herbst, R. S., J.-C. Soria, M. Kowanetz, G. D. Fine, O. Hamid, M. S. Gordon, J. A. Sosman, D. F. McDermott, J. D. Powderly, S. N. Gettinger, H. E. K. Kohrt, L. Horn, D. P. Lawrence, S. Rost, M. Leabman, Y. Xiao, A. Mokatrin, H. Koeppen, P. S. Hegde, I. Mellman, D. S. Chen and F. S. Hodi (2014). "Predictive correlates of response to the anti-PD-L1 antibody MPDL3280A in cancer patients." Nature **515**: 563.
Herreros-Villanueva, M., E. Hijona, A. Cosme and L. Bujanda (2012). "Adjuvant and neoadjuvant treatment in pancreatic cancer." World journal of gastroenterology: WJG **18**(14): 1565.
Herreros-Villanueva, M., E. Hijona, A. Cosme and L. Bujanda (2012). "Mouse models of pancreatic cancer." World journal of gastroenterology **18**(12): 1286-1294.

Hickman, J. A., R. Graeser, R. de Hoogt, S. Vidic, C. Brito, M. Gutekunst and H. van der Kuip (2014). "Three-dimensional models of cancer for pharmacology and cancer cell biology: capturing tumor complexity in vitro/ex vivo." Biotechnology journal **9**(9): 1115-1128.
Hilmi, M., L. Bartholin and C. Neuzillet (2018). "Immune therapies in pancreatic ductal adenocarcinoma: Where are we now?" World journal of gastroenterology **24**(20): 2137.
Hingorani, S. R., L. Wang, A. S. Multani, C. Combs, T. B. Deramaudt, R. H. Hruban, A. K. Rustgi, S. Chang and D. A. Tuveson (2005). "Trp53R172H and KrasG12D cooperate to promote chromosomal instability and widely metastatic pancreatic ductal adenocarcinoma in mice." Cancer Cell **7**(5): 469-483.
Hingorani, S. R., L. Zheng, A. J. Bullock, T. E. Seery, W. P. Harris, D. S. Sigal, F. Braiteh, P. S. Ritch, M. M. Zalupski and N. Bahary (2018). "HALO 202: randomized phase II study of PEGPH20 plus nab-paclitaxel/gemcitabine versus nab-paclitaxel/gemcitabine in patients with untreated, metastatic pancreatic ductal adenocarcinoma." J Clin Oncol **36**(4): 359-366.
Hirschhaeuser, F., H. Menne, C. Dittfeld, J. West, W. Mueller-Klieser and L. A. Kunz-Schughart (2010). "Multicellular tumor spheroids: an underestimated tool is catching up again." Journal of biotechnology **148**(1): 3-15.
Hoare, T. R. and D. S. Kohane (2008). "Hydrogels in drug delivery: progress and challenges." Polymer **49**(8): 1993-2007.
Holm, H. H. (1997). The history of interstitial brachytherapy of prostatic cancer. Seminars in surgical oncology, Wiley Online Library.
Hong, S. P., J. Wen, S. Bang, S. Park and S. Y. Song (2009). "CD44-positive cells are responsible for gemcitabine resistance in pancreatic cancer cells." International Journal of Cancer **125**(10): 2323-2331.
Horwitz, S. (1994). "Taxol (paclitaxel): mechanisms of action." Annals of oncology: official journal of the European Society for Medical Oncology **5**: S3-6.
Hrynyk, M., J. P. Ellis, F. Haxho, S. Allison, J. A. M. Steele, S. Abdulkhalek, R. J. Neufeld and M. R. Szewczuk (2015). "Therapeutic designed poly (lactic-co-glycolic acid) cylindrical oseltamivir phosphate-loaded implants impede tumor neovascularization, growth and metastasis in mouse model of human pancreatic carcinoma." Drug Design, Development and Therapy **9**: 4573-4586.
Hu, Y.-L., W. Qi, F. Han, J.-Z. Shao and J.-Q. Gao (2011). "Toxicity evaluation of biodegradable chitosan nanoparticles using a zebrafish embryo model." Int J Nanomedicine **6**(4): 3351-3359.
Hua, S. (2014). "Development of an effective topical liposomal formulation for localized analgesia and anti-inflammatory actions in the Complete Freund's Adjuvant rodent model of acute inflammatory pain." Pain physician **17**: E719-E735.
Huang, M., E. Khor and L.-Y. Lim (2004). "Uptake and cytotoxicity of chitosan molecules and nanoparticles: effects of molecular weight and degree of deacetylation." Pharmaceutical research **21**(2): 344-353.
Huxley, R., A. Ansary-Moghaddam, A. B. De González, F. Barzi and M. Woodward (2005). "Type-II diabetes and pancreatic cancer: a meta-analysis of 36 studies." British journal of cancer **92**(11): 2076.
Indolfi, L., M. Ligorio, D. T. Ting, K. Xega, A. R. Tzafriri, F. Bersani, N. Aceto, V. Thapar, B. C. Fuchs and V. Deshpande (2016). "A tunable delivery platform to provide local chemotherapy for pancreatic ductal adenocarcinoma." Biomaterials **93**: 71-82.
Innocente, F., D. Mandracchia, E. Pektok, B. Nottelet, J.-C. Tille, S. De Valence, G. Faggian, A. Mazzucco, A. Kalangos and R. Gurny (2009). "Paclitaxel-eluting biodegradable synthetic vascular prostheses: a step towards reduction of neointima formation?" Circulation **120**(11 suppl 1): S37-S45.
Iyer, S. S., W. H. Barr and H. T. Karnes (2007). "A 'biorelevant'approach to accelerated in vitro drug release testing of a biodegradable, naltrexone implant." International journal of pharmaceutics **340**(1-2): 119-125.
Jaccoulet, E., T. Daniel, P. Prognon and E. Caudron (2019). "Forced Degradation of Monoclonal Antibodies After Compounding: Impact on Routine Hospital Quality Control." Journal of Pharmaceutical Sciences.
Jain, D. and D. Bar-Shalom (2014). "Alginate drug delivery systems: application in context of pharmaceutical and biomedical research." Drug development and industrial pharmacy **40**(12): 1576-1584.

Jang, J., Y.-J. Seol, H. J. Kim, J. Kundu, S. W. Kim and D.-W. Cho (2014). "Effects of alginate hydrogel cross-linking density on mechanical and biological behaviors for tissue engineering." journal of the mechanical behavior of biomedical materials **37**: 69-77.
Janjic, M., F. Pappa, V. Karagkiozaki, C. Gitas, K. Ktenidis and S. Logothetidis (2017). "Surface modification of endovascular stents with rosuvastatin and heparin-loaded biodegradable nanofibers by electrospinning." International journal of nanomedicine **12**: 6343-6355.
Jiang, H., S. Hegde, B. L. Knolhoff, Y. Zhu, J. M. Herndon, M. A. Meyer, T. M. Nywening, W. G. Hawkins, I. M. Shapiro, D. T. Weaver, J. A. Pachter, A. Wang-Gillam and D. G. DeNardo (2016). "Targeting focal adhesion kinase renders pancreatic cancers responsive to checkpoint immunotherapy." Nature Medicine **22**: 851.
Jiang, L., L. Wang, N. Wang, S. Gong, L. Wang, Q. Li, C. Shen and L.-S. Turng (2018). "Fabrication of polycaprolactone electrospun fibers with different hierarchical structures mimicking collagen fibrils for tissue engineering scaffolds." Applied Surface Science **427**: 311-325.
Jin, H.-T., R. Ahmed and T. Okazaki (2010). Role of PD-1 in regulating T-cell immunity. Negative Co-Receptors and Ligands, Springer**:** 17-37.
Jun, E., S. C. Kim, C. M. Lee, J. Oh, S. Lee and I. K. Shim (2017). "Synergistic effect of a drug loaded electrospun patch and systemic chemotherapy in pancreatic cancer xenograft." Scientific reports **7**(1): 12381.
Junoh, H., J. Jaafar, M. N. A. M. Norddin, A. F. Ismail, M. H. D. Othman, M. A. Rahman, N. Yusof, W. N. W. Salleh and H. Ilbeygi (2015). "A review on the fabrication of electrospun polymer electrolyte membrane for direct methanol fuel cell." Journal of Nanomaterials **2015**: 4.
Kafka, D. and R. B. Gold (1983). "Food and Drug Administration approves vaginal sponge." Family planning perspectives **15**(3): 146-148.
Kamaly, N., B. Yameen, J. Wu and O. C. Farokhzad (2016). "Degradable Controlled-Release Polymers and Polymeric Nanoparticles: Mechanisms of Controlling Drug Release." Chemical reviews **116**(4): 2602-2663.
Kampan, N. C., M. T. Madondo, O. M. McNally, M. Quinn and M. Plebanski (2015). "Paclitaxel and its evolving role in the management of ovarian cancer." BioMed research international **2015**.
Kapałczyńska, M., T. Kolenda, W. Przybyła, M. Zajączkowska, A. Teresiak, V. Filas, M. Ibbs, R. Bliźniak, Ł. Łuczewski and K. Lamperska (2018). "2D and 3D cell cultures - a comparison of different types of cancer cell cultures." Archives of medical science : AMS **14**(4): 910-919.
Kau, Y.-C. and S.-J. Liu (2012). "Comparison of in vitro and in vivo release of lidocaine from biodegradable pellets: 9AP1-10." European Journal of Anaesthesiology (EJA) **29**: 134.
Khashi, M., S. Hassanajili and S. I. Golestaneh (2018). "Electrospun Poly-lactic Acid/Chitosan Nanofibers Loaded with Paclitaxel for Coating of a Prototype Polymeric Stent." Fibers and Polymers **19**(7): 1444-1453.
Kim, M. P. and G. E. Gallick (2008). "Gemcitabine Resistance in Pancreatic Cancer: Picking the Key Players." Clinical Cancer Research **14**(5): 1284.
Kim, V. M. and N. Ahuja (2015). "Early detection of pancreatic cancer." Chinese journal of cancer research = Chung-kuo yen cheng yen chiu **27**(4): 321-331.
Kim, Y.-C., J.-H. Park and M. R. Prausnitz (2012). "Microneedles for drug and vaccine delivery." Advanced drug delivery reviews **64**(14): 1547-1568.
Kleinberg, L. (2016). "Polifeprosan 20, 3.85% carmustine slow release wafer in malignant glioma: patient selection and perspectives on a low-burden therapy." Patient preference and adherence **10**: 2397.
Klopfleisch, R. and F. Jung (2017). "The pathology of the foreign body reaction against biomaterials." Journal of Biomedical Materials Research Part A **105**(3): 927-940.
Klug, F., H. Prakash, Peter E. Huber, T. Seibel, N. Bender, N. Halama, C. Pfirschke, Ralf H. Voss, C. Timke, L. Umansky, K. Klapproth, K. Schäkel, N. Garbi, D. Jäger, J. Weitz, H. Schmitz-Winnenthal, Günter J. Hämmerling and P. Beckhove (2013). "Low-Dose Irradiation Programs Macrophage Differentiation to an iNOS+/M1 Phenotype that Orchestrates Effective T Cell Immunotherapy." Cancer Cell **24**(5): 589-602.
Kowalewski, A., Ł. Szylberg, M. Saganek, W. Napiontek, P. Antosik and D. Grzanka (2018). "Emerging strategies in BRCA-positive pancreatic cancer." Journal of cancer research and clinical oncology **144**(8): 1503-1507.

Krzyszczyk, P., R. Schloss, A. Palmer and F. Berthiaume (2018). "The Role of Macrophages in Acute and Chronic Wound Healing and Interventions to Promote Pro-wound Healing Phenotypes." Frontiers in Physiology **9**(419).
Kuo, C. K. and P. X. Ma (2001). "Ionically crosslinked alginate hydrogels as scaffolds for tissue engineering: Part 1. Structure, gelation rate and mechanical properties." Biomaterials **22**(6): 511-521.
Kuznetsov, K. A., A. O. Stepanova, R. I. Kvon, T. E. L. Douglas, N. A. Kuznetsov, V. S. Chernonosova, I. A. Zaporozhchenko, M. V. Kharkova, I. V. Romanova, A. A. Karpenko and P. P. Laktionov (2018). "Electrospun Produced 3D Matrices for Covering of Vascular Stents: Paclitaxel Release Depending on Fiber Structure and Composition of the External Environment." Materials (Basel, Switzerland) **11**(11): 2176.
Kwilas, A., R. Donahue, M. Bernstein and J. Hodge (2012). "In the field: exploiting the untapped potential of immunogenic modulation by radiation in combination with immunotherapy for the treatment of cancer." **2**(104).
Lam, C. X., D. W. Hutmacher, J. T. Schantz, M. A. Woodruff and S. H. Teoh (2009). "Evaluation of polycaprolactone scaffold degradation for 6 months in vitro and in vivo." Journal of Biomedical Materials Research Part A: An Official Journal of The Society for Biomaterials, The Japanese Society for Biomaterials, and The Australian Society for Biomaterials and the Korean Society for Biomaterials **90**(3): 906-919.
Lammers, T., F. Kiessling, M. Ashford, W. Hennink, D. Crommelin and G. Storm (2016). "Cancer nanomedicine: Is targeting our target?" Nature reviews. Materials **1**(9): 16069.
Le, D. T., T. S. Crocenzi, J. N. Uram, E. R. Lutz, D. Laheru, E. A. Sugar, R. H. Vonderheide, G. A. Fisher, A. H. Ko and A. L. Murphy (2016). Randomized phase II study of the safety, efficacy, and immune response of GVAX pancreas (with cyclophosphamide) and CRS-207 with or without nivolumab in patients with previously treated metastatic pancreatic adenocarcinoma (STELLAR), American Society of Clinical Oncology.
Le, H. K., L. Graham, E. Cha, J. K. Morales, M. H. Manjili and H. D. Bear (2009). "Gemcitabine directly inhibits myeloid derived suppressor cells in BALB/c mice bearing 4T1 mammary carcinoma and augments expansion of T cells from tumor-bearing mice." International Immunopharmacology **9**(7): 900-909.
Leach, J. B. and C. E. Schmidt (2005). "Characterization of protein release from photocrosslinkable hyaluronic acid-polyethylene glycol hydrogel tissue engineering scaffolds." Biomaterials **26**(2): 125-135.
Lee, H. S. and S. W. Park (2016). "Systemic Chemotherapy in Advanced Pancreatic Cancer." Gut and liver **10**(3): 340-347.
Lee, J. W., C. A. Komar, F. Bengsch, K. Graham and G. L. Beatty (2016). "Genetically Engineered Mouse Models of Pancreatic Cancer: The KPC Model (LSL-Kras(G12D/+) ;LSL-Trp53(R172H/+) ;Pdx-1-Cre), Its Variants, and Their Application in Immuno-oncology Drug Discovery." Current protocols in pharmacology **73**: 14.39.11-14.39.20.
Lee, K. Y. and D. J. Mooney (2012). "Alginate: properties and biomedical applications." Progress in polymer science **37**(1): 106-126.
Lee, S. M., N. Kim, H. J. Son, J. H. Park, R. H. Nam, M. H. Ham, D. Choi, S. H. Sohn, E. Shin, Y.-J. Hwang, J. Sung, D. H. Lee and H.-N. Lee (2016). "The Effect of Sex on the Azoxymethane/Dextran Sulfate Sodium-treated Mice Model of Colon Cancer." Journal of cancer prevention **21**(4): 271-278.
Li, J. and D. J. Mooney (2016). "Designing hydrogels for controlled drug delivery." Nature Reviews Materials **1**(12): 16071.
Liling, G., Z. Di, X. Jiachao, G. Xin, F. Xiaoting and Z. Qing (2016). "Effects of ionic crosslinking on physical and mechanical properties of alginate mulching films." Carbohydrate polymers **136**: 259-265.
Lin, C.-C. and A. T. Metters (2006). "Hydrogels in controlled release formulations: network design and mathematical modeling." Advanced drug delivery reviews **58**(12): 1379-1408.
Liu, L., G. Zhao, W. Wu, Y. Rong, D. Jin, D. Wang, W. Lou and X. Qin (2016). "Low intratumoral regulatory T cells and high peritumoral CD8+ T cells relate to long-term survival in patients with pancreatic ductal adenocarcinoma after pancreatectomy." Cancer Immunology, Immunotherapy **65**(1): 73-82.
Liu, R., J. B. Wolinsky, J. Walpole, E. Southard, L. R. Chirieac, M. W. Grinstaff and Y. L. Colson (2010). "Prevention of Local Tumor Recurrence Following Surgery Using Low-Dose Chemotherapeutic Polymer Films." Annals of Surgical Oncology **17**(4): 1203-1213.

Locker, G. Y., S. Hamilton, J. Harris, J. M. Jessup, N. Kemeny, J. S. Macdonald, M. R. Somerfield, D. F. Hayes and R. C. J. J. o. c. o. Bast Jr (2006). "ASCO 2006 update of recommendations for the use of tumor markers in gastrointestinal cancer." **24**(33): 5313-5327.
Loh, J. W., G. Yeoh, M. Saunders and L.-Y. Lim (2010). "Uptake and cytotoxicity of chitosan nanoparticles in human liver cells." Toxicology and applied pharmacology **249**(2): 148-157.
Longati, P., X. Jia, J. Eimer, A. Wagman, M.-R. Witt, S. Rehnmark, C. Verbeke, R. Toftgård, M. Löhr and R. L. Heuchel (2013). "3D pancreatic carcinoma spheroids induce a matrix-rich, chemoresistant phenotype offering a better model for drug testing." BMC Cancer **13**: 95-95.
Lowenfels, A. B. and P. Maisonneuve (2006). "Epidemiology and risk factors for pancreatic cancer." Best Practice & Research Clinical Gastroenterology **20**(2): 197-209.
Lu, Y., J. Huang, G. Yu, R. Cardenas, S. Wei, E. K. Wujcik and Z. Guo (2016). "Coaxial electrospun fibers: applications in drug delivery and tissue engineering." Wiley Interdisciplinary Reviews: Nanomedicine and Nanobiotechnology.
Ma, Z. and L.-Y. Lim (2003). "Uptake of chitosan and associated insulin in Caco-2 cell monolayers: a comparison between chitosan molecules and chitosan nanoparticles." Pharmaceutical Research **20**(11): 1812-1819.
Mahoney, K. M., G. J. Freeman and D. F. McDermott (2015). "The Next Immune-Checkpoint Inhibitors: PD-1/PD-L1 Blockade in Melanoma." Clinical Therapeutics **37**(4): 764-782.
Makadia, H. K. and S. J. Siegel (2011). "Poly lactic-co-glycolic acid (PLGA) as biodegradable controlled drug delivery carrier." Polymers **3**(3): 1377-1397.
Malaise, S., L. Rami, A. Montembault, P. Alcouffe, B. Burdin, L. Bordenave, S. Delmond and L. David (2014). "Bioresorption mechanisms of chitosan physical hydrogels: A scanning electron microscopy study." Materials Science and Engineering: C **42**: 374-384.
Manoukian, O. S., M. R. Arul, N. Sardashti, T. Stedman, R. James, S. Rudraiah and S. G. Kumbar (2018). "Biodegradable Polymeric Injectable Implants for Long-Term Delivery of Contraceptive Drugs." Journal of applied polymer science **135**(14): 46068.
Mansoor, I., J. Lai, S. Ranamukhaarachchi, V. Schmitt, D. Lambert, J. Dutz, U. O. Häfeli and B. Stoeber (2015). "A microneedle-based method for the characterization of diffusion in skin tissue using doxorubicin as a model drug." Biomedical Microdevices **17**(3): 61.
Marabelle, A., R. Andtbacka, K. Harrington, I. Melero, R. Leidner, T. de Baere, C. Robert, P. A. Ascierto, J.-F. Baurain, M. Imperiale, S. Rahimian, D. Tersago, E. Klumper, M. Hendriks, R. Kumar, M. Stern, K. Öhrling, C. Massacesi, I. Tchakov, A. Tse, J.-Y. Douillard, J. Tabernero, J. Haanen and J. Brody (2018). "Starting the fight in the tumor: expert recommendations for the development of human intratumoral immunotherapy (HIT-IT)." Annals of Oncology **29**(11): 2163-2174.
Matsukawa, K., T. Masuda, A. M. Akimoto and R. Yoshida (2016). "A surface-grafted thermoresponsive hydrogel in which the surface structure dominates the bulk properties." Chemical Communications **52**(74): 11064-11067.
Matthes, K., M. Mino-Kenudson, D. V. Sahani, N. Holalkere, K. D. Fowers, R. Rathi and W. R. Brugge (2007). "EUS-guided injection of paclitaxel (OncoGel) provides therapeutic drug concentrations in the porcine pancreas (with video)." Gastrointestinal endoscopy **65**(3): 448-453.
Mazur, P. K., A. Herner, F. Neff and J. T. Siveke (2015). Current methods in mouse models of pancreatic cancer. Mouse Models of Cancer, Springer**:** 185-215.
McConville, C., P. Tawari and W. Wang (2015). "Hot melt extruded and injection moulded disulfiram-loaded PLGA millirods for the treatment of glioblastoma multiforme via stereotactic injection." International journal of pharmaceutics **494**(1): 73-82.
McGirt, M. J., K. D. Than, J. D. Weingart, K. L. Chaichana, F. J. Attenello, A. Olivi, J. Laterra, L. R. Kleinberg, S. A. Grossman, H. Brem and A. Quiñones-Hinojosa (2009). "Gliadel (BCNU) wafer plus concomitant temozolomide therapy after primary resection of glioblastoma multiforme." Journal of neurosurgery **110**(3): 583-588.

McLeod, E. J., A. D. Beischer, J. S. Hill and A. H. Kaye (1997). "Multicellular tumor spheroids grown from pancreatic carcinoma cell lines: use as an orthotopic xenograft in athymic nude mice." Pancreas **14**(3): 237-248.
Mehta, G., A. Y. Hsiao, M. Ingram, G. D. Luker and S. Takayama (2012). "Opportunities and challenges for use of tumor spheroids as models to test drug delivery and efficacy." Journal of controlled release **164**(2): 192-204.
Mellman, I., G. Coukos and G. Dranoff (2011). "Cancer immunotherapy comes of age." Nature **480**: 480.
Merck. (2019). "Cell Culture FAQs: Bacterial Endotoxin Contamination." from https://www.sigmaaldrich.com/technical-documents/articles/biology/what-is-endotoxin.html.
Mierzwa, M. L., M. K. Nyati, M. A. Morgan and T. S. Lawrence (2010). "Recent advances in combined modality therapy." The oncologist **15**(4): 372-381.
Minchinton, A. I. and I. F. Tannock (2006). "Drug penetration in solid tumours." Nature Reviews Cancer **6**(8): 583-592.
Mini, E., S. Nobili, B. Caciagli, I. Landini and T. Mazzei (2006). "Cellular pharmacology of gemcitabine." Annals of Oncology **17**(suppl_5): v7-v12.
Mirabedini, A., J. Foroughi, T. Romeo and G. G. Wallace (2015). "Development and characterization of novel hybrid hydrogel fibers." Macromolecular Materials and Engineering **300**(12): 1217-1225.
Mirabedini, A., J. Foroughi and G. G. Wallace (2016). "Developments in conducting polymer fibres: from established spinning methods toward advanced applications." RSC Advances **6**(50): 44687-44716.
Mondal, D., M. Griffith and S. S. Venkatraman (2016). "Polycaprolactone-based biomaterials for tissue engineering and drug delivery: Current scenario and challenges." International Journal of Polymeric Materials and Polymeric Biomaterials **65**(5): 255-265.
Moran, P. (2000). "Cellular effects of cancer chemotherapy administration." Journal of Infusion Nursing **23**(1): 44.
Mu, F., J. T. Lucas Jr, J. M. Watts, A. J. Johnson, J. Daniel Bourland, A. W. Laxton, M. D. Chan and S. B. Tatter (2015). "Tumor resection with carmustine wafer placement as salvage therapy after local failure of radiosurgery for brain metastasis." Journal of Clinical Neuroscience **22**(3): 561-565.
Munshi, A., M. Hobbs and R. E. Meyn (2005). Clonogenic cell survival assay. Chemosensitivity, Springer**:** 21-28.
Namekawa, T., K. Ikeda, K. Horie-Inoue and S. Inoue (2019). "Application of prostate cancer models for preclinical study: Advantages and limitations of cell lines, patient-derived xenografts, and three-dimensional culture of patient-derived cells." Cells **8**(1): 74.
Nasongkla, N. (2009). Biodegradable Polymeric Implants as Drug Delivery Systems for Brain Cancer Therapy. World Congress on Medical Physics and Biomedical Engineering, September 7-12, 2009, Munich, Germany, Springer.
Neesse, A., P. Michl, K. K. Frese, C. Feig, N. Cook, M. A. Jacobetz, M. P. Lolkema, M. Buchholz, K. P. Olive, T. M. Gress and D. A. Tuveson (2011). "Stromal biology and therapy in pancreatic cancer." Gut **60**(6): 861.
Newick, K., S. O'Brien, E. Moon and S. M. Albelda (2017). "CAR T Cell Therapy for Solid Tumors." Annual Review of Medicine **68**(1): 139-152.
Ng, I. W., Y. Y. Soon, D. Chen and J. C. S. Tey (2018). "Chemoradiotherapy versus chemotherapy for locally advanced unresectable pancreatic cancer: A systematic review and meta-analysis." **14**(6): 392-401.
Ng, S.-F. and N. Jumaat (2014). "Carboxymethyl cellulose wafers containing antimicrobials: A modern drug delivery system for wound infections." European Journal of Pharmaceutical Sciences **51**: 173-179.
Nunamaker, E. A., E. K. Purcell and D. R. Kipke (2007). "In vivo stability and biocompatibility of implanted calcium alginate disks." Journal of Biomedical Materials Research Part A: An Official Journal of The Society for Biomaterials, The Japanese Society for Biomaterials, and The Australian Society for Biomaterials and the Korean Society for Biomaterials **83**(4): 1128-1137.
Nunes, A. S., A. S. Barros, E. C. Costa, A. F. Moreira and I. J. Correia (2019). "3D tumor spheroids as in vitro models to mimic in vivo human solid tumors resistance to therapeutic drugs." Biotechnology and bioengineering **116**(1): 206-226.

Oberstein, P. E. and K. P. Olive (2013). "Pancreatic cancer: why is it so hard to treat?" Therapeutic advances in gastroenterology **6**(4): 321-337.
Okada, S., K. Vaeteewoottacharn and R. Kariya (2019). "Application of Highly Immunocompromised Mice for the Establishment of Patient-Derived Xenograft (PDX) Models." Cells **8**(8): 889.
Oshimura, M., A. Takasu and K. Nagata (2009). "Controlled Ring-Opening Polymerization of ϵ-Caprolactone Using Polymer-Supported Scandium Trifluoromethanesulfonate in Organic Solvent and Ionic Liquids." Macromolecules **42**(8): 3086-3091.
Ozipek, B. and H. Karakas (2014). 9 - Wet spinning of synthetic polymer fibers. Advances in Filament Yarn Spinning of Textiles and Polymers. D. Zhang, Woodhead Publishing**:** 174-186.
Pampaloni, F., E. G. Reynaud and E. H. Stelzer (2007). "The third dimension bridges the gap between cell culture and live tissue." Nature reviews Molecular cell biology **8**(10): 839.
Pan, S. T., Z. L. Li, Z. X. He, J. X. Qiu and S. F. Zhou (2016). "Molecular mechanisms for tumour resistance to chemotherapy." Clinical and Experimental Pharmacology and Physiology **43**(8): 723-737.
Pandol, S., M. Edderkaoui, I. Gukovsky, A. Lugea and A. Gukovskaya (2009). "Desmoplasia of Pancreatic Ductal Adenocarcinoma." Clinical gastroenterology and hepatology : the official clinical practice journal of the American Gastroenterological Association **7**(11 0): S44-S47.
Pardoll, D. M. (2012). "The blockade of immune checkpoints in cancer immunotherapy." Nature Reviews Cancer **12**: 252.
Parikh, A., J. Y.-L. Wo, D. P. Ryan, J. W. Clark, R. D. Nipp, L. S. Blaszkowsky, C. D. Weekes, E. V. Seventer, L. Ly, B. Foreman, R. B. Corcoran and T. S. Hong (2019). "A phase II study of ipilimumab and nivolumab with radiation in metastatic pancreatic adenocarcinoma." Journal of Clinical Oncology **37**(4_suppl): 391-391.
Park, H., R. B. Ambade, S. H. Noh, W. Eom, K. H. Koh, S. B. Ambade, W. J. Lee, S. H. Kim and T. H. Han (2019). "Porous Graphene-Carbon Nanotube Scaffolds for Fiber Supercapacitors." ACS applied materials & interfaces.
Park, K. (2016). "Drug Delivery Research: The Invention Cycle." Molecular pharmaceutics **13**(7): 2143-2147.
Park, S., S. Kang, X. Chen, E. J. Kim, J. Kim, N. Kim, J. Kim and M. M. Jin (2013). "Tumor suppression via paclitaxel-loaded drug carriers that target inflammation marker upregulated in tumor vasculature and macrophages." Biomaterials **34**(2): 598-605.
Passacantilli, I., V. Panzeri, F. Terracciano, G. Delle Fave, C. Sette and G. J. O. r. Capurso (2018). "Co-treatment with gemcitabine and nab-paclitaxel exerts additive effects on pancreatic cancer cell death." **39**(4): 1984-1990.
Patil, H., R. V. Tiwari and M. A. Repka (2016). "Hot-Melt Extrusion: from Theory to Application in Pharmaceutical Formulation." AAPS PharmSciTech **17**(1): 20-42.
Patnaik, A., S. P. Kang, D. Rasco, K. P. Papadopoulos, J. Elassaiss-Schaap, M. Beeram, R. Drengler, C. Chen, L. Smith and G. Espino (2015). "Phase I study of pembrolizumab (MK-3475; anti–PD-1 monoclonal antibody) in patients with advanced solid tumors." Clinical cancer research **21**(19): 4286-4293.
Pekkari, A. (2015). Controlled Drug-Release from Mesoporous Hydrogels. Master of Science, Chalmers University of Technology.
Pektok, E., B. Nottelet, J.-C. Tille, R. Gurny, A. Kalangos, M. Moeller and B. H. Walpoth (2008). "Degradation and Healing Characteristics of Small-Diameter Poly (ε-Caprolactone) Vascular Grafts in the Rat Systemic Arterial CirculationCLINICAL PERSPECTIVE." Circulation **118**(24): 2563-2570.
Peng, J. S., J. Wey, S. Chalikonda, D. S. Allende, R. M. Walsh and G. Morris-Stiff (2019). "Pathologic tumor response to neoadjuvant therapy in borderline resectable pancreatic cancer." Hepatobiliary & Pancreatic Diseases International.
Perez, E. A., E. H. Romond, V. J. Suman, J.-H. Jeong, G. Sledge, C. E. Geyer Jr, S. Martino, P. Rastogi, J. Gralow and S. M. Swain (2014). "Trastuzumab plus adjuvant chemotherapy for human epidermal growth factor receptor 2–positive breast cancer: planned joint analysis of overall survival from NSABP B-31 and NCCTG N9831." Journal of clinical oncology **32**(33): 3744.

Pitt, C. G., A. R. Jeffcoat, R. A. Zweidinger and A. Schindler (1979). "Sustained drug delivery systems. I. The permeability of poly (ϵ-caprolactone), poly (DL-lactic acid), and their copolymers." Journal of biomedical materials research **13**(3): 497-507.
Provenzano, Paolo P., C. Cuevas, Amy E. Chang, Vikas K. Goel, Daniel D. Von Hoff and Sunil R. Hingorani (2012). "Enzymatic Targeting of the Stroma Ablates Physical Barriers to Treatment of Pancreatic Ductal Adenocarcinoma." Cancer Cell **21**(3): 418-429.
Qi, L., Z. Xu, X. Jiang, Y. Li and M. Wang (2005). "Cytotoxic activities of chitosan nanoparticles and copper-loaded nanoparticles." Bioorganic & medicinal chemistry letters **15**(5): 1397-1399.
Qian, F., G. M. Saidel, D. M. Sutton, A. Exner and J. Gao (2002). "Combined modeling and experimental approach for the development of dual-release polymer millirods." Journal of controlled release **83**(3): 427-435.
Qiu, Y. and K. Park (2001). "Environment-sensitive hydrogels for drug delivery." Advanced Drug Delivery Reviews **53**(3): 321-339.
Quezada, S. A. and K. S. Peggs (2013). "Exploiting CTLA-4, PD-1 and PD-L1 to reactivate the host immune response against cancer." British Journal Of Cancer **108**: 1560.
Ranaldi, G., I. Marigliano, I. Vespignani, G. Perozzi and Y. Sambuy (2002). "The effect of chitosan and other polycations on tight junction permeability in the human intestinal Caco-2 cell line1 1Abbreviations: AP = apical; BL = basolateral; 2-DOG = 2-deoxyglucose; HBSS = Hanks balanced salt solution; FITC = fluorescein isothiocyanate; HEPES = N-2-hydroxyethyl piperazine-N-4-butanesulfonic acid; HMW = high molecular weight; LMW = low molecular weight; MES = morpholinoethane sulfonic acid; PBS+ = phosphate buffered saline; PEI = polyethylenimine; TEER = trans-epithelial electrical resistance; TRITC = tetramethylrodamine isothiocyanate." The Journal of Nutritional Biochemistry **13**(3): 157-167.
Rausch, M. P. and K. T. Hastings (2017). Immune checkpoint inhibitors in the treatment of melanoma: From basic science to clinical application. Cutaneous Melanoma: Etiology and Therapy [Internet], Codon Publications.
Ray, S., M. M. Bonafede and N. A. Mohile (2014). "Treatment Patterns, Survival, and Healthcare Costs of Patients with Malignant Gliomas in a Large US Commercially Insured Population." American Health & Drug Benefits **7**(3): 140-149 110p.
Reddy, A., E. V. Caler and N. W. Andrews (2001). "Plasma membrane repair is mediated by Ca2+-regulated exocytosis of lysosomes." Cell **106**(2): 157-169.
Rekha, M. and C. P. Sharma (2007). "Pullulan as a promising biomaterial for biomedical applications: a perspective." Trends Biomater Artif Organs **20**(2): 116-121.
Reneker, D. H., W. Kataphinan, A. Theron, E. Zussman and A. L. Yarin (2002). "Nanofiber garlands of polycaprolactone by electrospinning." Polymer **43**(25): 6785-6794.
Renner, A., M. Burotto and C. Rojas (2019). "Immune Checkpoint Inhibitor Dosing: Can We Go Lower Without Compromising Clinical Efficacy?" (5): 1-5.
Reynolds, C., D. Barrera, R. Jotte, A. I. Spira, C. Weissman, K. A. Boehm, S. Pritchard and L. Asmar (2009). "Phase II trial of nanoparticle albumin-bound paclitaxel, carboplatin, and bevacizumab in first-line patients with advanced nonsquamous non-small cell lung cancer." Journal of Thoracic Oncology **4**(12): 1537-1543.
Reynolds, R. B. and J. Folloder (2014). "Clinical management of pancreatic cancer." Journal of the advanced practitioner in oncology **5**(5): 356.
Richmond, A. and Y. Su (2008). "Mouse xenograft models vs GEM models for human cancer therapeutics." Disease Models & Mechanisms **1**(2-3): 78-82.
Riley, R. S., C. H. June, R. Langer and M. J. Mitchell (2019). "Delivery technologies for cancer immunotherapy." Nature Reviews Drug Discovery **18**(3): 175-196.
Rinoldi, C., M. Costantini, E. Kijeńska-Gawrońska, S. Testa, E. Fornetti, M. Heljak, M. Ćwiklińska, R. Buda, J. Baldi and S. Cannata (2019). "Tendon Tissue Engineering: Effects of Mechanical and Biochemical Stimulation on Stem Cell Alignment on Cell-Laden Hydrogel Yarns." Advanced Healthcare Materials: 1801218.
Rodriguez, A., S. R. Macewan, H. Meyerson, J. T. Kirk and J. M. Anderson (2009). "The foreign body reaction in T-cell-deficient mice." Journal of biomedical materials research. Part A **90**(1): 106-113.

Roland, L., M. Grau, J. Matena, M. Teske, M. Gieseke, A. Kampmann, M. Beyerbach, H. Murua Escobar, H. Haferkamp, N.-C. Gellrich and I. Nolte (2015). "Poly-ε-caprolactone Coated and Functionalized Porous Titanium and Magnesium Implants for Enhancing Angiogenesis in Critically Sized Bone Defects." International journal of molecular sciences **17**(1): 1.
Rosenberg, S. A. and M. E. Dudley (2009). "Adoptive cell therapy for the treatment of patients with metastatic melanoma." Current Opinion in Immunology **21**(2): 233-240.
Rowshanravan, B., N. Halliday and D. M. Sansom (2018). "CTLA-4: a moving target in immunotherapy." Blood **131**(1): 58-67.
Sachan, N. K., S. Pushkar, A. Jha and A. Bhattcharya (2009). "Sodium alginate: the wonder polymer for controlled drug delivery." Journal of pharmacy research **2**(8): 1191-1199.
Sadeghi, A., F. Dorkoosh, M. Avadi, M. Weinhold, A. Bayat, F. Delie, R. Gurny, B. Larijani, M. Rafiee-Tehrani and H. Junginger (2008). "Permeation enhancer effect of chitosan and chitosan derivatives: comparison of formulations as soluble polymers and nanoparticulate systems on insulin absorption in Caco-2 cells." European journal of pharmaceutics and biopharmaceutics **70**(1): 270-278.
Safran, H., T. P. King, H. Choy, P. J. Hesketh, B. Wolf, E. Altenhein, W. Sikov, A. Rosmarin, W. Akerley and K. Radie-Keane (1997). "Paclitaxel and concurrent radiation for locally advanced pancreatic and gastric cancer: a phase I study." Journal of clinical oncology **15**(3): 901-907.
Safran, H., T. Moore, D. Iannitti, T. Dipetrillo, P. Akerman, W. Cioffi, D. Harrington, D. Quirk, R. Rathore, D. Cruff, J. Vakharia, S. Vora, D. Savarese and H. Wanebo (2001). "Paclitaxel and concurrent radiation for locally advanced pancreatic cancer." International Journal of Radiation Oncology*Biology*Physics **49**(5): 1275-1279.
Saikia, C., P. Gogoi and T. Maji (2015). "Chitosan: A promising biopolymer in drug delivery applications." J. Mol. Genet. Med. S **4**: 006.
Salmon, H., K. Franciszkiewicz, D. Damotte, M.-C. Dieu-Nosjean, P. Validire, A. Trautmann, F. Mami-Chouaib and E. Donnadieu (2012). "Matrix architecture defines the preferential localization and migration of T cells into the stroma of human lung tumors." The Journal of Clinical Investigation **122**(3): 899-910.
Saluja, A. K. and V. Dudeja (2013). "Relevance of animal models of pancreatic cancer and pancreatitis to human disease." Gastroenterology **144**(6): 1194-1198.
Saraf, A., G. Lozier, A. Haesslein, F. K. Kasper, R. M. Raphael, L. S. Baggett and A. G. Mikos (2009). "Fabrication of nonwoven coaxial fiber meshes by electrospinning." Tissue Engineering Part C: Methods **15**(3): 333-344.
Sato-Dahlman, M., K. Wirth and M. Yamamoto (2018). "Role of Gene Therapy in Pancreatic Cancer-A Review." Cancers **10**(4): 103.
Schweizer, D., I. Vostiar, A. Heier, T. Serno, K. Schoenhammer, M. Jahn, S. Jones, A. Piequet, C. Beerli, H. Gram and A. Goepferich (2013). "Pharmacokinetics, biocompatibility and bioavailability of a controlled release monoclonal antibody formulation." Journal of Controlled Release **172**(3): 975-982.
Shabason, J., J. Chen, S. Apisarnthanarax, N. Damjanov, B. Giantonio, A. Loaiza-Bonilla, P. O'Dwyer, M. O'Hara, K. Reiss, U. Teitelbaum, P. Wissel, J. Drebin, C. Vollmer, M. Kochman, R. Mick, N. Vergara, N. Jhala, A. Doucette, J. Lukens, J. Plastaras, J. Metz and E. Ben-Josef (2018). "A phase I dose escalation trial of nab-paclitaxel and fixed dose radiation in patients with unresectable or borderline resectable pancreatic cancer." Cancer Chemotherapy Pharmacology. **81**(3): 609-614.
Shaikh, R., T. R. Raj Singh, M. J. Garland, A. D. Woolfson and R. F. Donnelly (2011). "Mucoadhesive drug delivery systems." Journal of pharmacy & bioallied sciences **3**(1): 89-100.
Shchipunov, Y. A. and I. V. Postnova (2011). "Formation of calcium alginate-based macroporous materials comprising chitosan and hydroxyapatite." Colloid Journal **73**(4): 565.
Sheikh, Z., P. J. Brooks, O. Barzilay, N. Fine and M. Glogauer (2015). "Macrophages, Foreign Body Giant Cells and Their Response to Implantable Biomaterials." Materials (Basel, Switzerland) **8**(9): 5671-5701.
Shekunov, B. Y., P. Chattopadhyay, H. H. Tong, A. H. Chow and J. G. Grossmann (2007). "Structure and drug release in a crosslinked poly (ethylene oxide) hydrogel." Journal of pharmaceutical sciences **96**(5): 1320-1330.
Shen, F., S. Chu, A. K. Bence, B. Bailey, X. Xue, P. A. Erickson, M. H. Montrose, W. T. Beck and L. C. Erickson (2008). "Quantitation of Doxorubicin Uptake, Efflux, and Modulation of Multidrug Resistance

(MDR) in MDR Human Cancer Cells." Journal of Pharmacology and Experimental Therapeutics **324**(1): 95-102.
Shen, J. and D. J. Burgess (2012). "Accelerated in-vitro release testing methods for extended-release parenteral dosage forms." Journal of Pharmacy and Pharmacology **64**(7): 986-996.
Shepard, H. M. (2015). "Breaching the Castle Walls: Hyaluronan Depletion as a Therapeutic Approach to Cancer Therapy." Frontiers in oncology **5**: 192.
Siepmann, J. and N. A. Peppas (2001). "Modeling of drug release from delivery systems based on hydroxypropyl methylcellulose (HPMC)." Advanced Drug Delivery Reviews **48**(2–3): 139-157.
Siepmann, J. and F. Siepmann (2008). "Mathematical modeling of drug delivery." International Journal of Pharmaceutics **364**(2): 328-343.
Sill, T. J. and H. A. von Recum (2008). "Electrospinning: applications in drug delivery and tissue engineering." Biomaterials **29**(13): 1989-2006.
Singh, S., S.-j. Tang, J. Sreenarasimhaiah, L. F. Lara and A. Siddiqui (2011). "The clinical utility and limitations of serum carbohydrate antigen (CA19-9) as a diagnostic tool for pancreatic cancer and cholangiocarcinoma." Digestive diseases and sciences **56**(8): 2491-2496.
Smidsrød, O. and G. Skja (1990). "Alginate as immobilization matrix for cells." Trends in biotechnology **8**: 71-78.
Smith, T. T., H. F. Moffett, S. B. Stephan, C. F. Opel, A. G. Dumigan, X. Jiang, V. G. Pillarisetty, S. P. S. Pillai, K. D. Wittrup and M. T. Stephan (2017). "Biopolymers codelivering engineered T cells and STING agonists can eliminate heterogeneous tumors." The Journal of Clinical Investigation **127**(6): 2176-2191.
Swain, S. M., J. Baselga, S.-B. Kim, J. Ro, V. Semiglazov, M. Campone, E. Ciruelos, J.-M. Ferrero, A. Schneeweiss and S. J. N. E. J. o. M. Heeson (2015). "Pertuzumab, trastuzumab, and docetaxel in HER2-positive metastatic breast cancer." **372**(8): 724-734.
Swords, D. S., M. A. Firpo, C. L. Scaife and S. J. Mulvihill (2016). "Biomarkers in pancreatic adenocarcinoma: current perspectives." OncoTargets and therapy **9**: 7459-7467.
Takahashi, H., H. Akita, T. Ioka, H. Wada, A. Tomokoni, K. Asukai, M. Ohue, M. Yano and O. Ishikawa (2018). "Phase I trial evaluating the safety of preoperative gemcitabine/nab-paclitaxel with concurrent radiation therapy for borderline resectable pancreatic cancer." Pancreas **47**(9): 1135-1141.
Talebian, S., J. Foroughi, S. J. Wade, K. L. Vine, A. Dolatshahi-Pirouz, M. Mehrali, J. Conde and G. G. Wallace (2018). "Biopolymers for Antitumor Implantable Drug Delivery Systems: Recent Advances and Future Outlook." Advanced Materials: 1706665.
Tariman, J. D. (2017). "Changes in cancer treatment: Mabs, mibs, mids, nabs, and nibs." Nursing Clinics **52**(1): 65-81.
Tempero, M., W. Plunkett, V. R. v. Haperen, J. Hainsworth, H. Hochster, R. Lenzi and J. Abbruzzese (2003). "Randomized Phase II Comparison of Dose-Intense Gemcitabine: Thirty-Minute Infusion and Fixed Dose Rate Infusion in Patients With Pancreatic Adenocarcinoma." **21**(18): 3402-3408.
Thanou, M., J. Verhoef and H. Junginger (2001). "Chitosan and its derivatives as intestinal absorption enhancers." Advanced drug delivery reviews **50**: S91-S101.
Therapeutic Goods Administration (2017) "Clinical Evidence Guidelines ".
Three Rs Microsite. (2019). "Humane Endpoints." from https://3rs.ccac.ca/en/care-and-techniques/pain-management/ct-humane-endpoints.html.
Tønnesen, H. H. and J. Karlsen (2002). "Alginate in drug delivery systems." Drug development and industrial pharmacy **28**(6): 621-630.
Torphy, R. J., Y. Zhu and R. D. Schulick (2018). "Immunotherapy for pancreatic cancer: Barriers and breakthroughs." Annals of Gastroenterological Surgery.
Torres, A. J., C. Zhu, M. L. Shuler and S. Pannullo (2011). "Paclitaxel delivery to brain tumors from hydrogels: A computational study." Biotechnology Progress **27**(5): 1478-1487.
Tsai, S., L. McOlash, K. Palen, B. Johnson, C. Duris, Q. Yang, M. B. Dwinell, B. Hunt, D. B. Evans, J. Gershan and M. A. James (2018). "Development of primary human pancreatic cancer organoids, matched stromal and immune cells and 3D tumor microenvironment models." BMC Cancer **18**(1): 335.

Twyman-Saint Victor, C., A. J. Rech, A. Maity, R. Rengan, K. E. Pauken, E. Stelekati, J. L. Benci, B. Xu, H. Dada and P. M. J. N. Odorizzi (2015). "Radiation and dual checkpoint blockade activate non-redundant immune mechanisms in cancer." **520**(7547): 373-377.
Valtonen, S., U. Timonen, P. Toivanen, H. Kalimo, L. Kivipelto, O. Heiskanen, G. Unsgaard and T. Kuurne (1997). "Interstitial chemotherapy with carmustine-loaded polymers for high-grade gliomas: a randomized double-blind study." Neurosurgery **41**(1): 44-49.
Van Hove, A. H., M.-J. G. Beltejar and D. S. Benoit (2014). "Development and in vitro assessment of enzymatically-responsive poly (ethylene glycol) hydrogels for the delivery of therapeutic peptides." Biomaterials **35**(36): 9719-9730.
Varricchi, G., M. R. Galdiero, G. Marone, G. Criscuolo, M. Triassi, D. Bonaduce, G. Marone and C. G. Tocchetti (2017). "Cardiotoxicity of immune checkpoint inhibitors." ESMO open **2**(4): e000247.
Ventola, C. L. (2014). "Medical Applications for 3D Printing: Current and Projected Uses." P & T : a peer-reviewed journal for formulary management **39**(10): 704-711.
Ventura, C. A., C. Cannavà, R. Stancanelli, D. Paolino, D. Cosco, A. La Mantia, R. Pignatello and S. Tommasini (2011). "Gemcitabine-loaded chitosan microspheres. Characterization and biological in vitro evaluation." Biomedical microdevices **13**(5): 799-807.
Vincent, A., J. Herman, R. Schulick, R. H. Hruban and M. Goggins (2011). "Pancreatic cancer." The Lancet **378**(9791): 607-620.
Vincente, E., Y. Quijano and B. Ielpo (2014). "Arterial resection for pancreatic cancer: a modern surgeon should change its behavior according to the new therapeutic options." Il Giornale di chirurgia **35**(1-2): 5-14.
Vinci, M., S. Gowan, F. Boxall, L. Patterson, M. Zimmermann, C. Lomas, M. Mendiola, D. Hardisson and S. A. Eccles (2012). "Advances in establishment and analysis of three-dimensional tumor spheroid-based functional assays for target validation and drug evaluation." BMC biology **10**(1): 1.
Vine, K. L., S. Lobov, V. I. Chandran, N. L. E. Harris and M. Ranson (2015). "Improved pharmacokinetic and biodistribution properties of the selective urokinase inhibitor PAI-2 (SerpinB2) by site-specific PEGylation: implications for drug delivery." Pharmaceutical research **32**(3): 1045-1054.
Visonneau, S., A. Cesano, M. H. Torosian, E. J. Miller and D. Santoli (1998). "Growth characteristics and metastatic properties of human breast cancer xenografts in immunodeficient mice." The American journal of pathology **152**(5): 1299-1311.
Vogelstein, B., N. Papadopoulos, V. E. Velculescu, S. Zhou, L. A. Diaz and K. W. Kinzler (2013). "Cancer genome landscapes." science **339**(6127): 1546-1558.
Von Hoff, D. D., T. Ervin, F. P. Arena, E. G. Chiorean, J. Infante, M. Moore, T. Seay, S. A. Tjulandin, W. W. Ma and M. N. Saleh (2013). "Increased survival in pancreatic cancer with nab-paclitaxel plus gemcitabine." New England Journal of Medicine **369**(18): 1691-1703.
Vonlaufen, A., S. Joshi, C. Qu, P. A. Phillips, Z. Xu, N. R. Parker, C. S. Toi, R. C. Pirola, J. S. Wilson and D. Goldstein (2008). "Pancreatic stellate cells: partners in crime with pancreatic cancer cells." Cancer research **68**(7): 2085-2093.
Wainberg, Z. A., H. S. Hochster, E. J.-H. Kim, B. George, A. Kalyan, E. G. Chiorean, D. M. Waterhouse, M. Gutierrez, A. R. Parikh and R. Jain (2019). Phase I study of nivolumab (Nivo)+ nab-paclitaxel (nab-P)+ gemcitabine (Gem) in advanced pancreatic cancer (APC), American Society of Clinical Oncology.
Walle, T., R. Martinez Monge, A. Cerwenka, D. Ajona, I. Melero and F. Lecanda (2018). "Radiation effects on antitumor immune responses: current perspectives and challenges." Therapeutic advances in medical oncology **10**: 1758834017742575-1758834017742575.
Walter, K. A., M. A. Cahan, A. Gur, B. Tyler, J. Hilton, O. M. Colvin, P. C. Burger, A. Domb and H. Brem (1994). "Interstitial taxol delivered from a biodegradable polymer implant against experimental malignant glioma." Cancer research **54**(8): 2207-2212.
Wanawananon, K., S. E. Moulton, G. G. Wallace and S. Liawruangrath (2016). "Fabrication of novel core–shell PLGA and alginate fiber for dual-drug delivery system." Polymers for Advanced Technologies.

Wanderley, C. W., D. F. Colón, J. P. M. Luiz, F. F. Oliveira, P. R. Viacava, C. A. Leite, J. A. Pereira, C. M. Silva, C. R. Silva and R. L. Silva (2018). "Paclitaxel reduces tumor growth by reprogramming tumor-associated macrophages to an M1 profile in a TLR4-dependent manner." Cancer research **78**(20): 5891-5900.
Wang, C., J. Wang, X. Zhang, S. Yu, D. Wen, Q. Hu, Y. Ye, H. Bomba, X. Hu and Z. Liu (2018). "In situ formed reactive oxygen species–responsive scaffold with gemcitabine and checkpoint inhibitor for combination therapy." Science translational medicine **10**(429): eaan3682.
Wang, C. X., C. Cowen, Z. Zhang and C. R. Thomas (2005). "High-speed compression of single alginate microspheres." Chemical Engineering Science **60**(23): 6649-6657.
Wang, N. X. and H. A. von Recum (2011). "Affinity-based drug delivery." Macromolecular bioscience **11**(3): 321-332.
Wang, Y., W. Deng, N. Li, S. Neri, A. Sharma, W. Jiang and S. H. Lin (2018). "Combining Immunotherapy and Radiotherapy for Cancer Treatment: Current Challenges and Future Directions." Frontiers in pharmacology **9**: 185-185.
Wang, Y., Q. Wen and S. Choi (2016). "FDA's regulatory science program for generic PLA/PLGA-based drug products." Am Pharm Rev **19**(4): 5-9.
Ware, M. J., V. Keshishian, J. J. Law, J. C. Ho, C. A. Favela, P. Rees, B. Smith, S. Mohammad, R. F. Hwang, K. Rajapakshe, C. Coarfa, S. Huang, D. P. Edwards, S. J. Corr, B. Godin and S. A. Curley (2016). "Generation of an in vitro 3D PDAC stroma rich spheroid model." Biomaterials **108**: 129-142.
Waugh, J. and A. J. Wagstaff (2004). "The Paclitaxel (TAXUS™)-Eluting Stent." American Journal of Cardiovascular Drugs **4**(4): 257-268.
Wedmore, I., J. G. McManus, A. E. Pusateri and J. B. Holcomb (2006). "A special report on the chitosan-based hemostatic dressing: experience in current combat operations." Journal of Trauma and Acute Care Surgery **60**(3): 655-658.
Weinberg, B. D., E. Blanco, S. F. Lempka, J. M. Anderson, A. A. Exner and J. Gao (2007). "Combined radiofrequency ablation and doxorubicin-eluting polymer implants for liver cancer treatment." Journal of biomedical materials research. Part A **81**(1): 205-213.
Weniger, M., K. C. Honselmann and A. S. Liss (2018). "The Extracellular Matrix and Pancreatic Cancer: A Complex Relationship." Cancers **10**(9): 316.
West, J. L. and J. A. Hubbell (1995). "Photopolymerized hydrogel materials for drug delivery applications." Reactive Polymers **25**(2): 139-147.
Westphal, M., D. C. Hilt, E. Bortey, P. Delavault, R. Olivares, P. C. Warnke, I. R. Whittle, J. Jääskeläinen and Z. Ram (2003). "A phase 3 trial of local chemotherapy with biodegradable carmustine (BCNU) wafers (Gliadel wafers) in patients with primary malignant glioma." Neuro-oncology **5**(2): 79-88.
Wilhelm, S., A. J. Tavares, Q. Dai, S. Ohta, J. Audet, H. F. Dvorak and W. C. Chan (2016). "Analysis of nanoparticle delivery to tumours." Nature reviews materials **1**(5): 16014.
Wu, C.-C., Y.-F. Tsai, L.-H. Hsu, J.-P. Chen, S. Sumi and K.-C. Yang (2016). "A self-reinforcing biodegradable implant made of poly (ε-caprolactone)/calcium phosphate ceramic composite for craniomaxillofacial fracture fixation." Journal of Cranio-Maxillofacial Surgery **44**(9): 1333-1341.
Xia, G., H. Zhang, R. Cheng, H. Wang, Z. Song, L. Deng, X. Huang, H. A. Santos and W. Cui (2018). "Localized Controlled Delivery of Gemcitabine via Microsol Electrospun Fibers to Prevent Pancreatic Cancer Recurrence." Advanced healthcare materials **7**(18): 1800593.
Xu, S., A. Tabaković, X. Liu and E. Schlangen (2018). "Calcium alginate capsules encapsulating rejuvenator as healing system for asphalt mastic." Construction and Building Materials **169**: 379-387.
Yada, E., S. Wada, S. Yoshida and T. Sasada (2017). Use of patient-derived xenograft mouse models in cancer research and treatment, Future Science.
Yan, E., Y. Fan, Z. Sun, J. Gao, X. Hao, S. Pei, C. Wang, L. Sun and D. Zhang (2014). "Biocompatible core–shell electrospun nanofibers as potential application for chemotherapy against ovary cancer." Materials Science and Engineering: C **41**: 217-223.
Yang, C.-P. H. and S. B. Horwitz (2017). "Taxol(®): The First Microtubule Stabilizing Agent." International journal of molecular sciences **18**(8): 1733.

Yang, C.-Y., C.-S. Wong, J.-Y. Chang and S.-T. Ho (1996). "Intrathecal ketamine reduces morphine requirements in patients with terminal cancer pain." Canadian Journal of Anaesthesia **43**(4): 379-383.
Yeadon, J. (2013). "Immunodeficient Mice for Cancer Studies: Which Host Strain Should I Use?", from https://www.jax.org/news-and-insights/jax-blog/2013/july/which-host-strain-should-i-use.
Yi, H.-G., Y.-J. Choi, K. S. Kang, J. M. Hong, R. G. Pati, M. N. Park, I. K. Shim, C. M. Lee, S. C. Kim and D.-W. Cho (2016). "A 3D-printed local drug delivery patch for pancreatic cancer growth suppression." Journal of Controlled Release **238**: 231-241.
Yilgor, P., K. Tuzlakoglu, R. L. Reis, N. Hasirci and V. Hasirci (2009). "Incorporation of a sequential BMP-2/BMP-7 delivery system into chitosan-based scaffolds for bone tissue engineering." Biomaterials **30**(21): 3551-3559.
Yip, D. and C. H. Cho (2013). "A multicellular 3D heterospheroid model of liver tumor and stromal cells in collagen gel for anti-cancer drug testing." Biochemical and Biophysical Research Communications **433**(3): 327-332.
Zayed, A. A., S. J. Mandrekar and P. Haluska (2015). "Molecular and clinical implementations of ovarian cancer mouse avatar models." Chinese clinical oncology **4**(3): 30-30.
Zentner, G. M., R. Rathi, C. Shih, J. C. McRea, M.-H. Seo, H. Oh, B. G. Rhee, J. Mestecky, Z. Moldoveanu, M. Morgan and S. Weitman (2001). "Biodegradable block copolymers for delivery of proteins and water-insoluble drugs." Journal of Controlled Release **72**(1–3): 203-215.
Zhan, Q., B. Shen, X. Deng, H. Chen, J. Jin, X. Zhang, C. Peng and H. Li (2013). "Drug-eluting scaffold to deliver chemotherapeutic medication for management of pancreatic cancer after surgery." Int J Nanomedicine **8**: 2465-2472.
Zhang, C. (2007). "Reversible gelation and glass transition: Towards a microscopic model of reversible polymer gel." J Phys Chem US **3**: 55-63.
Zhang, J., S. Seyedin, S. Qin, Z. Wang, S. Moradi, F. Yang, P. A. Lynch, W. Yang, J. Liu and X. Wang (2019). "Highly Conductive Ti3C2Tx MXene Hybrid Fibers for Flexible and Elastic Fiber-Shaped Supercapacitors." Small: 1804732.
Zhang, K., S. L. Loong, S. Connor, W. Sidney, S.-Y. Tan, R. T. Ng, K. M. Lee, L. Canham and P. K. Chow (2005). "Complete tumor response following intratumoral 32P BioSilicon on human hepatocellular and pancreatic carcinoma xenografts in nude mice." Clinical cancer research **11**(20): 7532-7537.
Zhang, L., S. Sanagapalli and A. Stoita (2018). "Challenges in diagnosis of pancreatic cancer." World journal of gastroenterology **24**(19): 2047-2060.
Zhu, Y., C. Hu, B. Li, H. Yang, Y. Cheng and W. Cui (2013). "A highly flexible paclitaxel-loaded poly(ε-caprolactone) electrospun fibrous-membrane-covered stent for benign cardia stricture." Acta Biomaterialia **9**(9): 8328-8336.
Zolnik, B. S. and D. J. Burgess (2008). "Evaluation of in vivo–in vitro release of dexamethasone from PLGA microspheres." Journal of controlled release **127**(2): 137-145.

Appendices

APPENDIX A: SINGLE FIBRE CHARACTERISATION

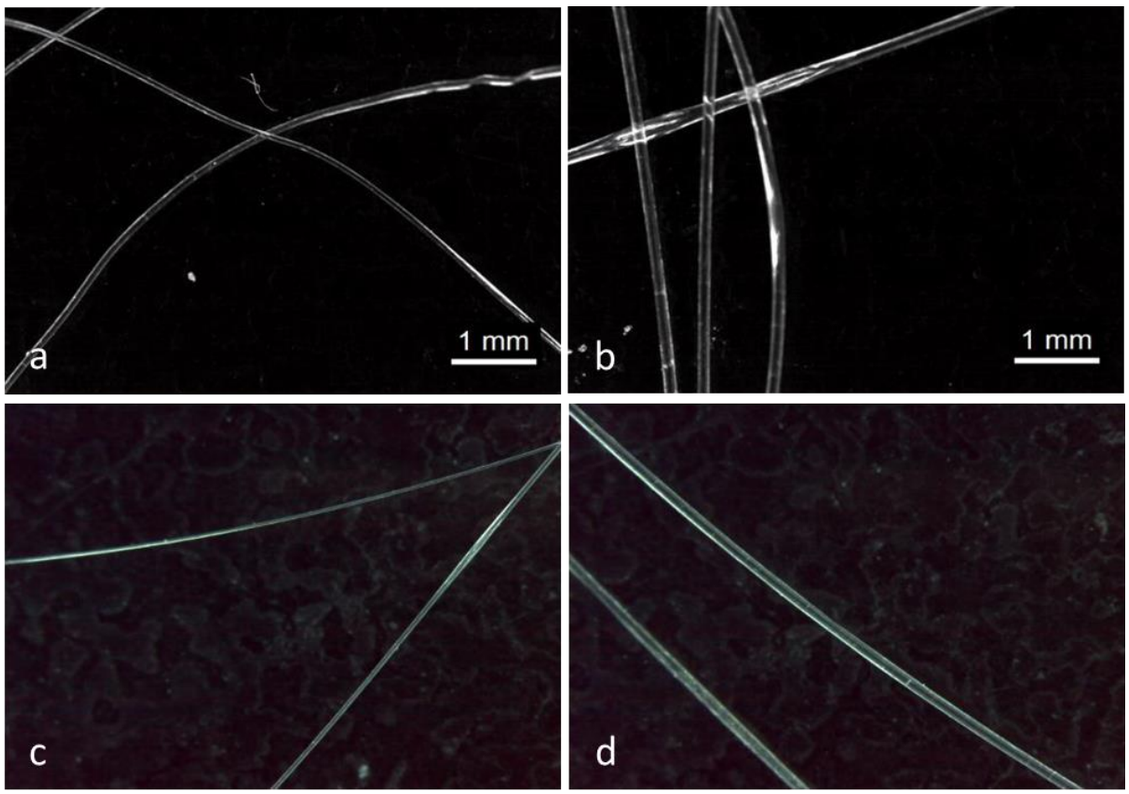

Figure A1: Optical light microscopy images of fibre formulations. Optical images at 20 × magnification of (a) 2 % alginate fiber containing no drug, (b) 3 % chitosan fiber containing no drug, (c) 2 % alginate fiber prepared with 2 mM gemcitabine and (d) 3 % chitosan fiber prepared with 2 mM gemcitabine. All optical images showed the fibers to be smooth and transparent

Table A1: Young's modulus values (GPa) for the complete range of empty and gemcitabine-loaded fibres.

	Young's Modulus (GPa)			
Conc. gemcitabine (mM) in spinning solution	**1 % alginate**	**2 % alginate**	**2 % chitosan**	**3 % chitosan**
0	0.6 ±0.1	1.5 ±0.2	1.9 ±0.2	2.0 ±0.3
0.2	0.8 ±0.3	2.0 ±0.3	1.3 ±0.3	1.9 ±0.4
2	0.8 ±0.4	3.5 ±0.1	2.2 ±0.2	2.1 ±0.2

APPENDIX B: SPHEROID FLUORESCENCE

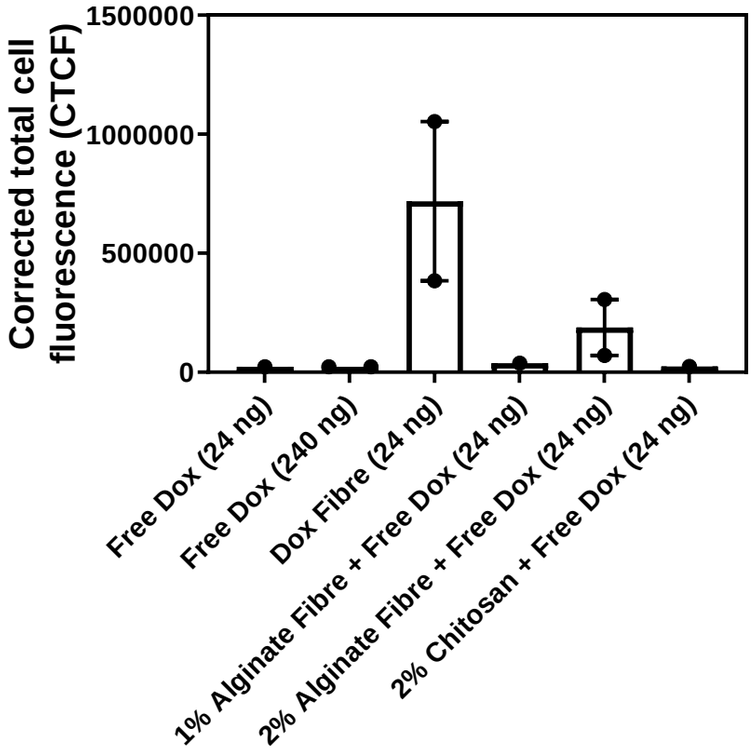

Figure A2: Total cell fluorescence was increased in spheroids treated with a doxorubicin eluting fibre Corrected total spheroid fluorescence was calculated using Image J software after treating MCF-7 spheroids for 4 h. Dox = doxorubicin.

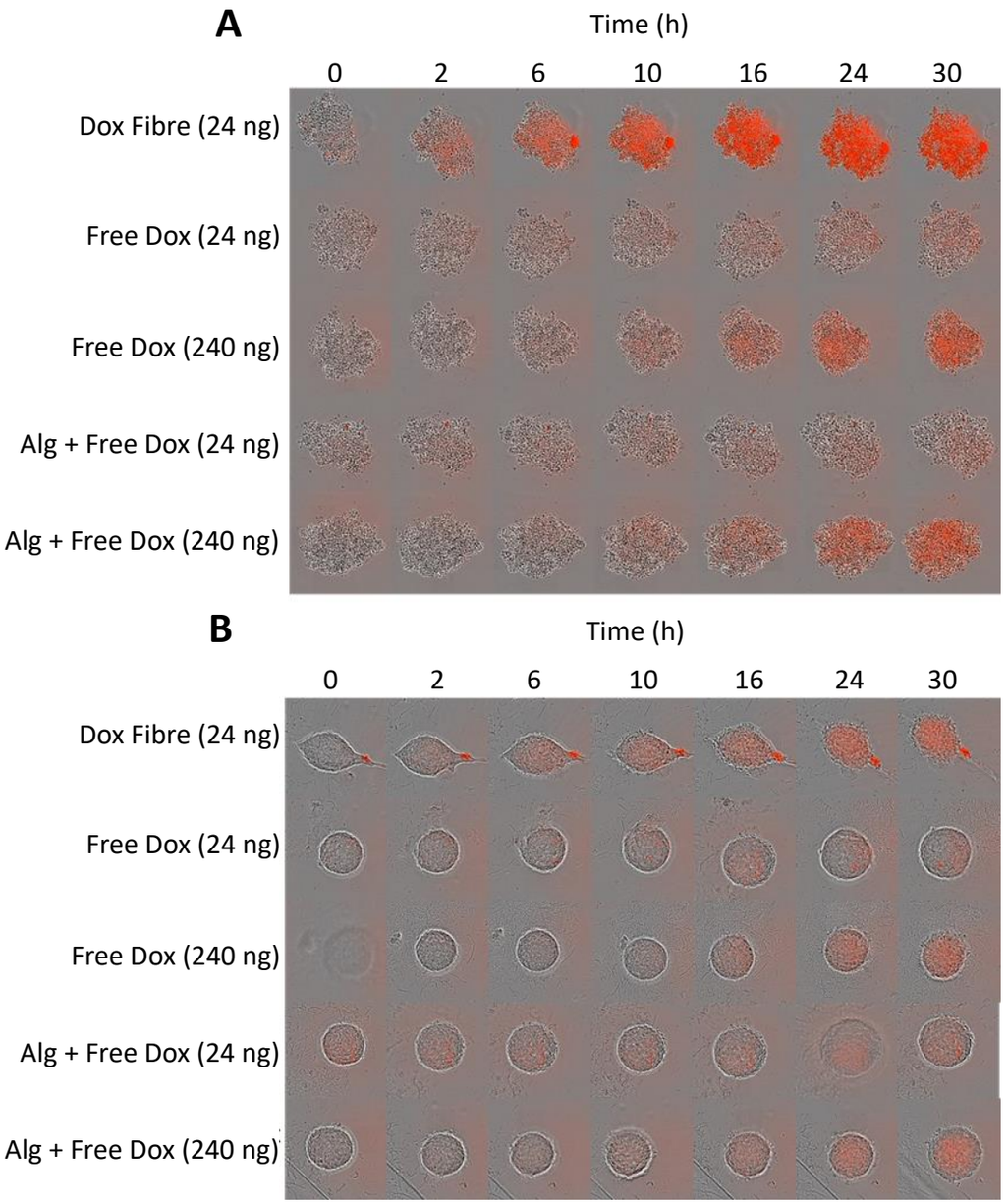

Figure A3: Effect of uncrosslinked polymer on drug uptake. A) PANC-1 tumour spheroids or B) MCF-7 tumour spheroids were treated with doxorubicin (24 ng) ± uncrosslinked 1 % alginate (15 % v/v) and imaged over 30 h. 2 cm doxorubicin fibre (1 × equivalent) contains 24 ng of doxorubicin. Dox=doxorubicin. Alg = alginate

APPENDIX C: COAXIAL FIBRE CHARACTERISATION

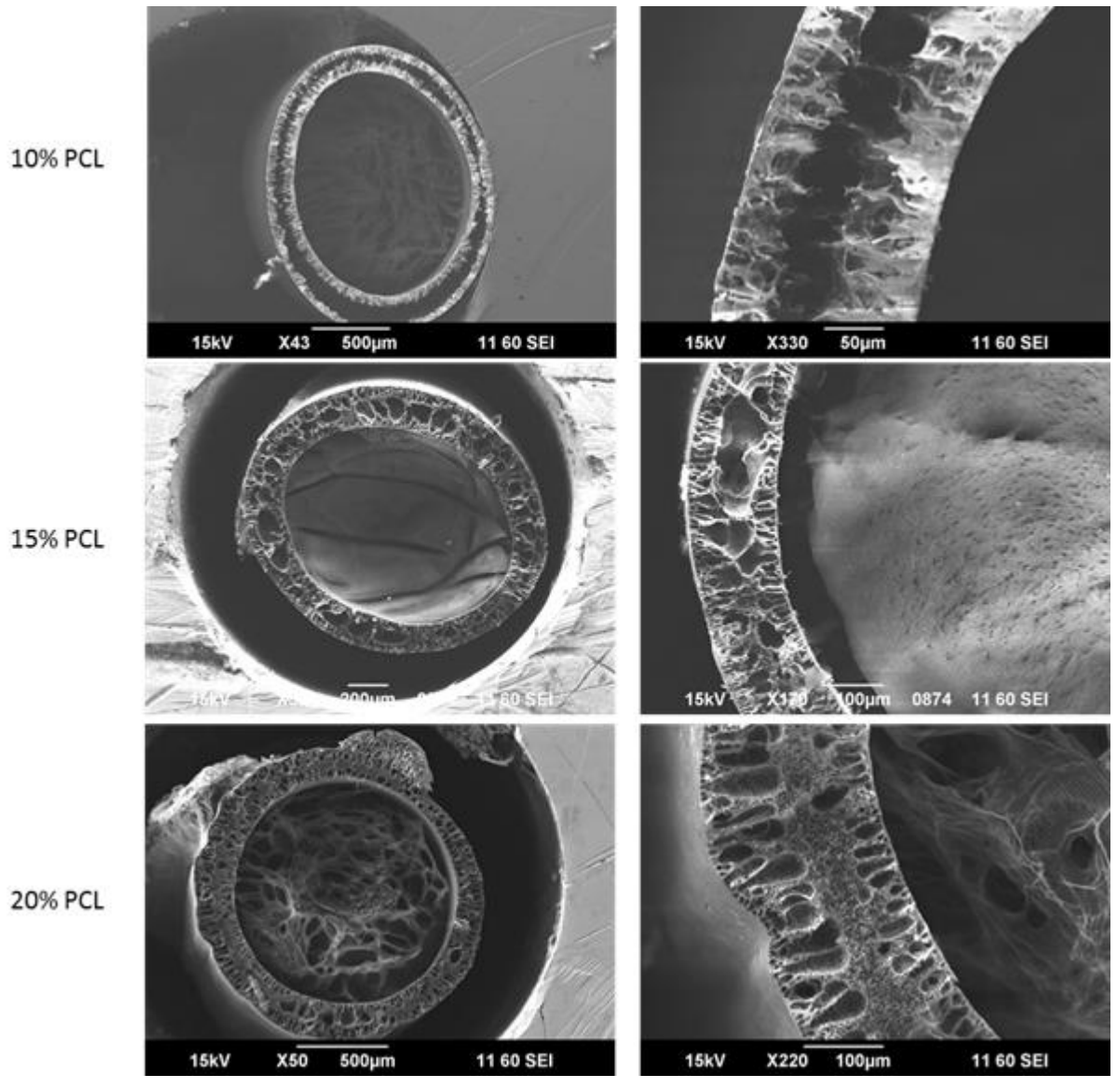

Figure A4: Internal cross sectional structures of coaxial fibres consisting of (A,B) 10 % PCL shell, (C,D) 15 % PCL shell, or (E,F) 20 % PCL shell.

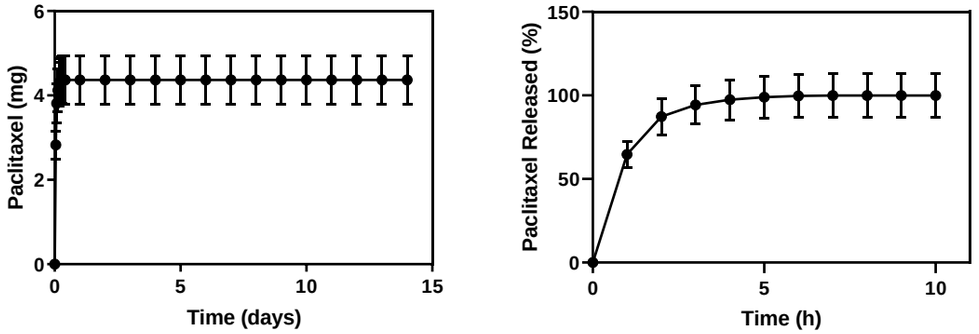

Figure A5: Paclitaxel release in ethanol. Cumulative release of paclitaxel release performed in absolute ethanol over (A) 14 days shows a release of 4.35 mg, with (B) 100 % being released in the first 7 h. Values are the mean (±SEM) of quadruplicates.

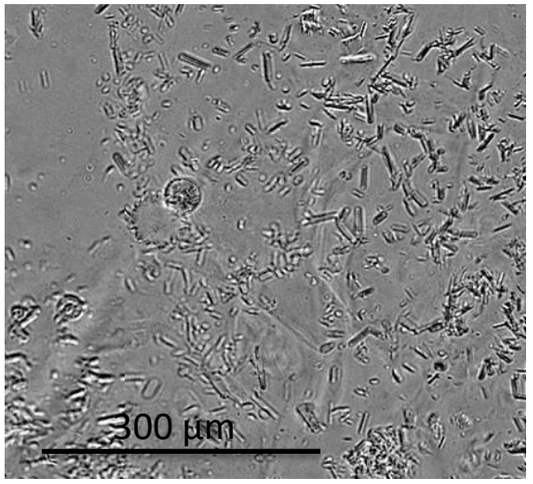

Figure A6: Paclitaxel crystals released from dual loaded fibre present in cell media. Images acquired at 10 × magnification

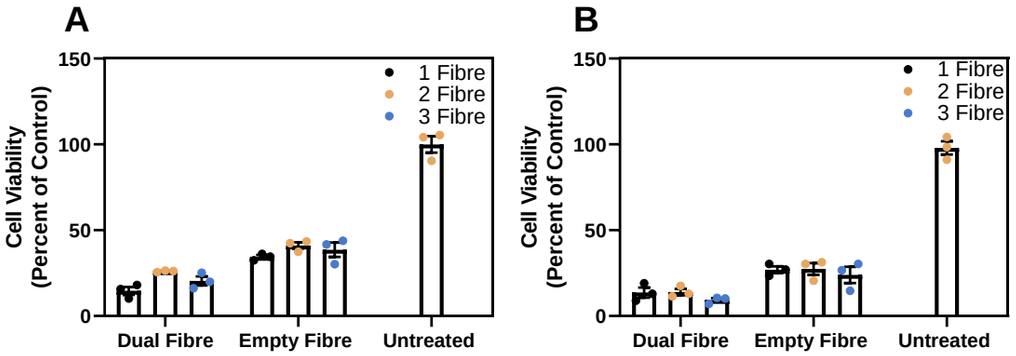

Figure A7: BxPC3luc and PANC-1 cells are more sensitive to both empty and drug loaded fibres. A dose response experiment was performed where 1, 2 and 3 pieces of empty or dual-drug loaded fibre (0.5 cm) were pre-incubated in media for 72 h before addition to a monolayer of A) BxPC3luc cells and B) PANC-1 cells and incubated for 72 h before and MTS assay was performed. Results are displayed as a percentage of an untreated control. Values are the mean (±SEM) of triplicates. Experiment performed in triplicate, one representative result shown.

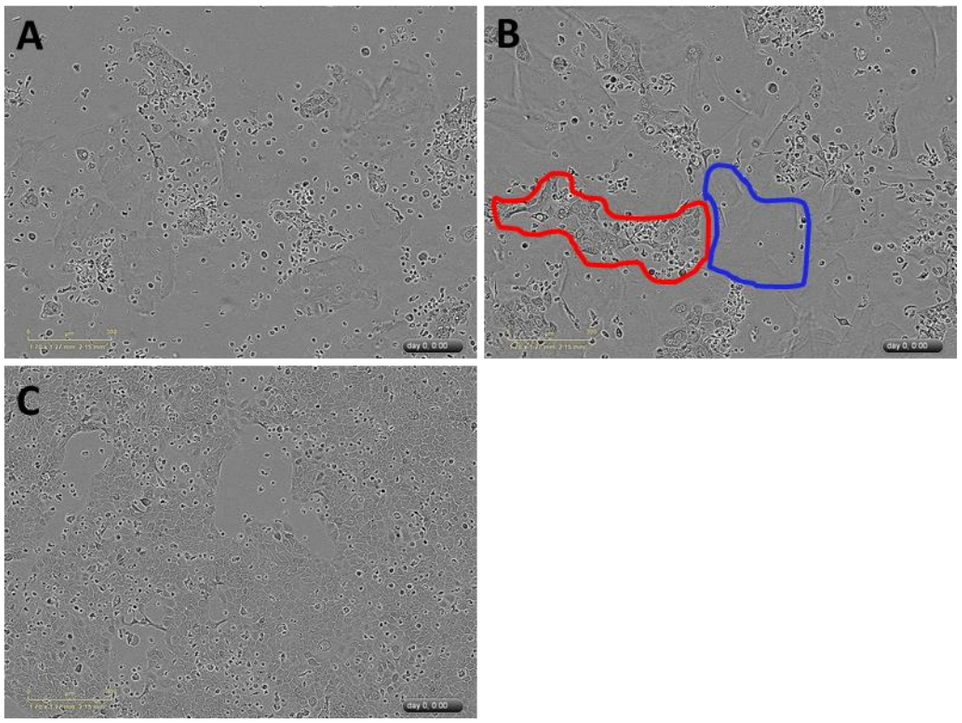

Figure A8: The presence of alginate interferes with cell growth. Images of BxPC3luc cells treated with A) dual-drug loaded fibre, B) empty fibre, or C) untreated were imaged. Red outline indicates areas of cell growth, while blue outline indicates presence of alginate. Images were taken using incuCyte ZOOM at 10 × magnification.

Figure A9: Cells pre-treated with the a gemcitabine loaded fibre and exposed to 2 Gy radiation had 100 % cell kill. Mia-PaCa-2 cells were pre-treated with 1 µM gemcitabine eluted from a gemcitabine loaded coaxial fibre and then irradiated with 2 Gy fraction of radiation. Cells were plated out using a clonogenic assay and stained with crystal violet.

APPENDIX D: HISTOLOGY

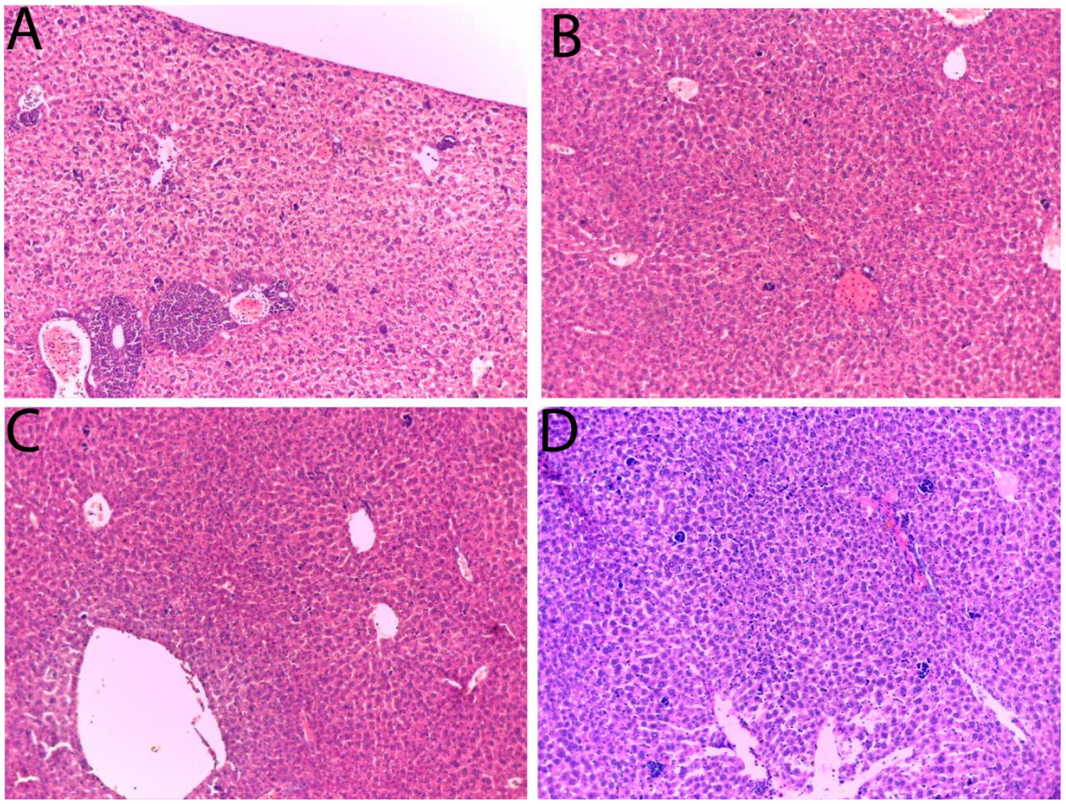

Figure A10: H&E staining of liver showed no metastatic lesions. A) Cohort A (i.v. saline control), B) Cohort B (empty implant + i.v. saline), C) Cohort C (empty implant + i.v. gemcitabine and paclitaxel), D) Cohort D (dual drug loaded implant (gemcitabine and paclitaxel))

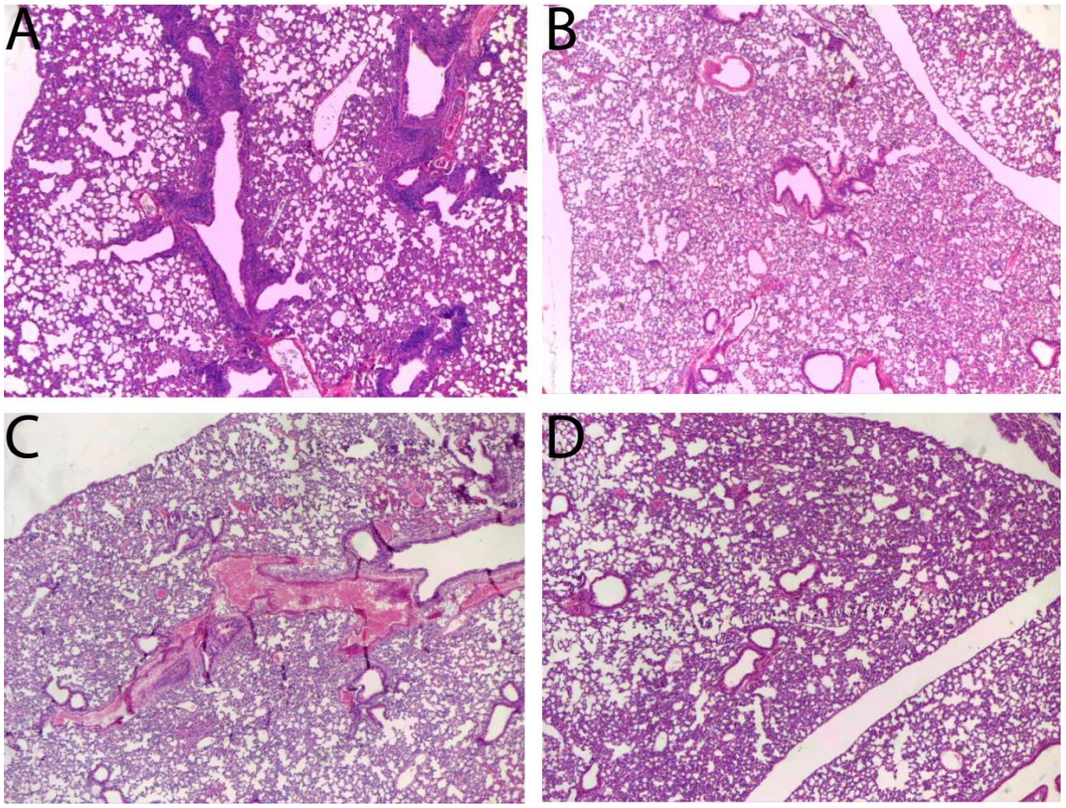

Figure A11: H&E staining of the lungs revealed no metastatic lesions. A) Cohort A (i.v. saline control), B) Cohort B (empty implant + i.v. saline), C) Cohort C (empty implant + i.v. gemcitabine and paclitaxel), D) Cohort D (dual drug loaded implant (gemcitabine and paclitaxel))